SCIENCE & TECHNOLOGY

ARS JOURNAL

A PUBLICATION OF THE AMERICAN ROCKET SOCIETY

FORMERLY JET PROPULSION

EDITORIAL

SURVEY ARTICLE

CONTRIBUTED ARTICLES

TECHNICAL NOTES

DEPARTMENTS

October 1959 Volume 29 Number 10 Part 1

LIQUID NITROGEN

...AT THE TOUCH OF A BUTTON

Supplies laboratory or plant needs swiftly and economically

Convenience is unmatched. A ready supply of liquid nitrogen always available —literally at the touch of a button. Supply is obtainable days, nights, weekends or holidays – it is not subject to outside influences over which you have no control such as routing or delivery schedules.

The Norelco Liquid Nitrogen Generator consists of a single atmosphere separation column that employs a Norelco Gas Liquefier as the nitrogen condenser. Operating as a completely integrated and self-contained system, the generator produces pure liquid nitrogen from air. *An oil-free product is assured since neither nitrogen nor air ever comes in contact with oily surfaces of working parts.* There are no moving parts in nitrogen separation column. The Norelco Nitrogen Generator does not require expert supervision for operation. Automatic controls provide continuous reliable service.

Startling economies are available with the Norelco Liquid Nitrogen Generator. The unit produces an average of six liters of pure, (99.5%) liquid nitrogen per hour over an uninterrupted period of up to 200 hours. (Production figures are based on average locations and operating conditions. Output will vary according to altitude, humidity, temperature, etc.) On a regular production basis, cost per liter is but a small fraction of most existing commercial rates.

Vaporization losses are reduced to an absolute minimum. Users of moderate quantities of liquid nitrogen order in excess of actual requirements in order to insure adequate supply of this vital product. Losses are considerable, particularly if the commercial source is some distance away.

The Norelco Liquid Nitrogen Generator is supplied as a packaged unit ready for immediate installation. Present users of the Norelco Gas Liquefier may add the nitrogen separation column and convert their unit to liquid nitrogen production. *Send for details today!*

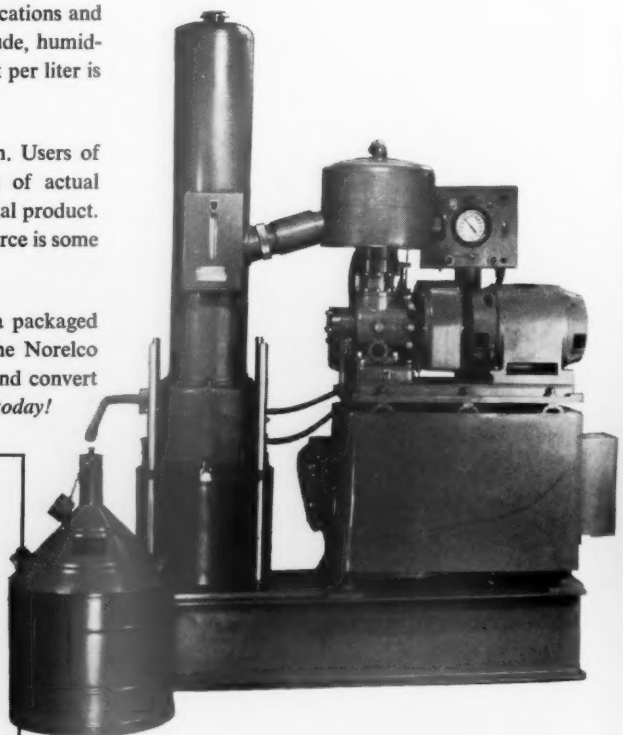

FEATURES

1. Low Cost
2. Fresh supply always available
3. Clean, *oil-free* product
4. High purity product
5. No evaporation or storage problems
6. No compressed air necessary
7. No expert supervision required
8. High production yield
9. Automatic controls for continuous reliable service

NORTH AMERICAN PHILIPS COMPANY, Inc.

Cryogenics Division 100 STEVENS AVENUE, MOUNT VERNON, N. Y.

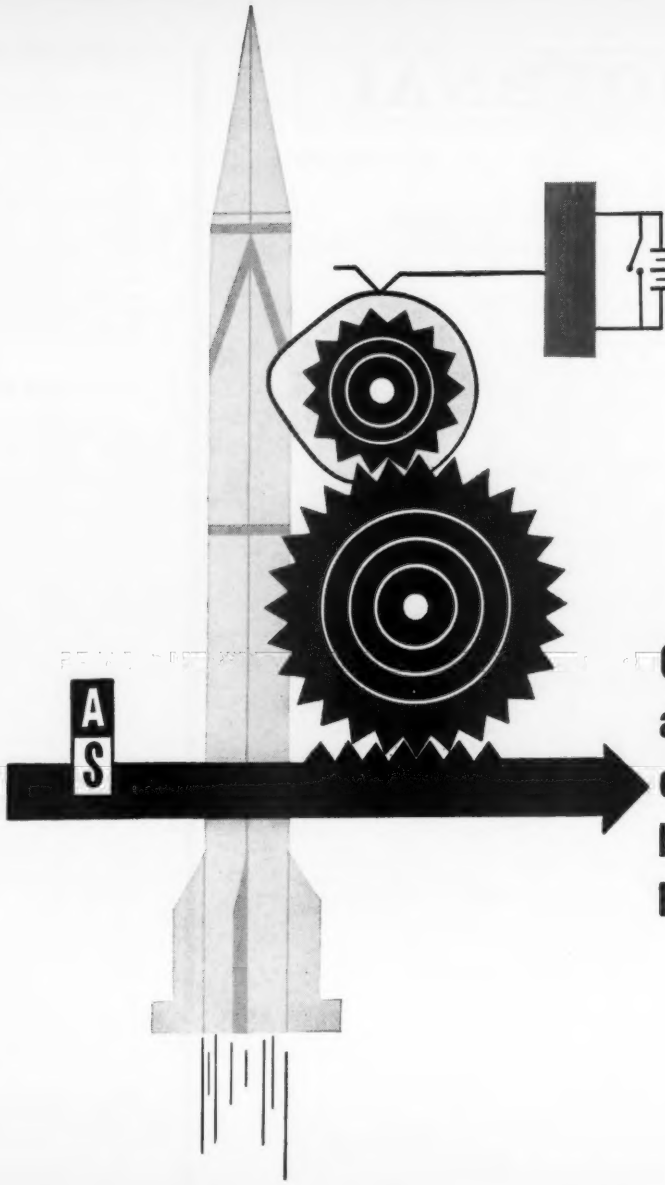

Over 10,000,000 arming devices delivered... by Bulova

Bulova—from conception to production—sets standards in reliability

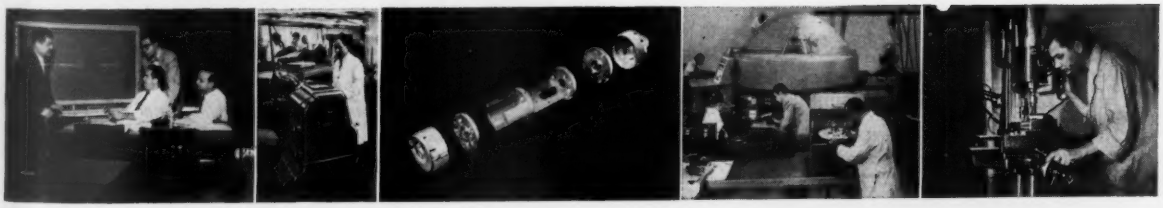

Bulova fuzes, safety and arming devices, timers and firing switches are designed and manufactured to the maximum degree of reliability.

Bulova's teams of electro-mechanical engineers are skilled in feasibility studies and analysis of parameters which lead to hardware meeting the most exacting safing and arming requirements.

Experience in precision design and manufacture is the Bulova tradition—the Bulova capability—it has been for over 80 years. For more information write—

Industrial & Defense Sales, 62-10 Woodside Avenue, Woodside 77, N.Y.

BULOVA

ARS JOURNAL

A PUBLICATION OF THE AMERICAN ROCKET SOCIETY

FORMERLY JET PROPULSION

American Rocket Society

500 Fifth Avenue, New York 36, N. Y.

Founded 1930

Scope of ARS JOURNAL

This Journal is devoted to the advancement of astronautics through the dissemination of original papers disclosing new scientific knowledge and basic applications of such knowledge. The sciences of astronautics are understood here to embrace selected aspects of jet and rocket propulsion, space flight mechanics, high-speed aerodynamics, flight guidance, space communications, atmospheric and outer space physics, materials and structures, human engineering, overall system analysis, and possibly certain other scientific areas. The selection of papers to be printed will be governed by the pertinence of the topic to the field of astronautics, by the current or probable future significance of the research, and by the importance of distributing the information to the members of the Society and to the profession at large.

Information for Authors

Manuscripts must be as brief as the proper presentation of the ideas will allow. Exclusion of dispensable material and conciseness of expression will influence the Editors' acceptance of a manuscript. In terms of standard-size double-spaced typed pages, a typical maximum length is 22 pages of text (including equations), 1 page of references, 1 page of abstract and 12 illustrations. Fewer illustrations permit more text, and vice versa. Greater length will be acceptable only in exceptional cases.

Short manuscripts, not more than one quarter of the maximum length stated for full articles, may qualify for publication as Technical Notes or Technical Comments. They may be devoted to new developments requiring prompt disclosure or to comments on previously published papers. Such manuscripts are usually published within two months of the date of receipt.

Sponsored manuscripts are published occasionally as an ARS service to the industry. A manuscript that does not qualify for publication, according to the above-stated requirements as to subject, scope or length, but which nevertheless deserves widespread distribution among jet propulsion engineers, may be printed as an extra part of the Journal or as a special supplement, if the author or his sponsor will reimburse the Society for actual publication costs. Estimates are available on request. Acknowledgment of such financial sponsorship appears as a footnote on the first page of the article. Publication is prompt since such papers are not in the ordinary backlog.

Manuscripts must be double spaced on one side of paper only with wide margins to allow for instructions to printer. Include a 100 to 200 word abstract. State the 'authors' positions and affiliations in a footnote on the first page. Equations and symbols may be handwritten or typewritten; clarity for the printer is essential. Greek letters and unusual symbols should be identified in the margin. If handwritten, distinguish between capital and lower case letters, and indicate subscripts and superscripts. References are to be grouped at the end of the manuscript and are to be given as follows: For journal articles: authors first, then title, journal, volume, year, page numbers; for books: authors first, then title, publisher, city, edition and page or chapter numbers. Line drawings must be clear and sharp to make clear engravings. Use black ink on white paper or tracing cloth. Lettering should be large enough to be legible after reduction. Photographs should be glossy prints, not matte or semi-matte. Each illustration must have a legend; legends should be listed in order on a separate sheet.

Manuscripts must be accompanied by written assurance as to security clearance in the event the subject matter lies in a classified area or if the paper originates under government sponsorship. Full responsibility rests with the author.

Submit manuscripts in duplicate (original plus first carbon, with two sets of illustrations) to the Editor, Martin Summerfield, Professor of Aeronautical Engineering, Princeton University, Princeton, N. J. Preprints of papers presented at ARS national meetings are automatically considered for publication.

ARS JOURNAL is published monthly by the American Rocket Society, Inc. and the American Interplanetary Society at 20th & Northampton Sts., Easton, Pa., U. S. A. Editorial offices: 500 Fifth Ave., New York 36, N. Y. Price: $12.50 per year, $2.00 per single copy. Second-class mail privileges authorized at Easton, Pa. This publication is authorized to be mailed at the special rates of postage prescribed by Section 132.122. Notice of change of address should be sent to the Secretary, ARS, at least 30 days prior to publication. Opinions expressed herein are the authors and do not necessarily reflect the views of the Editors or of the Society.

engineers • scientists

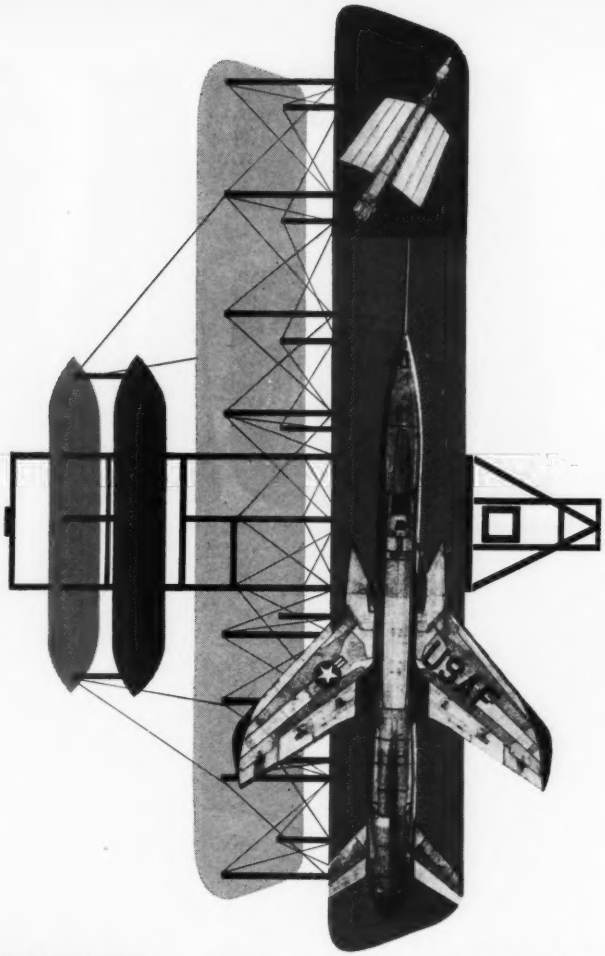

IDEAS CLEARLY IMAGINED BECOME REALITIES AT REPUBLIC AVIATION

During the early years of this century the airplane was only the dream of a few dedicated men. Yet in the short span of 5 decades this dream has evolved into such advanced aircraft as Republic's F-105 — the free world's most powerful fighter-bomber — which is capable of flight in the Mach 2 regime.

The same holds true for missiles and space vehicles. Thirty brief years ago they existed in only a few imaginations. Today at Republic the imaginations of many men are working to create the vehicles that will allow man to explore the last frontier — space. Included in this far-ranging research and development effort are plasma propulsion systems, electronic and hydraulic subsystems that will operate efficiently in extreme environments, and the calculation of super-accurate space flight trajectories.

Working across the total technology of flight, Republic engineers and scientists see their ideas become realities because the novel, the unique and the revolutionary in technical thinking are appreciated and encouraged by management. New investigations and new contracts mean you can put your ideas in motion at Republic Aviation.

Immediate Openings in Advanced Areas for Engineers and Scientists at all Levels of Experience:

ELECTRONICS: Inertial Guidance & Navigation • Digital Computer Development • Systems Engineering • Information Theory • Telemetry-SSB Technique • Doppler Radar • Countermeasures • Radome & Antenna Design • Microwave Circuitry & Components • Receiver & Transmitter Design • Airborne Navigational Systems • Jamming & Anti-Jamming • Miniaturization-Transistorization • Ranging Systems • Propagation Studies • Ground Support Equipment • Infrared & Ultra-Violet Techniques

THERMO, AERODYNAMICS: Theoretical Gasdynamics • Hyper-Velocity Studies • Astronautics Precision Trajectories • Air Load and Aeroelasticity • Airplane/Missile Performance • Stability and Controls • Flutter & Vibration • Vehicle Dynamics and System Designs • High Altitude Atmosphere Physics • Re-entry Heat Transfer • Hydromagnetics • Ground Support Equipment

PLASMA PROPULSION: Plasma Physics • Gaseous Electronics • Hypersonics and Shock Phenomena • Hydromagnetics • Physical Chemistry • Combustion and Detonation • Instrumentation • High Power Pulse Electronics

NUCLEAR PROPULSION & RADIATION PHENOMENA: Nuclear Weapons Effects • Radiation Environment in Space • Nuclear Power & Propulsion Applications • Nuclear Radiation Laboratories

Send resume in confidence to:
Mr. George R. Hickman
Engineering Employment Manager, Dept. 10-K

REPUBLIC AVIATION
FARMINGDALE, LONG ISLAND, NEW YORK

Keeping Our Eyes on Russian Astronautics

OUT OF sheer professional necessity, as well as intellectual curiosity, every research scientist and development engineer must keep alert to the findings and achievements of other scientists and engineers working in his field. In every phase of rocketry and astronautics, however, developments have been taking place so rapidly that it has become a rather difficult task just to keep up with American and English journals, not to mention proceedings of symposia, classified reports, new books, etc. It is understandable, therefore, that very few American scientists are really aware of the important work being done abroad, even in their own fields. Although most American scientists have been trained traditionally to read French and German, the two foreign languages that used to encompass the bulk of non-American science, even these languages represent barriers that discourage a great many scientists and engineers.

The problem has become still more acute in the past decade with the rapid advance of science and engineering in the USSR, as well as in a number of smaller countries. In the particular case of the Russians, the task of becoming informed of their work is especially difficult, aside from the question of how much they keep under security wraps. First, the traditional emphasis on French and German in Ph.D. training means that very few American scientists can read Russian. In fact, until a few years ago, it was not easy to buy Russian grammars or dictionaries, and only recently have scientific dictionaries begun to appear. Then, the language is more difficult to learn than French or German because of the unfamiliar alphabet and grammar. There is also the lack of familiarity on the part of American scientists with the names or relative importance of the 500-odd journals and serials in science and technology being published in the USSR. And, finally, we have only scant knowledge of Russian scientists and Russian institutions, the name-and-place clues ordinarily used in seeking out and evaluating publications in our own country.

Until a few years ago, keeping an eye on Russian science was of concern only to individual scholars (and probably to official intelligence agencies, but this is not pertinent here). Today, it is a matter of national policy, and several government agencies are now hard at work to inform American scientists of Russian published work. The Library of Congress publishes a *Monthly Index of Russian Accessions* that contains translated tables of contents of all Russian journals received in this country, and this is available from the Superintendent of Documents at $12 per year. The Office of Technical Services of the Department of Commerce publishes *Technical Translations*, a semimonthly that contains translated abstracts of Russian articles. This is available at $12 per year. An important program has been launched by the National Science Foundation to stimulate the translation and distribution of Russian journals in their entirety, and about 75 journals are now regularly available in complete translation, in technical fields ranging from agriculture to engineering, from medicine to physics. As a result of NSF subsidies given to the professional societies that carry out the translations, subscription prices are kept down to the same level as those of American journals, and academic institutions and libraries are finding it within their means to acquire these journals. A good deal more needs to be done along these lines, but it is an excellent national program even as it stands.

As part of this National Science Foundation program, the AMERICAN ROCKET SOCIETY has received a grant to finance the translation and dissemination of important Russian articles in astronautics. There is a novel aspect to the ARS project: In the interest of achieving the most effective distribution, the translated material is to be sent free of charge to all ARS members and subscribers to the ARS JOURNAL. The officers of the National Science Foundation agreed with the ARS representatives that it is not really enough to have the articles translated if the resulting price tends to limit the distribution to libraries. It is in the national interest to place these translations in the hands of the thousands of engineers who are expected to use the material, just as the ARS JOURNAL reaches them. Accordingly, the translations will appear quarterly as part of the January, April, July and October issues. The translations will not replace any part of the regular issue; the four issues named will, therefore, be considerably larger than normal. The extra cost will be covered by the NSF grant.

The Editors are faced with several problems in connection with this project. First, there is the problem of tracking down and securing the original articles that may qualify for translation and publication. If there were a single Russian journal equivalent to the ARS JOURNAL, the job would be a simple one: We would translate it in its entirety. Unfortunately, there is none, so articles must be selected from many different journals, quite a job for a scientific detective. Second, since we can't translate and publish within the limited NSF budget everything we uncover (nor do we want to do so), there is the problem of evaluation and ultimate selection of articles, a task that requires technical judgment. Another question is whether the selections should be concentrated in only a few subject areas or be spread out impartially over all the diverse subjects covered by our Society. Finally, the proposal has been made that articles should be abridged or condensed by the translator whenever possible, in order to achieve more extensive coverage within the available budget, but there are obvious dangers in this plan as well as advantages. Each of these questions raises problems of administration and execution. The Editors will attempt to develop workable solutions to all of them. Comments and suggestions from our readers will be welcome.

We trust that this project will prove successful, not only from the Society's standpoint, but, most important, from the standpoint of the profession we serve.

Martin Summerfield
Editor

Recent Advances in Space Propulsion

GEORGE S. SUTHERLAND
Boeing Airplane Co.
Seattle, Wash.

Dr. Sutherland received his B.S. in mechanical engineering from the University of Michigan in 1950 and his M.S. in the same field from Princeton University in 1952. In 1956, after completing a thesis on the burning mechanism of an ammonium-perchlorate solid propellant, he obtained his Ph.D. in aeronautical engineering. Since 1956 the author has worked at Boeing Airplane Co. on problems connected with large, rocket boosted weapon and space systems and in the field of advanced propulsion. He is currently head of the Advanced Propulsion Group of Boeing's Systems Management Office.

THOUGHTS on space propulsion have their beginning early in the history of mankind. Whenever man has paused to speculate on interplanetary or lunar journies, he has had to invent some method of getting to his destination. Possibly the first application of the rocket to space travel was made by Cyrano de Bergerac who, in 1656, described a vehicle festooned with firecrackers, the impulse from which would propel him toward the moon (140).[1] The giant gun, popularized by Jules Verne in 1865, had received considerable attention through the ages as a device for propelling man through space. A modified "gun," incidentally, has recently been proposed for launching missiles (150). As a matter of fact, at least one so-called "exotic" propulsion scheme (the ion rocket) was invented quite a few years ago, and other interesting ideas may lie undiscovered in old technical publications.

Although the concept of space propulsion is not new, recent political and engineering developments have stimulated a wide interest in this subject, and in the past several years considerable technical progress has been made.

Space Propulsion

The subject of space propulsion embraces three primary areas: The propulsive device itself, the energy source to drive it, and the interaction with gravity fields, i.e., space mechanics. Though embracing quite different technical disciplines, each of these areas will be discussed briefly, since most system analyses require consideration of all three in order to arrive at sound conclusions.

Large chemical booster rockets used to establish payloads in Earth orbits or escape trajectories are not considered here as space propulsion devices. Nuclear heat transfer rockets are discussed briefly, although their application to space propulsion, other than for boosters, has not yet been thoroughly explored.

Chemical Propulsion

The "conventional" chemical rocket will undoubtedly find application in space systems (10). For example, the development of new high energy solid propellants capable of withstanding temperature extremes can provide a compact, reliable source of high thrust per unit rocket weight. Storable, prepackaged liquid units can provide similar performance. Typical applications might include retrorockets for de-orbiting and landing, and propulsion for maneuvering.

Free Radical Reactions

Due to the relatively poor performance of the chemical rocket caused by the limited energy available from the usual combustion reactions, recent interest has centered on free radical reactions as a possible source of increased energy (8, 11). In particular, the recombination of atomic hydrogen to form molecular hydrogen is of special interest due to the high energy release coupled with the low molecular weight of the exhaust products. For example, if one could stabilize about 10 per cent by weight of atomic hydrogen in a molecular hydrogen matrix, the expected vacuum specific impulse would be about 700 sec (14).

In 1956, the National Bureau of Standards initiated a three-year program of fundamental research on free radicals (12). This work and similar research in other industrial and university laboratories, is primarily aimed at learning more about the formation and properties of free radicals, particularly at the liquid helium temperatures used to stabilize the free radicals.

This type of work must be done before an answer may be expected on the applicability of free radicals to propulsion. Initial results seem discouraging. For example, neglecting any question of special hardware required and the possibility of adverse mass ratios due to stabilization problems (8), there is some reason to doubt that practical quantities of a free radical, such as atomic hydrogen, can be stabilized by isolation in a solid matrix.

Theoretical statistical analyses by Golden (6) and Jackson and Montroll (7) have attempted to predict the number of free radicals that may be stabilized in a condensed phase. The mole fraction stabilized is a function of the condensed geometry (simple cubic, body-centered cubic, etc.) as well as of the concentration of free radicals in the condensing mixture. Neglecting diffusion in the solid phase, which may well make these estimates upper limits, both of these references predict mole fraction concentrations on the order of 10 to 14 per cent for 100 per cent free radical concentrations condensing into body-centered and face-centered lattice structures. This corresponds to weight fractions of only 5 to 6 per cent, which are somewhat low to be of interest for propulsion in the light of other probable disadvantages.

Evidence of the relatively strong tendency of atoms, such as H, O and N to diffuse in the solid matrix have been gathered from various sources (13). Future progress in free radical propulsion must await more knowledge of deposition and stabilization processes and of the diffusion of the radicals in the frozen matrix. It is interesting to note that, on the basis of these theoretically predicted concentrations of H atoms, Palmer (9) has calculated the linear burning rate of an H-atom propellant and finds a value of 125 cm per sec at 1-atm pressure.

Atmospheric Atom Recombination

Another possible way to employ chemical energy for propulsion, and one which may have possible applications to

Received Aug. 26, 1959.
[1] Numbers in parentheses indicate References at end of paper.

space travel, is the use of photo-dissociated atoms found in the upper atmosphere (1, 3, 4, 8). Though energy is available, the problem of utilizing it for propulsion is formidable. Analyses (3, 8) have indicated that at orbital speeds the thermodynamics and kinetics of recombination rule out the possibility of obtaining a net positive thrust, whereas at low supersonic speeds where thrust can conceivably be obtained, no practical means for supporting the vehicle at the required altitudes are available.

Nuclear Propulsion

The use of nuclear energy for propulsion received a fairly detailed examination by Shepherd and Cleaver in 1949 (32). Since that time a number of nuclear rocket studies have appeared, many of which deal with the application and performance aspect of the problem (16, 19, 21, 26, 27, 29).

Preliminary design studies on nuclear reactors for rockets have also been published (24, 25, 27, 29, 35). A great deal of this work is summarized in an excellent book by Bussard and DeLauer (18).

Heat Transfer Rocket

The development of the heat transfer nuclear rocket is under way at Jackass Flats, Nev., under the direction of the Atomic Energy Commission. Though details of technical progress are not available owing to security restrictions, an interesting progress report on the Rover program was recently given by Schreiber (31). The Rover program is aimed at demonstrating the feasibility of the heat transfer reactor for rocket propulsion. Recent tests (15) indicate that successful feasibility tests on Kiwi-A are well on their way to completion. This in turn means that in several years a flyable rocket reactor, capable of delivering a specific impulse of about 800 sec using hydrogen as the working fluid, will be ready for incorporation into a booster system. Such a single-stage booster system will be capable of placing in orbit about 10 per cent of its gross weight (29). Mass ratios (propellant weight/gross weight) obtainable are in the neighborhood of 0.75 to 0.80, and the reactor powerplant (reactor, shielding, pumps and nozzle) should develop about 20 to 30 lb of thrust per pound of engine weight.

Application of the Rover-type engine and possible successors to space missions has not yet been fully explored. Obviously, the nuclear rocket has the ability to impart the necessary velocity to establish a payload in the required interplanetary or lunar ballistic trajectory (98). Other facets of the problem, such as maneuver capability, control, starting, stopping and landing, could introduce unexpected difficulties. Also, in order to be economically feasible, ambitious space missions require better performance than the 800 to 1000-sec specific impulse probably available from the first and second generation Rover rockets.

Gaseous Reactor

The gaseous or "cavity" reactor offers the possibility of increasing the performance of the nuclear rocket by possibly 100 per cent or more. In this device, the material-temperature problems of the solid reactor core are traded for the material-temperature, chemical and hydrodynamic problems of the gaseous core (though at higher temperatures).

In an early analysis by Shepherd and Cleaver (32), a cavity radius of 120 m was estimated for a reactor using hydrogen and U^{235} at 100 atm. However, no reflector was assumed to surround their reactor.

In a more recent analysis, Safonov (28) has calculated that with a D_2O reflector, a cavity radius of about 1 m would require only 2 kg U^{235} for criticality. This is equivalent to a fissionable material density of less than 0.04 lb/ft^3, a value which indicates interesting possibilities for the gaseous reactor.

Bussard and DeLauer (18, p. 324) have shown that some method of separation of the fissionable material from the working fluid is required, or the cost of the escaping fuel becomes prohibitive. An initial analysis of the problem by Grey (22) indicates that a method based on centrifugal separation may prove successful. A major question, which cannot be completely answered until more data are available, is whether the radiative heat transfer to the walls of the cavity will be beyond the cooling ability of the incoming working fluid.

Fluidized Reactor

A partial compromise between the temperature limitations of the solid core reactor and the technical difficulties of the gaseous reactor may be afforded by the fluidized reactor (34). In this device, the propellant gas is passed through a bed of very small particles of fissionable material. At the proper flow rates, the bed is stabilized by gravitational or centrifugal forces, and very high heat transfer rates to the propellant gas may be achieved at relatively high temperatures. No recent experimentation appears to have been done on this concept.

Other methods for the direct utilization of nuclear energy for propulsion are discussed by Shepherd and Cleaver (32) and Bussard (139).

Thermonuclear Propulsion

Whether thermonuclear energy will be used directly for propulsion, as proposed by Clauser (37), or indirectly to generate electrical energy for an electrostatic or electromagnetic device, or even prove to be altogether impractical for propulsion applications, is a subject for speculative discussion.

Early studies by Tsien (42) and Sänger (41) present a somewhat pessimistic picture of the possibilities of using steady thermonuclear burning for propulsion. The requirement of large reactor volume combined with low volumetric energy release works against such applications.

Future prospects for thermonuclear propulsion rest largely on the success of Project Sherwood researchers in finding methods of igniting, confining and stabilizing the reacting plasma. For further information on this subject, the reader is referred to an excellent book by Bishop (36), which contains a semitechnical description of Project Sherwood from its inception until early 1958, plus a bibliography for those interested in further details.

Electric Propulsion

It is in the area of electric propulsion that current hopes are highest for early attainment of high performance space propulsion. For discussion purposes, electric propulsion is divided into three categories: (a) Arc heating or thermal-electric rockets, (b) electromagnetic accelerators, (c) electrostatic accelerators.

Arc Heating Rocket

The arc heating rocket, or plasma jet as it is more commonly called, is a thermal reaction device where an electric arc or discharge is used to heat a working fluid (43 to 48). Experimental results of Adams and Camac (43) indicate that specific impulse values between 1000 and 1200 sec are obtainable with at least 50 per cent efficiency (exhaust jet power/input power).

The very high temperatures in the arc chamber and electrode erosion are problems which, though not insurmountable, make successful application of these devices to any long duration mission somewhat doubtful. The plasma jet is in fairly wide use for heat transfer and materials testing research, and improved configurations may be expected to result from this work.

Electromagnetic Accelerators

Generally speaking, this category includes all those devices in which the interaction of a magnetic field with an electrically conducting gas or plasma produces a ponderomotive force in the plasma which may then be used to accelerate the plasma to produce thrust. These devices, therefore, have their roots in the technology of magnetohydrodynamics and plasma dynamics. Obviously, in such a fertile environment, a rapidly growing number of contributions are currently being made to the knowledge of handling plasma, and accelerating it to produce thrust. Much of the stimulus and knowledge concerning plasma dynamics has arisen from the United States' program on controlled fusion. However, for the present discussion, plasma operations at thermonuclear temperatures are not included. Only a few papers particularly concerned with propulsion will be mentioned here, and the reader is referred to such periodicals as *The Physical Review* and *The Physics of Fluids*, as well as several excellent books on the subject (61, 62, 65).

A number of interesting possibilities for electromagnetic accelerators have grown out of shock tube and shock wave investigations. Kolb (57) describes experiments utilizing a T-shape electrically driven shock tube, in which shock velocities are increased by factors of from 2 to 4 by means of ponderomotive forces induced by the magnetic field from the properly oriented return loop of the discharge circuit. Related experiments are described in the section "Magnetically Driven Shock Waves" in (61) as well as in (50 and 56).

Another series of experiments by Bostick and others have produced an interesting phenomenon called a "plasmoid," which is a toroidal-shaped entity of plasma produced by a discharge at the ends of two closely spaced conductors (52 to 54). Plasmoid velocities up to 2×10^7 cm per sec have been measured in a vacuum chamber. The interesting interaction of these plasmoids with magnetic fields and with each other provides stimulation for further experiments (54).

His work with plasmoids prompted Bostick to speculate on the potentialities of plasma motors (51), and he proposes various configurations, among which is the two-rail accelerator. This device, appealing in its simplicity, is shown in Fig. 1. Approximate calculations indicate that velocities of up to 10^8 cm per sec should be possible with this device.

Experimental studies of this type of accelerator have been carried out both in the United States and Russia (58, 49). Both investigations have provided evidence of plasma velocities up to 10^7 cm per sec. It was also shown (58) that the use of plates instead of rods materially aided in keeping the plasma in a fairly well-defined bunch.

A different approach was recently described by Kunen and McIlroy (60), in which nozzle-shaped electrodes are used to convert the well-known pinch effect in plasma into a high velocity axial exhaust stream. The inward moving "magnetic piston" caused by a discharge in a sufficiently high density gas drives a shock wave ahead of it. The transformation of the motion from the radial to the axial direction allows the very high velocity of the gas moving ahead of the piston to be used to produce thrust. Preliminary measurements indicate that specific impulse values of 2000 to 5000 sec were obtained.

Other experimenters have also had an eye on propulsion applications in shock tube work (55, 63, 64, 66). In general, time interval or streak camera measurements indicate shock front or plasma bunch speeds on the order of 10^6 to 8×10^6 cm per sec, which correspond to specific impulses in the range of 1000 to 8000 sec.

Preliminary measurements (60, 64, 66) suggest that the efficiency of conversion of stored energy into the moving plasma is probably in the range of 5 to 30 per cent. Further experiments are required to measure plasma energy more precisely, so that techniques for improving the conversion efficiency may be evaluated.

The electromagnetic accelerator is somewhat of a stepchild of research in shock tubes and magnetohydrodynamics. Calculations and experiments have certainly proved that very respectable exhaust velocities may be produced with this technique, and further experiments are now under way to improve the efficiency of energy transfer. Characteristics of this device which require further investigation include: (a) The necessity for pulsed operation, (b) the electric energy storage and transfer equipment, (c) optimum accelerator configuration and (d) potential for large thrusts for high-g maneuvers as well as its potential for low-g acceleration for long periods.

Electrostatic Propulsion

In the past few years, research in electrostatic propulsion has progressed from preliminary design and mission analysis to actual engine prototype testing.

Following the early discussions of Oberth (146) and Goddard (143), the first critical analysis of the ion rocket was given by Shepherd and Cleaver (91) who were somewhat dismayed by the problem of supplying the electrical energy required, particularly by means of rotating machinery.

Theoretical analyses by Spitzer (92) and Preston-Thomas (100) in the early 1950's were somewhat more optimistic about the prospects for ion propulsion, chiefly due to the fact that vehicle accelerations on the order of 10^{-4} g were assumed in their studies. More recent studies by Stuhlinger (102 to 104) and Bussard (73) also discuss the system design problem.

As a result of the studies mentioned above, it became evident that under the assumptions used, ion propelled space vehicles could be successfully employed for interplanetary missions, and that little or no effort had been devoted to developing the critical components for such a vehicle.

In the past few years this situation has improved, and several investigations on the characteristics of ion sources and accelerators are in progress, as well as efforts to develop new, lightweight power conversion equipment.

The ion accelerator is composed of an ion source, an elec-

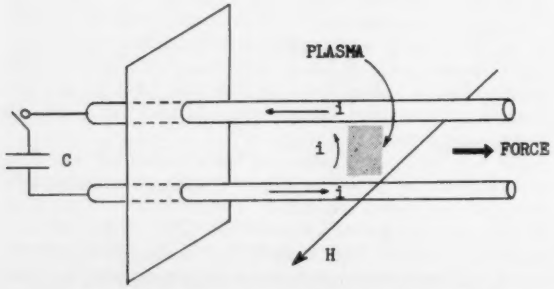

Fig. 1 Bostick's rail-type plasma accelerator

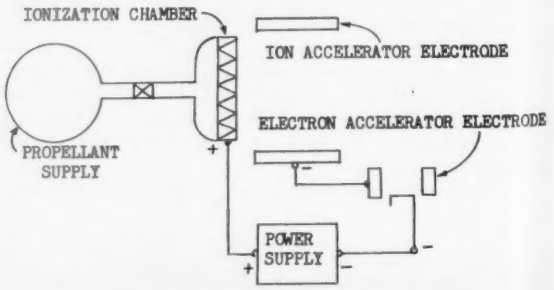

Fig. 2 Schematic of ion accelerator

trode arrangement for accelerating the ions and electrodes to neutralize the ion beam after passing the accelerating electrode. See Fig. 2.

Ion Sources

The ion source may utilize any one of a number of methods to produce ions (83, p. 483). These ion sources include the oscillating electron source, arc source, filament source, high frequency electrodeless discharge and surface ionization. Ion sources have been under intensive development by laboratories concerned with particle production for nuclear research and mass spectrographs. Most of these devices utilize either electrodeless, or low voltage discharges to produce ions, which are then extracted by means of an electric field (68, 69, 81).

An oscillating electron source which utilizes oscillating electrons trapped in a potential well to ionize the working gas is described in (84). This type of source appears capable of producing a high ion yield as well as relatively high currents. Ion source development for propulsion applications is just beginning, and it is premature to single out one type of source as most suitable for ion rockets. However, space vehicle requirements of long lifetime, high ion production efficiency and minimum energy expenditure per ion produced may eliminate many possibilities.

In order to reduce the power required per pound of thrust produced, the ion accelerator requires ions with a low charge to mass ratio. Cesium, which has the lowest ionization potential of the elements, has an atomic weight of 132.9 and is a logical contender as a propellant. Current cost of Cs is on the order of $540 per lb, but mass production could reduce this figure to less then $25 per lb (75). Due to its low ionization potential, Cs may be readily ionized on a tungsten surface. Initial research on the ionization of alkali metals on tungsten surfaces was done by Langmuir and others (93) more than 30 years ago. Recent work by Datz and Taylor (77) also indicates that ionization efficiencies of essentially 100 per cent can be achieved with Cs on a tungsten surface. These data, in conjunction with the low charge to mass ratio of Cs, have prompted several investigations of the suitability of the surface ionization of Cs (and other alkali metals) on tungsten as an ion source for propulsion applications (76, 79, 82, 85, 90).

One of the questions to be answered concerns the maximum ion current which can be drawn per square centimeter of emitting surface. This is a function of surface temperature and atom impingement rate. If the temperature is below a certain critical value, which depends upon the vapor pressure of the cesium, then Cs atoms form an adsorbed layer on the tungsten surface and lower the effective work function below the ionization potential of Cs. This occurs when more than about 20 per cent of the surface is covered with Cs. However, the ionization efficiency is seriously reduced even when more than 4 per cent of the surface is covered. Consequently, for 100 per cent conversion, the surface temperature must be slightly above the critical temperature. For example, Cs ion currents of 100 ma per cm^2 require a critical temperature close to 1450 K (82).

The early work on surface ionization was performed with ion current densities considerably less than would be of interest for ion propulsion. Consequently, Shelton et al. (90) have extended the results of Taylor and Langmuir up to Cs ion currents of 100 ma per cm^2. These results showed that even at these relatively high current densities, ionization efficiency was 100 per cent. Furthermore, the power required to produce the ions was only about 1 per cent of the jet power at a specific impulse of 7500 sec.

Ion Acceleration

After the ions are produced, they can be accelerated by an electric field. For Cs ions, a potential of 6700 v produces a specific impulse of about 10,000 sec. It is necessary for structural integrity and maximum efficiency that the ion beam be reasonably well-collimated and not impinge on the accelerating electrode. The high current densities will introduce space charge effects; hence the accelerator design must be accomplished by numerical analysis or analog techniques. Experience in the design of microwave tubes, electron microscopes and similar devices has uncovered a number of clever methods to deal with the design of particle accelerators or focusing devices. For example, space charge simulation in an electrolytic tank is discussed in a paper by Van Duzer and Brewer (94). Current research on ion optics and formation of high density beams is typified by work discussed in (72 and 78). Pierce, a pioneer in the field, has written an excellent book on electron beam design (87).

One trick that should be mentioned for overcoming space charge limitations is the accelerate-decelerate electrode configuration. For a net acceleration potential, higher current densities may be obtained, and a certain design flexibility achieved if the first electrode accelerates the ions to a high potential and the second electrode decelerates them to the potential corresponding to the desired specific impulse (85, 89). Finally, it is necessary to neutralize the positive ion beam by adding the required number of electrons. This is apparently somewhat difficult to accomplish in practice (76, 79, 90). Further experiments are needed to establish the best method for achieving neutralization.

Performance

The performance of the space charge-limited ion accelerator may be closely approximated by simple relations derived from Child's equation for plane-parallel geometry. These are

$$
\begin{aligned}
I_s &\sim V(q/m)^{1/2} \\
T/A &\sim (V/d)^2 \\
I/A &\sim (Vq/m)^{1/2}\, V/d^2 \\
P_j/T &\sim (Vq/m)^{1/2}
\end{aligned}
$$

where

I_s = specific impulse
V = accelerating voltage
q/m = charge to mass ratio of ion
T/A = thrust per unit area
I/A = maximum current density
P_j/T = power per unit thrust

One notes that, while it is desirable to have the accelerating voltage gradient as high as possible to produce maximum thrust per unit area, it is also desirable to have a low propellant charge to mass ratio in order to reduce the power required to produce a pound of thrust (70).

A great increase in particle mass may be obtained by utilizing charged particles of microscopic rather than atomic dimensions. Such a device was described at a recent ARS meeting in San Diego, and the title "colloid" rocket seems to have been adopted for this type of accelerator due to the fact that the particle sizes of interest are those found in colloids ($10^{-3}\ \mu < d < 1\mu$). Techniques for production of these charged particles are based on the effect of high electric fields on dielectric liquids (86, 88). For example, sprays of charged drops can be produced by certain electrode configurations and electrode voltages on the order of 5 to 10 kv.

Testing of ion accelerators and components requires special equipment and techniques not previously encountered by most propulsion engineers. For example, the high vacuum test chamber should be capable of providing a vacuum of 10^{-7} mm Hg in order to minimize the collision of ions with other atoms and molecules. Such an ion accelerator test facility is described by Childs (76) in an excellent discussion of ion rocket design criteria.

Solar Propulsion

This category includes those devices which directly utilize the sun for propulsion either by means of photon recoil or by means of heating a working fluid directly.

Use of solar photon momentum for propulsion by means of a solar sail is an intriguing possibility. Recent analyses by Garwin (96) and Tsu (97) have shown that accelerations on the order of 10^{-4} g can be obtained at 1 astronomical unit from the sun by utilizing commercially available 0.1-mil thick plastic sail material. A 10,000-lb vehicle (including sail) would require a sail area of 5.4×10^6 ft^2, or a circular sail about $\frac{1}{2}$ mile in diameter, and the sail would weigh about 3300 lb. (This simple calculation assumes that the sail lies flat.)

Tsu (97) has calculated the optimum sail setting for a logarithmic spiral trajectory, and computes a travel time of about 250 days to reach Mars' orbit with a 10^{-4}-g acceleration. No consideration was given to the problem of the capture maneuver required once the spiral trajectory intercepted Mars' orbit. Such a maneuver could be beyond the sail capability.

In any case, the solar sail technique deserves further attention. Even if not desirable for the primary system, it seems to deserve consideration as an emergency, "lifesaver" propulsion system.

The solar heat rocket, as envisioned by Ehricke (95) uses extremely thin coated plastic material similar to that assumed for the solar sail, to form spherical reflectors to concentrate the sun's energy on heat transfer tubes containing hydrogen. In a design study, he estimates that accelerations of 10^{-2} g can be obtained with a specific impulse of 450 sec.

Systems Analyses

A considerable number of preliminary designs of various types of space vehicles has appeared in the literature during the past several years. The early studies by Stuhlinger (103, 104) on ion propelled space vehicles are quite well-known. Excellent surveys of the general problem of electrical propulsion in space have been published by Shepherd (101) and Preston-Thomas (100). Detailed studies of nuclear powered turboelectric power supply systems have been made by Kovacik and Ross (99), and English et al. (127) among others.

These and other preliminary design and system analyses have demonstrated that low thrust space travel is practical. Further progress must await component development.

Space Mechanics

A complete coverage of the recent work done in the field of flight mechanics of space vehicles is beyond the scope of this review. However, since the performance of space propulsion systems is intimately linked with the path through gravity fields, a brief discussion of some of the unique characteristics of low thrust trajectories may be of value to the reader, and the accompanying references will at least help him find more detailed information.

A review of recent advances in the techniques of determining precision orbits has been prepared by Herrick and Baker (113). However, the emphasis here is placed on the results of approximate calculations, where simplifying assumptions allow a quicker approach to the gross behavior of the vehicle.

One of the first analyses of the problem was made by Tsien in 1953 (123), wherein he showed that the characteristic velocity required for escape from the Earth's gravity field increases with decreasing vehicle acceleration. In the particular case of circumferential acceleration, Tsien showed that the characteristic velocity more than doubled when the vehicle acceleration was reduced from 1 to 10^{-4} g.

However, circumferential thrust is considerably more efficient than radial thrust for developing escape velocity from a satellite orbit, and as pointed out by Lawden (115), is quite close to the optimum thrust direction. Though the instantaneous rate of increase of vehicle energy is a maximum when the thrust direction is tangent to the trajectory, both Lawden (115) and Michielsen (118) have shown that the optimum thrust direction is initially slightly offset toward the center of force, and gradually aligns itself with the trajectory tangent as the vehicle gains energy. Fortunately, tangential thrust is within 1 per cent of the optimum, and hence affords a simple approximation to the optimum thrust program.

Approximate treatments of the low thrust interplanetary trajectory problem generally break down into three parts:

1 The escape from a satellite orbit about the home planet.

2 The heliocentric trajectory to the vicinity of the target planet.

3 The capture of the target planet.

This method, in conjunction with the usual assumptions of circular, coplanar planetary orbits, divides the problem into a succession of "single-body" problems, i.e., two-body problems where one of the bodies has negligible mass.

As shown by Fox (112) and Perkins (120), if the tangential acceleration is less than about 10^{-2} g, the escape and capture calculations need only be performed once, since there are appropriate scaling laws which may be used to transform Earth escape maneuvers into escape (or capture) maneuvers about other planets.

Consequently, once a set of escape maneuvers is determined, the basic problem becomes one of finding the correct heliocentric trajectory to properly join the escape and capture trajectories. The problem is especially critical at the target planet, since only limited thrust is available for capture maneuvers. An interesting method suggested by Rodriguez (121) and also utilized by Levin (116) allows a simple solution to the problem which can eliminate or greatly reduce computer time.

In essence, this method transforms the trajectory from the real (r, θ) plane to the (E, h) plane, where E is the instantaneous energy per unit mass $[(v^2/2) - (\mu^2/r)]$, and h is the instantaneous angular momentum $r^2\dot{\theta}$. If at any instant the vehicle achieves a specific energy and specific angular momentum corresponding to those of any particular planetary orbit, then it is momentarily tangent to that orbit with the correct velocity to remain in the planetary orbit if the thrust is cut off at that instant. Hence, various steering programs are easily examined on the basis of being able to change from (E, h) of the initial planetary orbit to the (E, h) of the final planetary orbit. An example (121) of this method shows that an Earth-Mars trajectory may be accomplished by approximately 75 days of circumferential thrust followed by about 135 days of purely radial (inward) thrust.

Perkins (120) has presented a fairly detailed analysis of the escape (or capture) maneuver under tangentially directed thrust, and shows that low amplitude oscillations about the mean trajectory appear in the low thrust escape maneuver. In addition, his paper contains useful generalized graphs relating velocity, radius, distance and time, from which escape maneuvers can be plotted for any planet or tangential acceleration, as long as it is less than about 10^{-2} g.

The utility of the logarithmic spiral (111, 106) and the purely radial thrust trajectory (109) have been investigated by various authors, particularly in regard to simplification of the guidance problem.

Most analyses of the low thrust trajectory problem assume that the vehicle acceleration is constant in contrast to the constant thrust assumption usually associated with high thrust vehicles. Besides simplifying the analytical problem, the constant acceleration trajectory can result in higher terminal velocities than constant thrust operation. As pointed out by Fox (112, 98), if the vehicle is power-limited, i.e., operated at constant maximum power, then the exhaust velocity and propellant flow can be varied so that the total energy consumption and power-on time are minimized. Under the constraint that

$$\dot{m}_p v_e^2 = \text{constant}$$

where

$\dot{m}_p$ = propellant flow
v_e = exhaust velocity

the correct mass flow program results in constant vehicle acceleration.

Propulsion Power Sources

The fundamental problem of space propulsion is obtaining large quantities of power and converting it *efficiently* to a form useful for propulsion. For all of its disadvantages, chemical combustion solved the conversion problem very neatly.

Obviously, the subject of heat sources and the conversion of heat to electricity is a subject for a review in itself (138). However, due to the vital dependence of the space propulsion device upon its power source, the subject is included here to provide the interested reader with some suggestions on where to find more detailed treatments of certain aspects of the problem. It is assumed that for purposes of space propulsion electrical energy is required. Consequently, primary interest in energy conversion lies in the conversion of heat to electricity or in the generation of electricity directly.

Two sources of energy are considered: The sun and the nuclear fission reactor. As mentioned previously, the future prospects of fusion power are too uncertain to be discussed here. At normal incidence, solar radiation at Earth's orbit provides about 440 Btu/hr per ft², or 0.134 w per cm². This energy may be converted to electric energy directly by means of solar cells or by means of a conventional closed cycle converter. Nuclear energy may be converted to electricity by means of a closed cycle converter, or directly by means of thermoelectric converters.

Table 1 gives a comparison of the estimated specific weights of typical solar and nuclear systems.

Using the data from (138), it is apparent that for power requirements less than 10 kw the closed solar cycle offers the lowest specific weight, whereas for power levels above 10 kw, the nuclear reactor + turbo-alternator has the best performance. Solar cells become competitive only at relatively low power levels less than about 0.1 kw.

The data in Table 1 represent what can be done in the near future to provide power for electrical propulsion systems. Some improvement in specific weight may be obtained by using electrostatic generators instead of the usual electromagnetic devices (124), although 11-lb alternators producing 22 kw have recently been demonstrated (138). Other promising advances in direct conversion techniques are occurring in the field of thermionic vacuum diodes and thermionic gas-filled diodes (130, 132 to 136). Although it is too early to make any specific weight estimates on such devices, conversion efficiencies on the order of 25 to 30 per cent are expected in the near future. Current efficiencies are in the range of 10 to 15 per cent, and short circuit power densities of 30 w per cm² of emitter area have been reported. An intriguing possibility lies in the use of external load impedance matching by means of a transformer, where the alternating current is generated by a grid placed between the emitter and collector of a thermionic diode, and operated in a fashion similar to a vacuum tube. For the most recent advances in this important field, the reader is referred to (134).

Direct conversion of heat to electricity by means of magnetohydrodynamic apparatus has been suggested by Colgate and Aamodt (125) and Winterberg (137). Additional experimental research is needed to demonstrate feasibility.

Fox (112) has calculated that a propulsion system weight to exhaust power ratio of 22 lb/kw is adequate for a round trip to Mars with a 30 per cent payload. This figure appears to be in reach of our current technology.

Table 1 Comparison of typical solar and nuclear systems

System	Power level, kw	Specific weight, lb/kw	Reference
nuclear reactor (unshielded) + Rankine cycle	1	200	(138)
	10	25	
	100	4	
	1000	2	
nuclear reactor (min. equip. shield) + Rankine cycle	1	600	(99)
	10	70	
	100	10	
	1000	4	
nuclear reactor (shielded) + turbo-generator	20,000	6	(127)
nuclear reactor + turbo-alternator (unshielded)	1	500	(131)
	10	110	
closed solar cycle (requires large, low weight reflector)	1	60	(138)
	10	15	
	100	8	
	1000	10	
solar cells	1	250	(138)
	10	150	
	100	100	
solar cells (oriented; folding aluminum foil structure)	1	100	(131)
	10	100	

Conclusions

Space propulsion development is in a transition phase. An adequate number of preliminary design studies, mission analyses and trajectory computations have been accomplished to show, in general, the usefulness and applicability of the low thrust propulsion system to space missions.

In two areas, the nuclear rocket and the ion or colloid accelerator, research directed toward production of flight hardware is under way. A number of promising techniques have been demonstrated utilizing the principle of electromagnetic acceleration, and it is expected that further work on propulsion applications will produce high performance systems with considerably higher thrusts per unit system weight than can be achieved by the electrostatic accelerators. The problems arising from the necessity of working with high temperature plasmas will require considerable attention before adequate reliability and long operating lifetimes can be assured.

The possibilities for solar sailing are intriguing, but due to the difficulties of demonstrating feasibility, it is difficult to predict future developments. Similarly, the future application of fusion energy rests with the results of the current research on Project Sherwood, and any comment on applications at this time would seem premature.

Finally, the results of recent research on various methods of energy conversion are encouraging to the propulsion engineer, for his horizons widen as the power per unit weight of the energy conversion system increases.

References

Chemical Propulsion

1 Baldwin, L. V. and Blackshear, P. L., "Preliminary Survey of Propulsion Using Chemical Energy Stored in the Upper Atmosphere," NACA TN 4267, May 1958.

2 Bass, A. M. and Herzfeld, C. M., "Frozen Free Radicals," *Scientific American*, vol. 196, no. 5, March 1957, p. 91.

3 Charwat, A. F., "Photochemistry of the Upper Atmosphere as a Source of Propulsive Power," ARS JOURNAL, vol. 29, no. 2, Feb. 1959, pp. 108–114.

4 Demetriades, S. T. and Kretschmer, C. B., "The Use of Planetary Atmospheres for Propulsion," in "Advances in Astronautical Sciences," vol. 2, Plenum Press, Inc., New York, 1958.

5 Demetriades, S. T. and Farber, M., "Theoretical Study of Recombination Kinetics of Atomic Oxygen," ARS JOURNAL, vol. 29, no. 7, July 1959, pp. 528–530.

6 Golden, S., "Free-Radical Stabilization in Condensed Phases," *J. Chem. Phys.*, vol. 29, no. 1, July 1958, pp. 61–71.

7 Jackson, J. L. and Montroll, E. W., "Free Radical Statistics," *J. Chem. Phys.*, vol. 28, no. 6, June 1958, pp. 1101–1109.

8 Lee, Y. C. and Demetriades, S. T., "The Use of Free Radicals and Free Atoms for Purposes of Propulsion," paper 41C, presented at the SAE National Aeronautic Meeting, New York, April 8–11, 1958.

9 Palmer, H. B., "Burning Rate of an H-Atom Propellant," ARS JOURNAL, vol. 29, no. 5, May 1959, pp. 365–366.

10 Sutherland, G. S., "Solid and Liquid Rockets—A Comparison," paper 42A, presented at SAE National Aeronautic Meeting, New York, April 8–11, 1958.

11 Szego, G. C. and Mickle, E. A., "Free Radicals as High Energy Propellants," ARS preprint 525-57, presented at the ARS 12th Annual Meeting, New York, Dec. 2–6, 1957.

12 Nat. Bur. Standards, Administrative Bulletin 56-66, Oct. 29, 1956.

13 Nat. Bur. Standards, Free Radicals Research Newsletter, no. 11, Oct. 1, 1958.

14 Wort, D. J. H., "The Atomic Hydrogen Rocket," *J. Brit. Interplan. Soc.*, no. 4, July 1953, pp. 167–172.

Nuclear Propulsion

15 Aviation Week, "Kiwi-A Project Rover Reactor Fired in Test," June 29, 1959, p. 18.

16 Bagnall, L. M., "Some Data and Comments Concerning the Working Fluid Nuclear Rocket," ARS preprint 592-58, presented at the ASME-ARS Aviation Conference, Dallas, Texas, March 17–20, 1958.

17 Bonilla, C. F., "Nuclear Engineering," McGraw-Hill Book Co., Inc., New York, 1957.

18 Bussard, R. W. and DeLauer, R. D., "Nuclear Rocket Propulsion," McGraw-Hill Book Co., Inc., New York, 1958.

19 Cotter, T. P., "Potentialities and Problems of Nuclear Rocket Propulsion," *Aero/Space Engng.*, vol. 18, no. 2, Feb. 1959, pp. 50–53; *also* IAS Rep. no. 59-24.

20 Graves, G. A., "Radiation Problems in the Rover Program," ARS preprint 849–59, presented at ARS Semi-Annual Meeting, San Diego, Calif., June 8–13, 1959.

21 Green, L., Jr. and Carter, J. M., "Performance Calculations for Hybrid Nuclear-Chemical Rocket Propulsion Systems," ARS JOURNAL, vol. 29, no. 3, March 1959, pp. 180–186.

22 Grey, J., "A Gaseous-Core Nuclear Rocket Utilizing Hydrodynamic Containment of Fissionable Material," ARS preprint 848-59, presented at ARS Semi-Annual Meeting, San Diego, Calif., June 8–11, 1959.

23 Grey, J., "Nuclear Rockets—Basic Principles," *Nucleonics*, vol. 16, no. 7, July 1958, pp. 62–65.

24 Kaeppeler, H. J., "On the Problem of Cooling Nuclear Working Fluid Rockets Operating at Extreme Temperatures," *J. Brit. Interplan. Soc.*, vol. 14, no. 2, March-April 1955, pp. 89–97.

25 Levoy, M. M. and Newgard, J. J., "Rocket-Reactor Design," *Nucleonics*, vol. 16, no. 7, July 1958, pp. 66–68.

26 Logan, J. G. and Colichman, E. L., "Effect of Dissociation on the Performance of Working Fluids for Nuclear Propulsion," ARS JOURNAL, vol. 29, no. 6, June 1959, pp. 409–413.

27 Rosenblum, M. H., Rinehart, W. T. and Thompson, T. L., "Rocket Propulsion With Nuclear Energy," ARS preprint 559-57, presented at the ARS 12th Annual Meeting, New York, Dec. 2–6, 1957.

28 Safonov, G., "The Criticality and Some Potentialities of 'Cavity Reactors'," Rand Corp., Santa Monica, Calif., RM-1835, July 17, 1955; ASTIA Doc. no. AD112410.

29 Sams, E. W., "Performance of Nuclear Rocket for Large-Payload, Earth-Satellite Booster," IAS paper no. 59-94, presented at IAS National Summer Meeting, Los Angeles, Calif., June 16–19, 1959.

30 Sänger-Bredt, I., "Zur Thermodynamik der Arbeitsgase von Atomraketen," *Z. Naturforschung.*, vol. 8a, 1953, pp. 796–804.

31 Schreiber, R. E., "Nuclear Rocket Propulsion Program at Los Alamos," ARS preprint 689-58, presented at the ARS 13th Annual Meeting, New York, Nov. 17–21, 1958.

32 Shepherd, L. R. and Cleaver, A. V., "The Atomic Rocket, 1, 2, and 3," *J. Brit. Interplan. Soc.*, vol. 7, Sept. 1948, pp. 185–194; vol. 7, Nov. 1948, pp. 234–241; vol. 8, Jan. 1949, pp. 23–37.

33 Wang, C. J., Anthony, G. W. and Lawrence, H. R., "Thrust Optimization of a Nuclear Rocket of Variable Specific Impulse," ARS JOURNAL, vol. 29, no. 5, May 1959, pp. 341–344.

34 Went, J. J. and DeBruyn, H., "Fluidized and Liquid-Fuel Reactors with Uranium Oxides," *Nucleonics*, Sept. 1954.

35 Winterberg, F., "Besondere Brennstoffverteilungen und Kühlungsprobleme in Reaktoren von Kernraketen," *Astronautica Acta*, vol. IV, no. 2, 1958, pp. 138–165.

Thermonuclear Propulsion

36 Bishop, A. S., "Project Sherwood—The U.S. Program in Controlled Fusion," Addison-Wesley Publishing Co., Inc., Mass., 1958.

37 Clauser, M. U., "The Feasibility of Thermonuclear Propulsion," in "Conference on Extremely High Temperatures," John Wiley & Sons, Inc., New York, 1958, pp. 209–219.

38 Greenstein, J. L., "Comments on H. S. Tsien Paper," JET PROPULSION, vol. 26, no. 7, July 1956, p. 564.

39 Kaeppeler, H. J., "On Thermonuclear Power Plants," JET PROPULSION, vol. 27, no. 10, Oct. 1957, pp. 1098–1099.

40 Post, R. F., "Controlled Fusion Research: An Application of the Physics of High Temperature Plasmas," *Rev. Mod. Phys.*, vol. 28, no. 3, July 1956, pp. 338–362.

41 Sänger, E., "Stationäre Kernverbrennung in Raketen," *Astronautica Acta*, vol. I, no. 2, 1955, pp. 61–88; *also* NACA TM 1405, April 1957.

42 Tsien, H. S., "Thermonuclear Power Plants," JET PROPULSION, vol. 26, no. 7, July 1956, pp. 559–564.

Arc Heating Propulsion

43 Adams, M. C. and Camac, M., "The Arc Heated Plasma Thrust Chamber," ARS preprint 791-59, presented at the ARS Controllable Satellites Conference, MIT, April 30–May 1, 1959.

44 Brogan, T. R., "Electric Arc Gas Heaters for Re-Entry Simulation and Space Propulsion," ARS preprint no. 724-58, presented at ARS 13th Annual Meeting, New York, Nov. 17–21, 1958.

45 Ghai, M. L., "Plasma Generation Facility and Some Research Results," in "Conference on Extremely High Temperatures," John Wiley and Sons, Inc., New York, 1958, pp. 221–236.

46 Giannini, G. M., "The Plasma Jet and Its Application," in "Vistas in Astronautics," vol. I, Pergamon Press, Inc., New York, 1958, pp. 176–188.

47 Hogness, T. R., "Arc-Heated Plasma for Laboratory Hypersonics," ASTRONAUTICS, vol. 4, no. 3, March 1959, p. 40.

48 John, R. R. and Bade, W. L., "Stagnation Point Heat Transfer in a Subsonic Jet of Arc-Heated Air," ARS JOURNAL, vol. 29, no. 7, July 1959, pp. 523–525.

Electromagnetic Propulsion

49 Artsimovich, L. A. et al., "Electrodynamic Acceleration of Plasma Bunches," *Soviet Physics (JETP)*, vol. 6, no. 1, 1958.

50 Blackman, V. H. and Niblett, B., "Experiments Using a Hydromagnetic Shock Tube," in "The Plasma in a Magnetic Field," R. K. M. Landshaff, ed., Stanford University Press, Calif., 1958, pp. 87–98.

51 Bostick, W. H., "Plasma Motors," in "Conference on Extremely High Temperatures," John Wiley & Sons, Inc., New York, 1958, pp. 169–178; *also* "Advances in Astronautical Sciences," vol. 2, Plenum Press, Inc., New York, 1958.

52 Bostick, W. H., "Experimental Study of Ionized Matter Projected Across a Magnetic Field," *Phys. Rev.*, vol. 104, no. 2, Oct. 15, 1956, pp. 292–299.

53 Bostick, W. H., "Experimental Study of Plasmoids," *Phys. Rev.*, vol. 106, no. 3, May 1, 1957, pp. 404–412.

54 Finkelstein, D., Sawyer, G. A. and Stratton, T. F., "Supersonic Motion of Vacuum Spark Plasmas Along Magnetic Fields," *Phys. Fluids*, vol. 1, no. 3, May-June 1958, pp. 188–192.

55 Gauger, J., Vali, V. and Turner, T. E., "Laboratory Experiments in Hydromagnetic Propulsion," paper presented at the American Astronautical Society, Western Regional Meeting, Palo Alto, Calif., Aug. 18–19, 1958; *also* "Advances in Astronautical Sciences," vol. 2, Plenum Press, Inc., New York, 1958.

56 Jones, G. S. and Patrick, R. M., "The Production of High Temperature Gas by Magnetic Acceleration," in "Conference on Extremely High Temperatures," John Wiley & Sons, Inc., New York, 1958, pp. 3–10.

57 Kolb, A. C., "Production of High-Energy Plasmas by Magnetically Driven Shock Waves," *Phys. Rev.*, vol. 107, no. 2, July 15, 1957, pp. 345–350.

58 Korneff, T., Nodig, F. H. and Bohn, J. L., "Plasma Acceleration Experiments," in "Conference on Extremely High Temperatures," John Wiley & Sons, Inc., New York, 1958, pp. 197–207.

59 Kunen, A. E., "Electromagnetic Pinch Effect as a Space Propulsion System," in "Advances in Astronautical Sciences," vol. 2, Plenum Press, Inc., New York, 1958.

60 Kunen, A. E. and McIlroy, W., "The Magnetic Pinch Engine for Space Flight," American Astronautical Society preprint 59-13, presented at Western National Meeting, Los Angeles, Calif., Aug. 4–5, 1959.

61 Landshoff, R. K. M., "Magnetohydrodynamics," Stanford University Press, Stanford, Calif., 1957.

62 Landshoff, R. K. M., "The Plasma in a Magnetic Field," Stanford University Press, Stanford, Calif., 1958.

63 Patrick, R. M., Sr., "A Description of a Propulsive Device which Employs a Magnetic Field as the Driving Force," in "Vistas in Astronautics," vol. II, Pergamon Press, Inc., New York, 1959; *also* Avco Research Laboratory, Research Rep. no. 28, May 1958.

64 *Space/Aeronautics*, "Pulsed Plasma Accelerator Forecasts Spacecraft Control," March 1959, pp. 57–59.

65 Spitzer, L., Jr., "Physics of Fully Ionized Gases," Interscience Publishers, Inc., New York, 1956.

66 Starr, W. L., "Impulse from an Exploding Wire Plasma Accelerator," *J. Appl. Phys.*, vol. 30, no. 4, April 1959, pp. 594–595.

67 Yoler, Y. A., "On Plasma Propulsion," in "Advances in Astronautical Sciences," vol. 2, Plenum Press, Inc., New York, 1958.

Electrostatic Propulsion

68 Anderson, C. F. and Ehlers, K. W., "Ion Source for the Production of Multiply-Charged Heavy Ions," *Rev. Sci. Instr.*, vol. 27, no. 10, Oct. 1956, pp. 809–817.

69 Barnes, A. H., MacNeille, S. M., Starr, C. and Savage, H. W., "Problems of Physics in the Ion Source," Clinton Engineer Works–Tennessee Eastman Corp., Oak Ridge, Tenn., 1951.

70 Boden, R. H., "The Ion Rocket Engine," SAE preprint 41D, presented at the SAE National Aeronautic Meeting, New York, April 8–11, 1958.

71 Boden, R. H. "Ion Rocket Engines—A Summary," *Aero/Space Engng.*, vol. 18, no. 4, April 1959, pp. 67–71.

72 Brewer, G. R., "Formation of High-Density Electron Beams," *J. Appl. Phys.*, vol. 28, no. 1, Jan. 1957, pp. 7–15.

73 Bussard, R. W., "A Nuclear-Electric Propulsion System" *J. Brit. Interplan. Soc.*, vol. 15, no. 6, Nov.-Dec. 1956, pp. 297–304

74 Bussard, R. W. and DeLauer, R. D., "Nuclear Rocket Propulsion,' McGraw-Hill Book Co., Inc., New York, 1958, pp. 330–339.

75 *Chemical and Engineering News*, June 1, 1959, p. 50.

76 Childs, J. H., "Design of Ion Rockets and Test Facilities," IAS paper no. 59-103, presented at the IAS National Summer Meeting, Los Angeles, Calif., June 16–19, 1959.

77 Datz, S. and Taylor, E. H., "Ionization on Platinum and Tungsten Surfaces. I. The Alkali Metals," *J. Chem. Phys.*, vol. 25, no. 3, Sept. 1956, pp. 389–394.

78 Dietz, L. A., "Ion Optics for the V-Type Surface Ionization Filament Used in Mass Spectrometry," *Rev. Sci. Instr.*, vol. 30, no. 4, April 1959, pp. 235–241.

79 Eilenberg, S. L. and Huebner, A. L. C., "Engineering and Scientific Problems of Ion Propulsion," ARS preprint 880-59, presented at ARS Semi-Annual Meeting, San Diego, Calif., June 8–11, 1959.

80 Huebner, A. L. and Boden, R. H., "Critical Power Supply Problems

in Ion Propulsion," presented at IAS-ARS Space Exploration Meeting, San Diego, Calif., Aug. 1958.

81 Lamb, W. A. S. and Lofgren, E. J., "High Current Ion Injector," *Rev. Sci. Instr.*, vol. 27, no. 11, Nov. 1956, pp. 907–909.

82 Langmuir, D. B., "Problems of Thrust Production by Electrostatic Fields," in "Vistas in Astronautics," vol. II, Pergamon Press, Inc., New York, 1959.

83 Massey, H. S. W. and Burhop, E. H. S., "Electronic and Ionic Impact Phenonons," Oxford University Press, New York, 1952.

84 Meyerand, R. G., Jr. and Brown, S. C., "High-Current Ion Source," *Rev. Sci. Instr.*, vol. 30, no. 2, Feb. 1959, pp. 110–111.

85 Naiditch, S., "Experimental Ion Sources for Propulsion," ARS preprint 883-59, presented at ARS Semi-Annual Meeting, San Diego, Calif., June 8–11, 1959.

86 Pierce, E. T., "Effects of High Electric Fields on Dielectric Liquids. *J. Appl. Phys.*, vol. 30, no. 3, March 1959, pp. 445–446.

87 Pierce, J. R., "Theory and Design of Electron Beams," D. Van Nostrand Co., Inc., New York, 1954.

88 Pohl, H. A., "Some Effects of Nonuniform Fields on Dielectrics," *J. Appl. Phys.*, vol. 29, no. 8, Aug. 1958, pp. 1182–1188.

89 Seitz, R. N. and Raether, M. J., "A Pierce Gun Design for an Accelerate-Decelerate Ion Thrust Device," ARS preprint 884-59, presented at the ARS Semi-Annual Meeting, San Diego, Calif., June 8–11, 1959.

90 Shelton, H., Wuerker, R. F. and Sellen, J. M., "Generation and Neutralization of Ions for Electrostatic Propulsion," ARS preprint 882-59, presented at ARS Semi-Annual Meeting, San Diego, Calif., June 8–11, 1959.

91 Shepherd, L. R. and Cleaver, A. V., "The Atomic Rocket-4," *J. Brit. Interplan. Soc.*, Feb. 1949, pp. 59–70.

92 Spitzer, L., Jr., "Interplanetary Travel Between Satellite Orbits," *J. Brit. Interplan. Soc.*, vol. 10, no. 6, Nov. 1951, pp. 249–257.

93 Taylor, J. B. and Langmuir, I., "Evaporation of Atoms, Ions, and Electrons from Cesium Films on Tungsten," *Phys. Rev.*, no. 44, 1933, p. 423.

94 Van Duzer, T. and Brewer, G. R., "Space-Charge Simulation in an Electrolytic Tank," *J. Appl. Phys.*, vol. 30, no. 3, March 1959, pp. 291–301.

Solar Propulsion

95 Ehricke, K. A., "The Solar-Powered Space Ship," ARS preprint 310-56, presented at ARS Semi-Annual Meeting, June 18–20, 1956.

96 Garwin, R. L., "Solar Sailing—A Practical Method of Propulsion Within the Solar System," JET PROPULSION, vol. 28, no. 3, March 1958, pp. 188–190.

97 Tsu, T. C., "Interplanetary Travel by Solar Sail," ARS JOURNAL, vol. 29, no. 6, June 1959, pp. 422–427.

System Analyses

98 Fox, R., "Preliminary Studies on Electrical Propulsion Systems for Space Travel," ARS preprint 708-58, presented at the ARS 13th Annual Meeting, New York, Nov. 17–21, 1958.

99 Kovacik, V. P. and Ross, D. P., "Performance of Nuclear Electrical Propulsion Systems," IAS Rep. no. 59-25, presented at the IAS 27th Annual Meeting, New York, Jan. 20–29, 1959.

100 Preston-Thomas, H., "Interorbital Transport Techniques," *J. Brit. Interplan. Soc.*, vol. 11, no. 4, July 1952, pp. 173–193.

101 Shepherd, L. R., "Electrical Propulsion Systems in Space Flight," *Astronautica Acta*, vol. V, no. 2, 1959, pp. 144–157.

102 Stuhlinger, E., "Propulsion Systems for Space Ships," in "Vistas in Astronautics," vol. I, Pergamon Press, Inc., New York, 1958, pp. 191–196.

103 Stuhlinger, E., "Possibilities of Electrical Spaceship Propulsion," Bericht über den V. Internationalen Astronautischen Kongress (Fifth Int. Astro. Congress), Aug. 1954.

104 Stuhlinger, E., "Electrical Propulsion System for Space Ships with Nuclear Power Source," *J. Astronautics*, Part I, Winter 1955; Part II, Spring 1956; Part III, Summer 1956.

105 Willinski, M. I. and Orr, E. C., "Project Snooper, A Program for Unmanned Interplanetary Reconnaissance," JET PROPULSION, vol. 28, no. 11, Nov. 1958, pp. 723–729.

Space Mechanics

106 Bacon, R. H., "Logarithmic Spiral: An Ideal Trajectory for the Interplanetary Vehicle with Engines of Low Sustained Thrust," *Amer. J. Phys.*, vol. 27, no. 3, March 1959, pp. 164–165.

107 Baker, R. M. L., Jr. et al., "Efficient Precision Orbit Computation Techniques," ARS preprint 869-59, presented at ARS Semi-Annual Meeting, San Diego, Calif., June 8–13, 1959.

108 Benney, D. J., "Escape From Circular Orbit Using Tangential Thrust," JET PROPULSION, vol. 28, no. 3, March 1958, pp. 167–169.

109 Copeland, J., "Interplanetary Trajectories Under Low Thrust Radial Acceleration," ARS JOURNAL, vol. 29, no. 4, April 1959, pp. 267–271.

110 Faulders, C. R., "Low-Thrust Rocket Steering Program for Minimum Time Transfer Between Planetary Orbits," presented at SAE National Aeronautic Meeting, Los Angeles, Calif., Sept. 29–Oct. 4, 1958.

111 Forbes, G. F., "The Trajectory of a Powered Rocket in Space," *J. Brit. Interplan. Soc.*, vol. 9, no. 2, March 1950, pp. 75–79.

112 Fox, R. H., "Powered Trajectory Studies for Low Thrust Space Vehicles," ARS preprint 879-59, presented at the ARS Semi-Annual Meeting, San Diego, Calif., June 8–11, 1959.

113 Herrick, S. and Baker, R. M. L., Jr., "Recent Advances in Astrodynamics," JET PROPULSION, vol. 28, no. 10, Oct. 1958, pp. 649–654.

114 Irving, J. H. and Blum, E. K., "Comparative Performance of Ballistic and Low-Thrust Vehicles for Flight Missile Trajectories," in "Vistas in Astronautics," vol. II, Pergamon Press, Inc., New York, 1959.

115 Lawden, D. F., "Optimal Programming of Thrust Direction," *Astronautica Acta*, vol. I, no. 1, 1955, pp. 41–56.

116 Levin, E., "Low-Thrust Transfer Between Circular Orbits," Rand Corp. Rep. P-1536, Oct. 31, 1958.

117 Lorell, J. and Lass, H., "Low Thrust Takeoff from a Satellite Orbit," ARS preprint 872-59, presented at ARS Semi-Annual Meeting, San Diego, Calif., June 8–13, 1959.

118 Michielsen, H. F., "The Case for the Low Acceleration Spaceship," *Astronautica Acta*, vol. III, no. 2, 1957, pp. 130–152.

119 Michielsen, H. F., "Minimum Weight and Optimum Flight Path of Low-Acceleration Space Vehicles," in "Advances in Astronautical Sciences," vol. 3, Plenum Press, Inc., New York, 1958.

120 Perkins, F. M., "Flight Mechanics of Low-Thrust Spacecraft," *J. Aero/Space Sci.*, May 1959, pp. 291–297.

121 Rodriguez, E., "A Method of Determining Steering Programs for Low-Thrust Interplanetary Vehicles," ARS preprint 645-58, presented at the ARS Semi-Annual Meeting, Los Angeles, Calif., June 9–12, 1958.

122 Stuhlinger, E., "The Flight Path of an Electrically Propelled Space Ship," JET PROPULSION, vol. 27, no. 4, April 1957, pp. 410–414.

123 Tsien, H. S., "Take-off from Satellite Orbit," JOURNAL OF THE AMERICAN ROCKET SOCIETY, vol. 23, no. 4, July-Aug. 1953, pp. 233–236.

Propulsion Power Sources

124 Brosan, G. S., "An Electrical Machine for Use in Extra-Terrestrial Environment," *J. Brit. Interplan. Soc.*, vol. 14, no. 5, Sept. 1955, pp. 270–274.

125 Colgate, S. A. and Aamodt, R. F., "Plasma Reactor Promises Direct Electric Power," *Nucleonics*, vol. 15, no. 8, Aug. 1957, pp. 50–55.

126 Eisenberg, M., "Electrochemical Energy Sources for Space Flight Applications," ARS preprint 866-59, presented at the ARS Semi-Annual Meeting, San Diego, Calif., June 8–11, 1959.

127 English, R. E. et al., "A 20,000-Kilowatt Nuclear Turboelectric Power Supply for Manned Space Vehicles," NASA Memo 2-20-59E, March 1959.

128 Erlandson, P. M., "Direct Conversion of Solar Energy," Proc. World Symposium on Applied Solar Energy, Phoenix, Ariz., Nov. 1–5, 1955, p. 261.

129 Greer, W., "Solar Power Converter for Space Application," ARS preprint 865-59, presented at the ARS Semi-Annual Meeting, San Diego, Calif., June 8–11, 1959.

130 Grover, G. M., Roehling, D. J., Salmi, E. W. and Pidd, R. W., "Properties of a Thermoelectric Cell," *J. Appl. Phys.*, vol. 29, no. 11, Nov. 1958, pp. 1611–1612.

131 Hamilton, R. C., "Interplanetary Space Probe Auxiliary Power Systems," ARS preprint 864-59, presented at the ARS Semi-Annual Meeting, San Diego, Calif., June 8–11, 1959.

132 Hatsopoulos, G. N. and Kaye, J., "Analysis and Experimental Results of a Diode Configuration of a Novel Thermoelectron Engine," Proc. IRE, vol. 46, no. 9, Sept. 1958, p. 1574.

133 Houston, J. M., "Theoretical Efficiency of the Thermionic Energy Converter," *J. Appl. Phys.*, vol. 30, no. 4, April 1959, pp. 481–487.

134 Kaye, J. and Welsh, J. A., ed., "Direct Conversion of Heat to Electricity," a compilation of papers for the MIT Special Summer Program, July 6–17, 1959.

135 Webster, H. F., "Calculation of the Performance of a High-Vacuum Thermionic Energy Converter," *J. Appl. Phys.*, vol. 30, no. 4, April 1959, pp. 488–492.

136 Wilson, V. C., "Conversion of Heat to Electricity by Thermionic Emission," *J. Appl. Phys.*, vol. 30, no. 4, April 1959, pp. 475–481.

137 Winterberg, F., "Kernverbrennungsplasmen und magnetische Kernbrennkammern," *Astronautica Acta*, vol. IV, no. 4, 1958, pp. 235–263.

138 Zwick, E. B. and Zimmerman, R. L., "Space Vehicle Power Systems," ARS JOURNAL, vol. 29, no. 8, Aug. 1959, pp. 553–564.

General

139 Bussard, R. W., "Concepts for Future Nuclear Rocket Propulsion," JET PROPULSION, vol. 28, no. 4, April 1958, pp. 223–227.

140 Clarke, A. C., "Space Travel in Fact and Fiction," *J. Brit. Interplan. Soc.*, vol. 9, no. 5, Sept. 1950, pp. 213–230.

141 Cornog, R., "The Optimum Velocity of Propellant Ejection," in "Vistas in Astronautics," vol. I, Pergamon Press, Inc., New York, 1958, pp. 172–175.

142 Fisher, E., "Advanced Propulsion Concepts," ARS Preprint 847-59, presented at ARS Semi-Annual Meeting, San Diego, Calif., June 8–13, 1959.

143 Goddard, R. H., "Robert H. Goddard, An Autobiography," ASTRONAUTICS, vol. 4, no. 4, April 1959, p. 106.

144 Huth, J. H., Augenstein, B. W. and Holbrook, R. D., "Some Fundamental Considerations Relating to Advanced Rocket Propulsion Systems," Rand Corp., Santa Monica, Calif., RM-2194, March 11, 1958; ASTIA Doc. no. AD 133047.

145 Kaeppeler, H. J., "Aspects of Nuclear Power Application for Jet Propulsion," *J. Amer. Astro. Soc.*, vol. 2, nos. 2 and 3, Summer and Fall 1955.

146 Oberth, H., "Wege zur Raumschiffahrt," R. Oldenbourg, Munich, 1929.

147 Sänger-Bredt, I., "Die Eigenschaften von Wasserstoff und Wasser als Arbeitsgase für kernenergetisch beheizte Raketentriebwerke," *Astronautica Acta*, vol. III, no. 4, 1957, pp. 241–279.

148 Sänger-Bredt, I., "Über Arbeitsgase für nicht-konventionell beheizte Raketen," *Astronautica Acta*, vol. V, no. 2, 1959, pp. 97–115.

149 Seifert, H. S., "The Performance of a Rocket with Tapered Exhaust Velocity," JET PROPULSION, vol. 27, no. 12, Dec. 1957, pp. 1264–1266.

150 Tyler, V. M., Jackson, E. C. and Pierce, R. M., "Gun Barrel Launching," *Space/Aeron.*, Feb. 1959, pp. 52–54.

Some Economic Aspects of Hypersonic Flight

ROBERT CORNOG[1]

Thompson Ramo Wooldridge, Inc.
Los Angeles, Calif.

An examination is made of the influence of various flight performance characteristics on the direct flying costs of commercial aircraft whose average cruising speed is more than 1 mile per sec. Two types of aircraft are considered: Boost-glide vehicles and vehicles which cruise at constant speed. It is found that at hypersonic speeds, new features of flight operation become important. For example, for both types of vehicles, an important technical problem and economic factor is the initial acceleration to flying speed, which immediately follows takeoff. It is estimated that, granted reasonable extrapolations of contemporary technology, both types of vehicles may be expected to have total direct flying costs of less than 10 cents per ton-mile.

IMPORTANT military applications have been suggested for aircraft which fly through the atmosphere at hypersonic speeds (1).[2] However, the feasibility of commercial applications of hypersonic aircraft obviously depends on economic considerations. The object of this paper is to study the influence of various design parameters on the flight economics of hypersonic aircraft.

Hypersonic flight may be defined as flight at a speed which is large compared with the speed of sound in the flight medium. The hypersonic vehicles analyzed in this study are designed to fly in the atmosphere of the Earth at speeds ranging from 6 to 20 times the speed of sound.

Commercial hypersonic flight is of great interest for at least two reasons:

1 Hypersonic flight may be economical. With fixed payload, the faster a vehicle flies, the greater its gross revenue.[3] In the case of hypersonic vehicles this particular economic factor must, however, be weighed against the enormous and costly technical problems involved in the initial development of vehicles having adequate reliability and low direct flying costs.

2 The techniques used to bring manned commercial hypersonic vehicles up to flying speed can also be used to launch Earth satellites or vehicles intended for longer flights in space. Moreover, many of the techniques evolved for reducing the operating costs of commercial hypersonic flight will also be effective in reducing costs of all future space flights. Special interest, therefore, is attached to methods of reducing the cost of transportation at hypersonic speed.

Two features of hypersonic flight merit special discussion. First, unless special provisions are provided to maintain flight at subsonic speeds, a hypersonic vehicle cannot hover or cruise around the terminal airport before landing. "Stacking" is not feasible. Flight scheduling must be restricted so that every hypersonic vehicle can land immediately on arrival at destination. The feasibility of such scheduling has been assumed.

A second factor which must be considered is the possible adverse physiological effect which may be experienced by the passengers during flight. At takeoff, a prolonged period of acceleration is required to bring a hypersonic vehicle up to flight speed. The most cursory analysis will reveal that, at least for rocket boosted boost-glide vehicles, some sort of compromise must be made between the propulsion engineer who, in the interest of saving propellant, would like to use multi-g accelerations, and the aeromedical people, who, in the interests of passenger comfort and safety, would like to limit accelerations to a much lower value. The writer suggests that these two conflicting requirements can in large part be resolved by using variable thrust engines during boost.

The properties of two distinct types of hypersonic vehicles have been evaulated in this study, i.e., boost-glide vehicles and hypersonic airplanes.

Boost-Glide Vehicles

A boost-glide vehicle is one initially accelerated to maximum speed, and, at the end of that boost phase, the payload stage coasts as an unpowered glider to its destination. Landing of the payload stage is made at the same low subsonic speeds used by contemporary airplanes. A typical trajectory of a boost-glide vehicle is shown in Fig. 1.

The flight characteristics of boost-glide vehicles have been considered by previous workers in the field (5,6,7). The glide range of a momentum glider, such as would be used as the payload stage of a boost-glide vehicle, is shown in Fig. 2. If it is assumed that the lift to drag ratio is constant throughout the flight and that changes in the gravitational potential are ignored,[4] the range S in feet can be shown (8) to be

$$S = \frac{R}{2\epsilon} \log_e \left[\left(1 - \frac{v^2}{Rg}\right) \Big/ \left(1 - \frac{v_0^2}{Rg}\right) \right]$$

where

R = distance from flightpath to center of planet, ft
ϵ = drag to lift ratio
v_0 = initial speed, fps
v = final speed, fps
g = gravitational acceleration at flight altitude, fps²

Presented at the ARS 13th Annual Meeting, New York, N. Y., Nov. 17–21, 1958.

[1] Member of the Senior Staff, Ramo-Wooldridge Division. Member ARS.

[2] Numbers in parentheses indicate References at end of paper.

[3] Even if the ton-mile costs are greater than at lower flight speed, flight at hypersonic speed may be profitable and economically sound because significant increases in the speed of transportation and distribution of commodities have usually resulted in great increases in the variety of commodities being transported—in short, new markets are generated.

[4] Because a vehicle at hypersonic speeds has enormous kinetic energy, only a small error is introduced if, in computing the range of a momentum glider, changes in flight altitude are neglected. For example, neglecting resistance of the air and the Earth's rotational speed, a vehicle moving in free flight with an initial speed of 2 miles per sec at sea level will be still moving at 1.94 miles per sec when it has coasted up to an altitude of 100,000 ft, where it is above more than 98 per cent of the atmosphere.

Hypersonic Airplanes

A hypersonic airplane, like contemporary airplanes, cruises at constant speed. The propulsive power during cruise may be supplied by a rocket engine or by a ramjet engine. Since the hypersonic airplane must slow down to land, a deceleration period of flight, usually a momentum glide, must follow the cruise portion. The length of flightpath required for momentum gliding may be several hundred miles long; an appropriate allowance for this factor was made in all computations.

It has been assumed that the distances traveled in boosting a hypersonic airplane up to the cruise flying speed (usually less than 100 miles) are small compared to the total flight length. Accordingly, no allowance was made for this travel distance in computing the range of a hypersonic airplane. A typical trajectory of a hypersonic airplane is shown in Fig. 1.

The problems of aerodynamic heating may be less severe in a hypersonic airplane than in a boost-glide vehicle. For example, as shown in Fig. 2, a boost-glide vehicle having a lift to drag ratio of 5 must have an initial flight speed of more than 16,000 fps if a range of 3500 nautical miles is to be obtained. Despite the excellent work of Newtweiler(9), it is possible that both the structural weight and the aerodynamic performance of long-range boost-glide vehicles may be seriously compromised by the concessions in design made in order to cope with aerodynamic heating at speeds of 16,000 fps. Kooy and Uytenbogaart(10) have proposed rocket propelled airplanes, which, in order to avoid or reduce these problems of aerodynamic heating, cruise at a constant and lower speed. For example, at a flight speed of 8000 fps, the stagnation temperature in air is less than one third of its value at 16,000 fps, and, hence, many strong, lightweight, refractory metals can be used for constructing the skin of the vehicle, metals which would soften or melt at the higher speed and temperature. There are then valid technical reasons for considering the performance characteristics of hypersonic airplanes.

The range S in feet of a rocket powered hypersonic airplane cruising at constant speed v fps is

$$S = \frac{I_{sp} g_0 v}{\epsilon g[1 - (v^2/Rg)]} \log\left(\frac{M_0}{M}\right)$$

where

I_{sp} = specific impulse of engine, lb-sec/lb
g_0 = ratio of weight to mass, 32.2 lb/slug
M_0 = initial mass of airplane
M = final mass of airplane

Throughout this report, this formula has been used in computing the relevant properties of hypersonic airplanes (8).

Boosters

At takeoff, both boost-glide vehicles and hypersonic airplanes must be accelerated, or boosted, from rest to hypersonic speeds. In both cases, a jettisonable rocket is often specified as the booster. However, the use of various air-breathing engines has also been considered (2,3). In this study, the range of booster design parameters considered was deliberately made broad, so that several different types of single-stage boosters could be included and compared. Thus nuclear rockets and airbreathing, chemically-fueled turbojet or ramjet lifting engines are all considered as possible boosters.

The direct costs of launching a space vehicle can usually be reduced if the structural elements of the booster are recoverable and can be reloaded and used again and again (4). Accordingly, in the present study, it has been assumed that a recoverable (and reusable) booster is used. The details of the recover mechanism are not considered.

It should be noted that it is not always necessary or desirable to jettison the booster. It is often quite practical to incorporate all or part of booster machinery permanently into the payload stage. Such single-stage designs are usually most attractive for short-range flights—say less than 2000 to 3000 miles in length.

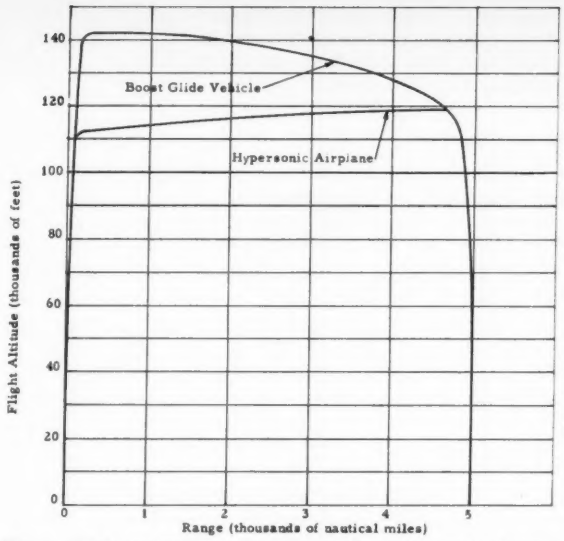

Fig. 1 Flight trajectories of a boost-glide vehicle and a hypersonic airplane

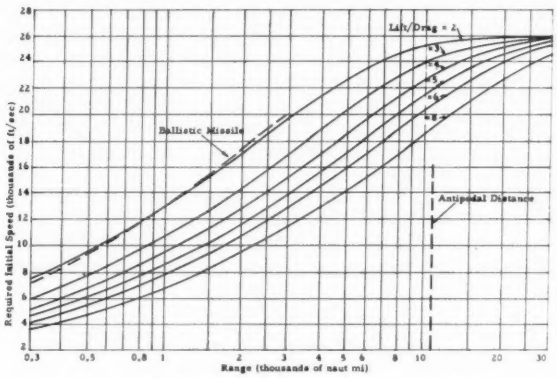

Fig. 2 Speed requirements of momentum glider

Economic Considerations

In order to aid in the discussion of transportation economics, certain conventions have been adopted in tabulating the operating costs of transportation enterprises. For example, the costs of operating a commercial airline are usually divided into two broad categories: Direct flying costs, and overhead or burden. Profit, sometimes lumped with direct flying costs, is here considered a separate category.

Direct flying costs average about 55 per cent of the total operating costs of most contemporary airlines, while overhead or burden makes up roughly 45 per cent of the total operating costs(10a). Profit is usually less than 5 per cent of total operating costs.

Direct Flying Costs

The following items are usually lumped together as direct flying costs:

The fuel and oil consumed during flight.

Interest on capital invested in flight equipment.

Depreciation allowance on the airplane.
Cost of overhaul, repairs and maintenance of the airplane.
Insurance and taxes on flight equipment.
Salaries of flying personnel.

Overhead Costs

The following expenses are included as "General Service and Administration" costs or "overhead":
Rents and other costs of maintaining airport facilities.
Salaries of ticket agents and other sales personnel.
Advertising costs.
Administrative and legal expenses.

Direct flying costs are of special interest not only to the operator of commercial aircraft, but also to the designer and to the manufacturer, since it is primarily the direct flying costs that are affected by operational characteristics of the airplane. Thus, a new type of airplane, having reduced direct flying costs, is attractive, first to the airline operator because of its potential for greater profit and, as a direct consequence, to the manufacturer because of its greater sales potential. In other words, direct flying costs are an essential element in the design of any new aircraft because they define its revenue and profit producing potential.

Overhead costs, on the other hand, are comparatively insensitive to the operational characteristics of the flight equipment; in other words, it is difficult to reduce the overhead costs of an airline by changes in airplane design. Consequently, only direct flying costs are analyzed in this study.

Cost Assignment

In this study, all of the component costs which are normally included under direct flying costs have been reassigned into one of two categories:

Fuel Costs. The costs of the propellants and fuels used to power the vehicles have been called fuel costs.

Structural Costs. All of the costs associated with procuring and maintaining the empty vehicle have been called "structural costs." They include:
Interest on the capital invested in the vehicle.
Depreciation and obsolescence of flight equipment.
Overhaul, repairs and maintenance.
Insurance and taxes on the flight equipment.

If other factors are unchanged, the labor costs of the flight crew, measured in cents per ton-mile, may be expected to decrease as flight speed is increased. This conclusion follows from the fact that an hour of effort on the part of the flight crew results in an amount of ton-miles of revenue output which is directly proportional to the flying speed. However, since, for vehicles designed for flight at hypersonic speeds, the salaries of the flying personnel are small compared with fuel costs and structural costs, and since salaries are relatively insensitive to the changes in design parameters considered in this study, a constant allowance of 0.5¢ per ton-mile was made for salaries of flying personnel.

Method of Computing Direct Flying Costs

Direct flying costs were computed for various types of hypersonic vehicles flying nonstop between cities separated by various distances. In every case, the fuel costs and the structural costs were computed for both booster stage and the payload stage. Direct flying costs would then be the sum of fuel and structural costs for booster stage and for payload stage, plus the labor costs of 0.5¢/ton-mile for the flight crew.

The parameters of a vehicle system which determine the fuel costs and the structural costs may be separated as follows:

1 The unit cost of the propellants and fuel consumed.

2 The specific impulse or specific fuel consumption obtained when the propellants and fuel are used.

3 The aerodynamic properties, especially lift to drag ratio, of the vehicle.

4 The total cost (including repairs and maintenance) of the dead weight structural elements which comprise the vehicle, and the number of hours which the vehicle can fly before it is worn out or obsolete. In other words, a depreciation factor. These two factors can be lumped together with no loss of generality. The resulting parameter measures the cost rate of owning and operating the vehicle structure. The cost units are cents per hour of flight per pound of structure.

5 The structural factors of the vehicle system. How much payload can be delivered per unit mass of vehicle structure?

The last two parameters, 4 and 5, affect only the structure costs, whereas only fuel cost is affected by the first parameter. Both fuel costs and structure costs are affected by parameters 2 and 3.

Representative numerical values were assigned to all five cost determining parameters, and direct flying costs were computed for various representative hypersonic vehicle configurations. Methods of reducing the direct flying costs were then investigated.

Discussion of Cost Determining Parameters

By choosing reference values for all but one of the five independent parameters listed above, the influence of the single remaining parameter on direct flying costs can be determined and plotted graphically. In many cases the conclusions thus obtained are rather insensitive functions of the numerical values chosen for the fixed parameters. Put more strongly, many valid design objectives for reducing direct flying costs of the aircraft can often be obtained from a cost analysis based on an inaccurate set of parametric assumptions. Nevertheless, good inputs improve the probability of good outputs; a discussion of each cost determining input parameter is therefore appropriate.

Unit Cost of Propellants and Fuel

Rocket Propellants. A combination consisting of petroleum oil and liquid oxygen was chosen as a reference rocket propellant because as shown in a previous study(7), in large-scale use, the cost of this propellant mixture may be less than 1 ¢/lb, and, in any event, much cheaper than any other chemical propellant combination having comparable specific impulse.

Liquid hydrogen, which might be used with a nuclear reactor, will probably cost at least 10 ¢/lb (7).

Turbojet and Ramjet Fuels. A gasoline- or kerosene-type petroleum fuel costing 2 ¢/lb (about 13 ¢/gal) is used as the reference standard for airbreathing powerplants.

Specific Impulse and Specific Fuel Consumption

Chemical Rockets. A value of 310 lb-sec/lb was chosen as the specific impulse of the reference low-cost rocket propellant combination consisting of petroleum oil and liquid oxygen. The methods used in selecting this value have been described elsewhere(11,12).

Turbojet or Ramjet Powerplants. Airbreathing engines, such as turbojets and ramjets may be used both as boosters used to accelerate vehicles up to flying speed and as cruise engines used to maintain flight speed in hypersonic aircraft. In both applications, an important property of such engines is their specific fuel consumption.

Ramjet engines may be computed to have the properties shown in Figs. 3 and 4 (8). The thermal efficiency of a ramjet is defined as the rate of thrust work output divided by the rate at which the chemical energy contained in the fuel is fed into the engine. The thrust coefficient is based on the cross sectional area of the undisturbed airstream entering the engine.

The compression efficiency of the diffuser is defined as the ratio of the work input required by a reversible adiabatic compressor producing the pressure ratio observed across the diffuser, to the loss in kinetic energy of the entering air while passing through the diffuser.

Combustion efficiency is defined in the normal manner. Nozzle efficiency is defined as the ratio of the observed increase in kinetic energy of the hot combustion products in passing through the nozzle, to the change in kinetic energy which would have been produced in the same gases flowing through the same pressure ratio in an ideal, reversible, adiabatic nozzle.

The ambient temperature of the air is assumed to be 220 K, corresponding to flight at stratospheric altitudes (i.e., greater than 35,332 ft in the standard NACA atmosphere).

As shown in Fig. 3, a ramjet may be expected to have a thermal efficiency of more than 0.50 when flying at 6000 fps. If a fuel, such as gasoline having a heat of combustion of 19,000 Btu/lb is used, the equivalent specific impulse, considering the ramjet to be replacing a rocket, is 1240 lb-sec/lb,[5] four times that of the reference rocket propellant. Thus even at 2 ¢/lb, the fuel costs per lb-sec of impulse of an airbreathing engine flying 6000 fps are about half of those of the reference rocket engine burning propellants costing 1¢/lb.

At lower flight speeds, such as are used during booster operation, even better relative performance can be obtained from airbreathing engines. For example, a turbojet having a specific fuel consumption of 1.0 lb/hr per lb of sea level static thrust has an equivalent specific impulse of 3600 lb-sec/lb. Thus, it is not inconceivable that airbreathing combination turbojet-ramjet booster units may be developed which will have high thrust to weight ratios and at the same time have equivalent specific impulses which are several times those obtainable with straight rocket engines using chemical propellants.

A further improvement factor of more than two and one-half can be obtained in the equivalent specific impulse of airbreathing engines if liquid hydrogen, with a heat of combustion of more than 50,000 Btu/lb, is used instead of gasoline for the fuel of an airbreathing engine. At present, economies resulting from this improvement in equivalent specific impulse are almost invariably more than offset by the greater cost of the liquid hydrogen.

It should be noted, however, that because of the falloff in thrust coefficient as indicated in Figs. 3 and 4, it is doubtful if flight speeds of much more than 6000 fps can be obtained with ramjets having subsonic combustion chambers. Consequently, a flight speed of 6000 fps was chosen as the maximum practical cruise speed of hypersonic airplanes when powered by airbreathing engines.

Nuclear Power. Instead of chemical energy, a solid core nuclear reactor can be used as an energy source for propulsion engines. Specific impulses as high as 1200 lb-sec/lb have been postulated for nuclear rockets in which hydrogen is used as the working medium(13). When used as part of a ramjet or turbojet engine with air as the working fluid, the same type of nuclear reactor will have vastly greater equivalent specific impulse than the chemically fueled engine; fuel costs will be trivial. However, instead of fuel consumption, the problems of developing a manned hypersonic airplane powered by an airbreathing nuclear reactor engine will be dominated by the weight problems of heavy components and shielding.

Transmitted Power. Conceptually, many of the difficulties of powering hypersonic vehicles could be avoided if the heavier components of the power generating equipment could remain motionless on the ground while the necessary propulsive power were somehow transmitted to a small, moving payload capsule. The difficulties and expense of accelerating and decelerating the heavy propulsion components would thus be

[5] The thrust developed in an engine when burning 1 lb/sec of fuel is the equivalent specific impulse. In an engine having a thermal efficiency of 0.5, flying at 6000 fps and burning 1 lb/sec of fuel having a heat content of 19,000 Btu/lb, the equivalent specific impulse I_{sp} is $I_{sp} = (19{,}000 \times 778 \times 0.5)/6000 \simeq 1240$ lb sec/lb.

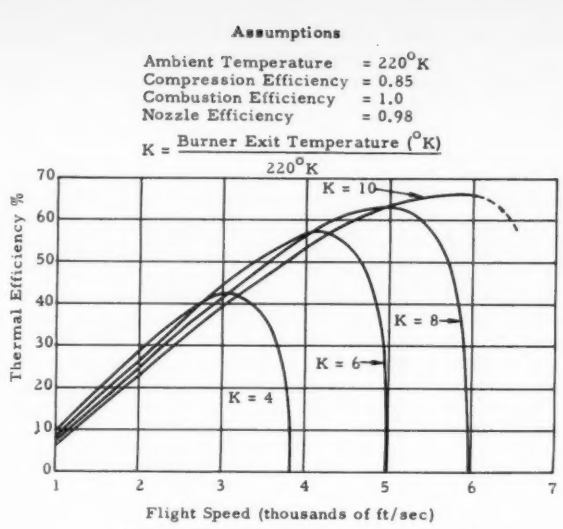

Fig. 3 Thermal efficiency of ramjets

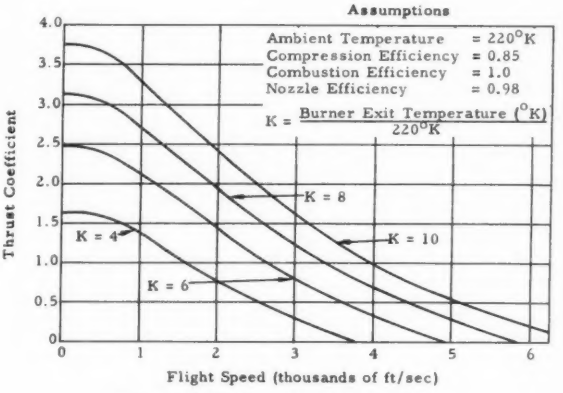

Fig. 4 Thrust coefficients of ramjets

avoided. Irving Langmuir has suggested that electromagnetic levitation be used to support and accelerate a manned capsule moving at high speed in an evacuated tube. Various other similar embodiments have also been suggested (8).

Lift to Drag Ratio

A lift to drag ratio of 6 was assumed for hypersonic aircraft cruising at 6000, 8000 or 10,000 fps. For boost-glide vehicles having an initial speed appreciably greater than 10,000 fps, lift to drag ratios of both 4 and 6 were assumed. It is believed that these aerodynamic assumptions are compatible with those made by others (14,1).

Unit Cost of Structure

Throughout this study, "structure" is used to include all parts of the complete vehicle except fuel, propellants and payload. Thus, the weights of guidance equipment, engines and flight crew are all included as a part of "structure."

Some insight into the probable unit cost of future hypersonic aircraft can be obtained as follows: The "fly-away" cost of a contemporary jet airplane, whose empty no-load weight is 100,000 lb, is roughly five million dollars. The initial cost of the vehicle is therefore $\$5 \times 10^6/10^5$ or \$50/lb. During a projected life of 10^4 hr, the depreciation and obsolescence costs are \$50/lb divided by 10^4 hr, or \$0.005/lb/hr. An additional \$100/lb may be needed during the life of the vehicle partly

to pay for interest, taxes and insurance, and partly to cover expenditures for maintenance and repairs. The total cost of the flying structure of contemporary jet aircraft is on the order of (\$50 + \$100)/10^4 hr or \$0.015/lb/hr of service life. In practice, service lives up to 30,000 hr are expected: the projected costs are correspondingly reduced.

There are at least two reasons for believing that the unit structural costs of future hypersonic aircraft as described here may be more than the 1.5¢/lb/hr suggested for contemporary jet airplanes. First, primarily because of the very different designs and construction materials used, both the cost of raw materials and the cost of fabrication will probably be appreciably greater for hypersonic aircraft and for recoverable boosters than for contemporary jet airplanes.

A second and related reason has to do with the fatigue life of the structural elements of hypersonic aircraft. In order to obtain the low structural factors (i.e., light structural weight) which it will be seen are an important factor in the economics of hypersonic aircraft, it seems likely that structural elements will be highly stressed. But when highly stressed, the fatigue life of materials is reduced. In short, the optimum design life for hypersonic aircraft may be much less than the 10,000 hr, or more, of flight often used for the design life of contemporary airplanes. There will be a corresponding increase in the dollars per pound per hour cost of the structure.

Because of these considerations, a cost of 10¢/lb/hr of flight was provisionally assumed for the unit cost of structure, both for boosters and for payload or cruise stages.

A numerical example may help clarify the assumption. A hypersonic vehicle may cost \$100/lb to fabricate and have a service life of 2000 flight hr. During this time, an additional \$100/lb may be spent on repairs, maintenance, taxes, insurance and interest on the \$100/lb investment. The direct structure costs of flying this vehicle are (\$100/lb + \$100/lb)/2000 hr, or 10¢/lb/hr.

Structural Factors

The term "structural factor" is used throughout this report to mean the ratio of the empty, unloaded weight of the stage under consideration to its initial gross weight, including both payload and propellants or fuel. The structural factor of contemporary air transports is about 0.5. However, structural factors of 0.1 (1) or less (17) have been suggested as appropriate for manned rocket powered hypersonic aircraft. Reference values of 0.1 and 0.2 have been used for the structural factor of payload stages; for boosters, reference structural factors of 0.05 and 0.1 were used.

Booster Costs

Assumptions

For both boost-glide vehicles and hypersonic airplanes, an initial acceleration to hypersonic speed is required. It seems appropriate, therefore, to compute the direct flying costs of accelerating a given payload, either a payload containing glider or a ramjet powered airplane, up to various hypersonic speeds. The accelerating mechanism, rocket powered or powered by airbreathing engines, is called the booster.

In all cases, it was assumed that the booster starts from rest and that the gravitational and aerodynamic losses experienced by the booster in climbing up through the atmosphere amount to 4000 fps. Thus a booster designed for a terminal speed of 6000 fps would, in field-free space, be capable of a terminal speed of 10,000 fps.

Based on a study of the German A-4 rocket, a 4000-fps allowance for acceleration losses seems appropriate, for vertical takeoff. It is probable that some improvement in booster performance could be obtained if the assumption of vertical takeoff thus implied were relaxed, and aerodynamic lift were used. Under these conditions, the assumption that gravitational and aerodynamic losses amount to 4000 fps may be too severe. On the other hand, restrictions on the acceleration program due to physiological limitations of the human body may decrease the acceleration efficiency of the boosters.

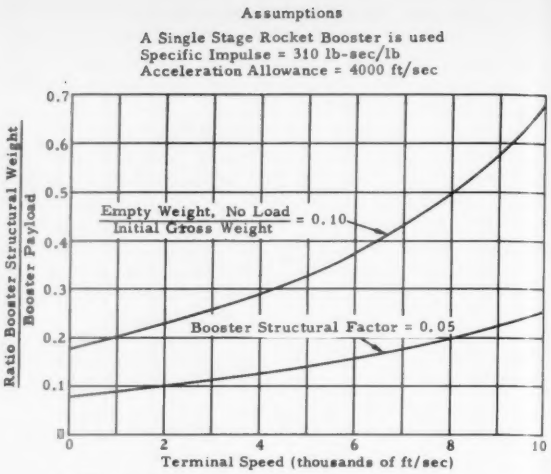

Fig. 5 Effect of terminal speed on structure

It was further assumed that each booster could be recovered and reused, and that an hour of flight time would be used to complete each launch cycle. Thus, using the reference value of 10 ¢/lb/hr, the booster structure costs would be 10 ¢/lb of booster structure each time the booster is used.

Results

A tabulation of the performance parameters of four boosters is given in Table 1. All are designed to accelerate to a final speed of 6000 fps. The contribution of the structural costs to the total direct flying costs of the booster may be obtained with the help of Figs. 5, 6 and 7.[6]

In Cases A and B, two boosters, both having a ratio of structural weight to payload of 0.15 (and thus the same structural costs), are compared. It is seen that the total launching costs of the airbreathing unit (Case B) are substantially less than those of the rocket unit (Case A).

Various changes can be introduced to reduce booster costs. For example, the structural costs can be reduced by improving the structural factor of the booster, and thus reducing the ratio of structural weight to payload. Numerically, a ratio of structural weight to payload of 0.05 can be assumed, rather than 0.15 as in Cases A and B. Then, to obtain this ratio, a structural factor of 0.0175 must be obtained in a rocket booster having a specific impulse of 310 lb-sec/lb, as shown in Fig. 6. Alternatively, even with infinite specific impulse, a booster unit must have a sea level thrust to weight ratio of 21 if it is to be used in vertical takeoff with payloads for which the booster structural weight to payload ratio is 0.05, i.e., 1/20.

[6] In Figs. 5, 6 and 7, the effects of various parameters on the ratio of booster structural weight to booster payload are shown. This particular ratio was chosen because it is easy to compute and may be used as a measure of the structural costs of the booster.

In Fig. 5 the effect of specific impulse on the ratio of booster structural weight to booster payload is shown. It may be seen that for the cases considered, comparatively little improvement in structural requirement is obtained by increasing specific impulse above 600 to 800 lb-sec/lb.

In Fig. 6 the effect of the booster structural factor on the ratio of booster structural weight to booster payload is shown. In all cases, a specific impulse of 310 lb-sec/lb was assumed for the booster engines.

In Fig. 7 the effect of booster burnout speed on the ratio of booster structural weight to booster payload is shown. As in Fig. 6, a specific impulse of 310 lb-sec/lb was assumed for the booster engines.

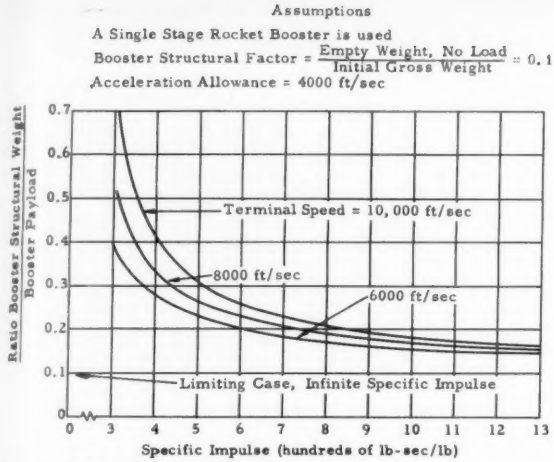

Fig. 6 Effect of specific impulse on ratio of booster structure

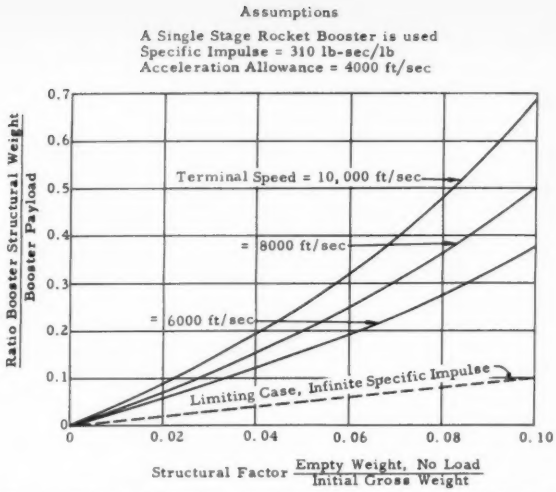

Fig. 7 Effect of booster structural factor on ratio of booster structural weight to booster payload

Turbojet lifting units having sea level thrust to weight ratios as high as 100/1 have been proposed (15). However, the development of airbreathing units, having a sea level static thrust to weight ratio of more than 20/1, into practical boosters capable of operating reliably over a wide range of Mach numbers would undoubtedly be a major undertaking, probably comparable to developing recoverable rockets having a structural factor of 0.0175.

Cases C and D of Table 1 show characteristics of two hypothetical booster designs in which these cost reducing changes have been incorporated. Again, the airbreathing configuration shows lower booster costs than the comparable rocket design. It is concluded first, that at terminal speeds of 6000 fps or less, a booster powered by airbreathing engines may be more economical to operate than its rocket powered counterpart, and second, that the cost of accelerating material (i.e., payload) to a speed of 6000 fps may be expected to lie somewhere in the range of 1 to 4¢/lb.

The cost of accelerating payloads to speeds greater than 6000 fps may be computed by using the same methods.

Other interesting conclusions can be derived from Table 1. For example, an upper bound can be placed on the value of a new propellant having improved specific impulse. In Case A, the total cost of boosting 1 lb of payload to 6000 fps is 3.5¢/lb. In Case D, the cost is 1.3 ¢/lb. Note that the only important difference between the two booster configurations, i.e., between Case A and Case D, is the increase in specific impulse from 310 lb-sec/lb (Case A) to 1240 lb-sec/lb (Case D). The total booster costs would again be 3.5¢/lb launched, if the price of fuel used in Case D were increased from 2 to 5.6¢/lb. Thus, given a Case A-type booster, and a 1 ¢/lb propellant combination having a specific impulse of 310 lb-sec/lb, only about 3.5 ¢/lb can be afforded for a propellant having a specific impulse of 1240 lb-sec/lb.

Under some circumstances, the economic incentive to increase specific impulse may be much greater than indicated

Table 1 Single-stage booster characteristics

Type of propulsion	A Chemical rocket	B Air-breather or nuclear rocket	C Lightweight chemical rocket	D Lightweight air-breather or nuclear rocket
Independent variables				
Speed at burnout, fps	6000	6000	6000	6000
structure/load	0.15	0.15	0.0575	0.069
specific impulse, lb-sec/lb	310	1240	310	1240
Dependent variables				
required thrust/weight ratio of engine for a thrust/weight = 1.2 at takeoff	25 (50)*	12	50 (100)*	24
structure/initial gross weight	0.048	0.10	0.02	0.05
load/initial gross weight	0.32	0.67	0.35	0.73
propellant/initial gross weight	0.63	0.23	0.63	0.22
propellant/load	1.97	0.35	1.82	0.30
Cost for each pound launched				
propellants at 1¢/lb	1.97	...	1.8	...
fuel at 2¢/lb	...	0.7	...	0.6
structure at 10¢/lb/launch	1.5	1.5	0.6	0.7
total	3.47	2.2	2.4	1.3

* The value in parentheses is probably more realistic, since no allowance has been made for the weight of propellant tanks in computing the first value. The tank weight of the airbreathing booster should be proportionally much smaller than the tank weight of a rocket powered booster, and thus much lighter.

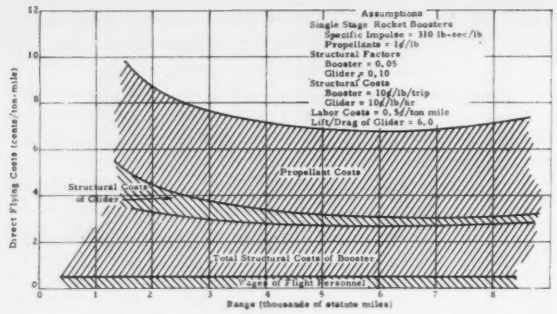

Fig. 8 Effect of range on direct flying costs of a reference boost-glide vehicle

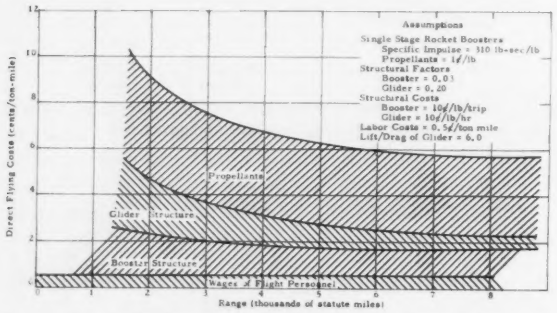

Fig. 9 Effect of altered structural factors on direct flying costs of a boost-glide vehicle

in the preceding paragraph. For example, in a ballistic missile system in which the boosters are not recovered, the structural costs may easily be 1000 times the 10¢/lb/trip cited above. Under these circumstances, more than 2600¢/lb can be afforded for a propellant having a specific impulse of 1240 lb-sec/lb.

Direct Flying Costs

Having determined a method of estimating the total costs of accelerating a payload to various terminal speeds, the direct flying costs of a boost-glide vehicle system can now be computed. A breakdown of the direct flying costs of a boost-glide vehicle is shown in Fig. 8, and a similar breakdown for a different boost-glide vehicle is shown in Fig. 9.[7] It will be noted that at all ranges, the structural costs of the booster are larger than those of the glider.

Fig. 9 may be compared with Fig. 8. The results of increasing the structural factor of the glider from 0.1 to 0.2 while at the same time reducing the structural factor of the booster from 0.05 to 0.03 may thus be determined. The total direct flying costs are thereby reduced at all ranges of more than 3400 miles.

It is worth noting that as long as rocket propellants costing 1¢/lb and having a specific impulse of 310 lb-sec/lb are used in the booster, there is a definite lower bound on the direct

[7] The allowance of 0.5 ¢/ton-mile made for salaries of the flight personnel is small by current standards. However, it should be noted that, because of the greater speed of flight, each man-hour of work by the crew members of a hypersonic airplane may be expected to produce about 10 times as much ton-mile revenue. It is not unlikely that the direct flying cost of transporting a pilot or crew member may be much larger than his salary. Thus, at 10 ¢/ton-mile the direct cost of transporting a 200-lb man on a 1-hr trip of 3000-mile length is $30. It is apparent that there are strong economic incentives for using a minimum number of lightweight personnel for the flight crew. It has been suggested that, at least for some unmanned cargo carriers, the entire airborne flight could be made completely automatic, that the need for a flight crew might then be eliminated.

Table 2 Limit case: Boost-glide vehicle

Range, thousands of statute miles	2	4	8
Required terminal speed, kilo fps, $L/D = 6$	10	13.7	18
Terminal speed with 4000-fps allowance	14	17.7	22
Initial weight/payload	4.05	5.86	9.0
Propellant/payload	3.05	4.86	8.0
Propellant costs, ¢/ton-mile	3.05	2.43	2.0
Assumed labor costs, ¢/ton-mile	0.5	0.5	0.5
Total direct flying costs, ¢/ton-mile	3.6	2.9	2.5

flying costs of a boost-glide vehicle. To illustrate this point, assume that both booster and glider have zero structural weight, and hence, there are no structural costs. See Table 2.

The results in the table are sobering. After making appropriate concessions for the structural weights, which will, in practice, always be required, it seems likely that the direct flying costs of commercial boost-glide vehicles using chemical rockets for acceleration will always be at least 5 or 6¢/ton-mile. As will be seen in the material which follows, it appears that ramjet propelled airplanes can be developed having direct flying costs that are as low as, or lower than, 5¢/ton-mile (see Table 4).

Cost of Midcourse Flight of Hypersonic Airplanes

In both Figs. 8 and 9, the propellant costs of the rocket booster are the largest single component of the direct flying costs. It seems likely that this component, at least, could be reduced if the speed at booster burnout were reduced, in other words if the booster requirements were reduced. Consider then, the direct flying cost breakdown of a hypersonic airplane which cruises at a speed lower than the initial speed of the boost-glide vehicles.

The costs of accelerating a payload vehicle up to hypersonic flying speed were discussed in an earlier section. The direct flying costs associated with the post boost portion of the flight, i.e., hypersonic airplanes containing cruise engines, will now be discussed. Since boost-glide vehicles have no midcourse flight costs other than those discussed in the preceding section, they need not be discussed further.

The structure costs of a reference rocket powered hypersonic airplane may be deduced from the data shown in Fig. 10. It is seen that the higher the cruise speed, the more economical the cruise portion of the flight. However, this advantage

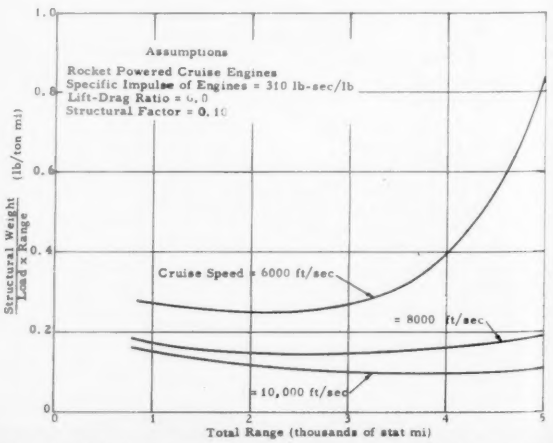

Fig. 10 Effect of range on structural use factor of a rocket powered airplane (various flight speeds)

may be partially offset by the greater costs of accelerating the airplane to the higher cruise speeds.

The effect of lift to drag ratio on the structural weights (and hence structural costs) of two airbreathing (or nuclear rocket powered) airplanes is shown in Fig. 11. It is seen that at least for the flight conditions specified, it is much more beneficial to reduce the airplane structural factor by 2 (0.2 to 0.1) than to increase the lift to drag ratio by the same factor (i.e., from 6 to 12, for example).

The effect of range on the structure requirements of four different hypersonic airplanes is shown in Fig. 12. Note that at a range of 3000 statute miles, two configurations show a structure requirement of only 0.1 lb/ton-mile. At flight speeds of more than 3000 mile/hr, the corresponding structural costs are less than 1¢/ton-mile.

The cost of the propellants or fuel used by a hypersonic airplane during midcourse can be computed by using the modified Brequet formula given earlier in the paper.

Total Direct Flying Costs of Hypersonic Airplanes

By adding booster costs, the structural and fuel costs of the midcourse cruise, and the labor costs of 0.5¢/ton-mile, the total direct flying costs of a hypersonic airplane can be obtained. For example, some of the data shown in Figs. 10 and 11 are shown in Table 3. It is seen that, using the stated assumptions, total direct flying costs range from roughly 5¢/ton-mile to almost three times this amount. Since the booster costs are much larger than the costs of structure and fuel, some reduction in ton-mile costs would be obtained if the length of flight path were increased to more than the 3000 statute miles assumed. This is shown in Fig. 13 for the reference hypersonic airplane, Case B of Table 3.

The magnitude of the booster costs relative to the other flight costs shown in Fig. 13 lead one to speculate on possible methods of reducing the booster costs. One method is to reduce the cruise flight speed assumed. A flight speed of 3000 statute miles/hr (4400 fps) was assumed in computing Fig. 14. Since the lift to drag ratio and the thermal efficiency of the engine (about 0.50 if gasoline or kerosene is used as fuel) are both unchanged, the fuel costs per trip per pound of airplane are unchanged. However, the structural costs per ton-mile are increased because:

1 The structural factor assumed for the airplane was increased from 0.1 to 0.2. In other words, there is more structure to pay for.

2 Because of the slower flying speed, each pound of the structure must be used longer to produce a ton-mile of revenue.

It is seen that using the stated assumptions, total direct flying costs of 5 to 6 ¢/ton-mile can be obtained at flight ranges between 2000 and 4000 miles.

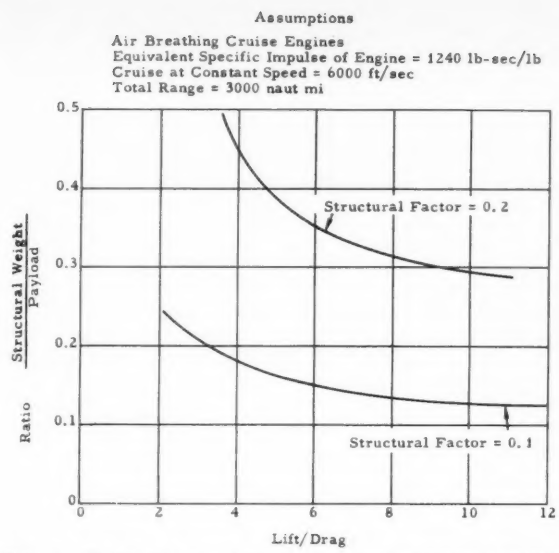

Fig. 11 Effect of lift to drag ratio on ratio structural weight

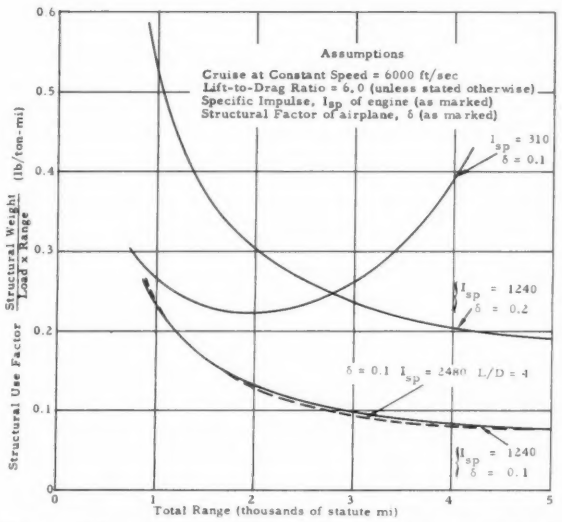

Fig. 12 Effect of range on structural use factors of hypersonic airplanes (various specific impulses and structure factors)

Table 3 Direct flying costs of various hypersonic airplanes (3000-nautical-mile range, chemical energy)

	A	B	C	D	E	F
Type of propulsion (cruise)	Breather	Breather	Breather	Breather	Rocket	Rocket
Specific impulse, lb-sec/lb	2480	1240	1240	1240	310	310
Flight, speed, fps	6000	6000	6000	6000	6000	10,000
Lift/drag	4	6	8	6	6	6
Structural factor	0.1	0.1	0.1	0.2	0.1	0.1
Costs, ¢/ton-mile						
structure at 10¢/lb/hr	1.2	1.0	0.9	2.4	2.7	1.0
fuel at 2¢/lb or propellant at 1¢/lb	0.8	0.5	0.3	0.6	1.7	0.2
booster: 3¢/lb at 6000 fps, 7.5¢/lb at 10,000 fps	3.6	3.0	2.7	3.5	7.9	7.3
labor, 0.5¢/ton-mile	0.5	0.5	0.5	0.5	0.5	0.5
Total costs, ¢/ton-mile	6.1	5.0	4.4	7.0	12.8	9.0

Other possible vehicle configurations will doubtless occur to the reader. For example, one is tempted to try to incorporate an integral booster mechanism into a hypersonic airplane of the types described in Figs. 13 or 14. Also, many airbreathing engines will "take hold" and produce thrust at speeds well below their design speed, and can thus be used to supply part of the boost acceleration. A weight breakdown of a typical embodiment incorporating these features is shown in Table 4.

Traffic Requirements

Commercial air traffic carries more passengers than inert cargo. Flights across the continental United States constitute the most heavily traveled route suitable for hypersonic aircraft (i.e., more than 2000 miles between stops). Current airline schedules provide an average of 4000 seat trips each way per day (16). Slightly less than half this number of seat trips each way per day are offered between North America and Europe. Assume each hypersonic vehicle makes six round trips per day (for a flight duty time of about 10 hr per day) and provides 33 seats each flight. It may be computed that only 20 vehicles will be needed for the trans United States traffic, and an additional 10 vehicles will suffice for the European traffic. It seems not unlikely that, in order to provide a reasonable frequency of service on the more lightly traveled routes, there will be a strong incentive to develop small vehicles of limited seating capacity, rather than large vehicles seating, say, several hundred passengers. Many of the same incentives to use aircraft having limiting seating capacity have been studied by the advanced research team at Lockheed (18).

Yet there appear to be operational economic advantages in favor of a large operator. First, every company must have at least one airplane in order to operate. Furthermore, to allow for time-consuming maintenance work, several vehicles are desirable. But if all the traffic on a given route can be handled by, say a dozen vehicles, there is apparently room for only a few companies to remain in business profitably.

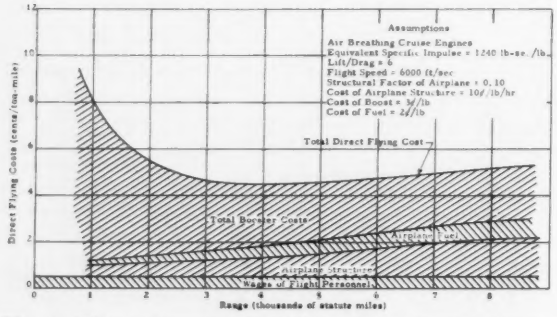

Fig. 13 Effects of range on direct flying costs of reference hypersonic ramjet airplane

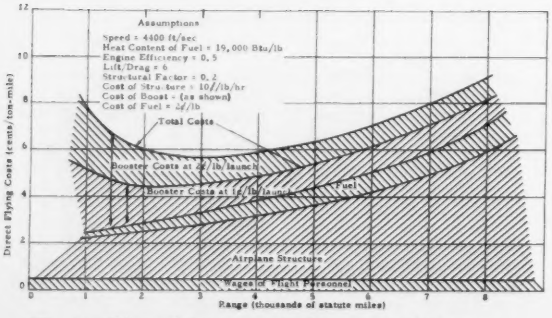

Fig. 14 Direct flying costs of a hypersonic airplane

Table 4 Projected performance characteristics of a hypersonic ramjet airplane using an airbreathing booster

General	
Type booster	integral air-breather
fuel for booster engine	gasoline
Type cruise propulsion	ramjet
fuel for cruise engine	gasoline
thermal efficiency during cruise	0.5
lift to drag during cruise	6
Design range, statute mile	4000
Cruise speed, fps	4400
Weights, lb	
Empty weight	5000
Gross payload	7500
Fuel used during boost	1900
Fuel used during cruise	5600
Initial gross weight	20,000
Performance, 100 per cent load factor	
Ton-mile/4000 mile trip	15,000
Ton-mile/flight hr	12,000
Cost fuel, 2 ¢/lb	1.0 ¢/ton-mi
Cost structure, 10¢/lb/hr	3.3 ¢/ton-mi
Flight crew, $75/trip	0.5 ¢/ton-mi
Total direct flying costs	4.8 ¢/ton-mi

A second advantage obtained by a company operating a large number of vehicles will be greater traffic flexibility. Unless hypersonic vehicles, as freight cars, are to be interchangeable between different airline companies, the larger airline should be able to make more effective scheduling of its vehicles between various flights than its smaller competitor.

The Future

Aside from growth due to increases in the world's population, the single factor which most affects air traffic is price to the customer. For example, it has been estimated that on many routes, each time the price is cut in half, the traffic density may be expected to increase by a factor of 10. Using what are believed to be fairly attainable assumptions, the estimated direct cost of flight at hypersonic speed appears to be about 5¢/ton-mile or, say, 1¢/seat-mile, assuming a load factor of 0.5 and 200 lb per passenger. Those rates are substantially lower than those achieved by current airplanes and probably close to those of most projected future airplanes. If these costs can be obtained, it is quite possible that long-range air traffic may increase by a factor of 10 within a decade.

Higher flight speed and the appeal to customers of the resultant reduction in travel time have often been used as a basis for developing new types of aircraft. However, if it takes 40 min to get to the airport and an additional 20 min to enplane, it seems unlikely that a hypersonic vehicle which will cross the United States in an additional 30 min will be, say, twice as desirable (to the paying passenger) as even a Mach 2 airplane, capable of flying the trip in about 130 min. In other words, as flight speed is increased, the numerical savings in travel time because of a given percentage increase in speed becomes quite small.

Concluding Remarks

Admittedly there are many factors which make it dangerous to be dogmatic in predicting trends in commerical air transport. Unforeseen technical developments, economic factors or political conditions may become of dominant importance. The following statements are, at least in part, subjective in nature and apply only to the flight conditions covered in this study.

Airplanes

At ranges up to several thousand miles, a ramjet propelled airplane burning a cheap gasoline- or kerosene-type fuel will probably have direct flying costs of about 5¢/ton mile, and as low or lower than those of a competing boost-glide rocket airplane using chemical propellants.

The cost of boosting the airplane up to its designed flying speed will be an important part of the total direct flying cost of hypersonic aircraft.

At ranges up to several thousand miles, the hypersonic airplane powered by a nuclear ramjet, if it is to compete economically, will probably need structural factors comparable with those of a competing chemical powered ramjet vehicle. This conclusion follows from the fact that in both cases the fuel costs are small compared to the structural costs.

Boosters

Up to speeds where a ramjet will no longer function effectively, boosters accelerated by airbreathing engines using chemical fuels are probably as cheap as competing chemical rocket boosters.

For applications considered here, the nuclear rocket is probably more expensive to operate than a competing chemical rocket, unless in the nuclear rocket the cost of the working fluid is less than 5¢/lb, and the structural factor is comparable to that of the competing chemical rocket.

Fuels and Propellants

For both rockets and ramjets using chemical energy for power, the most economical fuel is, and will remain, a cheap petroleum derivative, such as kerosene or gasoline.

For rocket applications, liquid oxygen is the most economical oxidizer.

Appendix: Direct Flying Costs of a Typical Contemporary Transport

It is of interest to compute the direct flying costs of a typical contemporary transport airplane, using the same methods and assumptions used in this paper.[8]

Consider a hypothetical turboprop transport which cruises at 400 miles/hr, has a range of 2000 statute miles, an empty weight of 60,000 lb, a payload of 30,000 lb and a gross weight of 120,000 lb.

Column A in the following table shows the direct flying costs if, as assumed in this study, fuel costs are 2¢/lb and structural costs are 10¢/lb/hr of flight.

	A	B
Fuel costs, ¢/ton-mile	2	2
Structural costs, ¢/ton-mile	100	15
Labor, ¢/ton-mile	0.5	5
Total, ¢/ton-mile	102.5	22

The structural costs are much too high. It is apparent, therefore, that the assumed 10¢/lb/hr of flight is probably unduly conservative. A lower figure, namely 1.5¢/lb/hr, was suggested in the text as being more appropriate for contemporary aircraft. At flight speeds of 400 miles/hr, crew costs of 5¢/ton-mile are probable compatible with the 0.5¢/ton-mile assumed for hypersonic vehicles. Using these values, Column B can be obtained. Although the allowances for structural costs and labor are probably still high, the picture is reassuringly close to contemporary experience.

[8] Some of the results of a most interesting analysis of the direct flying costs of an airbreathing airplane designed to fly at Mach 3 have recently been presented by Jamison (19). The Mach 3 cruising speed was chosen as a compromise between the reduced engineering and development requirements of designs having slower flight speeds and the increased economic prospects of designs having cruise speeds of Mach 5 or more.

Acknowledgment

The writer would like to acknowledge his indebtedness to R. Anders Park for editorial help during the preparation of this paper.

References

1 Sänger, E. and Bredt, J., "Über einen Raketenantrieb für Fernbomer" (A Rocket Drive for Long-Range Bombers), Ainring, Aug. 1944. English translation published by Robert Cornog, 1953.

2 Loebelson, R. M., "Marquardt Has High Hopes for Novel Ramjets," *Space/Aeron.*, Oct. 1958.

3 Rodgers, O. E., "Vistas in Aeronautics," Pergamon Press, 1958.

4 Romick, Knight and Black, "Meteor Jr., A Preliminary Design Investigation of a Minimum-Sized Ferry Rocket Vehicle of Meteor Concept," Eighth Annual Congress, IAF, 1957.

5 Sänger, E., "Gleitkorper für sehr hohe Fluggeschwindigkeiten" (Gliders for Very High Flight Velocities), D.P. 411/42, Berlin, 1939.

6 Thiel, A. K., "Untersuchungen an Gleitkörpen mit grossen Anfangsgeschwindigkeiten in Hoehen" (Investigations on Glide Vehicles Having High Velocities at High Altitudes), Dissertation submitted to the Institute of Technology, Darmstadt, Germany.

7 Cornog, R., "Economics of Rocket-Propelled Airplanes," *Aeron. Engng. Rev.*, Sept.-Oct. 1956.

8 Cornog, R. and Canright, "The Design of Liquid Fuel Rockets," Course notes for X 161 ABC, Univ. California, Engineering Extension, 1950.

9 Newtweiler, T. R. F., "Skin Heating During Re-entry of Satellite Vehicles to the Atmosphere," *J. Brit. Interplan. Soc.*, vol. 16, no. 1, Jan.–March 1957, p. 10.

10 Kooy and Uytenbogaart, "Ballistics of the Future," McGraw-Hill, 1946, chap. XI, sect. 15, pp. 399–400.

10a "Air Transport Facts and Figures," Official Publication of the Air Transport Assoc. of America, 20th ed.

11 Ley, W., "Rockets, Missiles and Space Travel," Viking Press, 1951, p. 354.

12 Sutton, G. P., "Rocket Propulsion Elements," John Wiley and Sons, 1956, 2nd ed.

13 Bollay, W., "Future Potentialities of Rocket Propulsion and Space Technology," *Western Aviation*, Oct. 1958.

14 Dorrance, W. H., "Two-Dimensional Airfoils at Moderate Hypersonic Velocities," *J. Aeron. Sci.*, Sept. 1952, vol. 19, no. 9, pp. 593–600.

15 Elliott, A. G., *Aviation Age*, April 1955, p. 18.

16 Studies by De Haviland Aircraft, Ltd., *Aviation Week*, Sept. 8, 1958.

17 Cornog, R. and van der Wal, F., "Optimum Proportions of Rocket Components," Vortrage gehalten auf dem. III, Internationalen Astronautischen Kongress, Probleme aus der Astronautischen Grundlagenforschung, Stuttgart, 1952.

18 Hibbard, H. and Bailey, R. A., "The Case for the Supersonic Transport," IAS National Summer Meeting, Calif., June 16–19, 1959.

19 Jamison, R. R., "Power for the Long Range Supersonic Airliner," IAS National Summer Meeting, Calif., June 16–19, 1959.

Project MIA (Mouse-in-Able), Experiments on Physiological Response to Spaceflight[1]

F. L. VAN DER WAL[2]
and W. D. YOUNG[3]

Space Technology Laboratories, Inc.
Los Angeles, Calif.

Mice carried in the nose cones of long-range ballistic missiles have successfully survived re-entry into the atmosphere. In most aspects, the environmental conditions experienced by these subjects exceeded in severity those which will be imposed on satellite passengers. This program represents an extension of the early pioneering flight experiments with mice and monkeys in relatively low performance sounding rockets. The relative success of these experiments permits a considerable degree of confidence in the ultimate successful recovery of biological payloads from future satellite vehicles. The project, known as Project MIA (Mouse-in-Able), was planned as a noninterference experiment in conjunction with the Project Able re-entry test program. The preparatory work was accomplished and the first flight occurred one month after official authorization. In each of the three Able flights, one mouse was carried in the nose cone. Although none of the nose cones was recovered, telemetered physiological records were obtained on the second and third Able flights. This report includes a description of the physical system, the preliminary tests, development of the instrumentation used in flight and the resulting signal pattern. The special problems associated with the use of living payloads in spaceflight vehicles are also discussed.

DURING April and July 1958, a series of tests of ICBM re-entry nose cones was performed, using as the launching vehicle a two-stage missile consisting of the Douglas Thor IRBM and the Aerojet 1040 liquid propellant rocket. This program, known as Project Able, was approved by the Air Force Ballistic Missile Division in December 1957, and the responsibility for assembly and instrumentation of the second stage and nose cone was given to the Space Technology Laboratories.

The nose cones used in these re-entry test flights were built by General Electric. They were encased in heat shields of various ablation materials, and provision was made for recovery of the nose cones for postflight inspection. Data were transmitted during flight from ablation gages and other instruments mounted in the nose cones. In addition to this instrumentation and the other supporting equipment, a certain amount of ballast was required to obtain the desired value of W/C_DA,[4] the parameter of critical importance in these re-entry experiments. A proposal was made by Space Technology Laboratories that a portion of this ballast be replaced by a minimum biological experiment which would be included in the vehicle as a secondary objective, on a noninterference basis.

This experiment consisted of flying a mouse in each Able nose cone in order to evaluate the effect of vehicle induced environmental parameters on a living animal. The proposal was officially approved by AFBMD on March 24, 1958, and the first MIA (Mouse-in-Able) package was flown in the first Able vehicle on April 23, 1958.

Equipment Development

Survival Equipment

The principal components of the MIA package are shown in Fig. 1. The physical system consisted of two aluminum cylinders connected end-to-end to form a closed circuit. The Mouse House cylinder housed the animal, its supporting equipment and a chemical canister containing silica gel for moisture absorption. The mouse was placed in an offset "cradle" mounted on bearings to permit automatic orientation in the optimum position for resistance to g loads.[5] The base of the cradle was filled with water which was made available to the mouse through an inserted wick. The second cylinder contained additional air purification chemicals and the circulation system used to assure continuous purification of the internal atmosphere. The ventilation system consisted of a small fan, driven by a 6-v motor powered by a pair of mercury cells. Chemical containers in this cylinder were filled with soda lime for absorption of carbon dioxide and additional silica gel.

This ventilation cylinder was connected by a hose to an oxygen regulator, which in turn was connected to a high pressure oxygen bottle. As the pressure in the closed system was reduced through chemical absorption of carbon dioxide and excess water vapor, more oxygen was admitted to the system. In this way a self-regenerating artificial atmosphere was maintained. The high pressure oxygen tank was a standard aircraft bailout bottle containing approximately 18 in.^{3} of oxygen at 2000 psi, the charged pressure. This amount of oxygen is sufficient to support a mouse for about two weeks if supplied only on demand. The oxygen regulator was a modified Alar A-2000 two-stage model.

Presented at the ARS 13th Annual Meeting, New York, N. Y., Nov. 17–21, 1958.

[1] For a more complete version of this report refer to ARS preprint 715-58.

[2] Member of the Technical Staff, Research and Development Division. Member ARS.

[3] Member of the Technical Staff, Research and Development Division.

[4] Ratio of gross weight of nose cone to the product of drag coefficient and area normal to flightpath.

[5] A similar concept has been proposed independently by Dr. Harald von Beekh in his paper "Multi-Directional G-Protection in Space Vehicles" for manned satellite applications, with due regard for the problems of emergency escape.

The system was completely self-contained; no external connections to any part of the Project Able equipment were required, other than simple mounting brackets and, in the two final flights, telemetry connectors. The MIA package was located foward in the nose cone, near the aerodynamic center, to minimize the lateral g loads associated with possible fishtail oscillations of the nose cone during re-entry.

Instrumentation of the Mouse

The problem of determining the condition of the mouse within the survival package was solved through the instrumentation system. It was necessary to determine, first, whether the subject was alive and, if alive, his health or his reaction to the environment. There were many parameters which could be measured to obtain a history of the animal's condition, behavior and response, but because of the limited telemetry capacity available, it was necessary to select the one parameter which would be most informative. Measurement of heart rate was settled upon.

Of the several possible transducers considered, an electrocardiograph-type pickup was chosen as a feasible and effective heart rate sensor because it was almost completely insensitive to environmental stimuli and the heart output was readily recognized. Since the mouse's skin is highly resistant to electrical currents, the electrodes were placed directly into the fascia, one connected ventrally to the right pectoral muscle, the other inserted diagonally across the heart, just below and to the left of the rib cage.

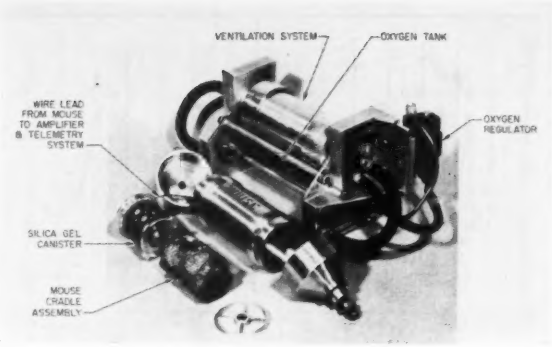

Fig. 1 Partially assembled MIA package

Fig. 2 Mouse in harness

Harness

The next problem was that of restraining the mouse in the package so that he would be unable to chew through or jerk loose the embedded wires.

During bench tests it became apparent that mice cannot tolerate near-total restraint under restricted sensory-input conditions for more than a few hours. This enforced immobilization frequently resulted in partial and temporary paralysis of the posterior quarters, probably accompanying a decrease in internal functions which could, in time, result in death. Apparently some less restrictive arrangement had to be developed. The ultimate solution, and the one used in the second and third flights, was a slipring assembly, restricting the motion of the mouse to single-point but unlimited rotation.

The slipring assembly was mounted on a metal saddle which was secured to the mouse with a harness made of Celastic, a special tape which provided an excellent bond to the subject's hair and skin. The harness was in two parts: A body band, with tabs for attachment of the saddle, and a metal-lined second layer used to discourage the mouse from chewing through the harness. (Fig. 2.)

After the mouse had been securely harnessed, the wires coming from the implanted electrodes were soldered to the slipring leads on the saddle. The slipring shaft was then inserted between brushes mounted on the cradle cover, thus completing the circuit to the telemetry system (see Fig. 1).

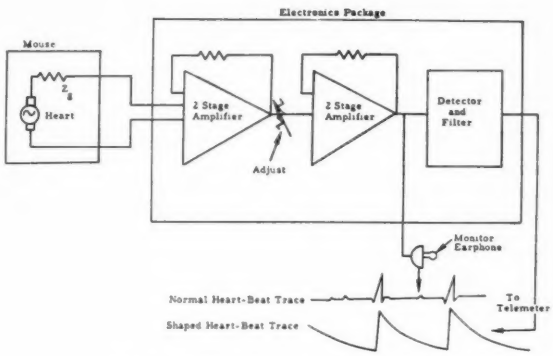

Fig. 3 Electronics unit block diagram

Electronics

The electronics unit (Fig. 3) was used to elongate the heart pulse and to amplify it by a factor of several thousand in order to produce the 5-v peak amplitude required for input to the telemeter. The pulse-elongation and filtering technique was employed to reduce the required transmission bandwidth, thus improving the system signal-to-noise ratio.

When the electronics circuit was being designed, the mouse was considered as an electrical generator with due regard for environmental stresses. The generator characteristics were found to be approximately as follows: Open circuit voltage, 1.5 mv peak-to-peak; impedance, 5000 ohms; characteristic frequency, 3 to 18 pulses per sec. A pair of two-stage transistorized amplifiers was included in the electronics unit, and an attenuator was inserted between the amplifiers in order to allow for variations in mouse output signal amplitude. Each amplifier circuit included about 10 db of negative feedback. This increased the input impedance to match the mouse impedance and stabilized the amplifier gain vs. environmental changes. Separate batteries were employed to power the two amplifiers so that only under very improbable circumstances could the amplifiers oscillate.

Initial attempts to amplify the mouse's pulse were impeded by large interference signals generated by the animal's respiration and physical motion. In order to reduce this interfer-

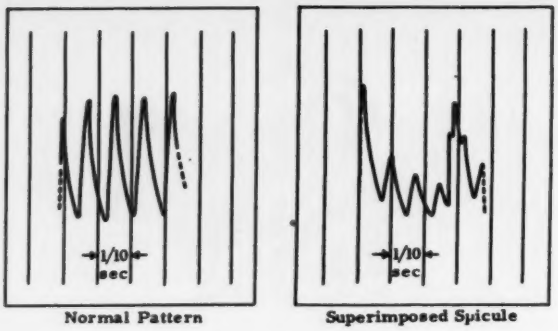

Fig. 4 Comparison of two heartbeat patterns

ence, the high frequencies were attenuated 20 db at 1000 cps by means of the feedback networks, thus making respiration noises negligible. Reducing the low frequency response about 20 db at 10 cps, by adjusting the coupling impedance values, adequately minimized motion-induced interference. Subsequent to amplification, silicon diodes rectified the heartbeat pulses and an RC filter in the output circuit elongated them to increase the low frequency component.

No evidence of adverse environmental effects on the electronics was detected in the records obtained from the flight tests. A typical section of an oscillograph record of the telemetered heartbeat is shown in Fig. 4 ("Normal Pattern").

Development Tests

The test program used in development of the MIA package consisted of testing individual components, including the mouse, under each of the anticipated stress conditions, then testing the assembled unit under the separately imposed stresses, and finally subjecting the complete system to a simulated flight by programming the tests to duplicate flight conditions. The individual stresses considered during this development test program included minimum acceptable operating duration, temperature, noise, vibration, acceleration and positive package sealing.

Recovery

Special MIA kits, data sheets and instruction booklets were provided to each of the recovery ships to assure proper care of the recovered mouse amd maximum experimental data from each flight.

MIA Flight Tests

History

Three Able vehicles were flown, each of which carried a mouse in a MIA package mounted in the nose cone. The first of these vehicles was launched on April 23, 1958 at 1910 EST. The mouse, a female, was not instrumented, since no telemetry was available for use in that flight. The nose cone was not recovered, and, since no mouse data were transmitted, no information on the physiological state of the passenger was obtained.

The second Able vehicle was launched at 2150 on July 9, 1958. It carried as a passenger a female mouse named Laska. Laska was installed in the Mouse House at 0750 on the launch date, and the package was mounted in the nose cone at 1200. Laska was exposed to the artificial atmosphere inside the Mouse House for 14 hr prior to launch.

The third Able flight occurred at 1715 on July 23, 1958. The mouse, a male named Benji was installed in the package at 0615 hours and mounted on the missile at 0930.

Data Received

Telemetry receiving stations are located at several points along the flightpath. Heartbeat signals were recorded at Cape Canaveral, Antigua and on the search ships for both instrumented flights. The duration of the telemetry reception at these stations is shown schematically in Fig. 5.

Data Interpretation

The physiological response of the mouse during this preliminary venture in spaceflight can best be interpreted by correlation of the heartbeat record with the physical parameters of the flight environment. Some difficulty was experienced in reducing the telemetered data due to masking of the anticipated heartbeat signal by muscle voltages generated during motion of the mouse or by respiratory signals and also by electronic noise during certain portions of the flight.

A typical signal interpretation problem is illustrated in Fig. 4. The left-hand trace is typical of the regular heartbeat signal recorded in the laboratory and during both of the instrumented MIA flights. The right-hand trace is a sample of the Able no. 2 data, in which the heartbeat was regularly interrupted by a superimposed spicule, thus complicating accurate counting of the number of pulses in a given signal segment. Since this characteristic appeared only during rocket burning and was most severe at times of highest acceleration, it is possible that the signal was associated with regular gasping respiration.

Since it had not proved feasible to obtain heartbeat records

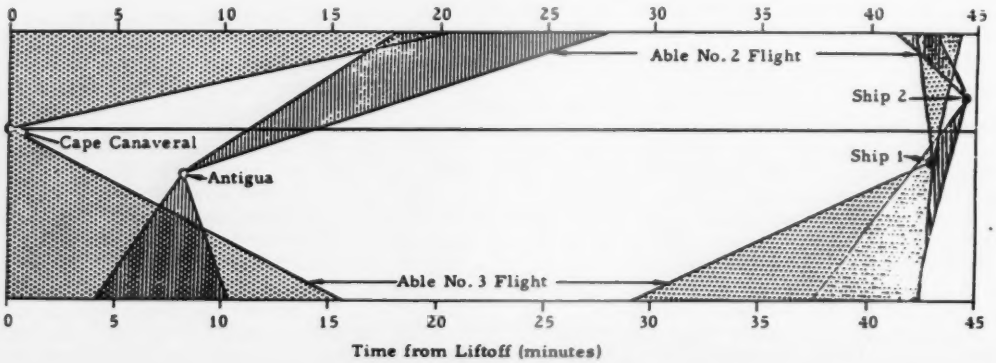

Fig. 5 Reception of physiological data

of these mice under known stress conditions in ground tests, interpretation of the flight data has been based on comparison with telemetered records obtained prior to liftoff. In Fig. 6, a plot is shown of the frequency of the heartbeat signals received from Laska and Benji at various times prior to liftoff.[6] It can be seen that Laska's "normal" heartbeat averaged about 12 impulses per sec, with variations between 11 and 13.5 per sec; the maximum spread in any continuous sample is on the order of 1 beat per sec. The mean value of Benji's heartbeat was much lower, about 5.2 impulses per sec, and the largest spread of "normal" values about the mean was only 1 beat per sec. This difference in mean values, though large, does not exceed the variation among healthy individuals as observed in bench tests.

In Fig. 7 are shown time-correlated plots of acceleration for Able no. 2 and heartbeat frequency for the mouse passenger Laska. There was a momentary sharp increase in heartbeat rate at liftoff. This settled immediately to a value equal to that recorded prior to liftoff, then increased fairly steadily with the increasing acceleration loads to a peak of 21.6 per sec just prior to first-stage burnout. The heart rate then began to drop slowly, but fluctuating; very high rates were maintained for about 35 sec. This relatively slow decrease to "normal" from maximum heart rate at maximum g is similar to the trend reported by the Russians for Laika the satellite dog when she entered the weightless state. Since Laska was not weightless at this time, however, one would instead expect a sharper decrease, such as had been observed in laboratory tests where the acceleration has been reduced suddenly from some high value to the normal 1 g.

During second-stage burning, the heart rate increased again, to a lower maximum (16.3 beats per sec), almost proportional to the g load. At second-stage burnout, when the vehicle and Laska became weightless, the rate dropped suddenly to the preflight value and remained quite steady.

As indicated in Fig. 5, no heartbeat signals were received in the time period from 28 to 41 min after liftoff of Able no. 2. This is also shown in Fig. 8, where Laska's heart rate during the weightless portion of the trajectory is presented with a time-correlated plot of vehicle altitude. When the down-range signal was picked up by the recovery ships at this later time, Laska's apparent heart rate had become very irregular, and the mean had dropped to less than half the earlier zero gravity mean of 12 beats per sec. Since the animal had already experienced 23 min of weightlessness prior to loss of the signal at Antigua without evidence of any distress, it seems unlikely that this decrease was in response to exposure to zero g. No conclusive explanation of this irregularity can be given at the present time for lack of supporting laboratory investigations or more comprehensive flight data.

An expanded plot of the down-range ship data is shown in Fig. 9. During high speed re-entry into the atmosphere, air particles near the nose cone are ionized due to the high temperature generated by friction. This ionized layer effectively blacks out transmission of signals from the nose cone telemetry, until the vehicle has slowed down considerably. The period during which signals are lost is approximately 30 sec long, and is shown by the break in recorded ship data indicated in Fig. 9. The mouse was experiencing about 60-g deceleration, following a higher peak value, when the heartbeat signal was regained. Values of deceleration during this re-entry phase were computed on the basis of known burnout conditions, followed by a ballistic trajectory. Because of uncertainties in predicting re-entry flight parameters from burnout conditions, a time error of perhaps 3 sec may exist in correlation of the trajectory characteristics with telemetered data. The quality of the data used in preparing Fig. 9 was severely compromised by the high noise level on the ship tapes; therefore, it would be quite unrealistic to attempt to

[6] In the following graphs, the heart rate data plots represent straightline connections between discrete points and have not been smoothed.

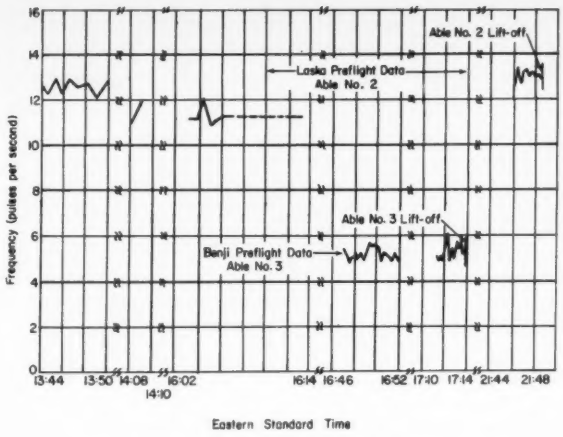

Fig. 6 Preflight heartbeat data

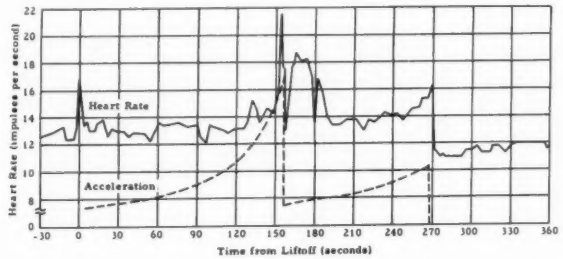

Fig. 7 Heart rate and acceleration during burning period, Able no. 2 (Laska)

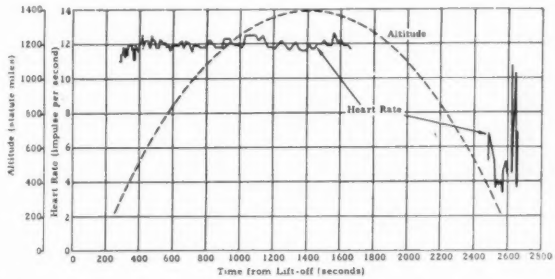

Fig. 8 Heart rate and altitude during weightlessness, Able no. 2 (Laska)

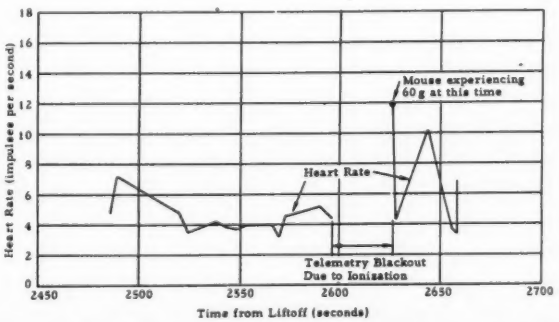

Fig. 9 Heart rate during re-entry, Able no. 2 (Laska)

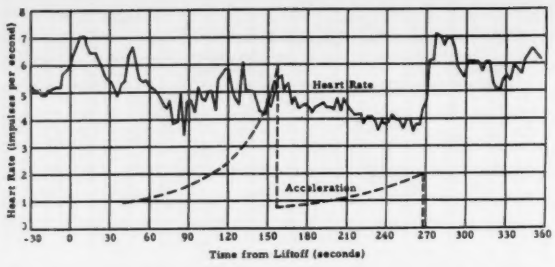

Fig. 10 Heart rate and acceleration during burning period, Able no. 3 (Benji)

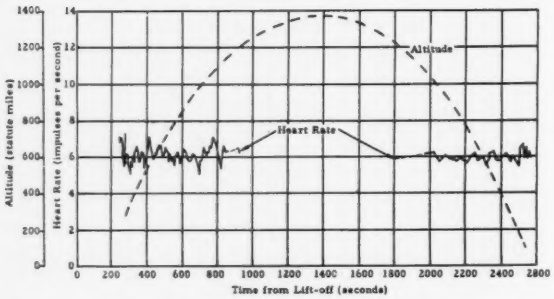

Fig. 11 Heart rate and altitude during weightlessness, Able no. 3 (Benji)

find meaningful trends in this fluctuating signal.

Two significant conclusions can, however, be drawn from this graph. First, Laska lived through the high deceleration and the external heating associated with re-entry without a catastrophic change in the recorded heart rate mean from the value observed just prior to re-entry. Indeed, the fluctuations noted after re-entry do not differ in magnitude from those measured just after the high g loads at first-stage burnout. Second, there is considerable evidence that the last data points were received when the nose cone was suspended from the recovery parachute. If this is so, the mouse survived all the major stresses associated with the re-entry and recovery operation, and one may state with some assurance that Laska returned to sea level alive after some 40 min of weightlessness.

In Fig. 10, a plot is shown of the heart rate of Benji, the male mouse flown in Able no. 3, with a time-correlated trace of acceleration during the burning period. It is immediately clear that the nature of these data is markedly different from data shown for Laska (Fig. 7), so that no generalizations regarding reaction to acceleration loads may be made from the results of these two instrumented tests. For the Able no. 3 flight, the heart rate just prior to liftoff was of the same order as the preflight mean, 5.2 beats per sec. The heart rate rose at liftoff, then dropped, then rose again. This erratic behavior continued throughout the entire burning period, with no detectable trends. The maximum excursion of values was from 3.4 to 7.1 beats per sec—3.7 beats total variation as compared to 9.5 for Laska. (It may be noted that the total excursion of measured heart rate about the "normal" value for each animal was about 75 per cent of the rate measured prior to the flight.)

No significant reaction occurred at first-stage burnout. At second-stage burnout, the heart rate rose sharply to 7.1 beats per sec as Benji was exposed to zero gravity, then settled down to a ± 1-beat fluctuation about a mean of 6 beats per sec, slightly higher than the preflight mean. This increase is not consistent with the sharp decrease in Laska's heart rate at the beginning of weightlessness, though both animals returned to near preflight "normal" almost immediately after the weightless period began.

The heart rate data for Benji during the entire weightless period, with a corresponding altitude trace, is presented in Fig. 11. As shown, the mean value of the heart rate did not shift during the loss of signal in the middle of the flight, and Benji appears to have been in very good shape throughout the duration of the record. In this flight, no telemetry signals were received following the ionization blackout at re-entry.

Summary of Results

Project MIA was a minimum biological experiment of secondary importance to the principal objective of the Able program, namely, the testing of ballistic re-entry nose cones. Consequently, the amount and nature of the data available were extremely limited, and certainly no generalized conclusions regarding the behavior of space mice may be drawn. However, some interesting observations were made, and may be summarized as follows:

1 Takeoff conditions were not severe enough to produce any evidence of violent or continuing response from the mice.

2 The acceleration loads during burning were essentially paralleled by Laska's heart rate, though this characteristic was not displayed by Benji under similar load conditions.

3 The observed decrease in Laska's heart rate at first-stage burnout was gradual; at second-stage burnout it was sharp. This is in opposition to the heart rate behavior reported for Laika the Russian satellite dog. No trend was detectable in Benji's heart rate at first-stage burnout, but a distinct increase to slightly above his preflight "normal" was apparent at the beginning of weightlessness.

4 Since both mice flew to a maximum altitude of 1400 statute miles (as compared to Laika's apogee of 1050 miles), they returned to Earth from a higher altitude than that reached by any other living organism.

5 Laska, and probably Benji, returned to sea level alive after experiencing re-entry conditions approaching those associated with satellite re-entry.

6 No evidence of distress due to weightlessness was noted in either flight. The mice were weightless for longer periods than any animal other than Laika.

7 There is every reason to believe that both Laska and Benji would have been recovered alive after their flights if the nose cones had been retrieved.

Acknowledgments

We would like to express our thanks to the entire Project Able staff, in particular to Dr. R. B. Morrison, Program Director, and Lt. Col. D. R. Latham, AFBMD Project Officer, for their interest, enthusiasm and cooperation. Project MIA could never have gotten off the ground, in several ways, without their help and support.

Transport Coefficients of Air to 8000 K[1]

ERNEST BAUER[2] and
MARTIN ZLOTNICK[3]

Avco Research and Advanced
Development Division
Wilmington, Mass.

The coefficients of viscosity and of frozen and reaction conductivity of air have been calculated for a temperature range 3000 K $< T <$ 8000 K, and a density range $10^{-2} < \rho/\rho_0 < 10$, where ρ_0 is the density of air at 1-atmosphere pressure and T = 273 K. We have used an intermolecular potential of form A/r^n, where r = intermolecular distance, and the exponent n = 6,8; this form of the potential is fitted to data derived from Amdur's scattering experiments. A critical discussion of uncertainties in calculations of this kind and a comparison with earlier work are given. The overall accuracy of the transport coefficients obtained here is estimated as ±25–30 per cent.

IN THE current developments in hypersonic flight, local temperatures of up to 8000 K are encountered. At these temperatures air is far from an ideal gas, because internal energy states are excited and many of the oxygen and of the nitrogen molecules are dissociated (1).[4] At present, there exist only very few calculations of the transport coefficients of air in this region (2 to 4), and they suffer from two major but related defects:

1 There is very little information on effective intermolecular potentials in the relevant energy or temperature range; about the best data are those inferred from experiments on the scattering of argon atoms on argon atoms and nitrogen molecules (5), and even this was not available in time for the previous calculations (2 to 4, 14). There was thus an inevitable tendency (2,3) to extrapolate low temperature intermolecular potentials (6) far beyond any reasonable range of validity of these data.

2 Presumably partly as a result of this uncertainty, no attempt was made in the early work to estimate the reliability of the results, both in terms of the numerical error or in terms of a display of the component parts of the calculation to indicate qualitative difficulties and limitations.

The philosophy of the present work is similar to that stated in Hansen's work (4), namely to provide an engineering approximation to the transport coefficients and to the dimensionless ratios used in aerodynamic analysis (Lewis, Prandtl and Schmidt numbers). We interpret this to mean that 10 per cent errors are to be regarded as satisfactory within the statement of the problem. In fact, we do not think that this can be achieved with the present state of knowledge. We estimate that the overall errors of our calculations are maybe ±25 to 30 per cent. The discussion of sources of error has deliberately been written up in some detail to point out the quantitative sources of error.

In addition to the quantitative errors which arise mostly from our incomplete knowledge of intermolecular potentials, there exists a major physical problem. The concept of a transport coefficient is based on the well-known Chapman-Enskog theory (6,7) which applies to the interaction of structureless point molecules, that is, of systems having no internal energy states. In fact, atoms and molecules have several types of internal degrees of freedom. Of these, molecular rotation can be treated in a way that is empirical but fairly satisfactory quantitatively (8). There is also molecular vibration, and electronic excitation of both atoms and molecules, which cannot necessarily be treated by a Eucken correction (8). Finally there is molecular dissociation or other kinds of chemical reaction, which are treated by a different method (9). The overall problem of internal molecular motion has been treated by Wang Chang and Uhlenbeck (10), but does not appear to have the definiteness of the theory for structureless molecules. Some of these problems are discussed in more detail elsewhere (11).

Physical Model

We consider the temperature range from 3000 to 8000 K, for values of ρ/ρ_0 lying between 10^{-2} and 10. The relative concentrations of the major chemical species of air in this region are shown in Table 1 (1). Roughly, we can break up our temperature range into a number of different regions, each with its own physical regime:

A $T <$ 3000 K—Room temperature regime. Here we may treat air as consisting of 21 per cent O_2 and 79 per cent N_2, neglecting 1 per cent A and traces of other materials. The molecules may be treated as interacting with conventional (6–12) or (exp–6) potentials, or even as rigid spheres of low temperature radius. This region has been treated thoroughly in the past (6), and thus we are not interested in making calculations for it.

B 3000 $< T \lesssim$ 4000 K—Oxygen dissociation region (nitrogen undissociated).

C 4000 $\lesssim T <$ 8000 K—Nitrogen dissociation region (oxygen dissociated).

D $T >$ 8000 K—Plasma region (no molecules; atoms, ions and electrons).

The usual kinetic theory concepts tend to break down in region D where there are mostly screened Coulomb (long-range) interactions, and there is significant electrical conductivity (12). This region is potentially of very great interest from the standpoint of magnetohydrodynamics, but we are not considering it here.

Thus we shall consider regions B and C, in terms of oxygen and nitrogen atoms and molecules interacting with inverse nth power repulsive potentials that are discussed in the next section. In region B we shall consider N_2 and the reaction $O_2 \rightleftarrows 2\,O$, in region C, O and the reaction $N_2 \rightleftarrows 2\,N$. Several remarks are in order.

Received Oct. 6, 1958.

[1] This work was supported by the U. S. Air Force, Ballistic Missile Division, Air Research and Development Command, under contract AF 04(645)-30. The same experimental data on intermolecular potentials have been used to calculate transport coefficients by Amdur and Mason ("Properties of Gases at Very High Temperatures," *Phys. Fluids*, vol. 1, 1958, p. 370). However, these authors do not examine possible errors as critically as we do.

[2] Principal Scientist, Physics Section; presently Research and Development Scientist, Aeronutronic Division of Ford Motor Co., Newport Beach, Calif. Member ARS.

[3] Senior Scientist. Aerodynamics Section.

[4] Numbers in parentheses indicate References at end of paper.

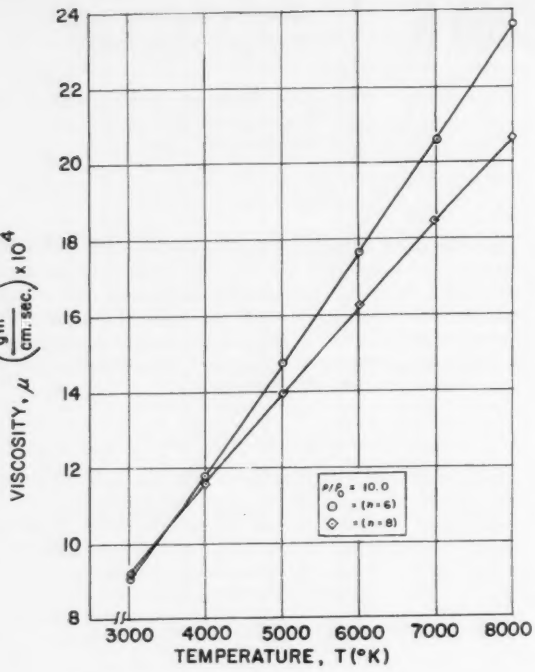

Fig. 1a Viscosity μ, $\rho/\rho_0 = 10.0$

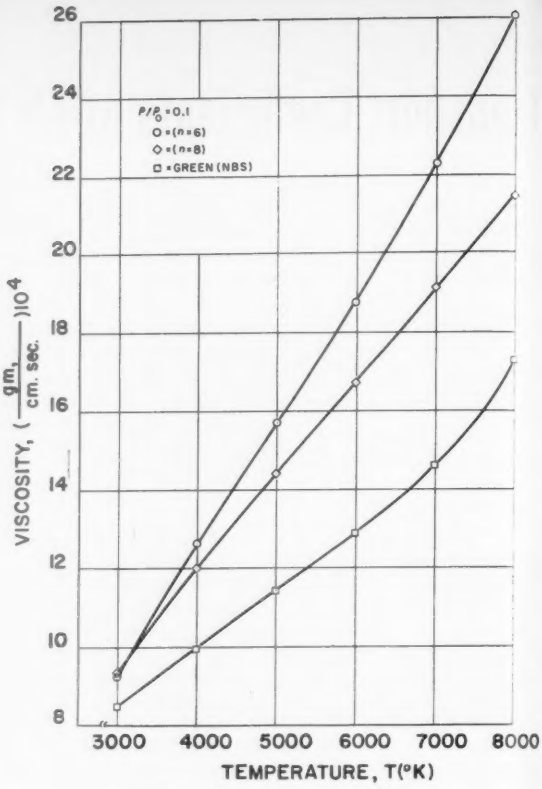

Fig. 1c Viscosity μ, $\rho/\rho_0 = 0.1$

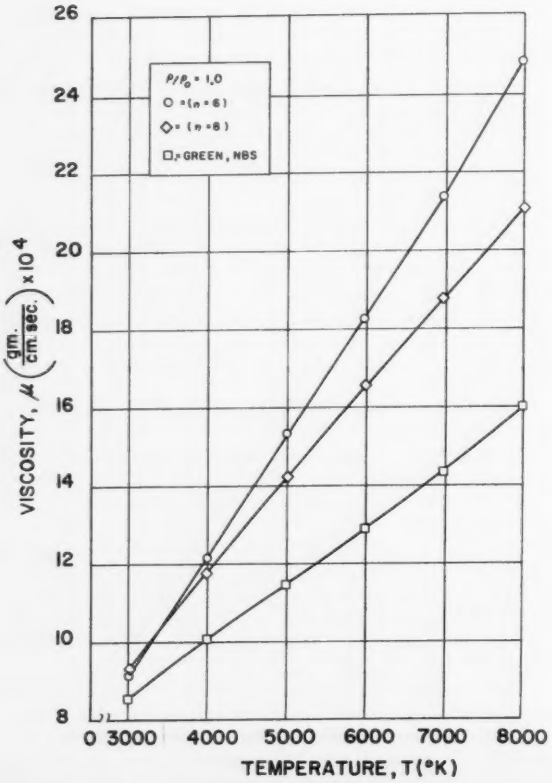

Fig. 1b Viscosity μ, $\rho/\rho_0 = 1.0$

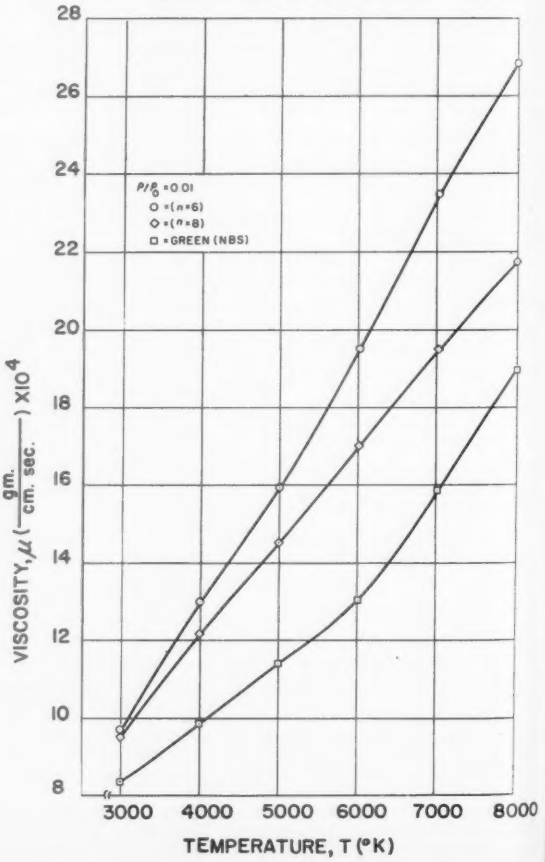

Fig. 1d Viscosity μ, $\rho/\rho_0 = 0.01$

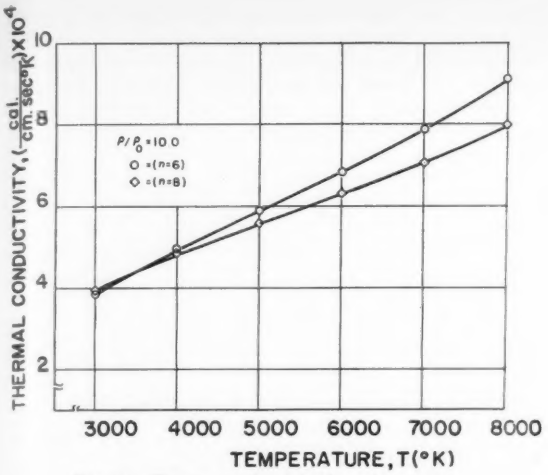

Fig. 2a Frozen conductivity k_f, $\rho/\rho_0 = 10.0$

1 Nitric oxide might have a significant effect on the reaction conductivity and also on the electrical conductivity, since NO has the lowest ionization potential of any of the major components of air. Thus as a further development, one might consider combining regions B and C to consider 5 components (N_2, O_2, NO, N, O) and three reactions ($N_2 \rightleftharpoons 2\,N$, $O_2 \rightleftharpoons 2\,O$, $NO \rightleftharpoons N + O$).

2 The reason for not going above 8000 K with the present calculation is that electron and ion contributions to the transport coefficients become important for electron concentrations $\gtrsim 10^{-3}$. This is discussed elsewhere (4,11).

Interatomic and Intermolecular Potentials

The potential energy between any two atoms or molecules, or between an atom and a molecule, is to be regarded simply as a function of r, the separation of the two centers of mass. The assumption of central forces is necessary for the Chapman-Enskog theory in its usual form to be applicable, and certainly the available data do not justify any more elaborate treatment. We shall describe the interaction potential by a power law expression

$$\phi(r) = A/r^n \qquad [1]$$

ble 1 Equilibrium composition of dry air (1), particles per air atom

perature (°K)	ρ/ρ_0	N_2	NO	O_2	N	O	e^-
000	10.0	3.807^{-1}	2.29^{-2}	9.25^{-2}	5.77^{-7}	2.31^{-3}	5.66^{-10}
	1.0	3.809^{-1}	2.26^{-2}	9.03^{-2}	1.83^{-6}	7.21^{-3}	3.64^{-9}
	0.1	3.813^{-1}	2.17^{-2}	8.34^{-2}	5.77^{-6}	2.19^{-2}	1.39^{-8}
	0.01	3.826^{-1}	1.92^{-2}	6.51^{-2}	1.83^{-5}	6.12^{-2}	4.26^{-8}
000	10.0	3.681^{-1}	4.79^{-2}	6.97^{-2}	6.26^{-5}	2.28^{-2}	1.44^{-7}
	1.0	3.711^{-1}	4.19^{-2}	5.29^{-2}	1.99^{-4}	6.28^{-2}	6.13^{-7}
	0.1	3.776^{-1}	2.85^{-2}	2.41^{-2}	6.35^{-4}	1.339^{-1}	1.73^{-6}
	0.01	3.848^{-1}	1.28^{-2}	4.75^{-3}	2.03^{-3}	1.883^{-1}	3.71^{-6}
000	10.0	3.616^{-1}	6.01^{-2}	3.91^{-2}	1.04^{-3}	7.19^{-2}	3.38^{-6}
	1.0	3.715^{-1}	3.80^{-2}	1.52^{-2}	3.32^{-3}	1.420^{-1}	1.05^{-5}
	0.1	3.788^{-1}	1.62^{-2}	2.70^{-3}	1.06^{-2}	1.890^{-1}	2.26^{-5}
	0.01	3.728^{-1}	5.49^{-3}	3.16^{-4}	3.33^{-2}	2.044^{-1}	4.18^{-5}
000	10.0	3.609^{-1}	5.58^{-2}	1.68^{-2}	6.78^{-3}	1.210^{-1}	2.44^{-5}
	1.0	3.683^{-1}	2.61^{-2}	3.61^{-3}	2.17^{-2}	1.772^{-1}	6.05^{-5}
	0.1	3.540^{-1}	9.15^{-3}	4.61^{-4}	6.72^{-2}	2.004^{-1}	1.16^{-4}
	0.01	2.939^{-1}	2.73^{-3}	4.95^{-5}	1.936^{-1}	2.076^{-1}	2.07^{-4}
000	10.0	3.560^{-1}	4.63^{-2}	6.75^{-3}	2.59^{-2}	1.506^{-1}	9.34^{-5}
	1.0	3.428^{-1}	1.82^{-2}	1.08^{-3}	8.04^{-2}	1.901^{-1}	2.04^{-4}
	0.1	2.753^{-1}	5.53^{-3}	1.24^{-4}	2.279^{-1}	2.045^{-1}	3.81^{-4}
	0.01	1.370^{-1}	1.26^{-3}	1.30^{-5}	5.084^{-1}	2.089^{-1}	7.59^{-4}
000	10.0	3.396^{-1}	3.48^{-2}	3.18^{-3}	7.01^{-2}	1.691^{-1}	2.52^{-4}
	1.0	2.846^{-1}	1.18^{-2}	4.33^{-4}	2.030^{-1}	1.975^{-1}	5.23^{-4}
	0.1	1.541^{-1}	2.87^{-3}	4.76^{-5}	4.723^{-1}	2.071^{-1}	1.11^{-3}
	0.01	3.50^{-2}	4.38^{-4}	4.88^{-6}	7.115^{-1}	2.095^{-1}	3.03^{-3}

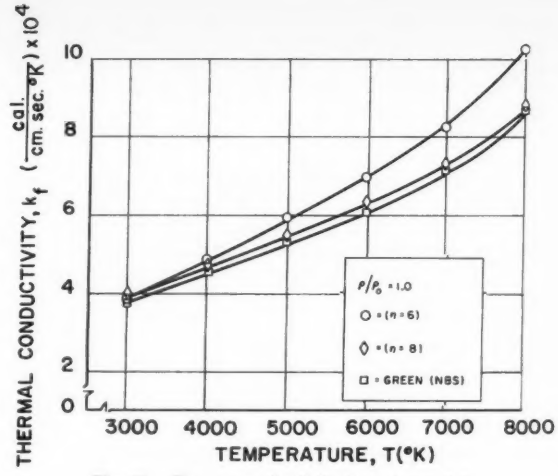

Fig. 2b Frozen conductivity k_f, $\rho/\rho_0 = 1.0$

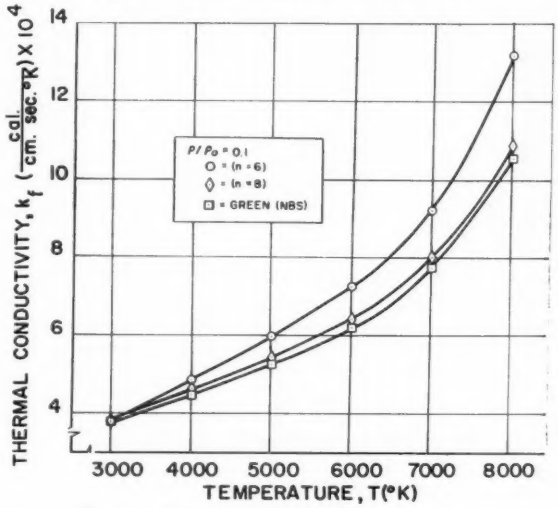

Fig. 2c Frozen conductivity k_f, $\rho/\rho_0 = 0.1$

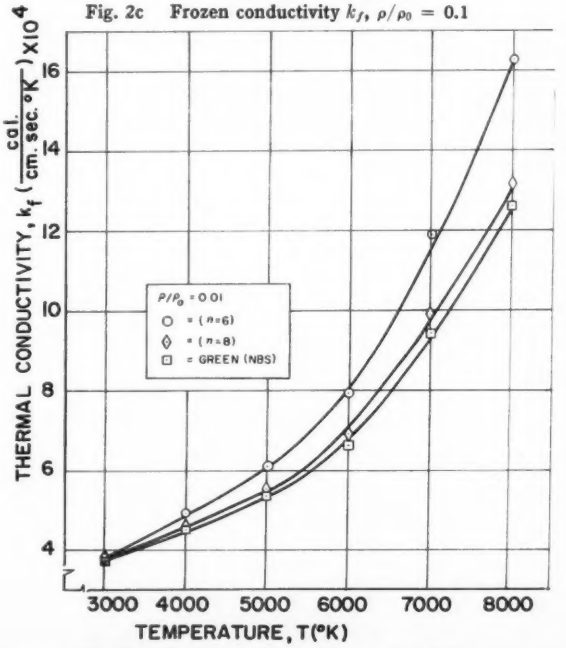

Fig. 2d Frozen conductivity k_f, $\rho/\rho_0 = 0.01$

The reason for using a power law, rather than an exponential which is more reasonable on physical grounds, is that the transport coefficients are given in closed form for a power law potential (7), and furthermore that over the relatively narrow energy range with which we are concerned, the experimental data can be described as well by a power law as by an exponential.

To find A, n parameters for nitrogen atoms and molecules, we shall use the data inferred by Amdur et al. (5) from experiments on the scattering of rare gases from one another and from nitrogen. It must be stressed that although the internal consistency of this work is quite good, to deduce N_2-N_2 interactions or even more N-N interactions is a fairly violent extension of the theory. However, there seem to exist no other data, theoretical or experimental, that are more relevant to our problem than these scattering results.

We shall assume that O-O, N-N, N-O interactions are all the same, with a potential $A_{atom}/r^{n_{atom}}$; that O_2-O_2, N_2-N_2, O_2-N_2 interactions are all the same, with a potential $A_{mol}/r^{n_{mol}}$, and that the customary "mixing rules" hold, so that an atom-molecule interaction is

$$(A_{atom}A_{mol})^{1/2}/r^{1/2(n_{atom}+n_{mol})} \quad [2]$$

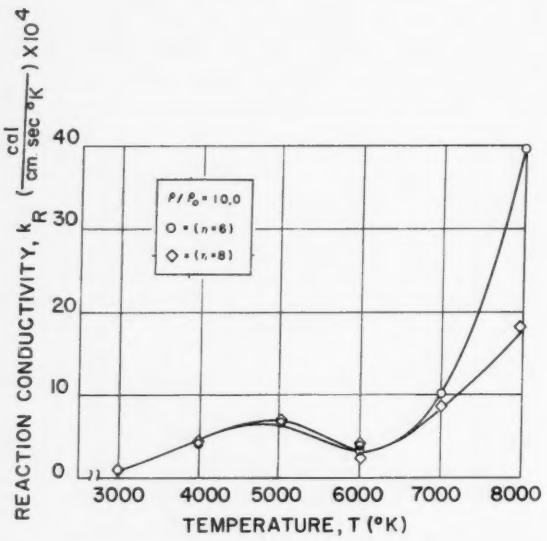

Fig. 3a Reaction conductivity k_R, $\rho/\rho_0 = 10.0$

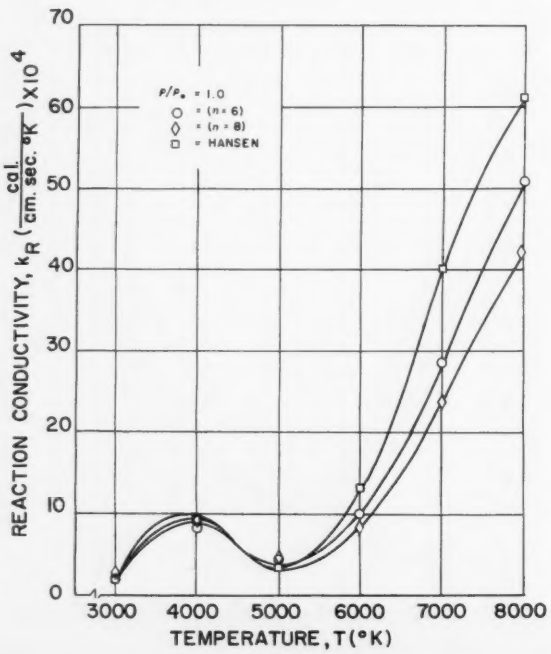

Fig. 3b Reaction conductivity k_R, $\rho/\rho_0 = 1.0$

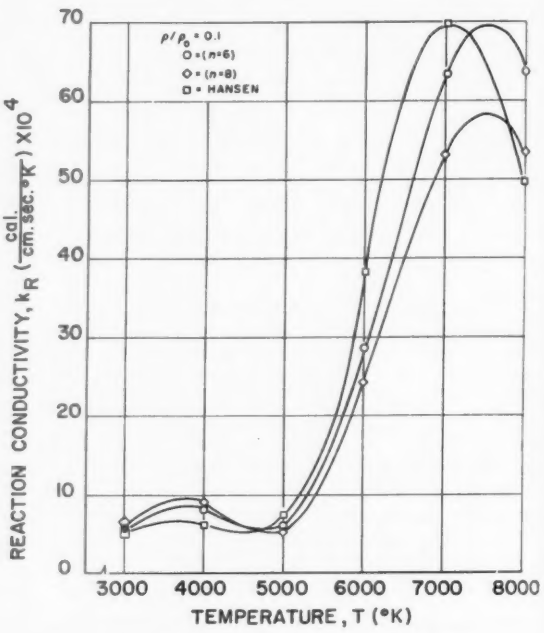

Fig. 3c Reaction conductivity k_R, $\rho/\rho_0 = 0.1$

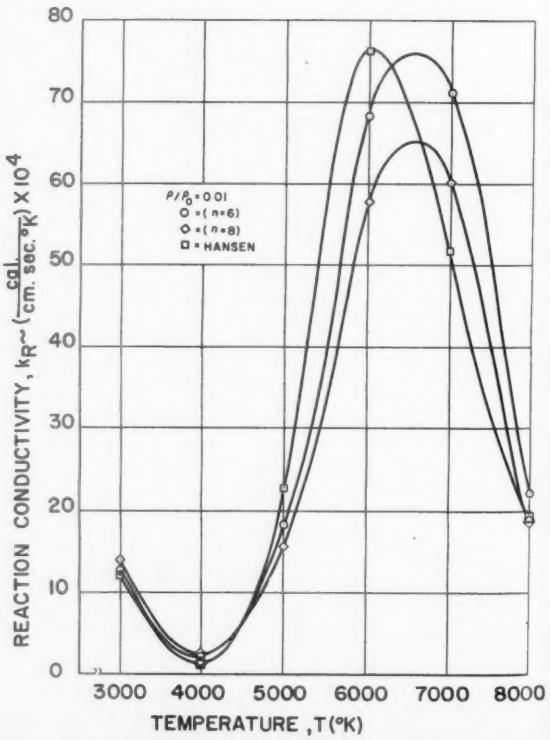

Fig. 3d Reaction conductivity k_R, $\rho/\rho_0 = 0.01$

In practice, we shall always take $n_{atom} = n_{mol} = n$, and work with $n = 6,8$ to give an idea of the effects of varying this parameter. The method of obtaining A_{atom}, A_{mol} from Amdur's work is to use a reference point r_1; $\phi(r_1) = A_n/r_1^n$; $\phi(r_1) \sim 1$ ev, which gives A_n once we have $\phi(r_1)$, r_1, n. We have used the following values of the force constants

$$n = 6: \quad A_{atom} = 4.02\,(10)^{-11} \qquad A_{mol} = 2.56\,(10)^{-10}$$

$$n = 8: \quad A_{atom} = 3.08\,(10)^{-10} \qquad A_{mol} = 1.97\,(10)^{-9} \qquad [3]$$

The dimensions of A are such that when distances are measured in Angstrom units, $\phi(r)$ is given in ergs.

A basic difference between the present and earlier calculations of transport coefficients (2 to 4) lies in the form of inter-

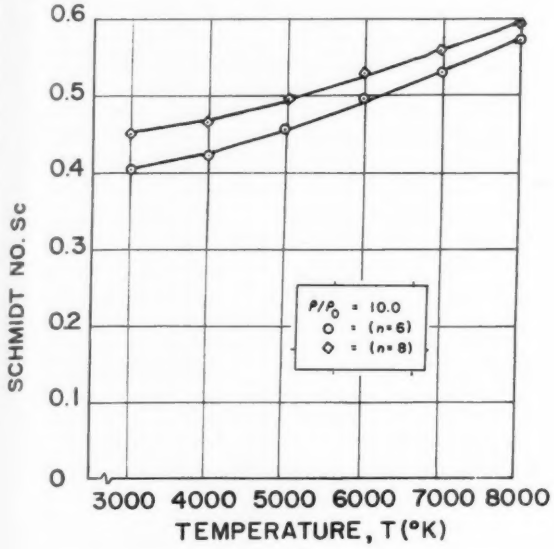

Fig. 4a Schmidt number $Sc = \mu/\rho D_{12}$, $\rho/\rho_0 = 10.0$

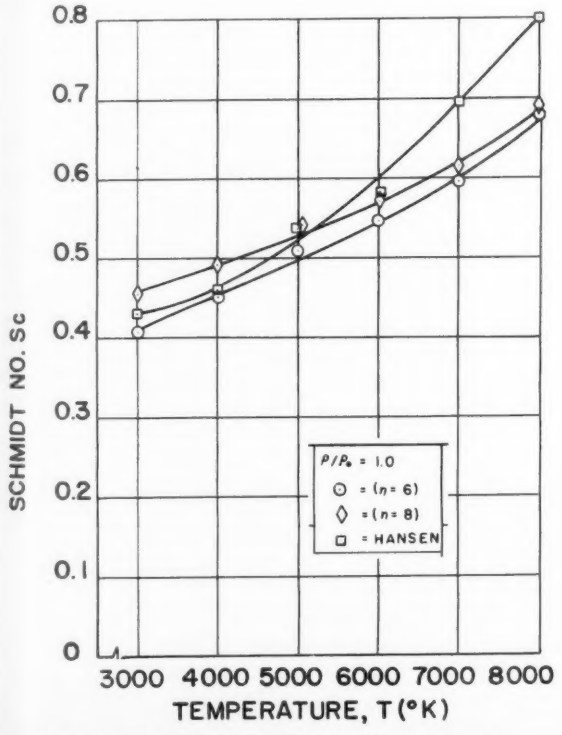

Fig. 4b Schmidt number $Sc = \mu/\rho D_{12}$, $\rho/\rho_0 = 1.0$

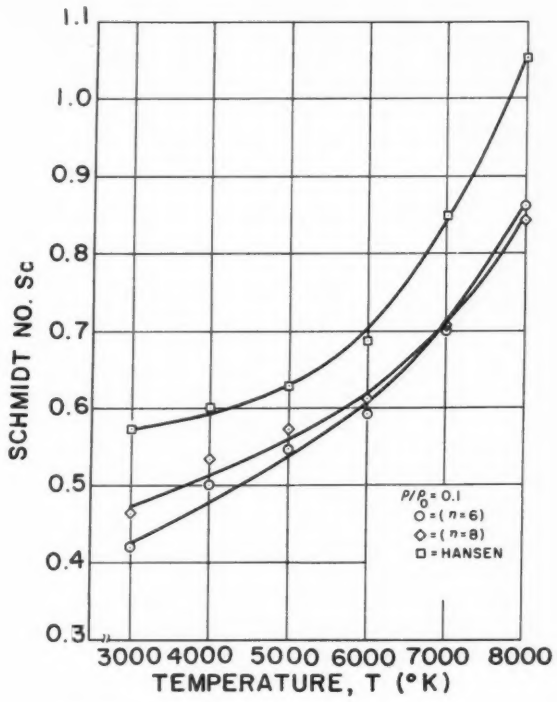

Fig. 4c Schmidt number $Sc = \mu/\rho D_{12}$, $\rho/\rho_0 = 0.1$

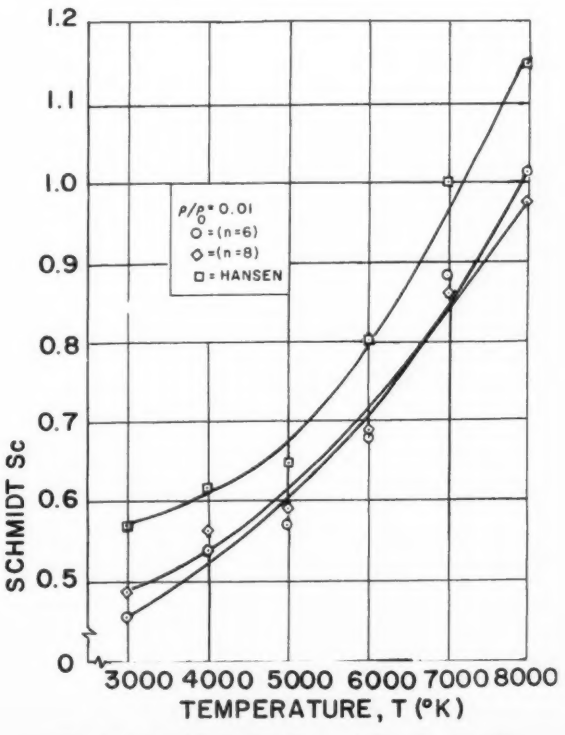

Fig. 4d Schmidt number $Sc = \mu/\rho D_{12}$, $\rho/\rho_0 = 0.01$

atomic potentials used, and this is certainly one of the principal advances of the present work. Green (3) and Baulknight (2) make apparently quite uncritical use of rigid sphere or (6–12) potentials, using numerical values derived from room temperature measurements, say 200 to 600 K (6). This is quite unsatisfactory because it involves an extreme extrapolation of results that are not particularly accurate and reliable in the first place. Hansen's calculations (4) are definitely superior to the earlier work (2,3) at least in basic concept; he recognizes the difficulties and derives effective rigid sphere diameters that vary with temperature in a consistent way.

There can be little question that Amdur's data (5) provide a better input than anything used previously (2 to 4), even though it must be realized that because of the experimental arrangement they do not give the effective intermolecular potential of nitrogen molecules at 6000 K, but rather an artificial interaction of 300 K nitrogen molecules in the 0.5-ev energy range (0.5 ev = 6000 K). This means that the effect of electronic states that are excited at 6000 K and not at 300 K is not taken into account. Such states are ^2P, ^2D for atomic nitrogen, and ^1S, ^1D for atomic oxygen. We know of no reliable way to remedy this deficiency with presently available data. Hansen (4) did make an attempt to take this into account, but it seems impossible to say whether his attempt would lead to better or worse results.

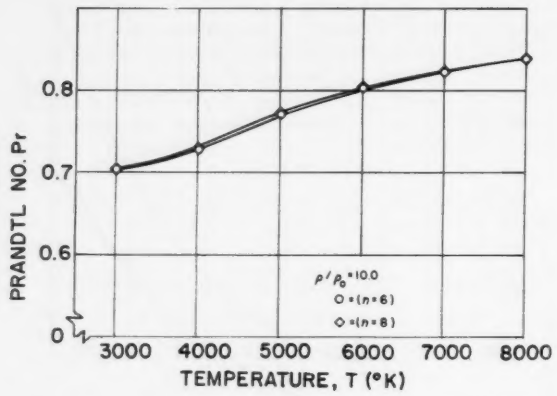

Fig. 5a Prandtl number $Pr = \mu c_p/k_f$, $\rho/\rho_0 = 10.0$

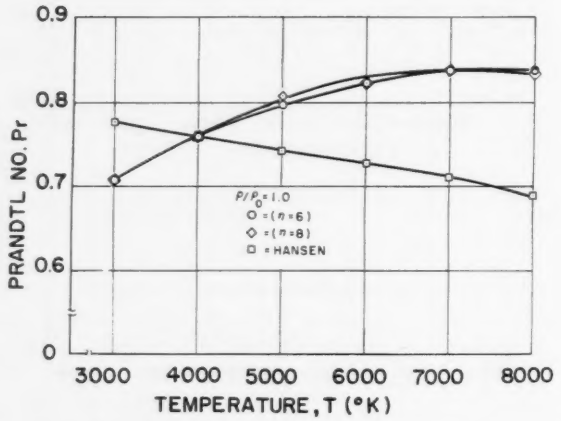

Fig. 5b Prandtl number $Pr = \mu c_p/k_f$, $\rho/\rho_0 = 1.0$

Computation Program and Results

Except for the reaction conductivity calculation where three components were used (O, O_2, N_2 or else O, N, N_2), the calculations have been carried out for a two-component mixture composed of atoms of atomic weight 15 and molecules of molecular weight 30, with specific heats the weighted averages between oxygen and nitrogen values.

The formulas used are entirely standard (6,7); they are stated explicitly elsewhere (11). For the viscosity and diffusion coefficients, the temperature variation is essentially given by

$$\mu, \mathfrak{D} \sim T^{(1/2 + 2/n)} \qquad [4]$$

except for relatively minor variations due to changes in composition. The viscosity (and diffusion) calculations are quite straightforward; the only limitations arise due to our limited knowledge of interatomic potentials and of the mixing rule for atom-molecule interactions. In calculating the thermal conductivity there are, of course, the basic problems of the internal degrees of freedom; within the standard techniques used here, the only additional uncertainty lies in the precise choice of Eucken correction (8), which gives a slight (±5 per cent, maybe) uncertainty to the frozen conductivity.

The results are given in graphical form in Figs. 1 through 6. The concept of a reaction conductivity k_R as indicated in

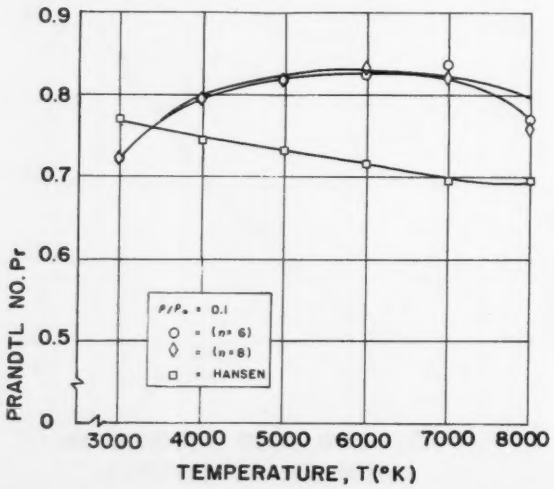

Fig. 5c Prandtl number $Pr = \mu c_p/k_f$, $\rho/\rho_0 = 0.1$

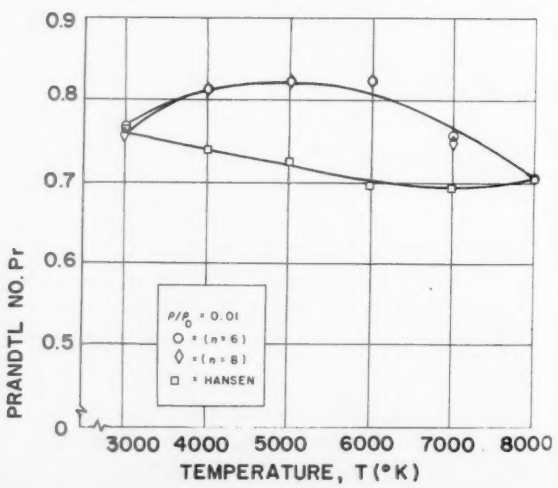

Fig. 5d Prandtl number $Pr = \mu c_p/k_f$, $\rho/\rho_0 = 0.01$

Figs. 3 was introduced explicitly by Hirschfelder and by Butler and Brokaw (9) to take into account the energy carried as chemical heat of reaction when there is a temperature gradient. k_R is to be distinguished from the "frozen" conductivity k_f, which is a measure of the energy carried as kinetic energy, and by the internal (rotational, vibrational and electronic) degrees of freedom. Thus, in a treatment in which the energy flux due to diffusion is taken into account separately, e.g., Fay and Riddell (13), the reaction conductivity is not to be used.

Estimate of Errors and Comparison With Earlier Work

The principal source of error that can be estimated lies in the choice of intermolecular and interatomic potentials. It seems reasonable to suppose that the amplitudes A may differ by a factor of 2 from the values listed in Equation [3]; such a factor of 2 would give an uncertainty of a factor $2^{1/n}$ in the hard sphere diameter of a molecule at a given temperature, and thus an uncertainty $2^{2/n}$ in the transport coefficients. Thus, for $n = 6$, $2^{2/6} = 1.26$, and for $n = 8$, $2^{2/8} = 1.19$, so that the error will be of order 20 to 25 per cent.

In addition to this scale error, we cannot distinguish empirically between $n = 6,8$; this gives rise to an uncertainty in the temperature dependence of the transport coefficients. From Equation [4] we see that $\mu \sim T^{0.833}$ for $n = 6$, and $\mu \sim T^{0.75}$ for $n = 8$. This gives rise to an uncertainty in the values of the transport coefficients of maximum amount 10 per cent over our temperature range.

In the case of the frozen conductivity, there is an additional but rather small (± 5 per cent) uncertainty in the precise value of the Eucken correction factor.

Thus we assign an overall uncertainty of ±25 to 30 per cent to the calculated values of the transport coefficients. This is made up mostly of three different possible sources of error:

1 The effect of excited electronic states.

2 The mixing rule approximation for atom-molecule interactions of Equation [2].

3 Possible errors in Amdur's scattering experiments.

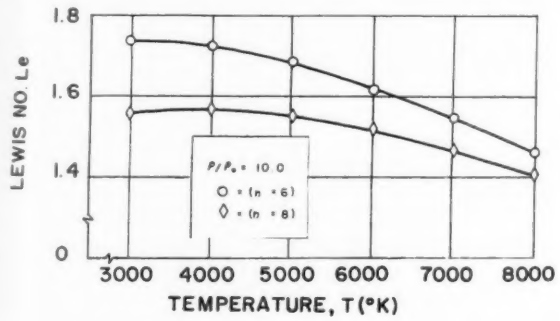

Fig. 6a Lewis number $Le = D_{12}c_p\rho/k_f$, $\rho/\rho_0 = 10.0$

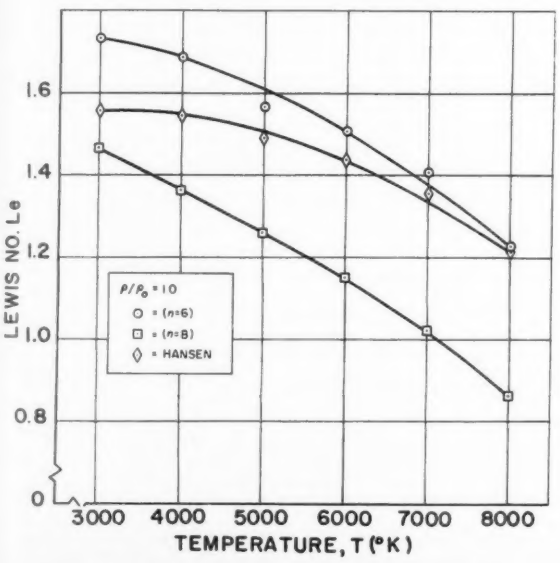

Fig. 6b Lewis number $Le = D_{12}c_p\rho/k_f$, $\rho/\rho_0 = 1.0$

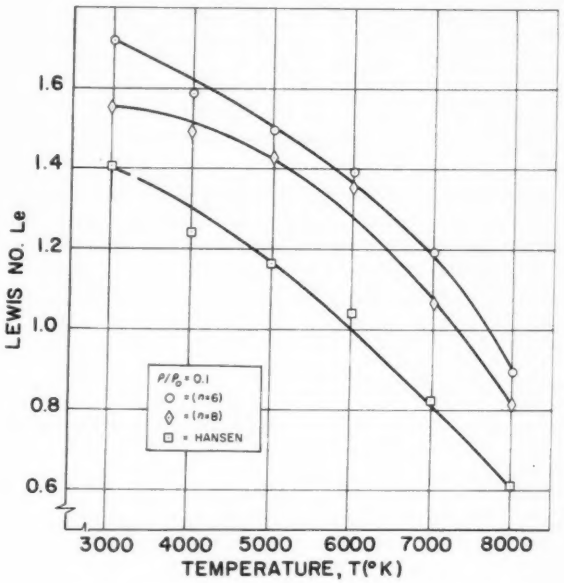

Fig. 6c Lewis number $Le = D_{12}c_p\rho/k_f$, $\rho/\rho_0 = 0.1$

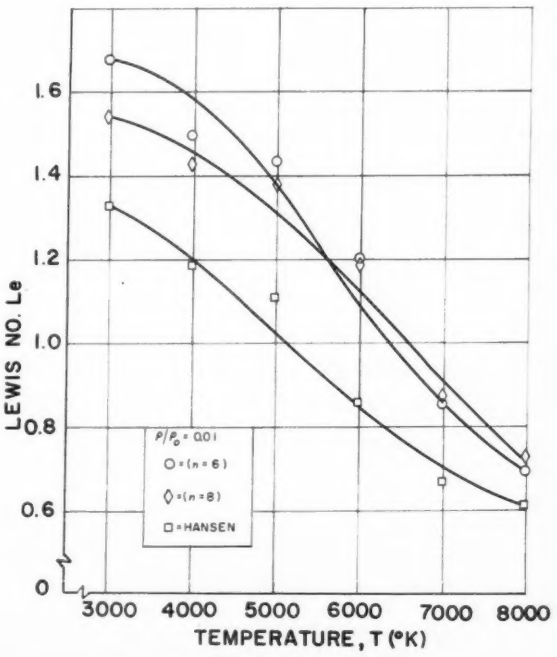

Fig. 6d Lewis number $Le = D_{12}c_p\rho/k_f$, $\rho/\rho_0 = 0.01$

Furthermore, there is the basic question of the applicability of the Chapman-Enskog theory of transport processes to molecules having internal degrees of freedom and undergoing chemical reactions. Some of these points are discussed elsewhere (11).

At this point it is worth giving a brief comparison of our results with previous work in the field (2 to 4). A comparison of viscosity and frozen conductivity calculations made by the present method with the calculations of Green (3) is included in Fig. 1. At the lower temperatures there is no substantial difference between the two sets of data, but at the higher temperatures the present values are substantially higher. This is to be expected: Green uses a Lennard-Jones 6–12 potential, so that at the higher temperatures he gets $\mu \sim T^{0.66}$ corresponding to a 12th power repulsion, whereas our 6th and 8th power repulsion potentials give $\mu \sim T^{0.83}$, $T^{0.75}$, respectively. The present reaction conductivity data are compared with Hansen's (4) in Fig. 3. An attempt was made to make the comparison on a uniform basis, and the agreement is generally fair.

The Schmidt number plotted in Fig. 4 is based on the binary diffusion coefficient $\mathfrak{D}_{\text{atom-mol}}$, which of course contains the full effect of atom-molecule interactions in the present calculation. The difference between the Schmidt numbers computed by Hansen (4) and those computed here is due primarily to the different atom-molecule interaction assumed in each case.

Acknowledgments

We are indebted to Dr. W. L. Bade of Avco-Rad and to Dr. T.-Y. Wu of the National Research Council, Ottawa, Canada for discussions, and to Paul Yannalfo for carrying out the computations.

References

1 Gilmore, F. R., "Equilibrium Composition and Thermodynamic Properties of Air to 24,000°K," Rand Rep. RM-1543, 1955.

2 Baulknight, C. W., "Calculation of Transport Properties at Elevated Temperatures" in "Transport Properties in Gases," Cambel, A. B. and Fenn, J., Eds., Northwestern Univ. Press, 1958, p. 89.

3 Green, M. S. and Klein, M., "Transport Properties of Air at Elevated Temperatures," Nat. Bur. Standards Rep. 5235-9.

4 Hansen, C. F., "Approximations for Thermodynamic and Transport Properties of High-temperature Air," NACA TN 4150, 1958.

5 Amdur, I., Mason, E. A. and Jordan, J., "Scattering of High Velocity Neutral Particles—X," *J. Chem. Phys.*, vol. 27, 1957, p. 527.

6 Hirschfelder, J. O., Curtiss, C.F. and Bird, R.B., "Molecular Theory of Gases and Liquids," John Wiley and Sons, New York, 1954.

7 Chapman, S. and Cowling, T. G., "Mathematical Theory of Non-Uniform Gases," Cambridge, 1939.

8 Ref. (6), p. 498 ff; Ref. (7), p. 237 ff, "The Eucken Correction."

9 Hirschfelder, J. O., "Heat Transfer in Chemically Reacting Mixtures I," *J. Chem. Phys.*, vol. 26, 1957, p. 274; *see also* Butler, J. N. and Brokaw, R. S., "Thermal Conductivity of Gas Mixtures in Chemical Equilibrium," *ibid.*, p. 1636.

10 Wang Chang, C. S. and Uhlenbeck, G. E., "Transport Properties of Polyatomic Gases," Engineering Research Institute, Univ. of Mich., CM-681, 1951.

11 Bauer, E. and Zlotnick, M., "Transport Properties of Air to 8,000° K," Avco Tech. Rep. RAD-TR-2-58-12, 1958.

12 Spitzer, L., "Physics of Fully Ionized Gases," Interscience Pub., New York, 1956, chap. 5.

13 Fay, J. A. and Riddell, F. R., "Theory of Stagnation Point Heat Transfer in Dissociated Air," *J. Aeron. Sci.*, vol. 25, 1958, p. 73.

14 Greifinger, P. S., "Transport Coefficients of Dissociating and Slightly Ionizing Air," Rand Rep. RM-1794, April 1957.

ARS JOURNAL

RUSSIAN SUPPLEMENT

J. George Adashko, Editor

Soviet Technical Literature in Translation

JOHN A. NEWBAUER

AMERICAN ROCKET SOCIETY
New York, N. Y.

THE October ARS JOURNAL brings to its readers a service designed to answer the question: What does USSR journal literature offer in astronautics?

This issue of the JOURNAL introduces selected and reviewed Russian journal articles on astronautics translated by Dr. J. George Adashko of the ARS Staff. These translated Russian papers will appear quarterly in the JOURNAL through the auspices of ARS and the National Science Foundation, which by a grant supports the program. Presentation of ARS Russian translations in a separate part of the JOURNAL represents an attempt to keep burgeoning technical literature centralized, recognizable and easily accessible.

ARS JOURNAL quarterly translations will spotlight technically significant Russian work in astronautics. The scientist or engineer wishing to pursue his field exhaustively in Soviet literature, however, needs knowledge of its form and extent, and how and where it is available in this country.

For this reason, there is presented here a digest of a government booklet discussing the form, content and availability of Russian Literature—*Providing U. S. Scientists With Soviet Scientific Information*, Revised Edition, May 1959—prepared by the NSF Office of Science Information Services, and available in its entirety from that office on request. "Keeping Up to Date on Soviet Astronautics," by F. J. Krieger in the April 1959 ASTRONAUTICS, points out the importance of newspaper coverage of science in Russia, a subject not broached by the NSF booklet. Also, the booklet assumes that such material as unpublished or informal Russian research reports are not available to Western scientists.

The principal means for recording and disseminating the results of research in Russia are substantially the same as in this country, that is, chiefly periodicals and books. The USSR publishes three types of scientific periodicals: Journals which are the equivalents of our scientific and engineering journals, compilations of papers which we call proceedings or transactions, and bulletins much like our science news bulletins. The term "book," as used in the USSR, applies to any onetime publication, and includes preprints, reprints and pamphlets, as well as conventional books as we know them.

The core of the Russian technical literature and the means to its access may be summarized as follows.

PRINCIPAL RUSSIAN JOURNALS AND SERIALS. The Soviet output seems to be about 500 regular scientific and engineering journals and serials, plus about 20,000 science and engineering books per year. The most important journal series are those published by the USSR Academy of Sciences, which appear in several subject series, in particular *Doklady Akademii Nauk SSSR* (*Proceedings*) and *Izvestiia Akademii Nauk SSSR* (*Bulletin*). Aside from these, most of the journals deal with specialized fields, and are sponsored or published by ministries or institutions.

Moreover, there are three important review series, each published in individual subject series. These are:

1 *Uspekhi* (*Progress*) review journals. For example, *Progress in Physical Sciences*, three issues per year, which is available in translation from the American Institute of Physics at $20 per year. Reviews in these journals are not limited to Soviet research, but cover narrow subject areas in foreign literature as well.

2 *Voprosy* (*Problems*) series. For example, *Voprosy Raketnoi Tekhniki* (*Problems in Rocket Technology*) devotes each issue to a specialized aspect of the field, and consists mainly of articles translated into Russian from the world literature (U. S., English, German, French, etc.). This particular series is not being translated into English, but some of the other publications in the *Voprosy* series, e.g., Economics, Virology, etc., are.

3 *Itogi Nauki* (*Summaries of Science*), covering a number of different fields; issued by the All-Union Institute of Scientific and Technical Information.

TRANSLATION OF COMPLETE JOURNALS (IN ENGLISH). Currently, about 75 Russian journals in various fields of science are being translated in their entirety. The names, with tables of contents, are listed in *Technical Translations*, issued semimonthly by the Office of Technical Services, Department of Commerce, at a price of $0.60 each or yearly subscription of $12. These include translations by private organizations (e.g., International Physical Index, Inc., Consultants Bureau, Inc., Pergamon Institute, etc.), by professional societies (American Institute of Physics, Instrument Society of America, ASME, etc.), and by government agencies. The publication of these translations is often subsidized by the NSF so that a relatively modest price is made possible, i.e., about two or three times the Russian subscription price. Thus, the *Journal of Technical Physics* is about $12.60 per year in the original Russian and $25 per year in English for universities from the American Institute of Physics.

ABSTRACTS AND INDEXES (IN ENGLISH). There are four major abstract or index sources:

1 *Monthly Index of Russian Accessions*, published by the Library of Congress and available from the Supt. of Documents for $12 per year. Contains translated tables of contents of journals received.

2 Abstracts of complete journals, by issue, announced in the Office of Technical Services' *Technical Translations*. About 140 Soviet journals, as well as journals of other countries, are currently being abstracted by various agencies. Instructions on how to obtain journal abstracts are included. (See below for additional information on OTS-TT.)

3 *Scientific Information Report*, available from the Office of Technical Services, Department of Commerce. Published semimonthly, at a cost of $28 per year, the Report contains translated abstracts of important Russian papers, covering a wide range of science.

4 *Express Abstracts*, in different subject series, are published by International Physical Index, Inc. and Consultants Bureau, Inc. For example, *Automation Express* is available at $57.50 per year. A *Rocket Technology Express* may soon be available.

BIBLIOGRAPHICAL AND ABSTRACT SOURCES IN RUSSIAN. There are three major sources of abstracts and bibliographies in Russian:

1 *Referativnyi Zhurnal* (*Abstract Journal Series*). This

appears in 13 different subject areas (see Table 1), each issued monthly or semimonthly, subscription price $10 to $100 per year, according to the size of the particular series. Entire set covers about 2000 Soviet journals and serials and about 12,000 non-Soviet. It is roughly equivalent to *Engineering Abstracts, Chemical Abstracts,* etc., in the U. S.

2 *Letopis Zhurnal'nykh Statei* (*Chronicle of Periodical Articles*). A weekly bibliography, it covers most Soviet periodicals (including nontechnical journals), about 2200 articles per week. Price: $12 per year.

3 *Knizhnaia Letopis'* (*Book Chronicle*). A weekly announcement of books published in the USSR, it covers about 1300 book titles per issue.

As of 1958, the *Abstract Journal* series have been issued in two editions—the library edition, which combines the subject sections into one volume, and the individual subscriber edition, in which each series is divided into two or three narrower subject areas, similar to the *Biological Abstracts* published in the U. S., and made available by parts.

Besides the few major U. S. agencies mentioned thus far, what government and private sources supply Soviet publications in the original and in translation?

First, there are a number of book dealers in the U. S. which import a substantial supply of Soviet publications. These are listed in Table 2.

Then many, although not all, of the publications of individual Soviet institutes are available on an exchange basis. The Processing Department of the Library of Congress maintains a list of Soviet institutions with which the Library of Congress has established exchange relations. Some of the Soviet institutional publications, especially those with limited circulation, are available on exchange only. This material is usually limited to a narrow subject field, and is exchangeable for equivalent publications in the same subject field. Information about these is practically nonexistent, or available only long after the supply is exhausted. In cases like this, however, scientists corresponding with their counterparts in the USSR have been able to learn of forthcoming publications in time to forewarn the libraries of their institutions to effect an exchange.

Although no accurate data on U. S. library holdings on Soviet science are available, the *Monthly Index of Russian Accessions* contains a listing of U. S. libraries which currently receive publications from the USSR. A report, *Russian and East European Publications in American Libraries,* prepared by Melville J. Ruggles and Vaclav Mastecky for the Committee on Slavic and East European Studies of the Association of Research Libraries, also includes some information on scientific literature.

Occasional collections of translated papers in special fields have been issued from time to time by several Government agencies, but on no regular schedule. Examples of these are translations in the field of electronics put out by the Air Technical Intelligence Center (available through OTS) and a compilation on photosynthesis issued by the Atomic Energy Commission (AEC-TR-2156). Such collections have also been issued by some commercial firms—for example, the *Chemistry Collection* series by the Consultants Bureau, Inc. and *Russian Literature on Satellites* by International Physical Index, Inc.

In addition to these more or less formal publications, an enormous number of separate Soviet papers are translated by and for numerous Government and private agencies. These are prepared individually, usually in response to specific requests. Copies of most of these separate publications are available either through translation depositories or commercial translating agencies.

At present, there are two main translation depositories in the U. S.: The Special Libraries Association Translation Center, located at the John Crerar Library in Chicago, and the Office of Technical Services (OTS) Technical Information Division, Department of Commerce, Washington, D. C.

Table 1 Series of the *Referativnyi Zhurnal* (*Abstract Journal*)

Referativnyi Zhurnal	No. of issues per year	No. of abstracts per year	
		1957	1958
Astronomy and Geodesy	12	10,000	7,902
Biology	24	103,445	113,375 (est.)*
Biochemistry	24	27,023	33,207
Chemistry	24	79,039	84,041
Electrical Engineering	12(1957) 24(1958)	39,829 (est.)	70,224 (est.)
Geography	12	27,601	30,197
Geology	12	18,394	22,203
Geophysics	12	10,750	9,650
Machine Building	24	53,450	86,925 (est.)
Mathematics	12	9,035	10,925 (est.)
Mechanics	12	13,649	15,105
Metallurgy	12	25,562	25,579
Physics	12	31,850	28,970
		449,627	538,303

* Wherever estimated totals are given, the last issue giving the exact number for the year has not been received in the United States.

All the translations are listed, with abstracts of the articles translated, in *Technical Translations,* published bimonthly since January 1959, by OTS as a sequel to the previous SLA Translation Center publication, *Translation Monthly.* As already noted, copies of *Technical Translations* are available individually or on subscription from the Office of Technical Services, U. S. Department of Commerce, Washington 25, D. C., at $0.60 a copy or $12 per year. Microfilm copies of the translations listed are available from both the SLA Translation Center and the OTS Technical Information Division at nominal rates. Translations prepared by commercial translating agencies are also listed in *Technical Translations.* However, commercial translation agencies usually provide the necessary bibliographic information on available translations, but sell copies of the translations themselves. Information on where such translations are available is included in the listing.

The OTS Technical Information Division acts as a clearing house for information on monographs translated, in process of translation, or being considered for translation by U. S. Government agencies. Information from commercial sources is also being added.

Translated monographs are published in many different ways—by commercial publishers, university presses as supplements to journals, by the Government Printing Office and as Government scientific reports. The monographs translated by Government agencies and published by the Govern-

Table 2 Subject Indexes to *Referativnyi Zhurnal* (as of July 1958)

Series	Years for which there are subject indexes
Astronomiia i Geodeziia (Astronomy and Geodesy)	1953, 1954, 1955, 1956
Matematika (Mathematics)	1953, 1954, 1955, 1956
Mekhanika (Mechanics)	1953, 1954, 1955, 1956
Metallurgiia (Metallurgy)	1956, 1957
Mashinostroenie (Machine Building)	1956

ment Printing Office or issued as Government scientific reports are listed in *Technical Translations*. Copies of translations issued as reports are also made available through OTS.

A relatively new feature in the entire translation activity is the translation of abstracts from the Soviet abstract journal series, *Referativnyi Zhurnal*. Although this Soviet abstracting service covers the world scientific and technical literature, the abstracts translated are those prepared from Soviet original sources, often including papers published in other Iron Curtain countries. Others, wherever applicable, are included in regular U. S. abstracting journals.

Recently, an entirely new program has been undertaken in the Government under the provisions of the Public Law 480. In addition, the Library of Congress is developing programs that will provide for the analysis and evaluation of foreign books, periodicals and other materials to determine whether they would provide the U. S. with information of technical, scientific, cultural or educational significance; to register, index, bind, reproduce, catalog, abstract, translate and disseminate books, periodicals and related materials determined to have such significance; and to acquire such books, periodicals and other materials; and to deposit them in appropriate U. S. libraries and research centers. The translated material resulting from this program will be disseminated through established U. S. channels, such as scientific societies, OTS and other translation depositories.

Reviews of Soviet scientific literature in this country present an even greater problem than abstracts. Although exact data on review coverage of Soviet literature are not available, references to Soviet research in regular review papers are painfully lacking. The only comprehensive review service in the U. S. which includes separate reviews of Soviet research is *Annual Reviews*, published by Annual Reviews, Inc., Stanford, Calif. Otherwise, what little material has been issued in the U. S. that is in any sense "review" in nature, has consisted of a relatively few reports and analyses, frequently based on compilations of abstracts, which summarized the state of the art in specific Soviet fields. Invariably, these have been prepared to meet specialized needs and have received little or no general distribution.

Table 3 Dealers of Soviet Publications in the United States*

Victor Kamkin, Inc. 2906 Fourteenth St., N. W. Washington 9, D. C.	Moore-Cottrell Subscription Agencies, Inc. North Cohocton, N. Y.
Imported Publications and Products 4 West Sixteenth St. New York 11, N. Y.	Universal Distributors 52–54 West Thirteenth St. New York 11, N. Y.
Four Continent Book Corporation 822 Broadway New York 3, N. Y.	Stechert-Hafner, Inc. 31 East Tenth St. New York 11, N. Y.

* This information has been prepared by C. A. Brophy Jr., Battelle Memorial Institute, Columbus, Ohio.

The Soviets have expressed preference that subscriptions be placed with dealers in the respective countries rather than directly with Mezhdunarodnaia Kniga (International Book), Soviet agency for publication export.

To insure prompt receipt of Soviet periodicals it is best to place orders about two months before the beginning of the year. Many periodicals can be ordered any time during the year, but this procedure seems to cause delay of receipt. Subscription for some periodicals are accepted only at specific intervals throughout the year. For example, a subscription to *Knizhnaia Letopis'* (Book Chronicle) is accepted from January and July only. These details are explained in the Soviet publication announcement, "Newspapers and Magazines of the USSR for 1959."

Plans have now been made within the U. S. Government, as well as by societies and commercial agencies, to extend such review services. A new service, for example, is the *International Geology Review*, published by the American Geological Institute under NSF sponsorship. Although this is intended to cover world literature, at present it is heavily concentrated on the Soviet Bloc.

Moreover, there are no comprehensive studies on the status and development of Soviet science to provide the U. S. scientist with the necessary background to orient himself in current Soviet literature or for a visit to the Soviet Union. There are also no comprehensive evaluations of Soviet research and publications in any one subject field. Only brief internal surveys of the latter have been made, and these primarily for translation purposes.

Recently, however, a number of organizations have begun to plan activities in this area, and at least one such study is under way—the American Institute of Physics' Committee to Study Publishing Problems in Physics assessment of the magnitude of the world's physics literature, including that of the Soviet Union, as sponsored by NSF.

There are also few studies in existence which provide information on matters closely related to or affecting Soviet scientific development, such as organization of science in the USSR, the philosophies of Soviet science, and its directions and rate of its growth. A number of smaller studies of this kind have been prepared by various Government agencies. These studies are usually treated as unpublished research reports, and as such are announced in the monthly journal *U. S. Government Research Reports*, issued by OTS.

Many of the general reference sources in science and technology, such as the *Bibliography of Agriculture*, issued by the Department of Agriculture, and the *Index of Medical Literature*, issued by the National Medical Library, also contain Soviet information. The reference aids pertinent to providing the U. S. scientist with Soviet scientific information can be divided into four major categories:

1 Bibliographic, such as bibliographies of original publications or bibliographies of translations. A major bibliographic source of Soviet publications is the *Serial Publications of the Soviet Union, 1939–1957: A Bibliographic Checklist*, issued by the Library of Congress in 1958. It lists publications in all subject fields, and contains a subject index.

2 Linguistic, such as dictionaries or transliteration tables. The problem of the need for Russian-English dictionaries in science and technology in the U. S. is presently being studied by New York University in science and by the Engineers Joint Council in technology. The results of these studies are expected within the near future. The Committee on Bibliography and Transliteration of the National Federation of Abstracting and Indexing Services is presently examining possible standardization of transliteration among the U. S. abstracting services. Possible standardization of transliteration is being discussed also by a Government committee headed by the Library of Congress.

3 Guides to information sources in the Soviet Union. The basic source of scientific information, of course, is the institution or the laboratory where the research is being done. Since in the Soviet Union many of these institutions publish their own research results, a listing of Soviet research institutes is a basic guide to Soviet scientific information. The only such list published in the U. S. at present is the *Directory of Medical and Biological Research Institutes of the USSR*, issued by the National Institute of Health in 1958. Data are being gathered for a comprehensive list of Soviet research institutes, but the date of publication has not been announced. Other sources for scientific information in the Soviet Union are the scientific and technical publishing houses, book dealers and libraries. *Publications and Publishing in the USSR* by B. Gorokhov, which describes such sources, is in publication.

4 Guides to information sources in the U. S. A source file is presently being established at the Science and Technol-

ogy Division of the Library of Congress under NSF sponsorship. This source file will contain references to reports and studies, both in Russian and in English, on Soviet science and information, such as reports on visits to the USSR by U. S. scientists. In addition, the Special Libraries Association has recently published a guide, *Translators and Translations: Services and Sources*, which was compiled at the Georgia Institute of Technology. This contains a directory of translators and translation pools throughout the world, and a bibliography of translation indexes.

Finally, *Providing U. S. Scientists With Soviet Scientific Information*, Revised Edition, May 1959, is available from the Office of Science Information Service, National Science Foundation, Washington 25, D. C.

Measurements of Thermodynamic Parameters of the Stratosphere With Aid of Meteorological Rockets

E. G. SHVIDKOVSKII

The Soviet Union's program of rocket investigations of the upper layers of the atmosphere provides also for the study of the thermodynamic parameters of the stratosphere (the region of the atmosphere extending from the tropopause to the region of the temperature minimum, lying at an altitude of approximately 80 km), both in the polar regions of the Arctic and Antarctic and the medium latitudes of the Soviet Union. The Arctic investigations were carried out on Heiss island (the Franz Josef Land Archipelago), and the Antarctic investigations of the lower and middle stratosphere were carried out on the diesel electric boat "Ob'" which has been engaged in various projects in the International Geophysical Year program.

THE ACCUMULATED data of the experimental investigations have not yet been completely interpreted. In particular, we do not include here the results obtained on the "Ob'." This communication is therefore of a preliminary character.

The plan of the rocket experiment, undertaken during the IGY investigation of the atmosphere, covers the following general phases:

(a) The temperature of the atmosphere is measured with resistance thermometers made up of thin tungsten wires.

(b) The pressure is measured with manometers modified to accommodate the necessary pressure range.

(c) The measuring elements of the instruments are mounted on a long thin rod projecting from the nose of the rocket. The remaining equipment required for the measurement is placed in various segments in the nose of the rocket.

(d) At a fixed altitude, the nose with the measuring apparatus separates from the body of the rocket and is parachuted down to Earth. The principal measurements are usually carried out during the descent. The readings of the instrument are transmitted to Earth by radio telemetry and are recorded on photographic film.

The theory of the methods used to measure temperature and pressure in this experiment involves an extensive set of problems pertaining to the interaction between the instrument and surrounding medium. This theory makes it possible to calculate the parameters of the free atmosphere from the actual readings of the instruments, which are greatly affected by the motion of the nose of the rocket. Here the interaction between the instrument and the atmosphere varies upon going from conditions corresponding to free molecular flow, through flow with slip, to conditions of continuous gasdynamics.

The processing of the telemetering data yields the values of the pressure and temperature dynamics as functions of the time. By using the equation of state of an ideal gas, the barometric formula, the laws of molecular dynamics and gasdynamics, and the results of preliminary laboratory experiments, it is possible to determine the pressure, temperature and density of the free atmosphere as functions of the altitude. Other important factors, such as the radiation transfer and the deviations from thermal and dynamic equilibrium between the instruments and the directly adjacent gas, are also accounted for here.

The experimental procedure and the procedure for the processing of the data does not require in principle that the trajectory of the nose of the rocket be tracked. This procedure is quite suitable in practice for the accumulation of systematic data on fields of thermodynamic parameters of the free atmosphere provided the altitude is restricted to the central portion of the stratosphere.

If the upper portion of the stratosphere is investigated, however, it is necessary to track the trajectory, in view of the increasing influence of the rarefaction of the medium, which

Translated from *Iskusstvennye Sputniki Zemli* (*Artificial Earth Satellites*), no. 2, USSR Acad. Sci. Press, Moscow, 1958, pp. 10–16.

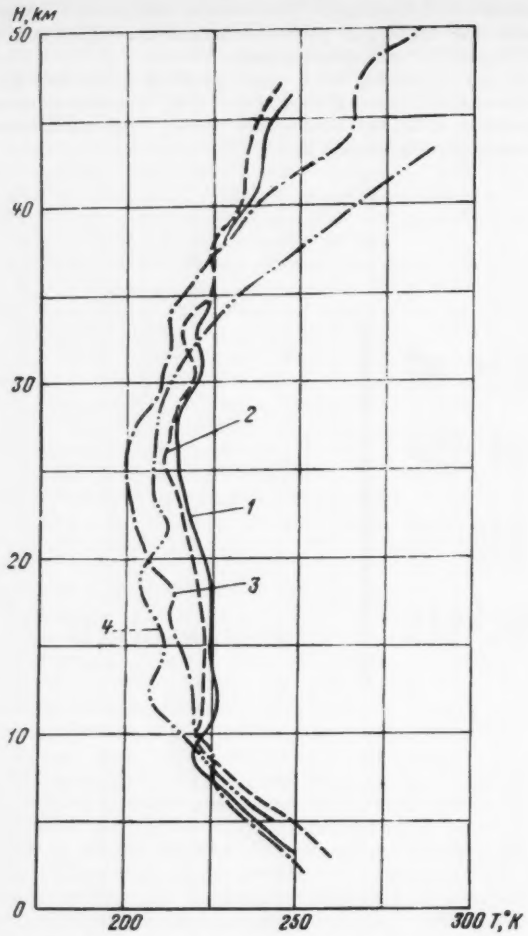

Fig. 1 Altitude distribution of temperatures above Heiss Island: 1—Oct. 1957; 2—Nov. 1957; 3—Dec. 1957; 4—Jan. 1958

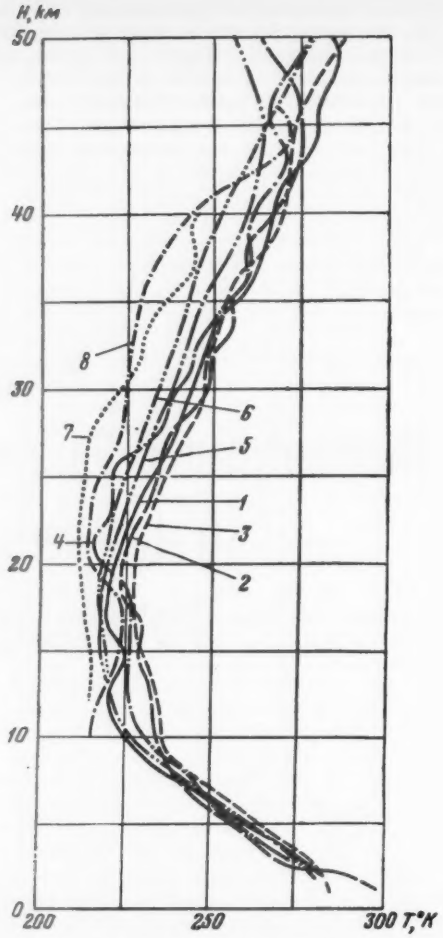

Fig. 2 Altitude distribution of temperatures in middle latitudes: 1—May 1957; 2—June 1957; 3—July 1957; 4—Aug. 1957; 5—Sept. 1957; 6—Oct. 1957; 7—Dec. 1957; 8—Feb. 1958

leads to a sharp increase in side effects. Otherwise, there are numerous experimental errors in the determination of the state of the atmosphere. In these cases the trajectory is tracked optically and by radio methods.

Measurements in the Free Atmosphere

Even before the start of the IGY, measurements were made of the parameters of the state of the free atmosphere up to approximately 80 km in the middle latitudes of the Soviet Union. Since these results have been published[1] in the form of averaged distribution curves for the temperature, pressure and density and in the form of corresponding tables for the fall-summer season, we shall dwell on them only briefly.

It must be noted first that in all the ranges of altitudes from the surface of the Earth to 80 km, one observes a good agreement between the readings of the thermometers and the temperature of the atmosphere as computed from the manometer readings. Such a comparison was made by tracking the trajectory of the nose of the rocket. This agreement served as the experimental basis for a program of investigations of the lower and middle atmosphere in which no tracking of the trajectory was necessary, thus considerably simplifying the experiments. The reliability of the data obtained is confirmed by the fact that the error of any individual temperature measurement at 75–80 km did not exceed ±15 deg. Our temperature curve is quite close to the well-known curve for the distribution of the temperature in the stratosphere, proposed in the U.S.A., but differs somewhat from the latter both in the altitudes and in the values of the temperature at the principal extremal points.

Seasonal Variations of Temperature

In the subsequent portion of this communication we propose to examine the character of the seasonal variations of the temperature field and the middle and low atmosphere, making use of results of rocket investigations in the Arctic and in the middle latitudes of the USSR. The following material therefore covers the altitude range up to 45 or 50 km.

We do not give the pressure-distribution curves because they do not present an easily interpretable picture, but note that the general character of these curves gives grounds for stating that the pressure diminishes from summer to winter. The changes in pressure are somewhat more strongly pronounced in the north than in the middle latitudes.

Figs. 1 and 2 give the temperature fields in various months on Heiss Island and in the middle latitudes. The analysis of the data leads to the following tentative conclusions:

(a) The temperature of the lower stratosphere in the region between 20 and 25 km diminishes from the summer to the winter months. The lowest temperatures occur in December or January.

[1] *Meteorologiya i Gidrologiya* (*Meteorology and Hydrology*), no. 8, 1957.

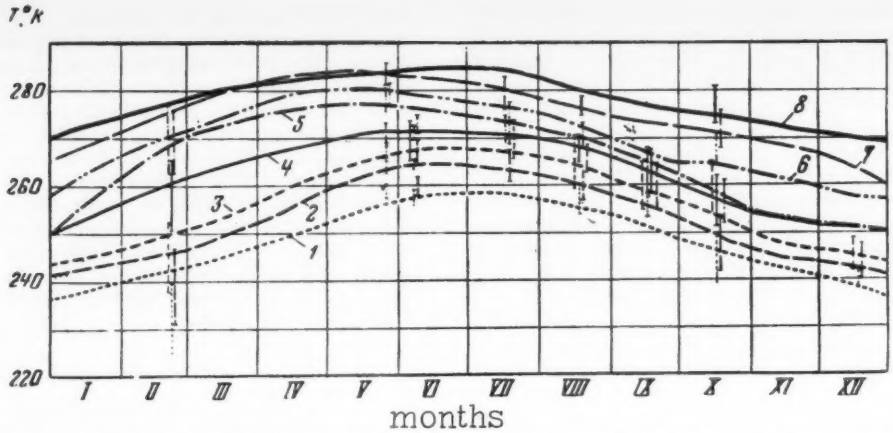

Fig. 3 Annual course of the temperature in the stratosphere (middle latitude): 1—36 km; 2—38 km; 3—40 km; 4—42 km; 5—44 km; 6—46 km; 7—48 km; 8—50 km. Abscissa, months

(b) This law breaks down at 40 or 50 km. Here we find a region where stratosphere temperature has a maximum, which, as can be seen from the curves, is higher in the north than in the middle latitudes.

(c) If we compare the curves for the northern and middle latitudes we note that the approximately isothermal layer extends to a higher altitude from the tropopause in the polar regions than in the middle latitudes. Furthermore, in the polar region, the height of the upper level of the layer of the atmosphere, which has a positive temperature gradient, rises from 26 km in October to 32 km in January. In the middle latitudes the corresponding change is from 21 to 26 km.

It is possible that these circumstances are connected with the fact that the temperature of the middle stratosphere is affected in the polar region by the end of the polar night, so that the January temperature curve for the latitude of Heiss Island reflects also the heating of the ionosphere by the sunlight. Consequently, in the north the gradient of the temperature, in the region up to the stratospheric temperature maximum, changes from 1.5 deg per km at the beginning of the polar night, to 5.5 deg per km at its end. In contrast to the above, the temperature gradient in the same region remains almost constant in the middle latitudes and amounts to approximately 2 deg per km.

The fluctuations of the temperature in middle latitudes near the stratospheric maximum, range from 260 to 280 K, and in the north they probably range from 270 to 300 K. Thus the middle stratosphere in the northern regions is not only somewhat warmer than in the southern ones, but the seasonal fluctuations of the temperature in the middle stratosphere are more strongly pronounced in the areas beyond the Arctic circle than in the middle latitudes.

As evidence that these variations of the temperature field, at any given place, are seasonal rather than synoptic, let us call attention to the character of the annual variation of the temperature at various altitudes in the region of the stratosphere. Fig. 3 shows the corresponding results for middle latitudes. In the lower stratosphere, at altitudes of 26 to 34 km, a clearly pronounced temperature maximum is observed during the summer. These curves exhibit an annual cycle of oscillations. For this region the amplitude of the oscillation is approximately 13 deg. As the altitude increases, the amplitude diminishes slightly to 10 deg in the region of 45–50 km. One can notice here that while the temperature maximum in middle latitudes is in fairly good agreement with the summer solstice at 45–50 km, it occurs in July at 26–34 km.

Since the results given for each month are not average

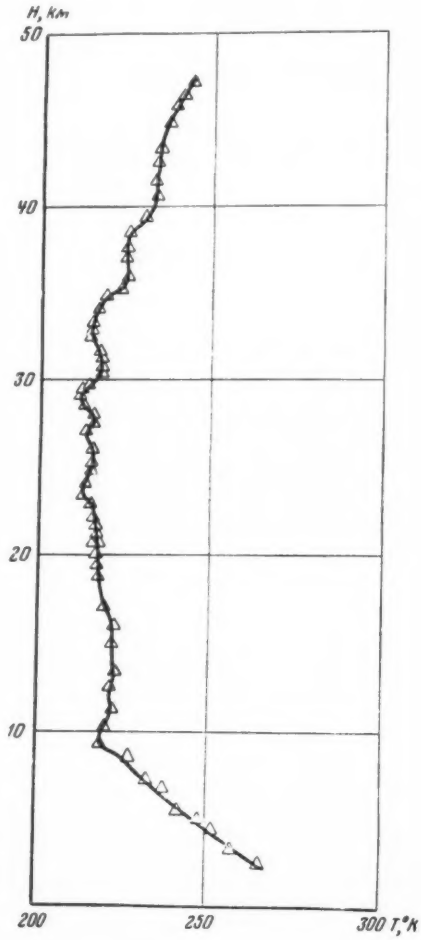

Fig. 4 Temperature field above Heiss Island as obtained by rocket soundings. Launching of Nov. 4, 1957 at 10:55 a.m. Temperature at Earth surface T_0 = 254.6 K. Data obtained during launching

values obtained from a very large number of observations, as is usually done in meteorology, but retain to a considerable degree the features of individual measurements, the observed annual fluctuations in the temperature in the stratosphere cannot be purely synoptic in nature, but should reflect the seasonal variations of the state of the atmosphere.

From Fig. 4, which shows the results of individual rocket soundings, it is clear that the temperature field in the lower and middle stratosphere can have a fine structure. The curve presented was obtained on Heiss Island. A similar structure of the temperature distribution has been frequently observed in the individual launchings of rockets. Although usually the observed temperature variations are small and reach 10 or 15 deg and rarely 20 deg, they are outside the measurement errors of the experiment. The cause of such a temperature stratification may be a large-scale turbulence, but the temperature stratification may have a more stable character. In any case, the experiment suggests that the concepts of simple and double tropopause are too approximate. Actually, the temperature field above the tropopause has in many cases a more complex character, as a consequence of many extrema in the altitude function.

The above features of the temperature field of the lower and middle atmosphere naturally require further refinement, which can be made only on the basis of a large number of experimental data and a more detailed analysis of these data. There is no doubt, however, that they contain many problems worthy of serious attention.

Research on the Flight of a Living Creature in an Artificial Earth Satellite

V. N. CHERNOV
and V. I. YAKOVLEV

DURING the last decade Soviet and other scientists have conducted many experiments with living organisms in rocket flight into the upper layers of the atmosphere. The data acquired clarified the nature of biological phenomena occurring under conditions approaching flight into cosmic space. With the rocket flights it was possible to study the influence on the organism of factors which could not be reproduced under conditions on Earth (weightlessness, radiation of various sorts, etc.).

A further step in this direction is the utilization of artificial satellites for biological experiments. In contrast to high altitude rockets which are generally employed for exploring the upper layers of the atmosphere and supply scientific data on brief flights by animals, artificial satellites permit us to study the behavior and condition of living organisms throughout the protracted period of the satellite's orbital motion. Therefore with the aid of artificial satellites conditions can be created which, from the biological point of view, approach (if they do not duplicate) the conditions of cosmic flight.

There are several special difficulties connected with carrying out scientific investigations involving a satellite.

First, just as in conducting experiments with high altitude rockets, there is the necessity for strict economy in the weight of all equipment, its cubage and electrical power requirements. Further, since we still have no devices that guarantee the safe descent of an animal and the scientific equipment, we are faced with the complicated problem of the recording and transmission of instrument data on the behavior of the animal and the pertinent hygienic and physiological index.

It can be said that the biological research with satellites takes two basic forms. First, there is the development of equipment and a system of regulating its functioning which will guarantee conditions necessary for the life of the animal at all stages of the satellite's flight. Second, there is the study of the biological effects of the factors of cosmic flight.

Unlike the high altitude rockets used in biological research, artificial satellites permit us to study the effects of protracted influence of acceleration, noise and vibration from the launching of the satellite until the moment of its entrance into orbit, and the effects of the state of dynamic weightlessness during orbital flight. The adequate study of the influence on the animals of a series of other factors, especially cosmic radiation, will be realized only with the launching of satellites which permit the equipment and animals to be safely recovered on Earth.

Obviously the conducting of experiments over a number of days demands the construction of equipment which can automatically sustain satisfactory living conditions for the animal during flight, supply it with the necessary amount of food and water and also dispose of excretions, etc. Also the experimental equipment must insure the uninterrupted recording of the scientific data and their transmission to the Earth receiving station.

Finally, such research demands the special preparation and training of the experimental animals, their careful preliminary inspection, and particularly their habituation to the effect of various flight factors.

The investigators' efforts were directed to the preparation and inspection of the animals and also (in cooperation with the instrument makers) to the devising and construction of every means necessary to preserve proper conditions for the animal during flight.

Cabin for the Animal, Its Equipment and Experimental Apparatus

Demands for economy in weight and size influenced the construction of the airtight cabin for the animal. The specifications for the airtight cabin were especially exacting, since

Translated from *Iskusstvennye Sputniki Zemli* (*Artificial Earth Satellites*), USSR Acad. Sci. Press, no. 1, Moscow, 1958. Translated by Prof. Donald A. McKenzie, University of New Mexico, Albuquerque.

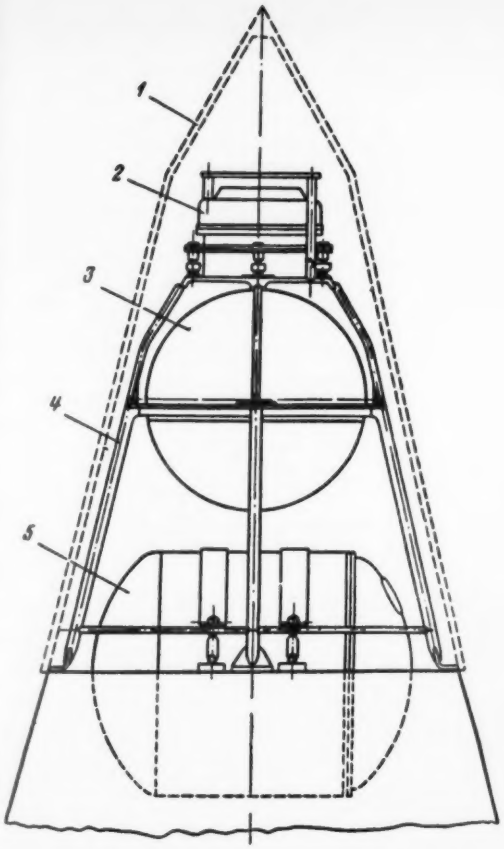

Fig. 1 Plan of the disposition of the apparatus and the airtight cabin for the animal in Sputnik II: 1 protective cone; 2 instrument for the study of ultraviolet and x-rays from the sun; 3 container with radio apparatus; 4 reinforced frame for strengthening the apparatus; 5 airtight cabin for the experimental animal

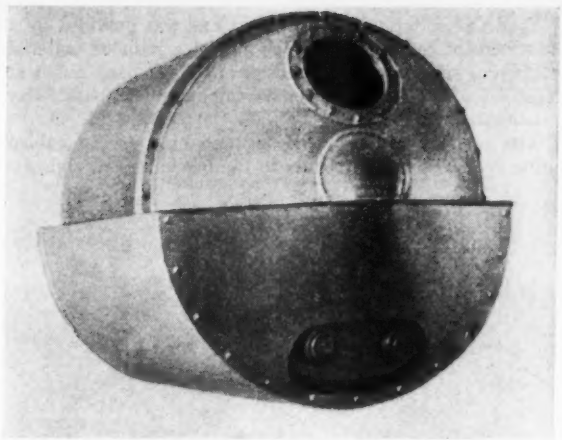

Fig. 2 External view of the airtight cabin for the experimental animal

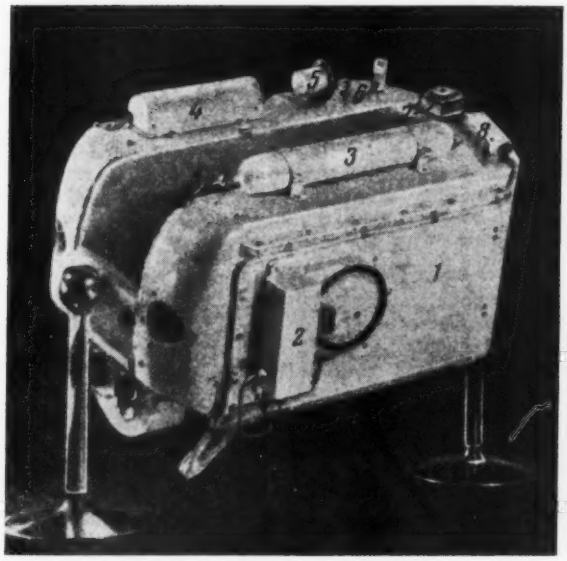

Fig. 3 General view of the demountable equipment of the animal's airtight cabin (one version): 1 box for the regenerative installation; 2 automatic water dispenser; 3 reservoir for the compressed air supplying pressure for the water-automat; 4 automat for measuring the animal's blood pressure; 5 indicator of air pressure in the cabin; 6 cabin air temperature indicator; 7 indicator registering the animal's movement; 8 a block including the indicator wires (circuits)

it had to protect the animal from extreme degrees of atmospheric rarification.

The airtight cabin, re-enforced by a sturdy frame (Fig. 1) was a cylindrical container 640 mm in diameter and 800 mm in length provided with a removable cover with an inspection hatch.

The removable cover was fitted with airtight joints through which electrical wires were introduced. The cabin for the animal was constructed of an aluminum alloy, and its outside surface was of the same material (Fig. 2). The container was able to accommodate the experimental animal and the necessary equipment without waste of space.

The equipment of the airtight cabin for the animal on Sputnik II consisted of installations for air regeneration and for temperature regulation in the cabin, troughs with a supply of food, a sanitary arrangement and a set of medical apparatus (Fig. 3).

The installation for air regeneration contained regenerative substance in the form of highly active chemical compounds. The regenerative substance absorbed the CO_2 and water vapor exhaled by the animal and released the necessary amount of oxygen. The ordinary supply of the regenerative substance filled the animal's oxygen requirement for seven days. Duplicate fractional horsepower motors provided ventilation for the regenerative equipment. The functioning of this equipment was regulated by a bellows pressure relay which, with the rise of barometric pressure in the cabin above 765 mm, shut off the main activity of the regenerative material.

The apparatus for the regulation of the air temperature consisted of a special heat conducting screen to which was conveyed the air from the animal and of a twin thermo relay which shut off the electric ventilator of the vent when the air temperature in the cabin got above +15 C (Fig. 4).

During the flight of the satellite the functioning of the above mentioned installations was checked by the readings of a potentiometric pressure indicator (working in a range of 200 to 1000 mm of mercury) and of wire rheostat temperature indicators situated inside and on the casing of the cabin.

Food and water supply for the animal was provided by a 3-liter metal container. The supply of gelatinous material containing the necessary amount of water and basic nutritive ingredients was computed for a completely adequate 7-day ration.

The sanitary arrangement consisted of a special rubber urine and feces receiver fitted to the pelvic region, and of a special "bodice" harnessed to the shoulder strap of the animal to assure a better fit of the receiver to his body (Fig. 5). By means of a rubber tube in the receptacle the animal's excretions were drained into an airtight "latrine" reservoir. For the purpose of deodorization and the absorption of liquid fractions the reservoir contained a certain amount of activated carbon and specially dried moss.

The arrangement for fitting the animal in the cabin—a light, woven garment and small restraining metal chains—restricted the animal's mobility in the cabin, while permitting him to stand, to sit, to recline and also to move a little back and forth along the longitudinal axis of the cabin.

The medical apparatus included an amplifying switching unit with two amplifiers and a set of pickups for registering the physiological functions and the motor reactions of the animal (Figs. 6 and 7).

Our research program provided for registering data which showed how the breathing and circulation of the experimental animal were functioning, namely: Frequency of systole, by a recording of the biopotentials of the heart (electrocardiogram); respiration frequency, by measurement of the perimeter of the thorax; the amount of the maximum arterial blood pressure, using the oscillation method to record the periodic contraction of the carotid artery which had been exteriorized by a special sleeve.

In order to judge the motor behavior of the animal we used an "actograph" with a motion indicator.

For recording the biopotential of the heart, indwelling silver electrodes were inserted under the dog's skin. The three-stage amplifier of the channel hooked into the amplifier-switching unit (coefficient of amplification—3000).

For recording the frequency of respiration we used strain gage indicators in the form of belts attached to the animal's thorax. The resistance of the indicators was from 0.3 to 25 kohm. The pickup was fitted in one branch of the potentiometric circuit. For greater operative reliability of the respiration pickup we used two indicators, hooked in parallel to the measuring circuit.

For registering the maximum blood pressure we used an oscillation pickup which, by means of a piezocrystal, transformed the pulsations of the walls of the carotid artery into fluctuations of electrical current. The amplifier of the oscillation channel was analogous to the amplifying circuit of the electrocardiogram and was housed in the same amplifier-switching unit. The automatic device responsible for air pressure in the cap consisted of a cylinder, the volume of

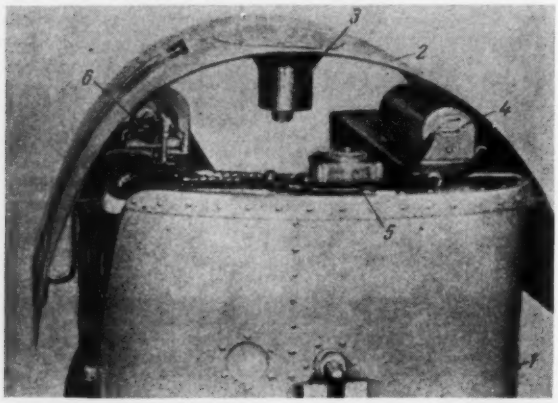

Fig. 4 Demountable equipment of the airtight cabin of the animal (rear view): 1 regenerative equipment container; 2 screen of the heat regulating device; 3 electric ventilator of the blower with air distributor; 4 device for measuring the animal's blood pressure; 5 indicator of the animal's motion; 6 indicators of temperature and air pressure in the cabin

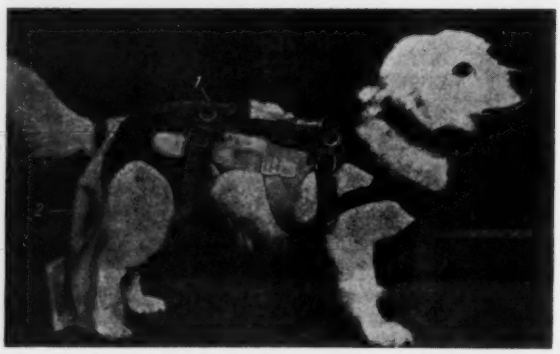

Fig. 5 Dog equipped with sanitary arrangement and restraining garments: 1 restraining cloth suit; 2 rubber sanitary arrangement

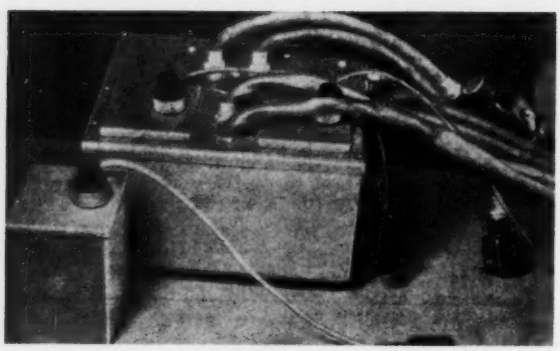

Fig. 6 Amplifier-switching set for medical apparatus

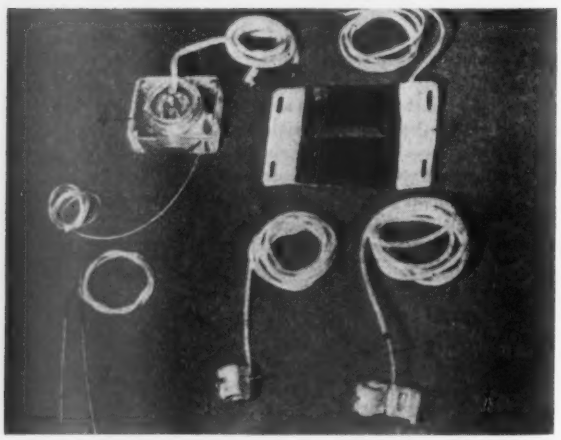

Fig. 7 Components of the medical apparatus: 1 respiration indicator; 2 blood pressure indicator; 3 electrocardiogram electrodes; 4 motion indicator

which (and consequently the air pressure) was changed by the motion of a piston operated by a special small electric motor.

The motion of the animal was registered by a potentiometric component which permitted us to determine the presence, the duration and amount of movement.

The controlling operational impulses and the power supply from special batteries were connected to the amplification block; the latter also supplied the output parameters for transmission to the radio-telemetric system. The diagram of equipment and apparatus setup in the airtight cabin is shown in Fig. 8.

All the fittings and apparatus in the cabin were checked for their functioning under conditions of vibration and acceleration; they were also subjected to protracted testing in the laboratory.

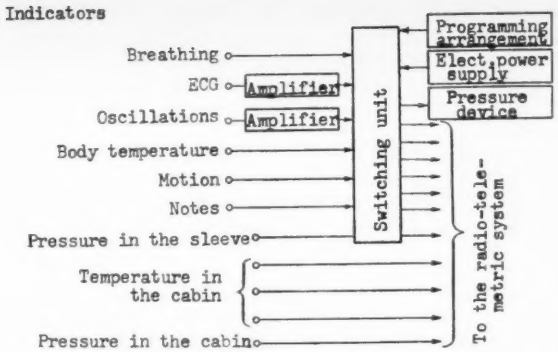

Fig. 8 Block diagram of apparatus. ECG—indication of channel of electrocardiogram

Preparation and Training of Experimental Animals

It could be assumed that for protracted experiments in satellites, dogs would prove just as suitable experimental animals as they had in our high altitude rocket research. However in the one case, a matter of mere hours was involved, and in the other, several days, during which the animal had to stay in a small cabin. It was therefore necessary to devote much attention to developing a system of preparation and gradual training of the dogs for a protracted and confined sojourn in a very small cabin.

First, the animal was made accustomed to the furnishings of the laboratory and to confinement in special cages. The size of these cages was gradually diminished, finally approximating that of the airtight satellite cabin designed to house the animal. Since the satellite cabin measures $600 \times 220 \times 450$ mm, we chose small dogs weighing about 6000 gm. The time the animals spent in these cages was gradually increased from some hours to 15 or 20 days. At the same time the animal was made accustomed to the wearing of special garments, a sanitary arrangement and contrivances for registering physiological functions (Fig. 9). During the training course an individual check of all equipment was made. We considered this phase of our work complete when the fully equipped animal had, without agitation, spent 20 days in its confining cage and exhibited no general or local bad effects.

Under these conditions there were the expected difficulties in training the animal to defecate and urinate. In the case of "untrained" dogs, the protracted limitation of their freedom of movement resulted in the retention of the stool and urine, and this, as a rule, was accompanied by restlessness, and sometimes by a deterioration of the general condition. The use of various pharmacological remedies (laxatives) gave no reliable results. Only a gradual and consistent training program insured a normal functioning of the animal's organs.

The next stage in the training was the habituation of the animal to a protracted sojourn in the airtight cabin. In this cabin was placed all the equipment essential for the projected flight of the satellite. The dogs were made accustomed to the furnishings of the cabin, to automatic feeding and to the noise of the operating assembly. The animals finally came to ignore the many sources of irritation connected with the operation of the apparatus, equipment and airtight cabin. During this period we carried out tests on the cabin equipment and our measuring devices which resulted in significant improvements.

The preparatory period included various operations on the animals for our research purposes. In order to record blood pressure we had to bring the whole carotid artery out to the cutaneous area of the neck. In order to make electrocardiograms, indwelling silver electrodes were introduced under the skin of the thorax in the area of the fifth intercostal. In the post-operational period we had to get the animal used to the cutaneous loop with its inserted artery.

It was no simple problem to provide food and water for the

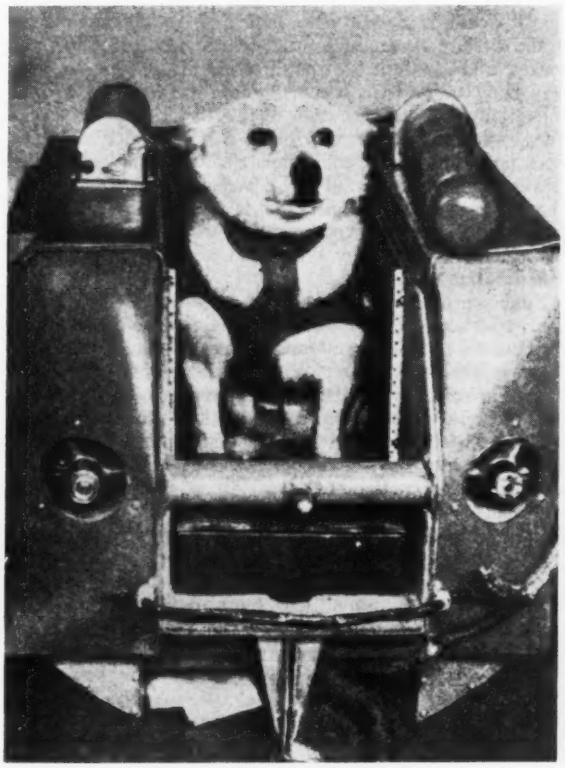

Fig. 9 Dog during training

experimental animal during its protracted isolation in the airtight cabin. It was not only necessary to develop and check various feeding devices for the preservation and dispensing of food, but we had also to determine the actual needs of the experimental animals with regard to caloric and general food composition, as well as their energy expenditure and water consumption. The Douglas-Holden method was used to determine the animal's expenditure of energy. It was indicated that the energy requirements of the animals varied within the limits of 400 to 650 kcal per day.

On the basis of these figures, test formulas of nutrients were devised and checked in numerous laboratory experiments. Completely satisfactory results were achieved with a dog food consisting of 40 per cent bread crumbs, 40 per cent powdered

meat and 20 per cent beef fat. One hundred gm a day of this pressed food supplied the needs of dogs weighing up to 7000 gm during the experimental feeding period of 20 days.

A study of the water consumption on this feeding regime showed that the dogs needed an average of 120 ml and not more than 200 ml per day.

We considered the possibility of employing a combined food mass in the form of a gelatinous mixture containing, besides the basic nutrients, a sufficient quantity of water and agar-agar to give the necessary mechanical consistency to the mixture. This process proved convenient and was used thereafter in the flight experiments.

After the animals were trained to the conditions of protracted confinement in the airtight cabin and all our protective measures and our experimental apparatus had been repeatedly tested, we could proceed to the next stage of the work.

We were very much interested in determining the stability of the animals under the effects of various flight factors, such as acceleration, noise and vibration. It was to be assumed that it would be most advantageous if the animal was placed in the satellite in such a way that the longitudinal axis of the rocket, and consequently the direction of acceleration, corresponded to the "chest-spinal" line of the animal. The toleration toward acceleration in this direction ("the transverse") is, as we know, very high. However, our literature does not contain any complete data about the protracted (several minutes) action of such "transverse" acceleration on the canine organism. Therefore, it was necessary to carry out several series of experiments in which we deliberately chose more than usually severe conditions both as to rate and duration of the acceleration.

Similar problems arose too in the investigation of the animals' resistance to vibration. In studying the effect of vibration, we were primarily interested in the resistance and finally in the individual reaction peculiarities of the different animals as well as concrete physiological changes due to vibration.

We carried out our experiments using laboratory stands which permitted us to develop acceleration and vibration approximating the accelerations and vibrations occurring during the real motion of the satellite.

In each instance there were two series of investigations. First, there was the conditioning of the animals, the eradication of their first tentative reactions to the equipment. Then we studied directly the influence of vibrations and accelerations and the resistance of the animals to their effect.

The first training tests in our series of experiments on the physiological influence of vibration were mainly devoted to the influence of sound, which was generated by the motors of a vibration stand. Under the influence of sound, the frequency of the animals' heart contractions increased one and one-half times, the respiration frequency was doubled and the blood pressure increased by 15 to 20 mm Hg. At the end of the conditioning experiments, the changes in these indexes did not exceed the limits of the usual physiological variations.

The conditioning was considered finished when the changes in the physiological indexes were insignificant and the general level of physiological indexes was not essentially different from the level prevailing before the conditioning.

The behavior of the animals (experiments were made on seven dogs), and the character and degree of change in their physiological functions while they were subjected to vibrations, were in all cases essentially the same. The animals satisfactorily stood the short-term action of general "transverse" vibrations. There were no noticeable variations in the behavior or general condition of the dogs. The vibrations caused a considerable increase in the frequency of the systole (almost double) and a moderate increase in the maximum arterial pressure (up to 30 to 65 mm Hg.). The changes noted had a transient character. The indexes of physiological functions involved returned to their original levels 5 min after the cessation of the vibration.

Our experiments indicated that there were no essential differences in the behavior and general conditions of the animals when they were subjected to sound alone or to a combination of sound and vibrations (with "vibration loads" up to 10). Changes in the functional indexes of the cardio-vascular and respiratory systems proved the same although differences in the expression of reaction were noted. The vibration caused greater functional changes in the organisms than did the sound.

In the next series of experiments, we studied the influence on the animals of changing velocities of centripetal acceleration acting in the chest-spine direction (2 to 10 "overload" for 6 to 15 min).

The results of the experiments (carried out on 14 dogs) showed that the behavior of the animals during the period of "overloads" was relatively calm. When the centrifuge began to rotate, the animals exhibited adaptational reactions accompanied by motor excitation. With the increase of the acceleration some of the animals calmed down while others showed a noticeable restlessness.

All the animals preserved the freedom of motion of their heads and bodies only up to a certain amount of acceleration. Then they were pressed to the surface of their rack but showed no noticeable restlessness. During the period of rotation an increased saliva excretion was noted which persisted for some time after the rotation stopped.

The frequency of systole in the animals increased quickly from the very beginning of acceleration, and exceeding the normal frequency by 1.5 to 2 times remained (with certain variations) at this level throughout the whole period of acceleration.

The frequency of respiration at the beginning of the rotation of the centrifuge increased generally by 1.5 to 2 times as compared with the initial frequency. With the increase in acceleration, the body of the animal was pressed more tightly against the surface of the rack, and as a result the respiratory action of the thorax was rendered more difficult; the breathing became more frequent and superficial. Throughout the whole period of acceleration the respiratory frequency exceeded the norm by 1.5 to 3 times.

The magnitude of maximum arterial pressure increased at the beginning of acceleration by 50 to 80 mm Hg and remained at this level throughout the whole acceleration period.

The assembled data showed that the effect of varying "transverse" accelerations, while accompanied by definite changes in the animals' behavior and the functioning of the cardio-vascular and respiratory systems, was satisfactorily tolerated by the experimental animals. As a rule, within 5 to 10 min after the cessation of acceleration, respiration and circulation returned to normal. During the subsequent observation period no deterioration in the animals' health was observed.

It was also important to determine in what measure variations in the hygienic properties of the environment may exert an influence on the condition of animals over a protracted period in the small airtight cabin.

It was of basic importance to clarify the admissible limits in the variations of temperature and of water and oxygen concentration in the cabin. Our work furnished data necessary for the regulation of the airconditioning system and the establishing of the maximum admissible concentration of oxygen at close to normal barometric air pressure.

Thus the result of all the preparatory labor was the development of the airtight cabin, its equipment and the experimental apparatus, and also the preparation of the experimental animals for the flight experiment. During the course of the experiments the assembled data indicated that animals would withstand a protracted stay (up to 20 days) in the airtight cabin as well as the effects of vibration, noise and acceleration.

We could thus proceed to the preparation and execution of experiments using the satellite itself.

From among the 10 animals that had gone through the

complete preparatory training we chose "Laika" for the final experiment, a female about 2 years old and weighing 6000 gm.

Results of Research With the Satellite

The individual steps of the experiment were different from one another and characterized by the action of different factors on the animal's organism.

For this reason it will be expedient to examine the results of the experiment with regard to three basic periods: The preflight period; the launching of the rocket and the satellite's escape into orbit; the orbital flight of the satellite.

The Preflight Period

This period includes the time from the moment of the animal's entrance into the airtight cabin to the launching of the satellite.

The conditions of the animal's stay in the airtight Sputnik cabin were completely satisfactory and were essentially the same as those which prevailed during the lengthy laboratory experiments with the animal. During the preflight period Laika's behavior as well as the indexes of the functioning of the cardio-vascular and respiratory systems in no way differed from the ordinary and did not exceed the observed normal limits.

The Launching of the Satellite

The launching (Nov. 3, 1957) involved a very high velocity which increased considerably from moment of launching to entrance into orbit. The acceleration of the motion of the satellite was several times the acceleration of the force of gravity. There was a corresponding increase in the apparent weight of the animal. Since the animal was situated perpendicular to the axis of the carrier rocket, the acceleration acted in the chest-spine direction (the direction in which the animal withstands an excess "weight" more easily). Simultaneously with acceleration the animal was subjected to the vibration and noise of the operating motors; the indicators of environmental conditions in the cabin showed the assigned values.

On the basis of the telemetered information received from this part of the flight and of the laboratory data, we may say that at the height of the acceleration the dog was pressed against the cabin rack but did not exhibit any sort of perceptible motor disturbance.

Immediately after launching the frequency of systole increased about three times as compared with the initial frequency. Later, when the acceleration was not only continuing but even increasing, the systolic frequency decreased. From the analysis of the electrograms no pathological signs at all were observable. The observed pattern was merely characteristic for a heightened frequency of heart beats of reflex origin.

The frequency of breathing at the maximum values of acceleration was three to four times the initial frequency, and in the more rapid respiration there were observed mechanical respiratory difficulties due to the effect of acceleration.

There are reasons to assume that the observed changes in the state of the physiological functions of the animal were in their origin connected primarily with the sudden action on the organism of powerful external irritants (the reactions were in the nature of defensive reflexes). Later we could observe the specific influence of these irritants (vibration, acceleration). For this reason the systolic frequency (even after a certain decrease) remained at a higher level than normal.

The analysis and comparison of our data with the results of the earlier laboratory experiments led to the conclusion that the animal withstood in a completely satisfactory fashion the satellite flight from the moment of launching to the entrance into orbit.

The Period of Motion in Orbit

After the satellite entered orbit there occurred a state of dynamic weightlessness, in which the weight of the animal, and all its organs and tissues, was practically equal to zero. In our experiments with high altitude rockets the ordinary period of partial or complete weightlessness did not exceed 5 to 6 min. In the flight of the satellite, in spite of its slow revolution, weightlessness was always practically complete. With the onset of weightlessness, the animal's body ceased to press against the floor of the cabin and easily pushed away from it

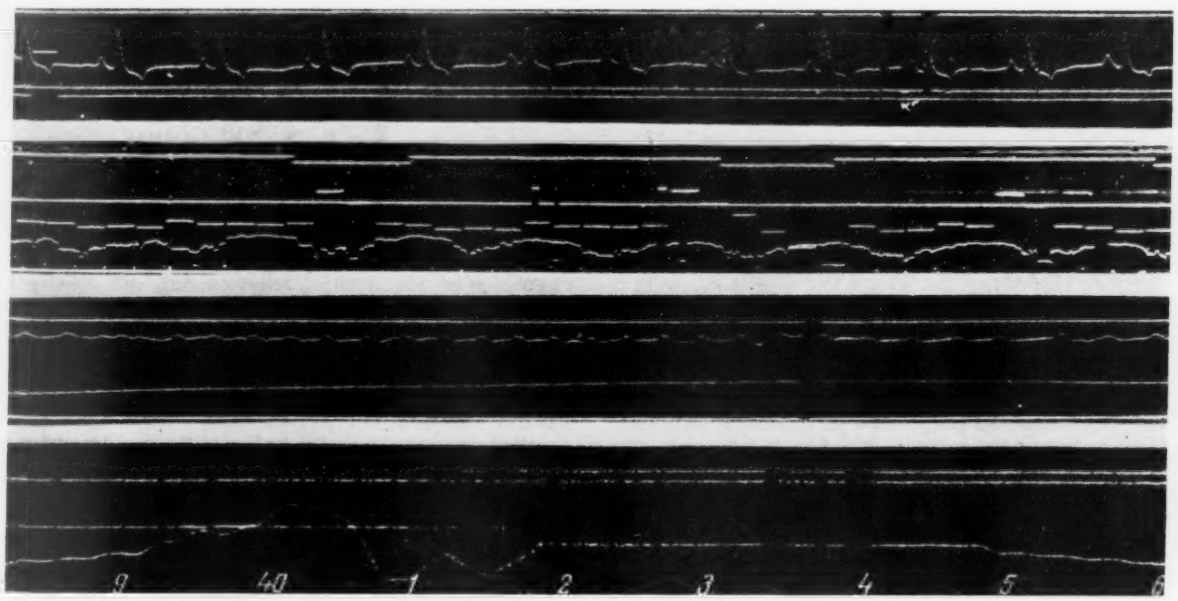

Fig. 10 Electrograms made during the satellite's flight: 1 electrocardiogram (thoracic lead, indwelling electrodes); 2 barometric pressure of air in cabin; 3 temperature at various points in the cabin; 4 the animal's respiration; 5 oscillation of the carotid artery; 6 air pressure in the sleeve of the pickup for measuring arterial pressure; 7 movements of the animal (actogram). (Translator's note: Figures on base line are not reported.)

by contracting the limb muscles. To judge from our records the motion was short-lived and smooth. Since the thorax was no longer subjected to compression, the frequency of respiration decreased. After a very brief and insignificant acceleration of heartbeat (as a result of the cessation of acceleration and vibration), the frequency of systole continued to decrease and to approach the initial rate. However, the time required for the heartbeat to return to normal after acceleration stopped was approximately three times as much as in our laboratory experiments where the animal was subjected in the centrifuge rotation to the same accelerations as those in the satellite.

It is probable that this is connected with the fact that, after the cessation of acceleration in our tests on Earth, the animal was once more subject to normal weight. With the shift to orbital motion, the accelerations changed with respect to the state of weightlessness.

Obviously this resulted in changes of the afferent impulses to the central nervous system (including those indicating the animal's body position in space); there was also a change in the functional state of the subcortical formations which regulate circulation and respiration. As a result there was a certain increase in the time needed for the indicated functions to return to normal after the effect of acceleration (after effect). It is also possible that this effect was somewhat strengthened by the action of accompanying factors (noise, vibration) the intensity of which was higher at launching than in the laboratory experiments.

The analysis of the electrocardiogram recorded at this time revealed certain changes in the configuration of its elements and of the duration of separate intervals. The changes noted did not bear a pathological character and were connected with the increased functional overload during the period preceding weightlessness (Fig. 10).

The electrocardiogram picture reflected the temporary shift in the reflex regulation of the heart activity (predominance of sympathetic influences). In the following period we observed the approach of this electrocardiogram picture to that characteristic for the initial state of the animal. In spite of the unusual state of weightlessness, the motor activity of the animal exhibited the normal pattern.

The fact that the indexes showing the functioning of circulation and respiration became normal during the period of weightlessness testified to the fact that this unique factor in itself did not cause any essential change in the condition of the physiological functions of the animal.

Certain deviations of the functional indexes which were observed later must apparently be explained by the change of air temperature in the airtight cabin.

An analysis of the data indicating the condition of the hygienic parameters of the atmosphere of the cabin showed that during the period of flight the supply of oxygen was completely adequate. The fact that there was no decrease of pressure in the cabin indicates that it was securely airtight. This is the more important since, as we know, the satellite passed through the region of meteor currents. Consequently, the construction and sturdiness of the cabin guaranteed the necessary protection from mechanical damage by meteoric material.

On the basis of this experiment we were unable to pass any definite judgment about the effect of cosmic radiation on the animal's organism. No clear physiological effect of the action of radiation was observed, but a detailed study of this question will necessarily require careful and prolonged research on the animal after the flight. The conditions of the experiment did not provide for this possibility.

An evaluation of the results obtained give every evidence that living creatures can satisfactorily survive conditions approaching those of cosmic flight. The positive result of the experiment in this respect permits us to continue and expand our research with even greater persistence.

The accumulation of experimental data with artificial Earth satellites will in the near future, we hope, permit us to arrive at definite conclusions regarding basic questions connected with the biomedical investigations of cosmic flight.

Investigation of Micrometeorites With the Aid of Rockets and Satellites

O. D. KOMISSAROV,
T. N. NAZAROVA,
L. N. NEUGODOV,
S. M. POLOSKOV
and L. Z. RUSAKOV

THE PRINCIPAL information concerning the solid component of interplanetary matter has so far been obtained by indirect means—by visual, photographic and radar tracking of meteors, observation of zodiacal lights, etc. All estimates of the distribution of meteoritic bodies are based on these investigations (1 to 4).[1]

Recently both the USSR and the United States began investigation of meteoric particles by direct methods—using apparatus raised into the upper atmosphere with rockets and satellites (5 to 11). To register meteoritic particles incident on rockets and satellites, we employ apparatus to count the number of collisions and to measure certain mechanical parameters of the meteoritic particles.

The measuring apparatus is based on the following idea. From the point of view of interest to us, we can characterize each particle by its momentum and energy (or by its mass and velocity). We cannot measure the momentum of a meteor particle as it strikes the particle detector, since the particle disintegrates on the surface of the detector and the momentum of the material expelled from the detector by this disintegration considerably exceeds the momentum of the particle itself. By measuring this "reaction" momentum, sensed by the detector, we determine not the momentum of the meteor particle, but rather its energy (within a certain transformation factor).

A theoretical calculation by K. P. Stanyukovich has shown that at high velocities the momentum registered is proportional to the energy of the incident particles. At the present time theoretical investigations and laboratory experiments

Translated from *Iskusstvennye Sputniki Zemli* (Artificial Earth Satellites), no. 2, USSR Acad. Sci. Press, Moscow, 1958, pp. 54–58.

[1] Numbers in parentheses indicate References at end of paper.

are being carried out to determine the proportionality ratio. It is possible that instead of $mv^2/2$, we may have to use an exponent of somewhat less than 2 for the velocity.

It would be natural to measure the momentum with a ballistic detector. Although the time of collision between a micrometeorite and the barrier is negligibly small (approximately 10^{-6} sec), it is advisable to make the natural frequency of the detector 400 cycles. The detector consists of a massive plate, mounted on a flat spring, and four ammonium phosphate piezoelectric elements attached to the plate (Fig. 1). We use not one but four piezoelements, in order to reduce the fluctuations in the detector emf, which depends on the place where the meteor particle strikes.

The plate displacement due to the impact of the micrometeorite causes deformation of the crystals, which in turn results in short damped voltage oscillations, sorted into four bands by a converter-amplifier that counts the number of pulses in each amplitude range. A block diagram of the converter is shown in Fig. 2. It is seen from the diagram that the signal from each detector goes to an individual amplifier, thus excluding the possibility of shunting of one detector crystal by the internal capacitance of another.

The signals are sorted into amplitude groups by counting circuits made up of binary triggers, one for each amplitude range.

To exclude repeated operation of the first triggers by signals in the form of damped oscillations, the input of each counting circuit contains a Kipp relay, which blocks the input for 0.06 to 0.08 sec. This determines the resolution of the entire system, which amounts to 12 to 17 impacts/sec.

The counting circuit of the most sensitive range has six triggers and counts up to 32. The Kipp-relay signal of this counting circuit comes from the last stage of the amplifier and assures the registration of detector signals from 0.001 v up.

The counting circuits of the next ranges contain five triggers counting up to 16 and three triggers counting up to four, respectively, and receive their signals from the intermediate amplifier stages.

The Kipp-relay signal of the least sensitive range is taken without amplification from the resistance summing network. The counting circuit of this range has only one trigger, i.e., every signal is registered.

Voltages from successive triggers are applied to an output circuit in which they produce voltages related as 1:2:4:8. Thus, any combination of states of the output triggers produces at the output a definite voltage, so that the state of each output trigger, and consequently the number of signals received prior to this instant in each band, can be readily determined at each instant of time.

This output circuit makes it possible to carry over one radio telemetering channel all the signals through the four ranges.

Fig. 3 shows the type of record produced by the telemetering system. The change in the height of the level indicates the number of impacts having amplitudes within the corresponding range, as recorded by the counting circuit.

Thus, our detector measures the momentum acquired by the surface, and is calibrated for momentum in the following manner. The detector is placed in a horizontal position, and a ball is dropped on it from a certain height. The ball bounces from the detector plate to a certain height. Knowing the height from which the ball was dropped and the height of the bounce, we obtain directly the momentum transferred to the detector.

This method simulates fully the disintegration occurring on the surface of the detector. Actually, the time of collision of the ball amounts to approximately 10^{-5} sec. Although this is three orders of magnitude greater than the time of contact with a meteoric particle, it is still much shorter than the natural period of the transducer and consequently, the detector really measures the momentum.

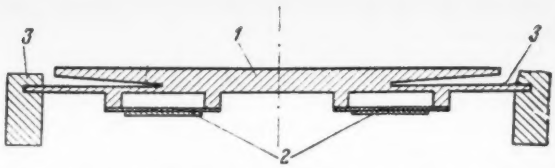

Fig. 1 Ballistic piezoelectric transducer. 1 plate; 2 ammonium phosphate crystals; 3 flat spring

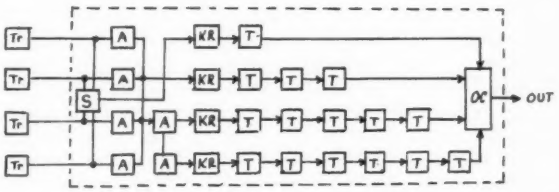

Fig. 2 Block diagram of converter-amplifier. Tr transducer; S summing network; A amplifier; KR Kipp relay; T trigger; OC output circuit; OUT output to telemetering channel

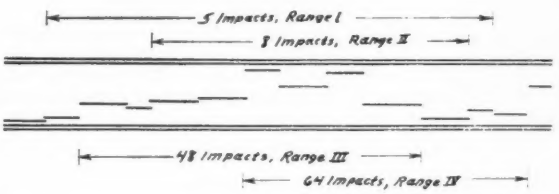

Fig. 3 Appearance of record produced with radio telemeter system. Five impacts, range I; eight impacts, range II; 48 impacts, range III; 64 impacts, range IV

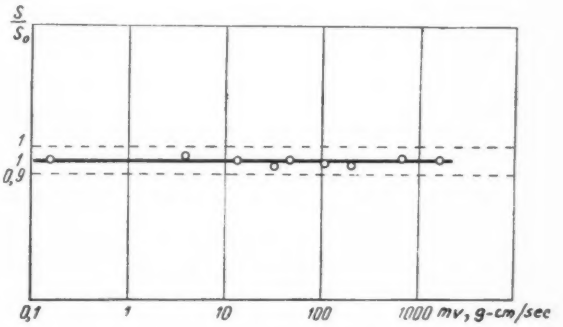

Fig. 4 Calibration curve of the system. The abscissa is in mv gm/cm/sec

The detectors were calibrated with balls ranging from 0.6×10^{-3} to 2 gm. By varying the balls and the height of the drop, we established that our detectors were linear in the range from 0.1 to 1000 gm/cm/sec.

Fig. 4 shows the dependence of the relative sensitivity of the system on the momentum of the ball. Since we wish to show merely that the detector records momenta within the foregoing range, the ordinates are marked in relative sensitivity S/S_0, where $S = U_b/mv$ is the sensitivity of the system, and S_0 is the nominal value of the sensitivity, which depends on the construction of the detector and on the converter, the noise level in the satellite, and other considerations.

A detector temperature change of ± 60 deg changes its

sensitivity by ±5 per cent, the sensitivity increasing with temperature.

If we assume 40 km/sec for the average velocity of a meteoric particle, and use the simplest theoretical law for the variation of the momentum acquired by the detector with the energy of the meteoric particle and with the coefficient for the conversion of momentum into energy (as calculated by K. P. Stanyukovich), we find that the detector can measure the energy of a meteoric particle of mass 10^{-9} gm and higher, without experiencing damage.

As already noted, the sensitivity of the system can be increased.

It thus becomes possible to measure one of the two quantities that characterize the mechanical properties of meteoric particles—perhaps the most important one, since the erosion of the satellite surface also is related to the particle energy.

The third Soviet satellite serves as a laboratory in space. It carries much scientific and auxiliary apparatus, some of which causes the satellite to vibrate as a whole. Consequently, if the sensitivity threshold is incorrectly chosen, the instrument may record not only impacts of meteoric particles, but also the vibration of the satellite itself.

To reduce the influence of these vibrations, the transducer is provided with rubber shock mounts; these reduce considerably the sensitivity of the transducer to noise and vibration of this type, but cannot eliminate it entirely.

To eliminate all false readings, the sensitivity of the system must be made greater than the noise level of the satellite.

As a result of all the precautions used, the apparatus was found to be insensitive to vibrations occurring in the satellite, but not to the stronger vibration and noise that accompany the flight of the carrier rocket during the active portion of its trajectory and during the time of rocket operation. However, this is of no importance since all the measurements began after the satellite separated from the rocket. It must be noted that the detector has a certain sensitivity to impact of meteoric particles against the surface of the satellite. In this case the sensitivity of the detector drops by a factor of 15 times or less, while when a particle strikes the body of the detector the sensitivity diminishes only by one half. These circumstances were taken into account in the interpretation of the experimental data.

To register meteoric particles, four detectors with a total area of 3410 cm², including housing, were installed on the cover of the satellite. All the transducers are located in one plane. Since the position of the satellite in space is known from data of magnetic instruments and solar-orientation transducers, the position of our detectors in space is, naturally, also known.

Based on preliminary data, the detectors registered on an average an impact frequency of approximately 1.7×10^{-3} impacts/cm² or 4.4×10^{-12} gm/cm²/sec (for two stellar magnitudes).

Along with such a density of meteoric matter, we registered a short-duration sharp increase in the number of impacts.

At the same time, while the satellite was in orbit, the detectors registered impacts of varying frequency. This result cannot be ascribed to a change in the number of meteoric particles with altitude, since not only the height, but also the position of the satellite in space varied along the orbit. The satellite, rolling and precessing in space, had varying orientations relative to the Earth over different parts of the orbit, and sometimes the Earth shielded the detectors from meteoric particles. It is possible that the change in the number of impacts during the motion of the satellite was also influenced by the direction of the meteoric stream.

During one instant of a sharp increase in the count, an average number of approximately 22 impacts/cm²/sec were registered at altitudes of 1700 to 1880 km. At 1300 to 1500 and 500 to 600 km, 10 and 9 impacts/sec/m² were recorded respectively, on the average.

Assuming that the momentum acquired by the transducer at the impact of a particle is proportional to the particle energy, the registered energy of a meteoric particle is approximately 10^4 ergs.

Acknowledgment

In conclusion, the authors express their deep gratitude to A. K. Bektabegov, M. A. Isakovich, G. M. Kurtev, N. A. Rozin, N. A. Roi and A. A. Trukhachev for their active participation in the work.

References

1 Watson, F. G., "Between the Planets," Harvard University Press, Cambridge, Mass., 1956.

2 Whipple, F. L., "Physics and Medicine of the Upper Atmosphere," University of New Mexico Press, Albuquerque, N. M., 1952.

3 Levin, B. Yu, "Physical Theory of Meteors and Meteoric Matter in the Solar System," USSR Academy of Sciences Press, 1956.

4 Fesenkov, V. G., "Meteoric Matter in Interplanetary Space," USSR Academy of Sciences Press, 1947.

5 Dubin, M., in "Rocket Exploration of the Upper Atmosphere," edited by Boyd, R. L. S., Seaton, M. J. and Massey, H. S. W., Pergamon Press, Inc., New York, 1954.

6 Berg, O. E. and Meredith, L. H., "Meteorite Impacts to Altitude of 103 Kilometers," *J. Geophys. Res.*, vol. 61, no. 4, 1956.

7 Marning, E. and Dubin, M., "Some Preliminary Reports of Experiments in Satellites 1958 Alpha and 1958 Gamma," in "Satellite Micrometeorite Measurements," National Academy of Sciences—National Research Council, Washington, D. C.

8 Dubin, M., "Cosmic Debris of Interplanetary Space," presented at the Second OSR Astronautics Conference, Denver, Colo., 1958.

9 La Gow, H. E., Schaefer, D. H. and Schaffert, I. C., "Micrometeorite Impact Measurements on a 20'-Diameter Sphere at 700 to 2500 Kilometers Altitude," USNRL, Washington, D. C., 1958.

10 Singer, S. F., "The Effect of Meteoric Particles on a Satellite," Jet Propulsion, vol. 26, no. 12, 1956.

11 Baum, S. A., Kaplan, S. A. and Stanyukovich, K. P., "Introduction to Cosmic Gas Dynamics," Fizmatgix, 1958.

Estimate of Internal Losses in a Liquid Fuel Jet Engine Chamber

A. V. KVASNIKOV

Moscow Aviation Institute

IN THIS ARTICLE we propose a system for estimating the thrust losses in a liquid fuel jet engine, based on the use of thermodynamic calculations and simple experimental facts. Such systems originated with M. V. Mel'nikov, who reconciled the experimental facts with computations by using maximum simplifying assumptions.

The definitions of the coefficients used in this article have the same meaning as the definitions adopted in heat power engineering, and the relations between them make it possible to strike a more correct loss balance.

It is assumed in thermodynamic calculations for liquid fuel jet engines that the cycle is performed by a gas with certain known real properties (the presence of dissociation and a change in composition during the time of equilibrium expansion). However, the real cycle is accompanied by collateral processes which occur because of the superposition of mixture-formation processes on the main cycle, and because of an interaction between the working medium and the walls of the chamber and the nozzle. This causes the gas to have different states at different points in the chamber cross section. The collateral processes are irreversible and lead to losses of energy and thrust, usually called internal losses. The power losses are characterized by the efficiency (η), and the thrust losses by the thrust coefficients (φ and ψ).

At the present time it is difficult to obtain reliable results from calculations of the internal losses. This is due above all to the complexity of the collateral processes and to the great difficulties in the performance of experiments that would yield direct indications concerning the magnitude of the more important losses.

Thus, for a direct estimate of the chemical losses, it is necessary to have data on the composition of the gas and on its temperature at characteristic cross sections of the chamber. However, if the gas has a complicated composition, if its thermal and chemical structure are not uniform, and if high chemical reaction velocities and high temperatures prevail, it is impossible to obtain satisfactory accuracy in the measurements of the temperature and composition of the gas. It would appear that an experimental determination of the hydraulic losses would be less complicated, but the gasdynamic processes in the nozzle channel combine with chemical and thermal processes, from which it is quite difficult to separate them.

It must be assumed that it is possible to determine in the experiment, with sufficient accuracy, the flow of working medium, the pressure in the chamber and the thrust. Starting with these reliable data and with data obtained by thermodynamic calculations, it is possible to obtain an estimate of the internal losses in the liquid fuel jet engine; this estimate is useful for work on the final detailed design of the engine. It must be borne in mind that its accuracy will affect not only the quality of the experiment, but also the accuracy of the thermodynamic computation, which contains simplifying assumptions.

Translated from *Izvestiia Vysshych Uchebnykh Zavedenii MVO* (*News of Higher Institutions of Learning*), Ministry of Higher Education, USSR, "Aviation Engineering" series, no. 1, 1958, pp. 95–105.

By thermodynamic computations we obtain

$$P_t,\ P_{spt},\ p_{ct}\ T_{ct}\ w_{at}\ G_{sec\ t}$$

where

P = thrust
p = pressure
T = temperature
w = velocity
G = flow
t = theoretical
sp = specific
c = chamber

i.e., the magnitude of the thrust, the specific thrust, the pressure, the temperature in the chamber, the exhaust velocity, and the mass flow rate of gas. Experimentally we obtain

$$P,\ P_{sp},\ p_c,\ T_c,\ w_a,\ G_{sec}$$

Comparison of the experimental and computed data makes it possible to determine the relative magnitude of the following:

the specific thrust

$$\xi_{sp} = P_{sp}/P_{sp\ t}$$

the pressure in the chamber

$$\xi_p = p_c/p_{ct}$$

the flow

$$\xi_g = G_{sec}/G_{sec\ t}$$

the absolute thrust

$$\xi_P = P/P_t$$

Starting with these data, we show how it is possible to approach the determination of the individual losses inside the chamber.

The operating conditions in the chamber can be of two extreme types:

$$G_{sec} = G_{sec\ t},\quad \xi_g = 1.0 \text{ and}$$
$$p_c = p_{ct},\quad \xi_p = 1.0$$

We shall assume that the speeds of the gas in the combustion chamber are small and that the pressure remains constant in it.

Let us consider the first case, when $\xi_g = 1$. Since not all the available heat is transferred to the gas ahead of the inlets to the jet, the thermal portion of the gas enthalpy in front of the jet is less than the available one, which is determined by thermodynamic computations. Furthermore, the enthalpy should drop further because of the heat losses in the chamber walls, and should rise because of heating of the fuel in the regenerative cooling jacket. On the whole, the gas temperature T_c will be lower than that obtained by thermodynamic computations T_{ct}.

Since the true flow of the gas is the same as the calculated one, and the temperature of the gas ahead of the jet is lower,

then if the throat of the jet is constant in dimension, the pressure in the chamber p_c should be less than the calculated p_{ct}. This follows from the fact that

$$G_{sec} = \mu F_{cr} \sqrt{\frac{kg}{R}\left(\frac{2}{k+1}\right)^{(k+1)/(k-1)}} \cdot \frac{p_c}{\sqrt{T_c}}$$

In most cases the true k and R differ from the computed values very little, and then, if the flow coefficient μ changes little when going to other values of p_c and T_c, we get

$$G_{sec} = A\,(p_c/\sqrt{T_c})$$

From this equation it is clear that as the temperature T_c is decreased, the pressure in the chamber should also decrease.

Taking into account that the thermal losses for cooling are small and that they are partially offset by the small amount of heat of regeneration, we do not introduce any corrections for regeneration and for external cooling. In those cases when the chamber walls are not cooled by the fuel, it is necessary to take into account the additional temperature drop, using either experimental or theoretical data on the heat losses at the wall. Such data are plentiful, and they are reliable.

The main losses in the nozzle channel are hydrodynamic, caused by friction of the gas against the wall, by internal friction and by separation of the jet, if it occurs. A feature of the process in this case is a complete or partial recovery of the heat that has not been given up in the combustion chamber. It is very difficult to separate the effect of afterburning and hydrodynamic losses on the exhaust velocity, either theoretically or experimentally with an operating engine.

The hydrodynamic losses of the nozzle can be determined in separate experiments, as is done for steam and gas turbines, i.e., by blowing gas or steam through models of the nozzles, without a chemical reaction occurring during the expansion.

If the calculated exhaust velocity in the model nozzle is w_{ab}, and the true rate is w_{an}, then the velocity of coefficient of the nozzle becomes

$$\psi_n = w_{an}/w_{ab}$$

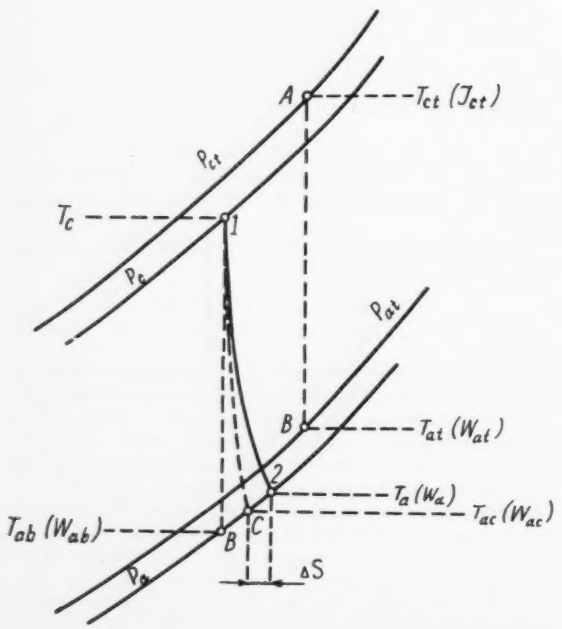

Fig. 1 Entropy diagram of the expansion of gas in a liquid fuel jet engine in the presence of hydraulic losses and afterburning

When using handbook data on the value of ψ_n it is necessary to know how the true exhaust velocity w_{an} is determined. Since the experimentally obtained impulse corresponds to the actual velocity, it is necessary to introduce, when calculating the value of w_{an}, a correction for the divergence of the jet resulting from the taper of the end portion of the nozzle.

In cases when the experimentally determined force includes a static component, the latter must be eliminated, and only the dynamic thrust must be determined.

The summary effect of the hydraulic losses and of the afterburning are characterized by a ratio of the true velocity to the calculated one, but for true values of p_c and T_c of the gas ahead of the nozzle. This ratio is in the form of a velocity coefficient of the nozzle of the operating liquid fuel jet engine. We shall call this the internal nozzle coefficient φ_n. By definition

$$\varphi_n = w_a/w_{ab}$$

The quantitative effect of the afterburning on the exhaust velocity is represented by the afterburning nozzle coefficient

$$\psi_{aft} = w_a/w_{an}$$

Obviously this coefficient should be greater than unity and

$$\varphi_n = \psi_n\psi_{aft} \qquad [1]$$

If the friction is small, and the afterburning is great, it is possible to obtain φ_n greater than unity. The quantity ψ_{aft} can also be called the coefficient of thrust recovery. The product $\varphi_T\psi_{aft}$ is a coefficient that estimates the overall loss in engine thrust due to incomplete chemical reaction in the chamber.

Losses in the combustion chamber alone lead to a reduction in the exhaust velocity and in thrust. Since

$$\frac{w_{ab}}{w_{at}} = \sqrt{\frac{T_c}{T_{ct}}}$$

the thrust coefficient of the chamber φ_T which shows how the thrust would decrease only for losses in the chamber, will be

$$\varphi_T = \frac{w_{ab}}{w_{at}} = \frac{P_{spb}}{P_{spt}} \qquad [2]$$

A further reduction of thrust results from losses in the nozzle itself. The internal nozzle coefficient φ_n gives an estimate of the additional reduction of velocity and of thrust

$$\varphi_n = w_a/w_{ab} \qquad [3]$$

Fig. 1 shows the entropy diagram of the expansion of the gas at two initial states: The theoretical one, and the case of incomplete combustion. The velocities and temperatures indicated in the foregoing formulas are marked on the diagram against the final points of the expansion lines.

We denote the dynamic thrust, corresponding to a velocity w_a, by P_a. The ratio of the axial thrust to the impulse, determined by the velocity w_a, gives a quantitative estimate of the thrust lost by radial divergence of the gas stream. If the span of the nozzle cone is 2α, then, with good accuracy, the thrust coefficient due to the taper of the nozzle, ψ_α, is determined from

$$\psi_\alpha = \frac{P_z}{P_a} = \frac{1+\cos\alpha}{2} \qquad [4]$$

where P_z represents the axial thrust.

If the pressure of the external medium is not equal to the pressure at the exit of the nozzle, P_z is not the true thrust P, since

$$P = P_z + (p_a - p_{un})F_a = \left[1 + \frac{\Delta p_a F_a}{P_z}\right] P_z = \psi_{un} P_z \qquad [5]$$

Here ψ_{un} is the external thrust coefficient, which may be greater or less than unity, and which provides an estimate of the change in the thrust due to incompleteness of the expansion process.

Consequently, in general

$$P = P_a\psi_\alpha\psi_{un} = (w_a/g)\psi_\alpha\psi_{un}\cdot G_{sec}$$

Dividing both parts of this equation by the computed value of the thrust, we find the so-called relative magnitude of the specific thrust

$$\xi_{sp} = \frac{P}{P_t} = \frac{P_{sp}}{P_{spt}} = \frac{w_a}{w_{at}}\,\psi_\alpha\psi_{un}$$

Multiplying Equations [2 and 3] we get

$$w_a/w_{at} = \varphi_T\varphi_n$$

after which

$$\xi_{sp} = \varphi_T\varphi_n\psi_\alpha\psi_{un} \qquad [6]$$

We call the velocity ratio, w_a/w_{at}, the relative magnitude of the internal specific thrust φ_{sp}. It follows from Equation [6]

$$\varphi_{sp} = \varphi_n\varphi_T = \xi_{sp}/\psi_\alpha\psi_{un} \qquad [7]$$

Were ξ_{sp} to be experimentally determined, and were the quantities ψ_α and ψ_{un} calculated from formulas [4 and 5], the relative magnitude of the internal specific thrust would become known.

Equation [7] establishes the relation between the relative magnitude of the specific thrust ξ_{sp} and the two coefficients that characterize the thrust losses due to the deviation of the true process from the theoretical one in the combustion chamber and in the nozzle channel separately. Using this, it is possible, by an indirect method, to determine the chemical losses in the chamber, i.e., the quantity φ_T.

The availability of experimental values of ξ_{sp} and ξ_p makes it possible to determine also the gas temperature at the edge of the nozzle. If $\xi_g = 1$, then

$$F_a w_a \gamma_a = F_a w_{at}\gamma_{at}$$

and

$$\frac{w_a}{w_{at}} = \frac{\gamma_{at}}{\gamma_a} = \frac{p_{at}}{p_a}\frac{T_a}{T_{at}} = \xi_p\frac{T_a}{T_{at}}$$

The temperature T_{at} can be calculated.

$$T_{at} = T_{ct}\left(\frac{p_{at}}{p_{ct}}\right)^{(k-1)/k} = \frac{T_{ct}}{\delta_n{}^{(k-1)/k}}$$

where δ_n is the degree of expansion in the nozzle channel. Thus

$$\frac{w_a}{w_{at}} = \frac{\delta_n{}^{(k-1)/k}}{\xi_p}\frac{T_a}{T_{ct}}$$

Taking Equation [7] into account, we get

$$\frac{T_a}{T_{ct}} = \frac{\varphi_{sp}\xi_p}{\delta_n{}^{(k-1)/k}} \qquad [8]$$

The ratio of the true temperature at a station in the nozzle to the calculated one in the chamber is determined by this formula with sufficient accuracy.

Let us proceed to show the relations between φ_T and φ_n and experimental data.

We first consider a case when the afterburning can be neglected, corresponding to $\psi_{aft} = 1$. We determine the quantity T_a in Equation [8] from the expression for the nozzle efficiency

$$\eta_n = \varphi_n{}^2 = \frac{I_c - I_a}{I_c - I_{ab}} \approx \frac{T_c - T_a}{T_c - T_{ab}}$$

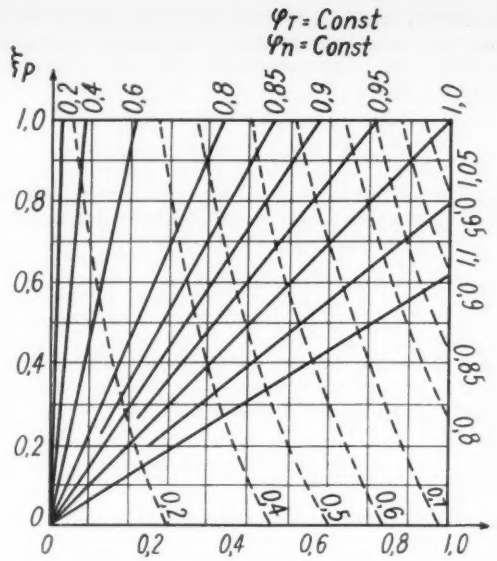

Fig. 2 Relation between the relative magnitude of the pressure in the chamber and the internal thrust coefficient at constant φ_T and φ_n ($G_{sec} = G_{sec\,t}$; $\delta_n = 100$, $k = 1.2$)

Hence

$$T_a = T_c[1 - \varphi_n{}^2\eta_i]$$

where

$$\eta_i = 1 - 1/\delta_n{}^{(k-1)/k}$$

Inserting T into Equation [8] we get

$$T_c\,[1 - \varphi_n{}^2\eta_i] = \frac{\varphi_{sp}\xi_p}{\delta_n{}^{(k-1)/k}}\,T_{ct}$$

But

$$T_c/T_{ct} = \varphi_T{}^2$$

and

$$\varphi_n = \varphi_{sp}/\varphi_T$$

These equalities lead to a formula for φ_T

$$\varphi_T = \sqrt{\varphi_{sp}[\xi_p - \eta_i(\xi_p - \varphi_{sp})]} \qquad [9]$$

This makes the value of the velocity coefficient of the nozzle

$$\varphi_n = \sqrt{\varphi_{sp}/[\xi_p - \eta_i(\xi_p - \varphi_{sp})]} \qquad [10]$$

Consequently, the thrust coefficient of the combustion chamber and the velocity coefficient of the nozzle are determined readily if δ_n, φ_{sp} and ξ_p are known. From the formulas obtained, it is seen that if identical ξ_p and φ_{sp} are obtained for two engines, the losses in the combustion chamber are greater, and those in the nozzle channel are less, for the nozzle having the greater degree of expansion.

Fig. 2 shows the diagram of the internal thrust losses, showing their dependence on the relative magnitude of the internal thrust and on the relative magnitude of the pressure in the chamber. When η_i is small and the difference $\xi_p - \varphi_{sp}$ is small, the second terms in the square brackets of Equation [9] can be neglected. In such cases we have

$$\varphi_T = \sqrt{\varphi_{sp}\xi_p}$$
$$\varphi_n = \sqrt{(\varphi_{sp}/\xi_p)} \qquad [11]$$

The corresponding expressions for φ_T and φ_n are readily obtained also for the case when the relative magnitude of the pressure is unity. The thrust coefficient of the combustion chamber at $\xi_p = 1$ is

$$\varphi_T = \sqrt{\varphi_{sp}\left[\frac{1}{\xi_g} - \eta_t\left(\frac{1}{\xi_g} - \varphi_{sp}\right)\right]} \qquad [12]$$

It is easy to see that expression [12] is similar to [9], the only difference being that ξ_p is replaced by $1/\xi_g$. If the quantity $\eta_t(1/\xi_g - \varphi_{sp})$ is close to zero, then

$$\varphi_T = \sqrt{\varphi_{sp}/\xi_g}$$

$$\varphi_n = \sqrt{\varphi_{sp}\xi_g} \qquad [13]$$

The specific thrust, as in the preceding case, diminishes with φ_{sp}; the absolute thrust diminishes to a smaller degree, since the flow of gas per second increases somewhat.

$$\frac{P}{P_t} = \frac{P_{sp}}{P_{spt}} \cdot \frac{G_{sec}}{G_{sec\ t}} = \varphi_{sp}\xi_g = \varphi_{abs}$$

Eliminating ξ_g with the aid of Equation [12] we get

$$\varphi_{abs} = \frac{\varphi_n^2\,[1 - \eta_t]}{1 - \varphi_n^2\,\eta_t} \qquad [14]$$

The relative magnitude of the absolute thrust is independent of the losses in the chamber. This is explained by the fact that the reduction in the initial gas temperature and the corresponding reduction in the specific thrust (proportional to $\sqrt{T_c}$) is offset by an increase in the flow per second.

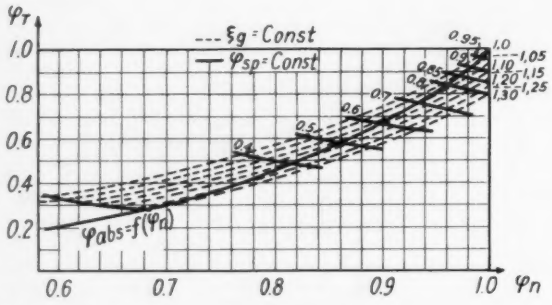

Fig. 3 Relation between the thrust coefficient of the combustion chamber φ_T and the internal nozzle coefficient φ_n($p_c = p_{ct}$; $\delta_n = 100$; $k = 1.2$)

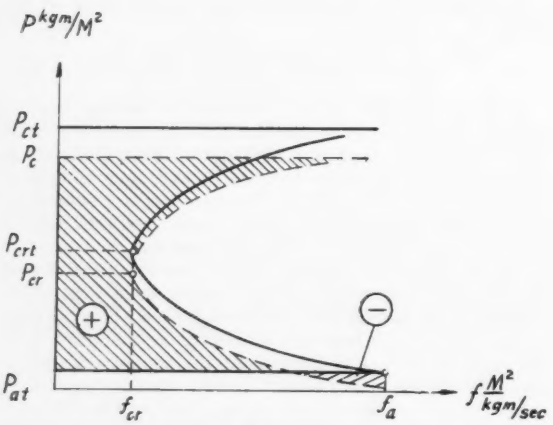

Fig. 4 Actual and theoretical p-f diagrams ($\xi_g = 1.0$). Abscissa, m²/kgm/sec; ordinate, kgm/m²

A diagram of the internal losses for the case $\xi_p = 1$ is shown in Fig. 3. When φ_T is not very high, say less than 0.96, an attempt must be made to determine the thrust afterburning coefficient, ψ_{aft}. Expansion without afterburning, but with hydraulic losses, corresponds to line 1—c on the entropy diagram. The true expansion, when afterburning takes place too, is given by line 1—2. The entropy diagram shown in Fig. 1 is hypothetical and is used to explain transitions from one expansion variant to another.

Let individual experiments establish the value of the hydraulic velocity coefficient of the nozzle, ψ_n. Then, comparing the expansion of the nozzle without losses and that with hydraulic losses alone, we can write

$$\varphi_n^2 = \frac{I_c - I_{an}}{I_c - I_{ab}} = \frac{T_c - T_{an}}{T_c - T_{ab}}$$

and also

$$\psi_n^2 = \frac{1 - (T_{an}/T_c)}{1 - (T_{ab}/T_c)} = \frac{1 - (T_{an}/T_c)}{1 - (1/\delta_n^{(k-1)/k})} = \frac{1}{\eta_t}\left[1 - \frac{T_{an}}{T_c}\right]$$

The thermal efficiency of the engine is determined here from the average value of isentropic exponent used in the thermodynamic calculations. From this expression we find the temperature T_{an} and, using T_a for [8], we obtain the ratio T_{an}/T_a, which characterizes the change in the final expansion temperature due to afterburning.

$$\frac{T_{an}}{T_a} = \frac{1 - \eta_t\psi_n^2}{\varphi_{sp}\xi_p}\,\delta_n^{(k-1)/k}\,\varphi_T^2$$

To find the unknown quantity φ_T, we write down the work balance for the gas with an initial state 1.

$$\frac{w_a^2}{2g} = \frac{w_{an}^2}{2g} + L_{aft}$$

Here L_{aft} is that portion of the work of expansion which is due to afterburning.

After suitable transformations we obtain the following equation for $\eta_T = \varphi_T^2$

$$m\delta_n^{2a}\eta_T^2 + \varphi_{sp}\delta_n^a[m\eta_t\delta_n^a\varphi_{sp} - \xi_p(3 - m)]\eta_T + \varphi_{sp}^2\xi_p[\eta_t\delta_n^a\varphi_{sp} + \xi_p] = 0 \qquad [15]$$

where

$$m = 1 - \eta_t\psi_n^2$$
$$a = (k - 1)/k$$

After determining φ_T we can calculate the gas temperature at the entrance to the nozzle

$$T_c = \varphi_T^2 T_{ct}$$

and next

$$\varphi_n = \varphi_{sp}/\varphi_T$$

hence

$$\psi_{aft} = \varphi_n/\psi_n = \varphi_{sp}/(\varphi_T\psi_n) \qquad [16]$$

The values of the specific thrust of the engine can be represented in graphic form, using the p-f diagram. The specific thrust can be calculated from

$$P_{sp} = \oint pdf$$

and the integration is over the internal and external contours of the entire chamber. Fig. 4 shows an example of the p-f diagram for the case when $\xi_g = 1.0$. The characteristic pressures p_c, p_{cr} and p_a diminish in proportion to ξ_p. The area bounded by the heavy line is proportional to $P_{sp\ t}$. The cross-hatched area, bounded by the dashed line, corresponds to P_{sp}. Fig. 5 is given for the case $\xi_p = 1.0$. In this variant of the chamber, the specific transverse cross sections

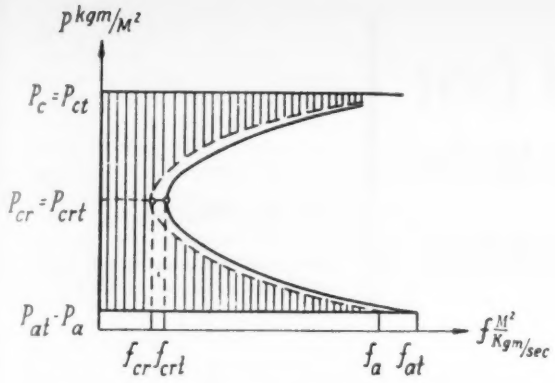

Fig. 5 Actual and theoretical *p-f* diagrams ($\xi_p = 1.0$)

f_{cr} and f_a are smaller than the calculated ones, since the flow of gas increases while the dimensions of the flow area remain constant.

It would be of great practical significance, in estimating the thrust losses in various portions of the flow area of the chamber, to plot the *p-f* indicator diagrams of an operating engine and compare them with calculations. It must be recalled that a comparison of the experimental indexes with the thrust coefficients can be made only if the composition and the excess-oxidant coefficients are the same both in experiment and theoretically. Otherwise the thermodynamic calculations must be carried out after the experiment is performed.

Table 1 lists a summary of the coefficients that characterize thrust losses in a $p = C$ liquid fuel engine.

The coefficients listed in Table 1 do not cover all the variety of problems that can arise in a study of internal losses in the combustion chamber. These losses can be differentiated in various ways. The incompleteness of combustion, for example, depends on the completeness of the mixture formation processes that occur near the head, on the amount of fuel reaching the walls, and on the degree of its utilization in the combustion chamber, on the placement of film cooling walls, on the physical and chemical properties of the fuel components that influence the rate of combustion, on the average speed of motion of gas in the chamber and on other less significant factors.

By carrying out special experiments, it is possible to investigate the effect of the above factors on the losses and to establish their quantitative shares in the coefficient φ_T. It is also possible to separate completely the internal nozzle losses. Among the hydraulic losses it is possible to separate the friction losses. Allowance for afterburning becomes more complicated if film cooling walls are located in the nozzle channel, and the problem arises of estimating the afterburning of the fuel entering the combustion chamber and the degree of combustion in the boundary layer.

The $p = C$ liquid fuel jet engine, considered in this article, is not the only thrust producer in modern rocket engines. More complicated thrust generators would be chambers with thermal and heat-flow channels or velocity chambers.

An estimate of the deviation from a hypothetical example of a velocity chamber can be made in an analogous manner, by assuming either the pressures at the chamber head p_{co} to be the same, or else the pressure at the gas entrance to the nozzle p_c.

Table 1 Coefficients that characterize thrust losses in a liquid fuel jet engine with $p = C$

Names	Symbols	Relation to other qualities
Thrust loss indexes		
thrust coefficient of combustion chamber	φ_T	
hydraulic thrust coefficient of nozzle (hydraulic velocity coefficient of nozzle)	ψ_n	
afterburning thrust coefficient	ψ_{aft}	
internal nozzle coefficient	φ_n	$\varphi_n = \psi_n\psi_{aft}$
thrust coefficient for divergence of stream	ψ_α	
external thrust coefficient	ψ_{un}	
internal thrust coefficient of liquid fuel jet engine (relative magnitude of internal specific thrust)	φ_{sp}	$\varphi_{sp} = \varphi_T\varphi_n$
total thrust coefficient of liquid jet engine (relative magnitude of specific thrust)	ξ_{sp}	$\xi_{sp} = \varphi_{sp}\psi_\alpha\psi_{un}$
Experimental indexes of deviations in operating conditions of the liquid fuel jet engine		
relative magnitude of fuel flow	ξ_g	$\xi_g = G_{sec}/G_{sec\ t}$
relative magnitude of absolute thrust	ξ_P	$\xi_P = P/P_t = \xi_g\xi_{sp}$
relative magnitude of specific thrust	ξ_{sp}	$\xi_{sp} = P_{sp}/P_{sp\ t} = \varphi_T\varphi_n\psi_\alpha\psi_{un}$
relative magnitude of pressure in combustion chamber	ξ_p	$\xi_p = p_c/p_{ct}$

Points on Lower Hugoniot Curve Describing Combustion Modes in Jet Engine Chambers[1]

YA. K. TROSHIN

Institute of Chemical Physics,
Academy of Sciences, USSR
Moscow

It is shown that under certain idealizing assumptions the lower branch of the Hugoniot curve describes real combustion modes in tubes, including the combustion modes in rocket engine chambers. A connection is established between the position of a point on this curve, corresponding to a definite combustion mode in the engine chamber, and the value of constriction of a Laval supersonic outlet nozzle. Relations are derived by which it is possible to make, in the first rough approximation, estimates of the principal parameters of the engine and to judge the degree of forcing of the combustion mode in a cylindrical combustion chamber.

It is known that the Hugoniot curve *LGABIM* (Fig. 1) is divided by secant lines 1*B* and 1*A* into a detonation branch (*BIM*) and a deflagration branch (*AGL*). Section *AB* has no physical significance, since points in this section would correspond to a process with imaginary velocity. Point *I* corresponds to a stationary detonation, propagating at minimum thermodynamic velocity. As indicated by Zel'dovich (1),[2] section *BI* corresponds to undercompressed detonation waves, which can occur only if artificial ignition of a gas in a tube (for example, by sparks) is realized at speeds greater than the thermodynamic velocity of detonation. During ignition of a shock wave, this section is forbidden from the energy point of view, since the states (on straight *MZ*) through which the shock-compressed gas should pass during the course of the chemical reaction, corresponds to higher thermal effects of the combustion reaction than the thermal effect corresponding to the given Hugoniot adiabatic. Section 1*M* corresponds to overcompressed detonation waves, observed for example in the passage of a detonation from a wide to a narrow tube, or immediately after the transition from combustion into detonation. Branch *AGL* is divided by the tangent 1*GT* into a section of weak deflagrations (*AG*) and of strong ones (*GL*). Points lying on section *GL* do not correspond to real combustion modes, since their realization would require, as in section *BI*, energies greater than liberated during the course of the reaction. Section *AG* is quite feasible from the energy point of view, but there is a widespread opinion (2 to 4) that the only deflagration that has physical significance among all the weak deflagrations is the one that occurs at nearly constant pressure, i.e., normal combustion with a speed u_n (point in the vicinity just below *A* on the branch *AG*).

On the basis of published works devoted to turbulent combustion (5, 6), we shall show that the entire branch *AG* corresponds to real combustion modes in tubes, the speed of which can vary from u_n to a maximum speed of combustion during fully developed deflagration (point *G*).

Deflagration Modes

The statements of Lewis and Elbe (2) and also those of Courant and Friedrichs (4), namely that only that portion of the curve *AG* which is very close to *A*, has physical significance, would be true in the case when the chemical reaction occurs stationarily in a perfectly plain front of a normal flame, perpendicular to the axis in the tube. We owe to Shchelkin and Damköhler a theoretical basis for the feasibility of combustion of a hot mixture in a wide zone of turbulent combustion. It is this, indeed, that permits us now to show that the entire branch of weak deflagrations *AG* has a fully defined physical meaning and describes real combustion modes in tubes.

Let us imagine combustion modes such as are shown, for example, in Fig. 2. Here the structure of the zone of the combustion flame is shown exactly as is now customary, after Shchelkin. It is bounded by control planes and is assumed, on the whole, to be a region of thermal jump, i.e., a discontinuity surface. It is assumed that this zone is stabilized in a tube of constant cross section. The initial gas, i.e., a homogeneous combustible mixture in a specified state 1 (p_1, ρ_1) is injected at a velocity u_1 into the stationary combustion zone II. The reaction products flow out of this

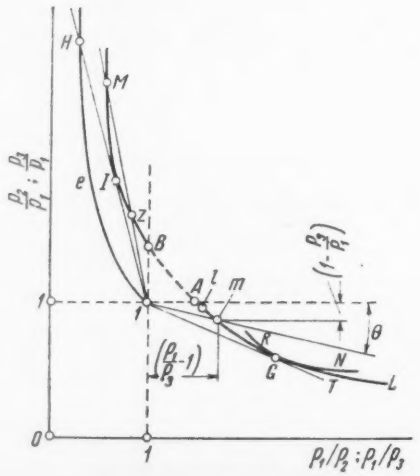

Fig. 1 The Hugoniot curve

Translated from *Izvestiia Akademii Nauk SSSR, Otd. Tekhn. Nauk, Energetika i Avtomatika* (*Bull. USSR Acad Sci., Tech. Sci. Div., Power and Automation*), no. 2, 1959, pp. 3–12.

[1] The author thanks K. I. Shchelkin for an evaluation of this paper and for valuable comments.

[2] Numbers in parentheses indicate References at end of paper.

zone with a velocity u_3 into region 3 (p_3, ρ_3.) It is furthermore assumed that the flow of gas in regions 1 and 3 is stationary and unidimensional. The gas in this region is ideal, and its specific heat is constant. We neglect all losses due to friction, heat transfer to the wall and other causes. The combustion modes are realized one after another by successive increase of the total flame surface S in zone II. The heat of combustion per unit mass Q and the ratio of the specific heats $k = c_p/c_v$ are specified.

Under these assumptions, the laws of conservation of mass, momentum and energy, applied to the case of a transfer of gas from state 1 into state 3 through the region of the thermal jump, give the equationing of the Michelson line

$$p_3 = p_1 - \rho_1 u_1 (u_3 - u_1) \qquad [1]$$

$$\frac{u_1}{a_n} = \frac{u_1}{\sqrt{p_1/\rho_1}} = \sqrt{\frac{1 - p_3/p_1}{\rho_1/\rho_3 - 1}} = \sqrt{\tan\theta} = M_1\sqrt{k} \qquad [2]$$

and the equation of the Hugoniot deflagration curve

$$\frac{p_3}{p_1} = \frac{\kappa - \rho_1/\rho_3 + 2Q/(p_1/\rho_1)}{\kappa\rho_1/\rho_3 - 1} \qquad \left(\kappa = \frac{k+1}{k-1}\right) \qquad [3]$$

The law of conservation of mass relates the velocity of motion of the gas in the states 1 and 3

$$u_3 = u_1\frac{\rho_1}{\rho_3} = M_3 a_3 \qquad M_3 = \frac{u_3}{a_3} = \sqrt{\frac{\tan\theta}{k}\frac{(\rho_1/\rho_3)}{(p_1/p_3)}} \qquad [4]$$

It is seen from Equation [1] that the combustion modes can be realized only if p_3 is less than p_1 by an amount equal to the change in the momentum of the gas that has passed through the region of the thermal jump.

The requirements imposed by Equation [1] can be realized by creating various conditions for the escape of the reaction products. For example, let the state of the initial gas correspond to normal atmospheric conditions. We join mentally a pressure chamber to the right end of the tube and continuously pump out from it the reaction products. We maintain the pressure in the pressure chamber constant for a given combustion mode at exactly the value called for by Equation [1]. The combustion mode at which the surface of the flame is exactly equal to the transverse cross section of the tube F (Fig. 2, A) corresponds to normal combustion $u_1 = u_n$. This mode is shown on curve AG in the vicinity just below point A. As the total surface of the flame increases, $S > F$ (Fig. 2, l,m) the speed of flow of the initial gas $u_1 = u_n S/F$ and the velocity of u_3 of the reaction products increases, while the pressure p_3 decreases. These combustion modes correspond to incompletely developed deflagrations (points 1 and m on curve AG). Upon further increase in the surface of the plane, the speed of flow of the reaction products reaches the local velocity of sound (Fig. 2, G) and then the fully developed deflagration mode occurs (point G on curve AGL).

It is seen from Equations [2 and 3] and Fig. 1 that the first intersection between the Michelson line and the Hugoniot deflagration curve makes it possible to choose, from all the possible final states of the gas on section AG, the particular one corresponding to the definite combustion mode with a definite flow speed of the initial gas in combustion zone II. Furthermore, the tangent of the angle of inclination (θ) of the Michelson line, for example line 1 m, exactly characterizes the value of this speed. From conditions of simultaneous tangency of the Michelson line 1GT to the Hugoniot deflagration branch AGL and to the Poisson adiabatic RGN, passing through point G, we obtain (7) the following equation

$$\frac{(u_1)_G}{\sqrt{p_1/\rho_1}} = \sqrt{\frac{k^2-1}{2}\frac{Q}{p_1/\rho_1} + k} - \sqrt{\frac{k^2-1}{2}\frac{Q}{p_1/\rho_1}} = (M_1)_G\sqrt{k} \qquad [5]$$

It is easy to determine from this equation the speed of the gas at the inlet to the combustion zone during fully developed deflagration. For the density and the pressure of the gas in region 3 in fully developed deflagration, we have the following relations

$$\left(\frac{\rho_1}{\rho_3}\right)_G = \frac{k(1+\beta)}{(k+1)\beta} \qquad \left(\frac{p_3}{p_1}\right)_G = \frac{1+\beta}{k+1} \qquad \beta = \frac{(u_1)_G^2}{p_1/\rho_1} \qquad [6]$$

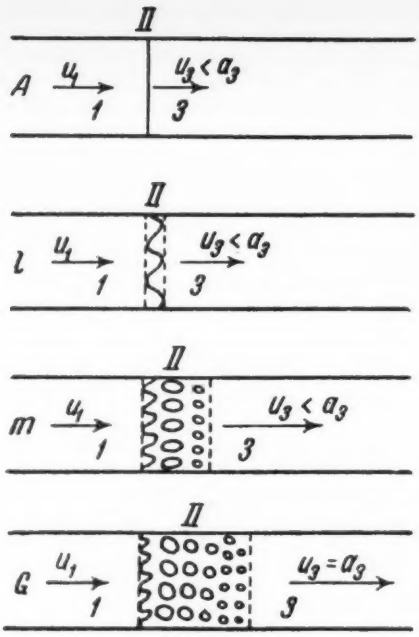

Fig. 2 Modes of deflagration

We remark that in deflagration modes the Michelson line physically, so to speak, characterizes successive averaged states of the gas over the width of the zone of turbulent flame. At each intermediate cross section of this zone, a portion of the gas has not reacted at all, and some portion has fully reacted. The local state of these two parts (composition, temperature, density) are quite different. All they have in common is the pressure, which is practically the same in a given cross section of the zone, and the average value of the composition, temperature and density of the gas, which changes from one cross section to another. Following, for example, the Michelson line 1m from the point 1 to the point m (Fig. 1), we follow, as it were, the course of burnup in zone II (Fig. 2, m). Corresponding to the very beginning of the zone (in the region near the left control surface) is a point on the line 1m located close to point 1 of this line. Here the percentage of burned-up gas is close to 100. Thus, we see that under definite boundary conditions, it is possible to realize deflagration modes for all values of velocity u_1 from u_m (the Michelson line—the nearly isobaric 1A) to maximum velocity $(u_1)_G$, corresponding to the critical condition (tangent 1GT).

The deflagration modes shown in Fig. 2 can be realized also in that case, when the pressure in the region 1 (p_1) is much greater than atmospheric, for example, under the condition when the escape of the reaction products from region 3 into the atmosphere is throttled. In this case the pressure p_3 is again maintained somehow constant for a given combustion mode and is exactly as it should be in accordance with Equation [1]. Under real conditions, for example, in chambers of liquid fuel jet engines, the role of the throttle is carried out by the constricting (subsonic) portion of the Laval supersonic nozzle (Fig. 3).

Let us arbitrarily divide such a combustion chamber along its length into regions 1, 2 and 3. Let us assume that in region 1 the finely dispersed liquid and the oxidant are fully evaporated and are well mixed, forming a homogeneous oxygen mixture,[3] the state of which is characterized by a pressure p_1 and density ρ_1, while its velocity of motion is u_1.

We assume that the previously assumed idealization (uniformity of flow of ideal gas in regions 1 and 3, invariance of specific heats, neglect of losses) is fully retained in this case. The flow of gas is stationary not only in regions 1 and 3, but also in the connected Laval nozzle, and the condition of isentropic expansion of the reaction products in such a nozzle to a state $4(p_4, \rho_4)$, at which they flow out of the engine with a velocity u_4 into the atmosphere, at a pressure of $p_0 << p_3$. The area of the transverse cross section of the cylindrical combustion chamber F and the quantities Q, k, p_1, ρ_1 and p_0 are all specified. The assumed idealization makes it possible to express the dependence of the constriction of the nozzle F/F_* on the number M_3 by the well-known equation

$$\frac{F}{F_*} = \frac{[1 + (1/2)(k-1)M_3^2]^{(1/2)\kappa}}{M_3[(1/2)(k+1)]^{(1/2)\kappa}} \qquad \left(\kappa = \frac{k+1}{k-1}\right) \qquad [7]$$

Here F_* is the area of the critical cross section.

Let us compare Equations [7 and 4] and see the close connection between the positions of the point on the deflagration branch, corresponding to a given combustion mode in the chamber of this engine, with the constriction (taper) of the nozzle. In fact, on the one hand M_3 is connected through Equation [4] with the position of the point on the deflagration branch, corresponding to a definite combustion mode in the engine chamber, and on the other hand it is connected via Equation [7] to the value of the constriction of the nozzle. Thus, it turns out that the points lying on the deflagration branch describe the states of the reaction products, corresponding to combustion modes of an entire series of combustion chambers (with constant values of F, k, Q, p_1 and ρ_1), which differ from each other by the value of the critical cross section of the supersonic Laval outlet nozzle F_*.

The lower the point is located on this branch, the more developed is the deflagration and the less must the channel be constricted in order to raise the speed of escape of the reaction products to sonic, and then also to supersonic in the expanding portion of the nozzle. In the case of a full deflagration, the speed of escape of the reaction products in region 3 equals the local velocity of sound ($M_3 = 1$), there is no need for constricting the channel, and we have a semithermal nozzle with a combustion mode forced to the limit.

[3] One uses most frequently liquid oxidants such as oxygen, tetranitromethane and nitric acid, which contain 1.14, 1.07 and 0.96 kg of oxygen per liter, respectively, and therefore a homogeneous mixture of fuel and oxidant can be called by convention an oxygen mixture in all liquid fuel jet engines.

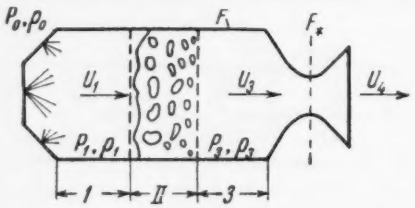

Fig. 3 Mode of incompletely developed deflagration in a combustion chamber of a liquid fuel jet engine

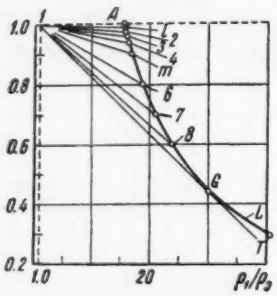

Fig. 4 Lower branch of the Hugoniot curve for a stoichiometric mixture of ethyl alcohol with oxygen (ordinates, p_3/p_1; abscissa, ρ_1/ρ_3)

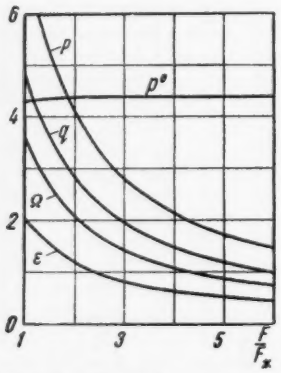

Fig. 5. Dependence of the thrust ($^3/_5 \times 10^{-3}$ P, kg), specific thrust (2×10^{-2} P^0, kg-sec-kg^{-1}), the flow per second of the fuel and oxidant mixture (10^{-1} q, kg/sec), the productivity of combustion chamber per liter (0.5 Ω, kg/sec^{-1} l^{-1}) and degree of forcing of the combustion chamber (2ε) on the constriction of the nozzle F/F_* (k = 1.2 yields a value of P^0 which is 11 per cent greater)

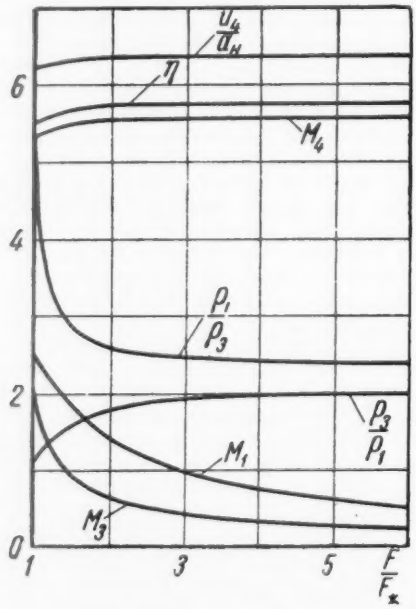

Fig. 6 Dependence of the speed of flow [$^3/_4$ u_4/a_H], the engine efficiency [10 η], the Mach numbers ($20M_1$, $2M_3$ and $2M_4$), the degree of change in pressure ($2p_3/p_1$) and the density [$^3/_2$ 10^{-1} ρ_1/ρ_3] on the constriction of the nozzle F/F_*

Table 1 Position of the point on the deflagration Hugoniot curve and the parameters of liquid fuel jet engine

Points	P_3/P_1	M_3	F/F_*	u_1, m/sec	P, kg	P, kg-sec/kg	u_4, m/sec	$\eta\ 10^3$	Ω, kg/sec/l	S/F
l	0.99	0.09	6.522	6.58	1989	219.96	2160	580	0.31	2.19
2	0.98	0.126	4.69	9.12	2751	219.8	2158	579	0.81	3.04
3	0.96	0.179	3.326	12.65	3819	219.62	2155	578	2.52	4.22
4	0.94	0.226	2.558	15.7	4731	219.34	2150	576	3.13	5.23
m	0.9	0.30	2.056	20.0	6037	219.31	2148	576	3.99	6.67
6	0.8	0.45	1.457	26.8	8038	218.02	2140	569	5.34	8.95
7	0.7	0.586	1.205	30.9	9205	216.91	2122	564	6.15	10.3
8	0.6	0.73	1.07	33.4	9920	216.04	2110	559	6.65	11.1
G	0.443	1.0	1.0	34.6	10245	214.98	2100	553	6.91	11.5

2 Approximate Comparative Estimate of the Parameters of a Liquid Fuel Jet Engine

The possibility of describing the combustion modes in liquid fuel jet engine chambers by means of points on the deflagration Hugoniot curve makes it possible, in the first rough approximation, to make a comparative estimate of the principal parameters of the engine and of the degree of forcing of the combustion modes in cylindrical chambers. Figs. 4, 5 and 6 and Table 1 give the results of such a comparative estimate of the parameters of a liquid fuel engine, operating at sea level and using for fuel a stoichiometric mixture of ethyl alcohol with oxygen. The initial data, taken for the calculation, were as follows:

$$\begin{aligned} k &= 1.3 \\ Q &= 960 \text{ kcal/kg of mixture} \\ p_1 &= 310{,}000 \text{ kg/m}^2 \\ p_1/p_0 &= 30 \\ \rho_1 &= 4.84 \text{ kg}\cdot\text{sec}^2/\text{m}^4 \\ p_1/\rho_1 &= 6.42 \times 10^4 \text{ m}^2/\text{sec}^2 \\ Q/(p_1/\rho_1) &= 62.7 \\ F &= 290 \text{ cm}^2 \\ V_k &= 6.9 \text{ l} \\ H_u &= 2080 \text{ kcal/kg of mixture} \\ u_n &\approx 3.0 \text{ m/sec} \end{aligned} \qquad [8]$$

Since the state of the reaction products in the liquid fuel jet engine chamber is close to the state of the detonation products, the magnitude of the effective heat of combustion Q can be determined from the relation that is well known from the theory of detonation (1)

$$D = 91.5\sqrt{(k^2-1)Q} \text{ kcal/kg of mixture} \qquad [9]$$

From known experimental values of the speed of detonation, $D = 2356$ m/sec. The value of Q computed in this manner corresponds to the value of the axially liberated chemical energy, compared with the lower caloric value H_u, since the speed of detonation is a unique measure of the degree of dissociation. By way of proof to justify such a method of determining the value of Q, we can refer to the successful attempts of using experimental values of the velocities of gas detonation for quantitative thermodynamic investigations at very high temperatures, for example, to find more exact values of the heats of dissociation of N_2 and CO (8, 9).

Let us describe the sequence of computation. For a mode with a fully developed deflagration ($M_3 = 1$, $F/F_* = 1$), the quantities $(M_1)_G(\rho_1/\rho_3)_G(p_3/p_1)_G$ are determined from relations [5 and 6], respectively. In the case of modes of an incompletely developed deflagration, we assume the values of p_3/p_1 and, finding from Equation [3] the corresponding values of ρ_1/ρ_3, we construct the lower branch of the Hugoniot curve (Fig. 4) and locate on it the point G, which describes the mode of a fully developed deflagration. We next find M_1, M_3, F/F_* from relations [2, 4 and 7]. The consumption q per second of a system consisting of fuel and oxidant, the speed of escape of the reaction products u_4, the thrust P, the specific thrust P^0, and the number M_4 are determined from the following obvious relations

$$q = \frac{u_1}{a_n} Fg\sqrt{p_1\rho_1} \qquad \left(g = 9.81\ \frac{\text{m}}{\text{sec}^2}\right) \qquad [10]$$

$$\frac{u_4}{a_n} = \left\{\left(\frac{p_3}{p_1}\right)\left(\frac{\rho_1}{\rho_3}\right)\frac{2k}{k-1}\left[1-\left(\frac{p_4}{p_3}\right)^{\chi}\right] + M_3^2\right\}^{1/2} \qquad \left(\chi = \frac{k-1}{k}\right) \qquad [11]$$

(for the rated mode $p_4 = p_0$)

$$P = \frac{q}{g}u_4, \qquad P^0 = \frac{u_4}{g} \qquad [12]$$

$$M_4 = \frac{(u_4/a_n)}{\sqrt{k(p_3/p_1)(\rho_1/\rho_3)(p_4/p_3)^{\chi}}} \qquad \left(\chi = \frac{k-1}{k}\right) \qquad [13]$$

The thermodynamic efficiency of the cycle can be expressed (10) in the form of a ratio of the fraction of the heat content per unit mass of gas, converted into useful work in the engine, to that increase in the heat content per unit mass of the gas which would have been obtained as a result of combustion at constant pressure. On the one hand, Q is equal pneumatically to the increase of the heat contents of the gas, which would result from combustion at constant pressure (isobar $1A$, Fig. 1), since $p_3/p_1 = 1$ for the point A in the Hugoniot equation [3] and then

$$Q = \frac{k}{k-1}\left[\left(\frac{p_3}{\rho_3}\right)_A - \left(\frac{p_1}{\rho_1}\right)\right] = i_A - i_1 \qquad [14]$$

On the other hand, from the law of conservation of energy for the region 1 and for section 4 we have

$$Q = i_4 - i_1 - \frac{u_1^2}{2} + \frac{u_4^2}{2} \qquad [15]$$

Consequently

$$\eta = \frac{i_A - i_4}{i_A - i_1} = \frac{(u_4/a_n)^2 - (u_1/a_n)^2}{2Q/(p_1/\rho_1)} \qquad [16]$$

To estimate the characteristics of the chamber from the point of view of completeness of the combustion process occurring in its volume V_c, let us determine the per liter productivity of the combustion chamber

$$\Omega = \frac{\bar{\tau}q}{V_c}\ \frac{\text{kg/sec}}{\text{liter}} \qquad [17]$$

To judge the degree of forcing of the combustion mode in

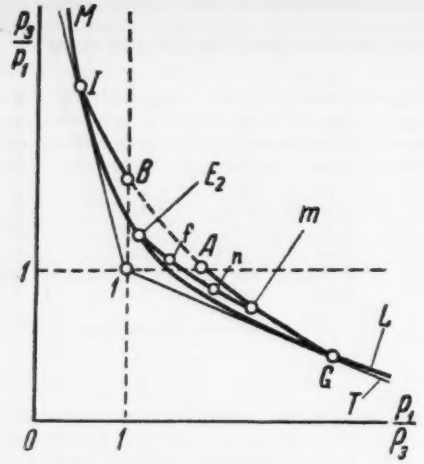

Fig. 7 Schematic representation of the curves of the usual Hugoniot adiabatic and the generalized one

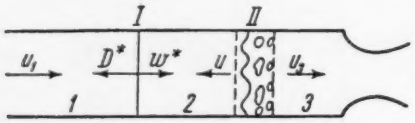

Fig. 8 Diagram showing propagation of nonstationary double discontinuity

the engine chamber we use the relation

$$\epsilon = \frac{q}{q_G} = \frac{u_1}{(u_1)_G} = \frac{M_1}{(M_1)_G} \qquad [18]$$

We see that this dimensionless criterion, introduced by Knorre (11) on the basis of consideration of the thermal choking (12), characterizes the relative position of the point on the lower branch of the Hugoniot curve, describing the combustion mode in the chamber of the engine. In the limiting case, during a completely developed deflagration $\epsilon = 1$.

Assuming that there occurs in the chamber of the engine a frontal turbulent combustion, let us estimate the relative increase in the surface of combustion

$$\frac{S}{F} = \frac{u_1}{u_n} = M_1 \frac{\sqrt{k(p_1/\rho_1)}}{u_n} \qquad [19]$$

to where u_n is the normal speed of the flame. The assumption concerning the existence of such a mechanism of ignition makes it possible to visualize very clearly the degree of forcing of the mode from the point of view of the required development of the surface of the flame in zone II. From Table 1 and relations [5 and 19], it is seen that the maximum required development of the combustion surface occurs in the fully developed deflagration mode, and that for a high caloric oxygen mixture it is not so large [$(S/F)_{max} \sim 11.5$]. If the combustion in zone 2 occurs in accordance with some other mechanism, for example, the mechanism of successive centered self-ignition of the combustible fuel mixture, heated through mixing with the final reaction products, the entire analysis above will be correct also for this case. What is most important is that the amount of mixture consumed per unit time remain constant for the specified deflagration mode. In the case of combustion by the mechanism of successive centered self-ignition, this quantity is determined by the number of self-ignition centers and their dimensions in zone II.

Appendix

The problem of the propagation of flame in the hot gas mixture in a tube with escape of reaction products into the atmosphere through a nozzle will be discussed.

Any combustion mode, describable by some point on the curve AG (Figs. 1 and 4) is characterized not only by definite values p_2/p_1, ρ_1/ρ_2, u_1, u_3, M_3, F/F_*, but also with a value of S/F in the combustion zone II. What happens if the length of the combustion chamber (region 1) is sufficiently large and, for some reason (for example, owing to instability (13)), the surface S of the flame increases, and the rate of injection of the cold gas u_1 and the value of the constriction of the nozzle F/F_* does not change? It is clear that in this case the conditions in the zone of the thermal jump, owing to the increased velocity of combustion, will satisfy the conservation laws, and the thermal jump will break up into a new thermal jump II and the shock wave I, which will begin to propagate opposite the injected cold gas. If the surface of combustion S begins to increase progressively during the mode of fully developed deflagration ($M_3 = 1$, $F/F_* = 1$), this case will not differ from the previously considered (7) case of propagation of a flame, occurring after completely developed deflagration is reached. The subcritical modes of propagation of the flame will be absent, and all the critical modes will fall on the Oppenheim curve (GE_2I, Fig. 7) which is described by the generalized Hugoniot equation

$$\frac{p_2}{p_1} = \frac{\mu\left[\kappa - \frac{\rho_1}{\rho_2}\left(\frac{\kappa\mu+1}{\kappa+\mu}\right) + \frac{2Q}{p_1/\rho_1}\left(\frac{\kappa\mu+1}{\kappa+\mu}\right)\frac{1}{\mu}\right]}{\kappa\frac{\rho_1}{\rho_2}\left(\frac{\kappa\mu+1}{\kappa+\mu}\right) - 1} \qquad [20]$$

However, if the combustion surface S increases in the mode of incomplete deflagration, for example, in modes describable by point m (Figs. 1, 4, 7) the pattern of propagation of the nonstationary double discontinuity will be analogous to that shown in Fig. 8. Such modes of flame propagation can also be described by Equation [20], by finding a connection between ρ_1/ρ_2 and μ, a connection which in this case is much more complicated than in the previously considered cases (7).

As before, we shall specify values of the amplitude of the shock wave $\mu = p_2/p_1$. Then to determine the velocity and the density of the shock-compressed gas (2) and also the velocity of the shock wave itself, we have

$$\varphi = \frac{\rho_2}{\rho_1} = \frac{\kappa\mu+1}{\kappa+\mu}$$

$$\frac{w}{a_n} = (\mu-1)\sqrt{\frac{2}{(k-1)+(k+1)\mu}} \qquad [21]$$

$$Dw/(p_1/\rho_1) = \mu - 1$$

As we examine Fig. 8, we see that the front of the shock wave I moves with respect to the gas 1 with a velocity D, and with respect to the walls of the tube with a velocity $D^* = D - u_1$. Gas 2 moves relative to gas 1 with a velocity w, and relative to the walls of the tube with a velocity $w^* = w - u_1$. In the case of weak shock wave, when $w < u_1$, the gas 2 flows to the right relative to the wall of the tube; at sufficiently strong shock waves, when $w > u_1$, the shock compressed gas moves to the left relative to the walls of the tube. We see, furthermore, that in subcritical regions, as well as in both weak and strong shock waves, zone II moves; relative to the gas in region 2 its velocity is

$$u = v - w^* \qquad [22]$$

relative to the walls of the tube its velocity is

$$v = u + w^* \qquad [23]$$

and relative to the gas in region 3 its velocity is

$$u_3 + v < a_3 \qquad [24]$$

Consequently, considering the transition of the gas from state 2 into 3, one can imagine (Fig. 9) that zone II is at rest, that the shock compressed gas 2 enters this zone with velocity u, and that the product of reaction leaves this zone with velocity $u_3 + v$. Since the combustion zone II in accordance with Equation [24] moves during subcritical modes of flame propagation, at a velocity relative to the gas 3 smaller than the speed of sound in these reaction products, the pressure and density in the entire region 3 for a specified mode of flame propagation (for specified μ) remains constant. And since the constriction of the nozzle does not change, at subcritical modes, the number M_3 remains unchanged in the entire region 3 for all values of u

$$M_3 = u_3/a_3 = \text{constant} \qquad [25]$$

Solving Equations [23 and 25] and the equations for the conservation of mass, momentum and energy in the transition of the gas from state 2 into state 3 through combustion zone II, we obtain for the subcritical modes the following relations which connect ρ_1/ρ_3 with μ in the generalized Hugoniot equation [20]

$$\left(\frac{a_3}{a_n}\right)^4 + \left(\frac{a_2}{a_n}\right)^3 b + \left(\frac{a_3}{a_n}\right)^2 c + \left(\frac{a_3}{a_n}\right) d + e = 0 \qquad [26]$$

$$b = -\frac{4M_3\left(\frac{w}{a_n} - \frac{u_1}{a_n}\right)\left(\frac{1}{k} + M_3^2\right)}{\frac{4}{k(k-1)^2} - \frac{2M_3^2}{k} - M_3^4}$$

$$c = \left\{2\left(M_3^2 + \frac{1}{k}\right)\left[\left(\frac{w}{a_n} - \frac{u_1}{a_n}\right)^2 + \frac{\mu}{\varphi}\right] - 2\left[\frac{2Q}{(a_n)^2} + \frac{\mu}{\varphi}\frac{(k+1)}{(k-1)}\right]\frac{k+1}{k(k-1)} - 8\left(\frac{w}{a_n} - \frac{u_1}{a_n}\right)^2 M_3^2 - \frac{4M_3^2}{\varphi}\mu - \frac{4}{k}\left(\frac{w}{a_n} - \frac{u_1}{a_n}\right)^2\right\}\left\{\frac{4}{k(k-1)^2} - \frac{2M_3^2}{k} - M_3^4\right\}^{-1}$$

$$d = -\frac{\left[4M_3\left(\frac{w}{a_n} - \frac{u_1}{a_n}\right)^2 + 4M_3\frac{\mu}{\varphi}\left(\frac{w}{a_n} - \frac{u_1}{a_n}\right)\right]}{\frac{4}{k(k-1)^2} - \frac{2M_3^2}{k} - M_3^4}$$

$$e = \frac{\left[\frac{2Q}{a_n^2} + \frac{\mu}{\varphi}\left(\frac{k+1}{k-1}\right)\right]^2 - \left[\left(\frac{w}{a_n} - \frac{u_1}{a_n}\right)^2 + \frac{\mu}{\varphi}\right]^2}{\frac{4}{k(k-1)^2} - \frac{2M_3^2}{k} - M_3^4}$$

$$\frac{u_3}{a_n} = \frac{a_3}{a_n} M_3 \qquad [27]$$

$$\frac{v}{a_n} = \frac{\frac{2Q}{(a_n)^2} + \frac{2k}{k-1}\frac{\mu}{\varphi} - \frac{2}{k-1}\left(\frac{a_3}{a_n}\right)^2 + \left(\frac{w}{a_n} - \frac{u_1}{a_n}\right)^2 - \left(\frac{u_3}{a_n}\right)^2}{2\frac{u_3}{a_n} + 2\left(\frac{w}{a_n} - \frac{u_1}{a_n}\right)} \qquad [28]$$

$$\frac{u}{a_n} = \frac{v}{a_n} - \left(\frac{w}{a_n} - \frac{u_1}{a_n}\right) \qquad \frac{\rho_1}{\rho_3} = \frac{(v/a_n + u_3/a_n)}{\varphi u/a_n} \qquad [29]$$

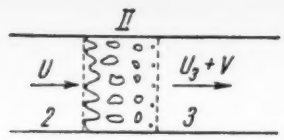

Fig. 9 Transition of gas from state 2 into 3 through the combustion zone II

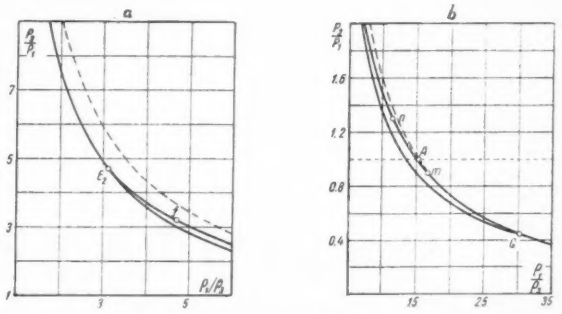

Fig. 10a and b: Sections of curves of the ordinary and generalized Hugoniot adiabatic

Since the quantities M_3 and u_1 (along with p_1, ρ_1, k and Q) are known for a definite deflagration mode, then, by specifying μ and finding φ and w/a_n from Equation [21] we calculate the coefficients b, c, d and e. We then determine a_3/a_n from Equation [26], followed by u_3/a_n, v/a_n, u/a_n and ρ_1/ρ_3 from Equations [27, 28 and 29] respectively.

Having thus established a connection between ρ_1/ρ_3 and μ, we can now, starting with Equation [20] determine p_3/p_1, i.e., find the place on the p-p diagram for a given subcritical unsteady mode of flame propagation (for given u). Such subcritical modes correspond to points on the curve $mnfE_2$ (Figs. 7 and 10). This curve originates on the Hugoniot deflagration branch and ends on the Oppenheim curve. The point E_2 corresponds exactly to the transition from the subcritical mode to the critical one, at which the surface of the flame S rises so much, that the combustion zone II begins to move relative to gas 3 with local velocity of sound. Obviously the "family of points m" on the deflagration Hugoniot curve will correspond to a "family of corresponding points E_2" on the Oppenheim curve and only in completely developed deflagration do the two points m and E_2 coalesce into one point G.

The speed of propagation of the flame, the shock wave and the pressure in regions 3 and 2, occurring in combustion modes describable by the points of curve m and fE_2, can be estimated from Table 2.

A solution of this problem may be useful to the analysis of fluctuations of combustion in jet engine chambers.

References

1 Zel'dovich, Ya. B. and Kompaneets, A. S., "Theory of Detonation," Gostekhizdat, Moscow, 1955.

2 Lewis, B. and Elbe, G., "Combustion, Flames and Explosions of

Table 2 Velocities of the gas, combustion front, shock wave, density and pressure in subcritical modes of flame propagation

Points	p_3/p_1	ρ_1/ρ_3	u, m/sec	v, m/sec	u_3, m/sec	$\mu = p_2/p_1$	D^*, m/sec
m	0.9	16.96	20	0	338	1.0	
n	1.3	11.75	27.6	99.6	337.8	1.5	336
f	3.18	4.72	53.5	450	335	5	595
E_2	4.67	3.15	76	722	333	10	845

Gases," Cambridge Univ. Press, 1938, p. 246.
3 *Ibid*, 1951 ed., p. 597.
4 Courant, R. and Friedrichs, K. "Supersonic Flow and Shock Waves," 1948, pp. 231, 234.
5 Shchelkin, K. I., "On the Theory of Occurrence of Detonation in Gas Mixtures and Tubes," *DAN SSSR* (*Transactions, Academy of Sciences, USSR*), vol. 23, 1939, p. 636. "Combustion in a Turbulent Stream," *J. Tech. Physics*, USSR, vol. 13, 1943, p. 520.
6 Damköhler, G., "Der Einfluss Turbulenz auf die Flamengeschwindigkeit in Gasgemischen," *Zeitschrift für Elektrochemie*, vol. 46, 1940, p. 601.
7 Troshin, Ya. K., "Gas Dynamic Analysis of Non-Stationary Processes of Flame Propagation in Tubes," *Izvestiia AN SSSR, OTN* (*Bull. Acad. Sci. USSR, Div. Tech. Sci.*), no. 1, 1956, p. 80.
8 Zel'dovich, Ya. B. and Ratner, S. B., "Calculation of the Speed of Detonation in Gases," *J. of Experimental and Theoretical Physics* (USSR), vol. 11, 1941, p. 170.
9 Kistiakowsky, G. B., Knight, H. T. and Malin, M. E., "Gaseous Detonation III. Dissociation Energies of Nitrogen and Carbon Monoxide," *J. Chem. Phys.*, vol. 20, no. 5, 1952, p. 767.
10 Zel'dovich, Ya. B., "On the Energy Utilization of Detonation Combustion," *J. Tech. Phys.* (*USSR*), vol. 10, no. 17, 1943, p. 1453.
11 Knorre, G. F., "Comparative Analysis of the Characteristics of Flame Furnaces," *Transactions of NII-1*, published by the Bureau of New Technology, no. 1939, 1947.
12 Abramovich, G. N., "Motion of Heated Gas in Cylindrical Tubes," *Transactions of NII-1*, no. 5, 1945; *see also* "Going Through the Speed of Sound in Gas Flow," *DAN SSSR*, no. 3, 1946.
13 Troshin, Ya. K. and Shchelkin, K. I., "Structure of the Front of Spherical Flames and the Instability of Normal Combustion," *Izvestiia AN SSSR, OTN*, no. 9, 1955.

Structure of Turbulent Flame of Homogeneous and Heterogeneous Mixtures

V. YA. BASEVICH and S. M. KOGARKO

Institute of Chemical Physics Academy of Sciences, USSR Moscow

It is known that the initial nonreacting fuel can be found in the tongue of a turbulent flame of homogeneous mixtures, and even in combustion products. This is confirmed also by the existing concepts of the possible mechanism of turbulence of the flame, for example, the surface model(1,2).[1] However, the quantitative aspect of this problem has apparently not been sufficiently investigated.

It is the purpose of this investigation to determine the concentration and the temperature of fuel and its rate of combustion in turbulent flames, so that an approach can be made to the study of its structure.

Description of Experiments

THE MAIN diagram of the setup is shown in Fig. 1. The apparatus consisted of a compressor, electric heater 1 to heat the air, interchangeable fuel atomizers 3 and a combustion chamber 6, in the input of which one could place the turbulizer 5. The two-dimensional tongue of the flame is stabilized by hydrogen burners 7. By rearranging the atomizers and by varying the temperature it was possible to obtain either a completely evaporated homogeneous mixture or fuel dispersed in the form of droplets with a negligible content of the vapor phase. The magnitude of the vapor phase was registered with special apparatus (parts 9–16). The fuel used was benzol and paraffin base kerosene, with a specific gravity 0.82 gm/cm³ and a boiling range 140–300 C (85.7 per cent C, 14 per cent H and 0.3 per cent remainder).

When operating with homogeneous mixtures, the concentration of the fuel (benzol) in the combustion zone was determined from its absorption spectrum. The measurements were carried out after collecting the gases in a quartz window cell provided with an electric heater. The cell was heated to the stream temperature at the entrance to the combustion chamber (125 C). Gas samples were gathered by periodically turning on the feed of the main fuel for a short period (1–2 sec). The gas collector and the connecting line did not become noticeably heated during the test. It was also possible to make the measurements directly in the combustion chamber through the quartz walls.

The light source used to photograph the benzol absorption spectra was an ion arc, the spectrum of which displayed a strong absorption of the lines in the wave length range λ = 2529 to 2531 Å. In the measurements, the intensity of the λ = 2529.1-Å line was compared with the intensity of λ_0 = 2527.4 Å, which practically experienced no absorption (Fig. 2).

A calibration curve showing the connection between the ratio logarithm $i = \log (I_\lambda / I_{\lambda_0})$ (where I and $I_{\lambda 0}$ are the readings of the microphotometer with correction for the emulsion characteristics for λ and λ_0 respectively) and the concentration of the benzol is shown in Fig. 3. Several samples were analyzed with a mass spectrometer.[2]

When working with atomized fuel, the trajectories (or more accurately the stream lines) of the drops in the combustion zone were first determined from direct photographs of the flame. The next step was to note one or several trajectories and determine the size distribution of the fuel drops and their number at various points of the trajectories. For this pur-

Translated from *Izvestiia Akademii Nauk SSSR, Otd. Tekhn. Nauk, Energetika i Avtomatika* (*Bull. USSR Acad. Sci., Tech. Sci. Div., Power and Automation*), no. 2, 1959, pp. 13–20.

[1] Numbers in parentheses indicate References at end of paper.

[2] The authors express their gratitude to V. L. Tal'roze for performing the mass spectroscopic measurements.

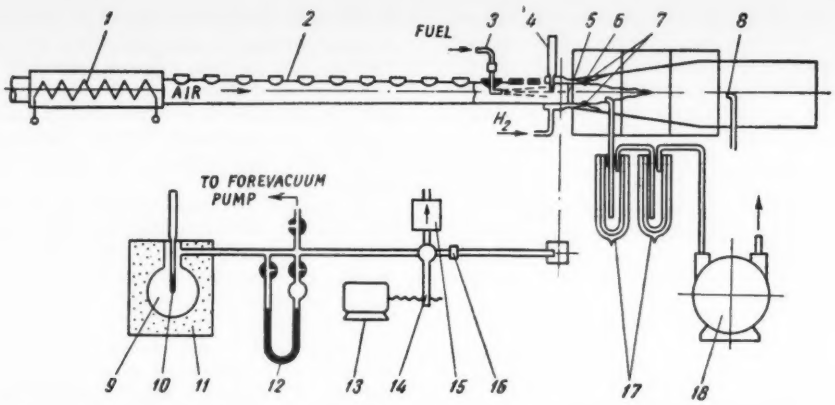

Fig. 1 Experimental setup: 1 electric heater; 2 tube; 3 nozzle; 4 thermometer; 5 turbulizer; 6 combustion chamber; 7 burner; 8 gas collector; 9 vessel; 10 thermometer; 11 thermostatic oven; 12 manometer; 13 electric motor; 14 valve; 15 electric stopwatch; 16 calibrated aperture; 17 trap with liquid nitrogen; 18 flow meter

pose we registered the prints of drops on rods covered with lamp black and magnesium oxide, the rod being rapidly drawn through the combustion zone. This was done by a special mechanism introduced into the combustion chamber (Fig. 4). The exposure of the rod, i.e., the time during which drops could settle through the slit and cover of the mechanism (height 0.5 to 6 mm) on the open surface of the rod, was determined with the aid of oscillographic pips produced by two pulses from a photocell. The latter was briefly illuminated through holes suitably placed in the rod. The exposure time was $\tau = \tau'\Delta/l$ where Δ is the height of the slit, l the distance between holes in the rod, and τ' the time between two pips. The rods with the prints of the drops were studied under a microscope (60×).

The travel time of the drop along any one trajectory was estimated by photographically scanning the flame through a suitably located slit. In experiments with homogeneous mixtures, the speed of the gas was determined by the same photographic scanning method, by mixing minute particles of magnesium into the stream.

For quantitative calculation of the completeness of combustion in experiments with pulverized fuel, note was also taken of local composition α' of the mixture at trajectory points located directly before the entrance of the mixture into the combustion zone. For this purpose a certain amount of fuel-air mixture was drawn through the flow meter 18, and the amount of fuel that settled in liquid-nitrogen traps (17, Fig. 1) was measured.

The Orth instrument was used to determine the concentration of CO_2, O_2 and CO in the reaction products, where they were gathered from the combustion zone by a water cooled gas collector.

In addition, the usual methods were used to determine the flow of air, fuel and other quantities.

Results of the Experiment

Homogeneous Mixtures

At first the changes in concentration of the initial fuel and of the final combustion products were compared along the combustion zone. To obtain a homogeneous mixture the temperature of the stream was maintained at 125 C and the atomizer was placed at the maximum distance from the combustion chamber. The conditions under which the experiments with benzol were made are listed in Table 1, where V is the stream velocity at the entrance to the combustion chamber, α is the coefficient of excess air and ϵ is the degree of turbulence in per cent.

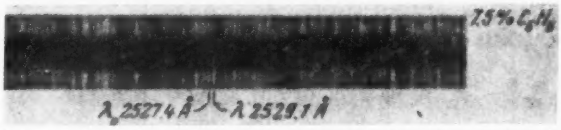

Fig. 2 Absorption spectrum; iron lines in benzol, wave length range from 2529 to 2531 Å

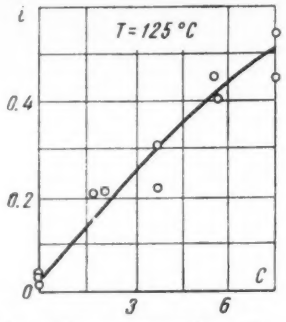

Fig. 3 Calibration of benzol absorption: C concentration of benzol by weight

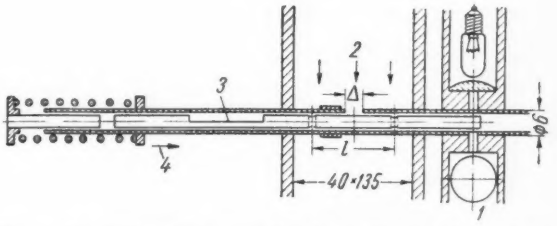

Fig. 4 Mechanism for transporting the rod through the combustion chamber: 1 photocell; 2 flow direction; 3 slug; 4 direction of motion of rod

Table 1 Conditions under which experiments with benzol were made

Experiment no.	V, m/sec	Mixture composition	Turbulizer	ϵ%
1	45	1.25	none	5
2	45	1	none	5
3	90	1	none	5
4	90	1	used	12

Fig. 5 shows for the sake of illustration the results of the experiment with $V = 90$ m/sec and $\alpha = 1.0$. The abscissas indicate here the length of the combustion chamber, and the ordinate the completeness of combustion. The completeness of combustion was determined from the decrease in the benzol, in accordance with the equation

$$\eta = I - (C/C_0) \qquad [1]$$

where C_0 and C are the initial benzol concentration and the concentration at a given point (obtained by analysis of the samples in the cells). The same figure shows the completeness of combustion as determined by the content of CO_2 and CO.

$$\eta = [CO_2 + CO]/[CO_2 + CO]_{max} \qquad [2]$$

where the square brackets denote the summary concentrations at the given point and the maximum value, calculated for the local values of the excess air coefficient. The content of other products in the combustion zone obtained by mass spectroscopic analysis, was not more than one per cent and was therefore disregarded in the balance. The speed of the gas was estimated from measurements made of the inlet and outlet of the combustion chamber and amounted to 90 and 120 m/sec. Fig. 5 shows the corresponding average time scale.

An attempt was made to estimate the temperature variation of the initial fuel in the combustion zone. For this purpose we obtained, for a mixture containing 7.5 per cent benzol, the temperature dependence $i = \log(I_\lambda/I_{\lambda_0})$, from which the contents of benzol in the sample were estimated (Fig. 6).

This ratio diminishes rather sharply with increasing temperature and approaches zero above 210 C. Thus, the method used makes it possible to register the presence of benzol vapor having a temperature not more than 210 C.

Fig. 7 shows the completeness of combustion determined from the decrease in the benzol contents in the analysis of the samples in cells, and determined directly in the combustion chamber. In the latter case we determine the concentration of the fuel by assuming for the initial concentration the calibration curve at 125 C. Here, as in other experiments, the values of η, determined from Equations [1] and [2] in the interval from 0 to 0.8, i.e., in the combustion zone, are practically the same. Thus, the fuel registered in the combustion zone has a temperature close to initial.

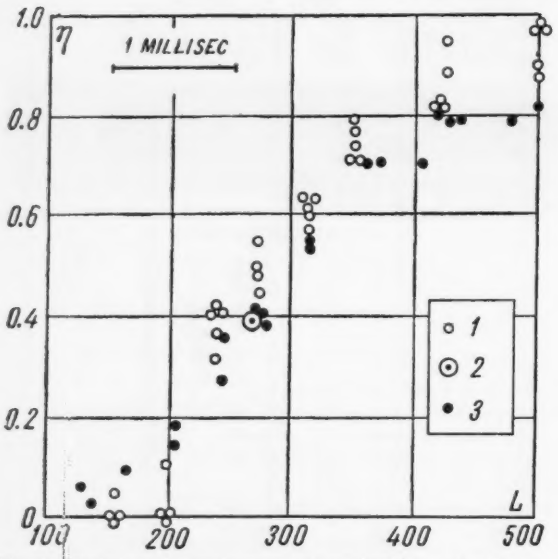

Fig. 5 Variation of completeness of combustion η of a homogeneous mixture along the length L (mm) of the combustion zone: 1 obtained by spectroscopic analysis of the benzol; 2 obtained by mass spectroscopic analysis; 3 obtained by analysis of the combustion products (experiment 4, Table 1)

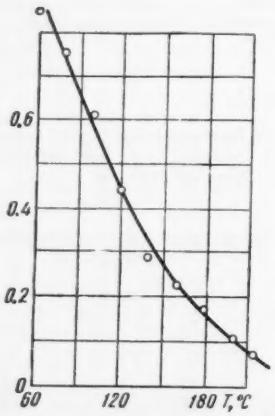

Fig. 6 Dependence of the calibration of benzol (7.5 per cent C_6H_6) absorption on the temperature T (deg C)

Heterogeneous Mixtures

In experiments with atomized liquid fuel the distribution of the drops by dimensions, their number and the contents of combustion products were determined along the stream lines in the combustion zone. The initial dimensions of the drops corresponded to those used in practice, amounting to 20 to 180 μ.

To determine the time dependence of the reduction in the drop diameter during combustion, use was made of the re-

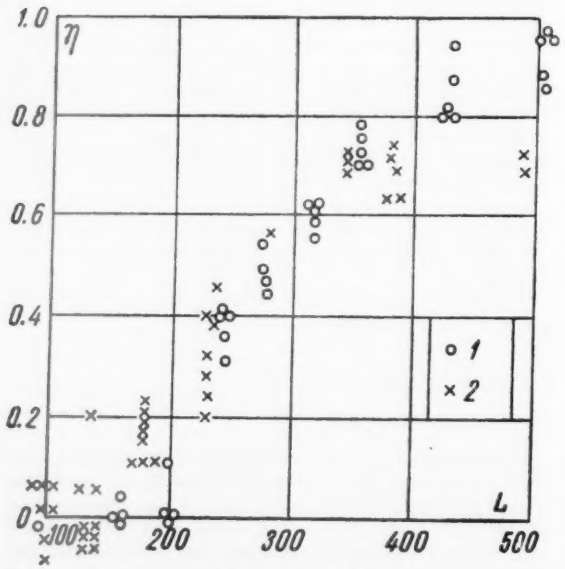

Fig. 7 Variation of completeness of combustion η of a homogeneous mixture along the length of the combustion zone L (mm): 1 obtained by analysis of benzol samples in the cell; 2 obtained by analysis of the benzol directly in the combustion zone (experiment 4, Table 1)

Table 2 Conditions of the experiments with atomized liquid fuel

Experiment no.	V, m/sec	Fuel	α	α'	$D\mu$
1	33	kerosene	1	...	175
2	33	"	1	...	192
3	33	"	2.55	...	88
4	10	"	0.71	1.9	192
5	56	"	1.05	1.36	192
6	33	benzol	1.1	3.36	192
7	10	"	1.83	2.3	159

distribution curves as shown in Fig. 8. Here the abscissa represents the diameters of the drops and the ordinates the relative concentration of drops of a given size $n = N/FV\tau$, where N is the counted number of particles of the given dimension group (deviation from normal $\pm 8\ \mu$), F is the measured area of the rod, V the local velocity of the stream in the combustion chamber and τ the exposure time of the rod. The points where the distribution curves for the various cross sections of the combustion zone intersect with the line of constant relative concentration, n = const (shown dotted in the figure), give successive values of the drop dimensions at a given initial diameter group.

For a known distance between droplets on the photographs and known speed of the gases, it is easy to calculate the corresponding combustion time and to obtain the actual variation of the drop diameters with time during the combustion process.

Experiments were carried out at an initial air temperature of 25 to 30 deg and with the atomizer placed in the closest position in the combustion chamber. Under these conditions the prior evaporation of the fuel was negligibly small.

The conditions of the experiments with atomized liquid fuel are given in Table 2, where V is the speed of the stream at the inlet to the combustion chamber, α and α' are the summary and local coefficients of excess air and D is the maximum drop dimension in the given experiments.

Fig. 9 shows the results of the experiments in the absence of combustion, from which the methodical errors can be estimated. The solid lines (almost straight, parallel to the abscissa) are the theoretical values of the diameters, based on the well-known formula

$$D_0^2 - D^2 = k\tau \qquad [3]$$

where D_0 and D are the initial and current group diameters of the drop, τ is the time and k is an evaporation (combustion) constant, with a value of 0.0035×10^{-2} cm²/sec. This corresponds to the theoretical value for the evaporation of kerosene under the experimental condition (simplified computation, using a coefficient of diffusion of 0.1 cm²/sec and a vapor tension of 30 mm mercury at the temperature of the experiment). As can be seen here, there was practically no reduction in the drop diameters, owing to the short evaporation time.

Figs. 10 and 11 show the relations obtained for the reduction in the group diameter of the drops in combustion. As a result of the considerable scattering of the points, no attempts were made to ascertain the influence of the conditions of each experiment on the speed of combustion. The solid lines here, too, correspond to theoretical values D, in accordance with Equation [3], with a value of the constant $k = 0.0059$ cm²/sec, previously obtained by the gas analysis method (τ is the combustion time).

In spite of the great scatter in the experimental points, it is seen that when $D_0 = 180$ to $100\ \mu$, within the limits of the indicated time, the experimental values are more or less in satisfactory agreement with the theoretical curves. However,

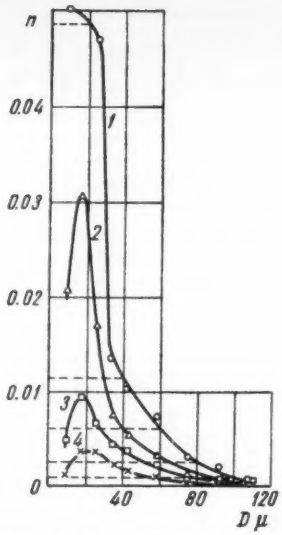

Fig. 8 Dependence of relative droplet concentration (n, mm³) on the diameter (D) at various distances (L, mm) along the combustion chamber: 1, 120; 2, 200; 3, 270; 4, 350

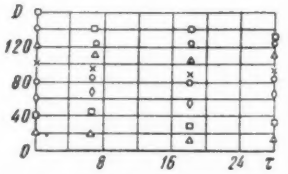

Fig. 9 Dependence of the droplet group diameter D (μ), in evaporation without combustion, on the time τ (millisec)

starting with $D_0 = 80\ \mu$ and below, one observes already quite clearly a noticeable reduction in the speed of combustion compared with the calculated values, and the smaller the size of the drops the greater this reduction.

This reduction in the speed of combustion cannot be the consequence of the fragmentation of larger drops into smaller ones, for the same results were observed in an experiment where only small drops were used (experiment 3).

Fig. 12 shows a comparison of the completeness of combustion, calculated on the one hand from the photographs of the drops, using

$$\eta' = \left(\sum_i n_i D_{0i}^3 - \sum_i n_i D^3\right) \Big/ \sum_i n_i D_{0i}^3 \qquad [4]$$

where i is the index of the given group of size D_0; and calculated on the other hand from Equation [2], with allowance for the experimentally determined local excess-air coefficients. Although the transverse velocities of the drops and of the gases were different, the error introduced by this difference in the computed value of η was disregarded. The solid lines correspond to purely diffusion mechanism of combustion.

Discussion of Results

It follows above all from the experiments with homogeneous mixtures that a gradual decrease in the concentration of the initial fuel and a corresponding increase in the combustion

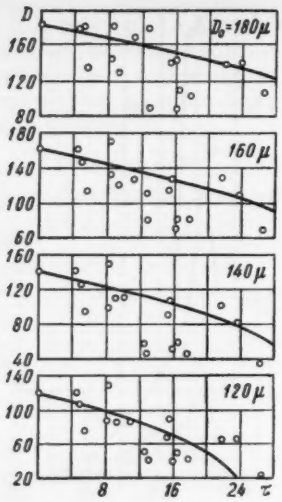

Fig. 10 Dependence of the droplet group diameter D (μ) during combustion on the time τ (millisec); D_0 = 180 to 100 μ

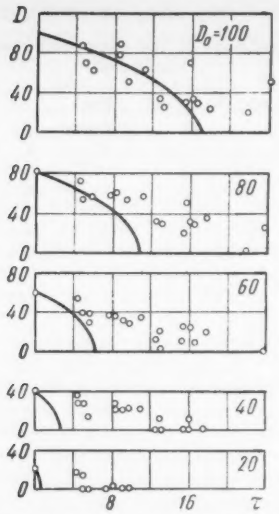

Fig. 11 Dependence of the droplet group diameter D (μ) during combustion on the time τ (millisec); D_0 = 80 to 20 μ

products occurs over the combustion zone. The discrepancy between the points obtained by measuring the concentration of the benzol and those obtained by measuring the composition of the combustion product does not exceed 1 millisec. This time is quite close in order of magnitude to the time of conversion in laminar flames, approximately 0.5 millisec.

In addition, it follows from results of the experiments that the fuel temperature in the combustion zone is practically equal to initial. This indicates that there is no noticeable mixing of the combustion products with the initial mixture.

It can be stated that if the initial conditions are $P = 1$ atmos, $\tau \leq 125$ C, the combustion zone of homogeneous hydrocarbon-air mixtures, even at speeds up to 90 m/sec and strong turbulence, consists of unmixed volumes of the initial mixture (at a temperature close to initial) separated by the zone of the chemical reaction from combustion products. This confirms the conclusion, previously made on the basis of spectroscopic and temperature measurements (3), that at any point in the combustion zone, both at its beginning and its end, the conditions under which the chemical reaction takes place are identical, and there are no grounds for adopting the three-dimensional combustion model of a turbulent flame, proposed by Summerfield (4).

Let us estimate the errors of the procedure employed in experiments with atomized liquid fuel. One of the sources of errors may be the known fact that, when a blast passes over an obstacle, only sufficiently large particles settle, and small particles settle either incompletely or not at all. The effectiveness of the settling is characterized by so-called settling coefficient, which depends on the Stokes number.

Using the known experimental data on the inertial settling of aerosols (5), and estimating the Stokes number for the worst case, for the minimum stream velocity at which the investigation was carried out (10 m/sec) and for drops of the smallest size (20 μ) at a gas temperature of 900 C (the average of the maximum and minimum temperatures in the combustion chamber), we obtain a value of 50 per cent for the settling coefficient. At larger velocities and at larger particle dimensions the settling coefficient is also greater and approaches unity. Owing to the incompleteness of the theory of inertial settling and of the relatively large dimensions of the drops used in this investigation, no correction for the settling coefficient was made in our calculations. It is important to point out here, however, that a decrease in the settling coefficient during combustion may lead only to an increase in the observed combustion rate but not to a reduction, i.e., it can lead to a faster decrease in the drop diameters.

Another source of errors that results from the turbulence of the flow may be the transverse transfer of drops, the settling of drops on the walls of the chamber and their breaking up, and also coalescence of drops. A slight effect of all these factors was observed during the experiment in the absence of combustion, since a satisfactory agreement was obtained between the experimental and calculated values of the drop diameters.

In experiments with atomized liquid fuel, in the case of sufficiently large drops, a correspondence was found between the values of the drop diameters in the combustion zone, determined experimentally, and those calculated with Equation [3], using the diffusion mechanism.

For small drops ($D_0 \leq 80$ μ), merely the use of Equation [3], with a value of τ equal to the total time of stay of the drop in the combustion zone, obviously cannot describe satisfactorily the experimentally observed speed of combustion. The experimental data on homogeneous mixtures indicate a possible cause of this disagreement: Apparently not every drop is surrounded by a zone in which combustion takes place, but such a zone is produced for a group of drops, leaving many cold unignited drops. It follows therefore that the deviation from this formula does not indicate that the diffusion mechanism of

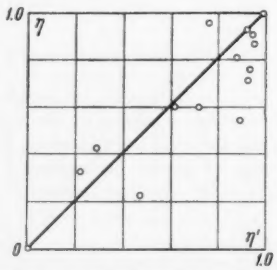

Fig. 12 Comparison of completeness of combustion η', obtained from droplet photographs and Equation [4], and η, obtained by gas analysis and Equation [2]

combustion of the drops does not apply. It is possible that the use of Equation [3] for minute drops in turbulent stream will lead to correct results if one introduces in it a function $f(p)$ of the probability p of drop ignition.

$$D_0^2 - D^2 = kf(p)\tau \qquad [5]$$

At the beginning of the combustion zone $p = 0$, and after a certain time τ^* it approaches unity. One can assume that this time, at any rate for small drops, is on the order of magnitude of the time of combustion of a homogeneous mixture, defined as a ratio of the length of the flow line in the combustion zone to the velocity. A large drop, having a greater mass, follows the turbulent pulsations to a lesser degree, and it is therefore possible to assume a greater probability of such a drop becoming ignited by the fluctuating combustion zones. It is probable that the values of τ^* for large drops are less, and the rate of increase of the ignition function $f(t)$ is greater, so that the deviation from the combustion law given in Equation [3] manifests itself to a lesser degree.

An agreement was obtained in the experiment between the amount of fuel in the combustion zone, in the liquid phase in the form of drops, and the concentration of the final combustion products, although a certain deviation toward lower values of completeness of combustion does exist. This means that the mechanism of the diffusion combustion of the drops is fundamental, although deviations from it are possible, particularly under conditions that differ noticeably from the conditions under which these experiments were performed (for example, in an accelerating stream).

Conclusions

1 In a turbulent flame of homogeneous oxygen-air mixtures with initial conditions $P = 1$ atmos and $T \leq 125$ C, a change occurs in the concentration of the initial fuel and there is a corresponding increase in concentration in the combustion products over the entire length of the combustion zone. The time of transformation is less than one millisec; the fuel-air mixture in the combustion zone has a temperature close to initial.

2 In the combustion of atomized fuel in a turbulent stream, the decrease in the group diameter of the large particles (180 to 100 μ) is satisfactorily represented by Equation [1] under the conditions of the experiment.

3 In the combustion of small drops (≤ 80 μ), formula [1] is inadequate for the description of the change in the group diameter, and corrections must be introduced to take into account the probability of ignition and combustion of the drops.

References

1 Damköhler, G., "Der Einfluss der Turbulenz auf die Flammengeschwindigkeit in Gasgemischen," *Z. Electrochemie*, vol. 46, p. 601, 1940.

2 Shchelkin, K. I., "Combustion in Turbulent Flow" *Zhurnal Tekhnicheskoi Fiziki* (*J. Tech. Phys.*), vol. 13, p. 520, 1943.

3 Basevich, V. Ya., "Spectroscopic Investigation of a Turbulent Flame," *Zhurnal Fizicheskoi Khimii* (*J. Phys. Chem.*), vol. 32, p. 1077, 1958.

4 Summerfield, M., Reiter, S. H., Kebely, V. and Mascolo, R. W., "The Structure and Propagation Mechanism of Turbulent Flames in High Speed Flow," Jet Propulsion, vol. 25, p. 377, 1955.

5 Fuks, N. A., "Mekhanika Aérozolei" (Mechanics of Aerosols), USSR Academy of Sciences Press, 1955.

Effect of Flow Pulsations on the Turbulent Speed of Flame Propagation

L. S. KOZACHENKO

The mechanism of flame propagation in a turbulent stream is considered. A burner is described in which the degree of turbulence can be varied from 1.7 to 15.7 per cent. Measurement of the turbulent characteristics by means of a glow-discharge anemometer and a thermal anemometer has shown that the glow discharge exhibits no time delay at a pulsation rate up to 20 kc and that it can be used under laboratory conditions. An experimental estimate is made of the role of flow pulsations in the transfer of the flame through the combustible mixture. Certain results are reported on the measurement of flow pulsations behind various turbulizing devices under conditions of isothermal flow and combustion of a homogeneous fuel-air mixture. It is shown that the turbulent flame speed can be represented in the form of the sum

$$u_t = u_n + u' + u''$$

where u_n is the normal speed of propagation of the flame, u' the mean square pulsation of the isothermal flow and u'' the additional pulsation generated by the flame. The setup included a fixture for measuring the flow of air and fuel in a Töpler chamber for recording on motion film the dimensions of the combustion zones by means of a series spark discharge.

Measurement of Turbulence With Glow-Discharge Anemometer

WITHOUT dwelling in detail on the advantages and shortcomings of thermal anemometers, we note that a glow-discharge anemometer is free of many shortcomings inherent in thermal anemometers, mostly since it has no inertia, is small and permits the recording of high-frequency pulsations.

Fig. 1 shows the diagram and the basic power-supply circuit for a glow discharge, based essentially on the schemes of Lindwall (1)[1] and Zakharov (2).

Fig. 1 shows schematically a discharge gap, in which the electrodes are two sharply-pointed tungsten wires.

Translated from *Izvestiia Akademii Nauk SSSR, OTN, Energetika i Avtomatika* (*Bull. Acad. Sci. USSR, Div. Tech. Sci., Power and Automation*), no. 2, 1959, pp. 21–25.

[1] Numbers in parentheses indicate References at end of paper.

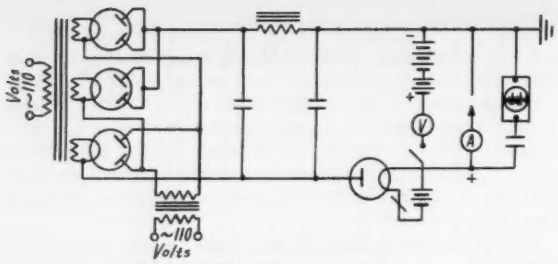

Fig. 1 Glow-discharge circuit

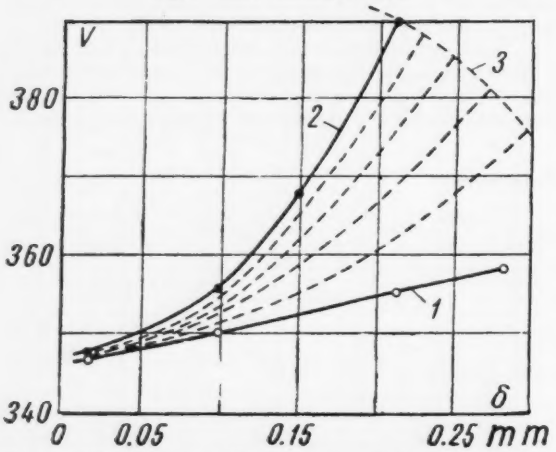

Fig. 2 Voltage across electrodes of glow discharge as function of the gap and of the rate of flow. Curve 1: speed zero m/sec. Curve 2: speed 25 m/sec. The dotted curves are drawn for velocity intervals of 5 m/sec. Curve 3 corresponds to the limits at which the glow discharge breaks up

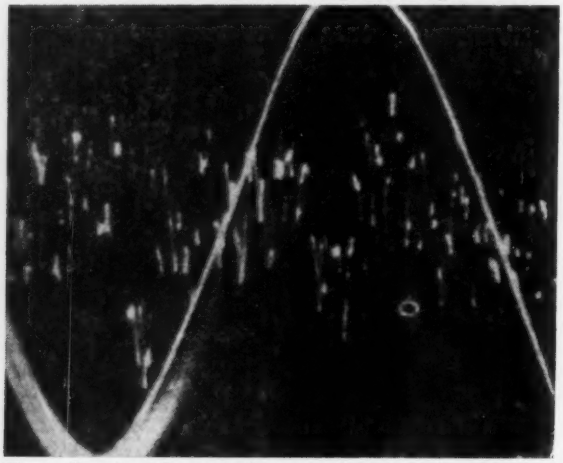

Fig. 3 Sample of flow pulsations recorded with a glow-discharge anemometer

Table 1

No.	Turbulizer	Mesh	2 mm diam	Smooth tube	5 mm diam	8 mm diam
1	ϵ_1	1.7	4	4.9	8.5	15.7
2	ϵ_2	...	...	5.05	7.4	14.2
3	ϵ_3	...	5.6	...	10.0	17.0
4	ϵ_4	5.7	10.3	12.0	17.0	23.5
5	ϵ''	4.0	4.37	1.45	4.5	4.55
7	$\epsilon_1 + \epsilon''$	5.70	8.37	9.35	13.0	20.25
8	$\frac{\epsilon_1}{\epsilon_1 + \epsilon''} 100\%$	1.0	1.29	1.29	1.28	1.18

With a total of 1300 v d-c applied, the current in the glow discharge was adjustable from 7 to 20 milliamp.

The electrode voltage of the glow discharge is plotted in Fig. 2 as a function of the gap and of the rate of flow, at a glow-discharge current of 10 milliamp.

If the gap between electrodes is fixed and the current is constant, the voltage across the terminals of the glow discharge varies in direct proportion to the change in flow velocity over the entire interval, until the glow discharge breaks down.

Fig. 3 shows an oscillogram of the voltage pulsations across the electrodes of the glow discharge, obtained in a section of the tube behind a turbulizer with $d = 5$ mm under conditions of isothermal flow of air with $Re = 20{,}000$, as compared with a sinusoidal voltage amplitude 2.7 v and frequency 50 cycles.

Oscillograms of the pulsations of the voltage (flow velocity) show the possibility of employing a glow discharge for registration of higher frequencies of flow pulsation up to 20 kcs, as compared with the thermal anemometer; furthermore, this is not the limit.

An analysis of the pulsation spectra obtained shows the presence of pulsations that exceed the mean square value of the pulsating component of the current by a factor of 3 or 3.5. The distribution of the pulsations is Gaussian.

Among shortcomings of flow-pulsation estimates made with a glow discharge are the following:

1 The cumbersome procedure required to process the oscillograms.

2 Instability of the glow discharge at the slightest contamination of the air with carbonic acid or with oil aerosols.

3 The plot of the variation of the voltage per meter of velocity and the subsequent oscillographic record must be made without changing the gap of the glow discharge.

4 Breakdown of the glow discharge at increased flow velocity.

Results of Measurements of the Degree of Turbulence

A glow-discharge anemometer was developed and the turbulent characteristics of the flow were measured in the laboratory using a burner section measuring 40 × 40 mm. Engineer Yu. A. Bokhon of the Institute of Chemical Physics, Academy of Sciences, USSR and diploma student K. V. Yushko of the Moscow Engineering Physics Institute participated in the project.

The results of the measurement of turbulent characteristics, as represented by the degree of turbulence $\epsilon = u'/V$ (per cent), are given in Table 1.

Measurements of the degree of turbulence by means of a thermal anemometer were set up for the same burner, under the same technical conditions, at the laboratory of E. S. Shchetinkov. The results of these measurements are also listed in the table, together with the degree of turbulence calculated from the data of Baines and Peterson (3).

Baines and Peterson's higher values of the degree of turbulence can be attributed to the double-row gratings used in that investigation, with perpendicular placement of the bars, whereas in our case, we used a single row of parallel bars spaced $2d$ apart.

The d degree of turbulence measured with glow-discharge and thermal anemometers deviates from the mean by a maximum of ±6.5 per cent, which can be considered good agreement for measurements of this type.

An estimate of the degree of turbulence based on flame measurement was carried out using Töpler photographs of the combustion zone, obtained with the burner shown in Fig. 4.

Two faces of a square 40 × 40-mm burner were shortened by 40 mm and were joined to quartz optical plates measuring 150 × 240 mm. In the case of flames of large size, the number of plates was doubled, so that a flame up to 480 mm long could be photographed. The two other faces of the channel, located between the quartz plates, were equipped with a de-

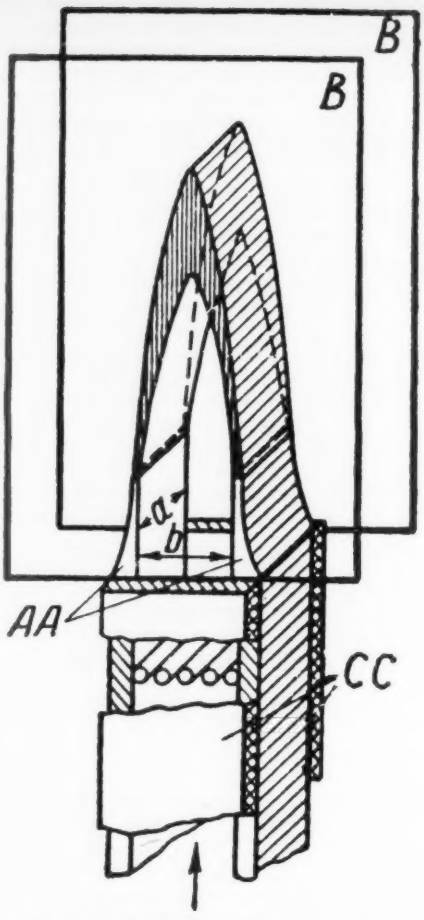

Fig. 4 Diagram of experimental burner

vice for the feed of additional fuel mixture to the section of the burner serving as a stabilizing source of ignition of the initial mixture.

As shown schematically in Fig. 4, a fixture for the insertion of a turbulizer was located at a distance of 55 mm from the section of the burner. The turbulizers used were either wires of diameter $d = 2$, 5 and 8 mm, installed in a single row with a spacing of $2d$ between axes, or a wire mesh with 625 holes per cm^2. Commercial smooth tubing having a natural turbulence was also used.

Fig. 5 shows diagrams of the combustion zone at combustible-mixture constant speed $V = 33$ m per sec and a normal flame speed $u_n = 0.52$ m per sec.

In these drawings, the lower half shows the outline of the actual combustion zone, obtained by taking moving pictures of the flame with a spark discharge, using the Töpler method.

Figs. 5a, 5b and 5c show the combustion zones obtained with turbulizers with $d = 8$ mm, smooth tubing, and mesh. The respective degrees of turbulence were found to be, for isothermal flow, 15.7, 14.9 and 1.7 per cent.

The upper half of Fig. 5c shows the scheme whereby the flame is transferred by the pulsations of the flow. Toward the center of the tube, on the side of the fresher fuel mixture, the rate of transfer of the flame is $u_t = u' + u_n$ while on the combustion product side, we have $u_t = u' - u_n$. In the case of isotropic turbulence, the longitudinal and transverse pulsations are equal to each other. Consequently, the degree of turbulence determined from the combustion zone will be

$$\epsilon = \tan(\alpha/2) \times 100 \text{ per cent} \qquad [1]$$

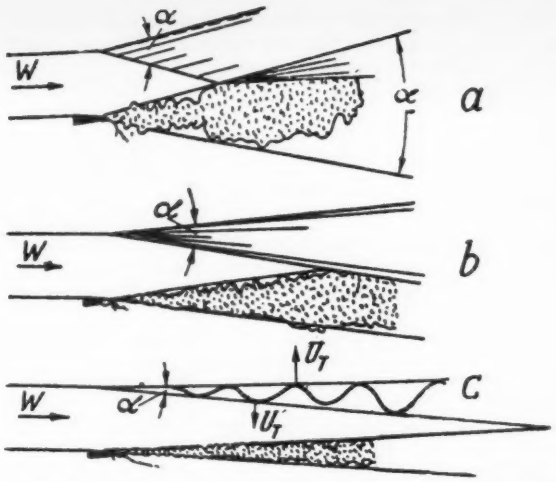

Fig. 5 Combustion zone at constant flow velocity $V = 33$ m/sec, $u_n = 0.52$ m/sec, and variable degree of turbulence of isothermal flow: (a) $\epsilon = 15.7$ per cent, (b) $\epsilon = 4.9$ per cent, (c) $\epsilon = 1.7$ per cent

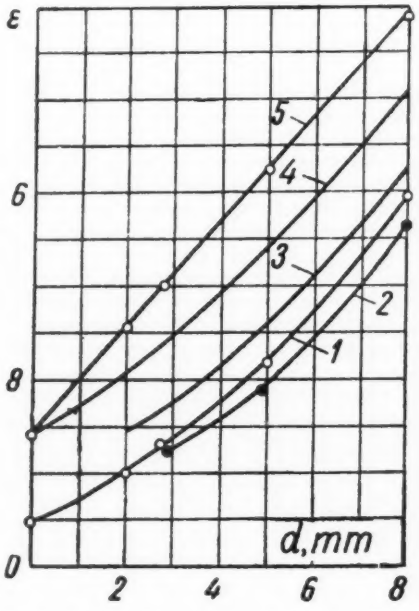

Fig. 6 Degree of turbulence after various data

Thus, the effective pulsation is

$$u' + u'' = V \tan \alpha/2 \qquad [2]$$

The measured values of the degree of turbulence, obtained by this method at an average flow rate of 33 m per sec, are shown in Fig. 6 and in the table.

As can be seen from Fig. 6 and from the table, the degree of the turbulence, measured in the combustion zone, increases in direct proportion to the diameter of the wires of the turbulizing mesh and exceeds considerably the degree of turbulence measured in isothermal flow.

Using the method of Bela Karlovitz (4) to estimate the pulsations of the flow and putting

$$\cos \alpha = u_n/(u_n + u')$$

where α is the angle between the normal to the local surface of the flame and the direction of propagation of the turbulent flame, the degree of turbulence generated by the flame can be estimated from

$$\epsilon'' = \frac{u''}{V} = \frac{\pi - 1}{V3^{1/2}} u_n \left(1 - \frac{u_n}{u_n + u'}\right)^{1/2} \qquad [3]$$

where

π = increase in the specific volume of the gas after the passage of the flame front, with a numerical value of 6
u' = mean square pulsation of the isothermal stream in m per sec
u_n = normal speed of propagation of the flame, equal to 0.52 m per sec

The table and Fig. 6 show, for a mean flow velocity of $V = 33$ m per sec, the values of the degree of turbulence as functions of the turbulizing grids: ϵ_1—curve 1, measured with a glow-discharge anemometer in isothermal flow; ϵ_2—curve 2, measured with a thermal anemometer under the same conditions; ϵ_3—curve 3, in which u' is calculated after Baines and Peterson; $\epsilon_1 + \epsilon''$—curve 4, the total value of the turbulence; ϵ''—degree of turbulence measured with a flow-discharge anemometer and generated by the flame; ϵ_4—curve 5, the degree of turbulence measured in the combustion zone.

The degree of turbulence ϵ_4 estimated for the trail of the combustion zone exceeds by a maximum of 29 per cent that measured with allowance for the turbulence generated by the flame.

Considering that the degree of turbulence of isothermal flow was measured at a point located on the axis of the tube 135 mm away from the turbulizing mesh, or at a distance $2D = 80$ mm from the flame, the average value of the pulsations acting on the entire surface of the flame apparently differs somewhat from that obtained by these measurements, and this explains the 29 per cent discrepancy between these two methods of measurement.

The fact that individual pulsations may exceed the mean square value by a factor of several times also contributes, under combustion conditions, to the possibility of exceeding the summary pulsations, measured by means of the trail of the flame.

Consequently, the turbulent speed of the flame is the result of the normal flame speed and of the flow pulsation produced by the mixture combustion conditions

$$u_t = u_n + u' + u'' \qquad [4]$$

The results obtained confirm essentially the Damköhler-Shchelkin (5, 6) theory concerning the mechanism of flame transfer in a turbulent stream at a normal flame speed u_n and flow pulsations. However, the first approximation, made by Shchelkin, equating the pulsation that participates in the transfer of the flame to the mean square pulsation of the isothermal incident flow, is insufficient. Once the pulsations of the generated flame are taken into account, the Damköhler-Shchelkin mechanism is confirmed by our experiments.

One must also note that, starting with a physical representation of flame transfer by centers that project to a maximum extent opposite the direction of the fresh gas (7), our experiments confirm the mechanism of the flame transfer by flow pulsations and by the normal flame speed. When investigating the turbulent velocity u_t by the burner method, it is necessary to estimate the per unit flow across the internal envelope surface passing through the peaks of the projecting flame centers or through the internal cone of the flame. An estimate of the flow of gas per unit surface passing through the maximum area of the flame cone, as made by Karlovitz et al. (4), has no physical meaning, since both the original mixture and the combustion product pass through this surface. Unfortunately, these experiments (4) cannot be used for comparison with our data.

One must also note that the pulsation u'' generated by flame depends on the normal velocity of the flame u_n, and thus increases the value of the normal velocity of the flame during combustion of mixtures in turbulent flow. Thus, for the conditions of our experiments, with $u' \geq 3\, u_n$, we can assume

$$u'' = \frac{\pi - 1}{\sqrt{3}} u_n \approx 2.9\, u_n$$

Hence

$$u_t = 3.9\, u_n + u' \qquad [5]$$

References

1 Lindwall, F. C. A., "Glow Discharge Anemometer," *Electrical Engng.*, July 1934, p. 1068.
2 Zakharov, Yu. T., "Glow-Discharge Anemometer," *J. Tech. Phys. USSR*, vol. 9, 1939, p. 1971.
3 Baines, H. D. and Peterson, E. G., "An Investigation of Flow Through Screens," *Trans. ASME*, vol. 73, no. 5, 1951, p. 467.
4 Karlovitz, B., Denniston, D. and Wells, F., "Investigation of Turbulent Flames," *J. Chem. Phys.*, vol. 19, no. 5, 1951, p. 541.
5 Damköhler, G., "Der Einfluss der Turbulenz auf die Flammengeschwindigkeit in Gasgemischen," *Zeitschrift fur Elektrochemis*, vol. 46, 1940, p. 601.
6 Shchelkin, K. I., "Combustion and Turbulent Flow," *J. Tech. Phys.*, vol. 8, nos. 9–10, 1943, p. 520.
7 Zel'dovich, Ya. B., "Remarks on Combustion of a Fast Stream in a Tube," *J. Tech. Phys. USSR*, no. 3, 1944.

Effect of Pressure on the Speed of Flame Propagation in a Turbulent Stream

S. A. GOL'DENBERG and V. S. PELEVIN

Power Institute
Academy of Sciences, USSR
Moscow

The authors consider the propagation of a flame at pressures below atmospheric in thoroughly premixed combustible mixtures.

Heretofore, various persons have investigated mostly the response of the turbulent speed of the flame (u_t) to changes in the rate of flow w in the turbulence characteristics of the incident stream, the nature of the fuel and its concentration in the mixture, and also in the initial temperature of the mixture. It is noted that V. E. Doroshenko and A. I. Nikitov have carried out simultaneously research along the same lines as the authors.

Procedure and Experimental Setup

THE MOST convenient method for investigating the effect of pressure on the speed of flame propagation and on the size of the combustion zone in front of the flame, in the case of turbulent flow, is apparently the burner method. The choice of this method is also dictated by the need of determining, under comparable conditions, the effect of pressure on flame propagation under reduced pressures in laminar and turbulent flow, inasmuch as this method has already yielded results that establish the effect of pressure on the normal flame speed (1).[1]

The experiments were carried out with a gasoline-air mixture in the same experimental setup and the same burner (d = 16 mm, L = 900 mm) with which the normal flame speed was determined (1).

It is known that at relatively large flow rates, the normal speed of the flame and the stream speed are not equal even in one point in space. It is therefore necessary, under conditions of turbulent flow, that the front of the flame be stabilized. At reduced pressure, as established by Klaukens and Wolfhard (2) and Cullen (3), the limiting pressure and the limiting flame propagation speed depend on the diameter of the burner if the combustion process occurs without an artificial source of ignition. To exclude the influence of the burner diameter we used in this investigation, as in our earlier work (1), a stabilizer in the form of a flame ring around the orifice of the burner; the ring was produced by burning a gas-oxygen mixture. The source was of sufficient intensity not to affect the speed of flame propagation.

The speed of flame propagation was determined by directly photographing the internal glowing cone, using a time exposure. The image of the flame was projected from the negative on a screen, to natural size. As in our earlier work (1), the speed of the flame was determined from the size of the angle at the vertex of the cone. The pressure in the chamber varied from 760 to 100 mm mercury. The Reynolds number R was varied from 4×10^3 to 20×10^3. Most experiments were carried out at constant Reynolds numbers. Under these conditions, the pressure at the burner outlet increased with decreasing pressure in the chamber. The experiments were carried out at variable rates of combustible mixture flow, with constant flow at the burner outlet, and at varying pressures in the chamber. During the time of the experiments, the intensity of the turbulence remained practically constant with varying length of the burning flame. This latter circumstance makes it possible to evaluate more clearly the dependence of the process of flame propagation on the variation of pressure.

Results of the Experiments

Fig. 1 shows typical curves of the dependence of the turbulent flame speed (u_t) on the pressure and concentration of fuel in the mixture, at a constant Reynolds number. It is obvious from the course of the experimental curves that if the Reynolds number is constant, one observes in a turbulent stream, in the entire investigated region, a regular increase in the linear speed of flame propagation with decreasing pressure.

Thus, if the Reynolds number is constant, the general tendency of the pressure, with varying pressure, is the same in laminar and turbulent flows. As in the experiments with laminar flow, the positions of the maxima of the flame-speed curves remain constant with varying pressure, and occur at a fuel concentration of 2.4 to 2.5 per cent. The ignition boundaries become somewhat constricted with decreasing pressure.

On the basis of curves similar to Fig. 1, it is possible to plot the variation of the turbulent flame speed u_t with varying pressure at differing concentrations of fuel in the mixture. An example of such a plot, in logarithmic coordinates, is shown in Fig. 2 for values of the concentration C of 2.45 and 2.9 per cent. This dependence is of the same type for all concentrations and shows that the linear flame speed increases with decreasing pressure. An analogous dependence was observed also in laminar gas flow (1).

The curves of Fig. 2 make it possible to establish a power-law relation between the turbulent speed of flame propagation

Translated from *Izvestiia Akademii Nauk SSSR, Otd. Tekhn. Nauk, Energetika i Avtomatika* (*Bull. USSR Acad. Sci., Tech. Sci. Div., Power and Automation*), no. 2, 1959, pp. 26–31.

[1] Numbers in parentheses indicate References at end of paper.

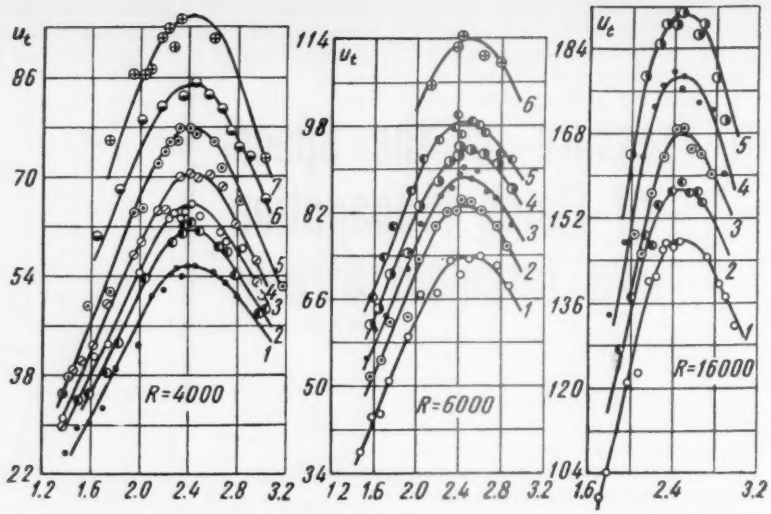

Fig. 1 Dependence of turbulent speed of flame propagation (u_t, cm/sec) on different values of pressure and concentration (C, per cent) of fuel. For R = 4000, curves 1, 2, 3, 4, 5, 6 and 7 correspond to p = 760, 500, 400, 300, 210, 152 and 100 mm mercury, respectively. For R = 6000, curves 1, 2, 3, 4, 5 and 6 correspond to p = 760, 500, 400, 300, 228 and 142 mm mercury, respectively; for R = 16,000, curves 1, 2, 3, 4 and 5 correspond to p = 760, 610, 500, 400 and 300 mm mercury

and the pressure. At all values of fuel concentrations, the exponent of p was found to range from 0.24 to 0.28, with 0.25 as the average. For practical calculations, the following empirical relation can be established

$$u_t = u_{t_0}(p/p_0)^{-0.25} \qquad [1]$$

where u_{t_0} and p_0 are respectively the flame speed and the pressure (at atmospheric pressure). Thus, $u_t \approx p^{-0.25}$. An analogous dependence was established also for the normal speed of flame propagation (1).

It can be concluded from the experiments that if the mass velocity is constant (R = const) the laws of variation of the speed of flame propagation with pressure are identical in laminar and turbulent flows.

Along with these results, we found it interesting to investigate the influence of pressure under varying values of R, but at constant rates of flow of combustible mixture from the burner. Such a method of investigation makes it possible to estimate the influence of physical and chemical factors on the process of flame propagation in a turbulent stream.

Fig. 3 shows the dependence of u_t on p at constant rate of flow w, equal to 1960 cm/sec, at concentrations C equal to 2.45, 2.1 and 1.72 per cent. On the same curves are marked the experimental points at flow velocities close to the foregoing value (the numerical values of the flow velocities are indicated near each point). In this case, the turbulent speed of flame propagation decreases with diminishing pressure. For a further analysis of the process it is important that the same relation be obtained also when the abscissa represents not the pressure, but the values of R corresponding to each value of the pressure. These results are evidence that the decrease in flame speed with diminishing pressure is due to the reduction in the Reynolds number as a consequence of the reduction in the density of the medium and the increase in kinematic viscosity.

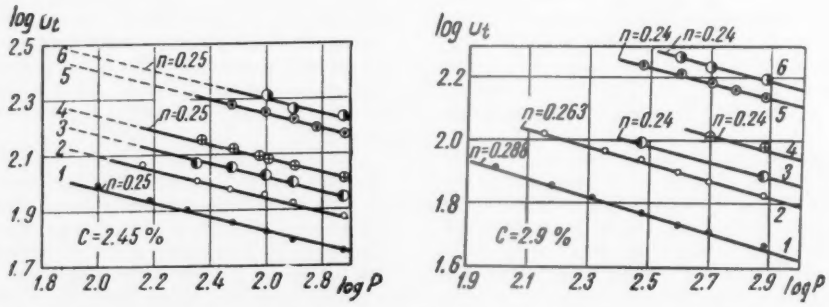

Fig. 2 Dependence of log u_t on log p for C = 2.45 per cent; lines 1, 2, 3, 4, 5 and 6 correspond to Reynolds number R = 4, 6, 8, 10 and 20 × 10³. The exponent of p was found to be n = 0.25 for all lines. For C = 2.9 per cent, the lines 1, 2, 3, 4, 5 and 6 correspond to R = 4, 6, 8, 10, 16 and 20 (×10³), the exponent of p is respectively n = 0.288, 0.263, 0.24, 0.24, 0.24 and 0.24

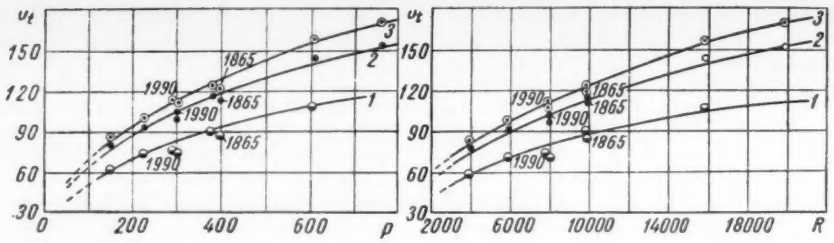

Fig. 3 Dependence of u_t (cm/sec) on p (mm mercury) and R at constant rate of flow w = 1960 cm/sec; curves 1, 2, and 3 correspond to concentrations C = 1.72, 2.1 and 2.45 per cent

Plotting the resultant data on logarithmic scale (Fig. 4) makes it possible to establish a clear-cut empirical relation between u_t and p at a constant rate of flow of combustible mixture

$$u_t/u_{t_0} = (p/p_0)^{\beta} \qquad [2]$$

Since $\beta = 0.45$, the velocity u_t is approximately proportional to the square root of the pressure.

For a theoretical analysis of the data obtained, we turn to modern concepts of the process of turbulent propagation of a flame. At present, not one of the theories permits an analytic derivation of the dependence of the turbulent speed of flame propagation on the pressure, without resorting to experimental data. The theoretical can therefore be formulated only for the purposes of ascertaining the general tendency of the process.

According to various theories and experimental investigations (4 to 9), the speed of propagation of a flame in turbulent stream depends in general on the following parameters:

$$u_t = f(u_n, u', l) \qquad [3]$$

where u_n is the normal flame speed, u' is the intensity fluctuating velocity component and l is the scale of the turbulence.

In the particular case when the propagation of the flame occurs in a stabilized stream leaving a cylindrical burner, in the absence of screens to generate turbulence, one can write instead of [3]

$$u_t = \varphi(u_n R^n, d^m) \qquad [4]$$

According to Damköhler (4), for a small-scale turbulence we have

$$\frac{u_t}{u_n} \approx \sqrt{\frac{a_t}{a}} \qquad [5]$$

where a_t is the coefficient of turbulent temperature conductivity and a is the coefficient of molecular temperature conductivity.

For the case of a large-scale turbulence

$$\frac{u_t}{u_n} \approx \frac{a_t}{a} \qquad [6]$$

Gol'denberg (10) established the relationships $a_t \approx aR^{0.84}$ for $R \leq 100 \times 10^3$ and $a_t \approx aR$ for $R \geq 100 \times 10^3$.

We can therefore write instead of [6]

$$u_t \approx u_n R^{0.84} \qquad [7]$$

It was found experimentally that $u_t \approx u_n R$ for $R \geq 100 \times 10^3$.

Thus, for two limiting cases—small-scale and large-scale turbulences—we obtain different dependences of the speed of flame propagation on the value of R. In a real stream, particularly at small values of R, one always has a range of scales and intensities. The foregoing division by scale and by intensity therefore pertains to two extreme regions. In view of these circumstances, one can barely expect the computed and experimental dependences of u_t on R to agree.

The experimental data obtained by us at normal pressure and for R ranging from 4000 to 16,000 permits us to establish (with accuracy to within a constant factor) the following relationship.

$$u_t \approx u_n R^{0.715} \qquad [8]$$

Since the burner diameter was not varied in our experiments, the scale of turbulence is included in this case as a constant factor. According to [3], the effect of pressure on the turbulent speed of flame propagation is a function of u_n, u' and l.

Inasmuch as in our case $u' = f(R)$ and $l \approx d$, our experimental data can be analyzed either by using Equation [7], which is derived by calculation, or by Equation [8], which we obtained experimentally. Let us examine the effect of pressure when R = const. In both cases it is obvious that $u_t \approx u_n$. Consequently, the dependence of u_t on the pressure should obey under these conditions the laws established for normal flame speed.

It was established by us earlier (1) that $u_n \approx p^{-0.25}$. The dependence given by Equation [1], which we obtained experimentally for u_t, is the same.

Let us see now what conclusions can be drawn from Equations [7 or 8] when the pressure is varied but the rate of flow is constant.

As indicated, a reduction in pressure brings about a reduction in the R number when the rate of flow is constant. If

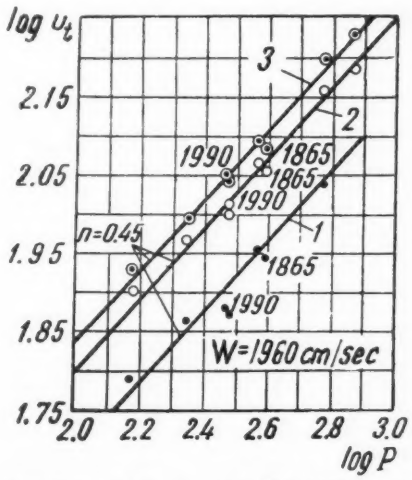

Fig. 4 Dependence of log u_t on log p at constant rate of flow w = 1960 cm/sec; lines 1, 2 and 3 correspond to concentrations C = 1.72, 2.1 and 2.45 per cent

the Reynolds number under our conditions is a hydrodynamic characteristic of the flow, then $R \approx p$ at constant rate of flow and at constant burner diameter. If one takes it into consideration that u_n is proportional to $p^{-0.25}$, we get from [8]

$$u_t \approx p^{-0.25} p^{0.715}$$

or approximately

$$u_t \approx \sqrt{p} \qquad [9]$$

The agreement between Equation [9] and the data obtained directly from experiment (Eq. [2]) are evidence that the theoretical considerations advanced are well founded. Furthermore, this is additional proof of the pressure dependence we established for the normal speed of flame propagation.

Thus, based on an analysis of the results obtained, we can conclude that, in turbulent flow at reduced pressures, the decisive factor in flame propagation is the density of the medium ρ, and consequently the kinematic viscosity ν, on which the characteristics of turbulence depend. In connection with this, it is of interest to examine the propagation of flames under conditions different from ours, namely, under conditions approaching isotropic turbulence as produced by screens. As is known, in this case the Reynolds number is not a hydrodynamic characteristic of the flow, determined by the values of u' and l. The problem consists therefore of finding a direct functional relation between u', l and ν.

From the theory of attenuation of isotropic turbulence past a screen we have (11)

$$u' \approx \text{const } (\nu t)^{-5/4} \qquad (t = \text{time}) \qquad [10]$$

If the speed is constant and the pressure is variable, it is obvious that for a given point in space the fluctuating velocity component will depend on ν in the following manner.

$$u' \approx \text{const } \nu^{-5/4} \quad \text{or} \quad u' \approx p^{5/4} \qquad [11]$$

Usually, the relation for u_t is written in the form

$$u_t \approx (u_n)^{\gamma}(u')^{\delta} \qquad [12]$$

Inserting into [12] the dependence [11] and the dependence $u_n \approx p^{-0.25}$ obtained in (1), we obtain

$$u_t \approx (p^{-1/4})^{\gamma}(p^{5/4})^{\delta} \qquad [13]$$

In particular, if $\gamma = \delta = 0.5$ we should obtain Equation [9] for conditions corresponding to attenuation of turbulence.

Such a dependence of the speed of flame propagation on the pressure was indeed obtained, under conditions of isotropic turbulence, by V. E. Doroshenko and A. I. Nikitskii. Direct measurements of u' by means of a thermo-anemometer, first performed in their research, under conditions of reduced pressures (600 to 100 mm mercury), have confirmed that the intensity of turbulence ϵ decreases with diminishing pressure (ϵ is proportional to u' if the rate of flow is constant). Experimentally, however, the dependence of u' on p was found to be weaker than called for by the theoretical Equation [11].

In analyzing the experimental relation [9] in light of the theory of K. I. Shchelkin (5,12), V. E. Doroshenko and A. I. Nikitskii have found that u_t is proportional to p^n ($n = 0.25$) and have concluded that the observed discrepancy between experiment and theory is due to the character of attenuation of the turbulence past the grid, a factor usually disregarded. As the distance from the edge of the burner is increased, the value of u' actually decreases, but since the speed of flame propagation is usually averaged over the entire surface of the front, it is essential to compare not local but mean effective values of u_t and u'. In this case the proportionality coefficient usually enters into equations similar to [12].

It must be emphasized that the essential result of our research and of the research of Doroshenko and Nikitskii is the rather good agreement between the experimental data on the dependence of u_t on p at constant flow velocity, obtained under different experimental conditions. This is evidence that the effect of pressure on the turbulent speed of flame propagation, as already noted, is due essentially to the change in the turbulence characteristics that depend on the kinematic viscosity of the medium. Furthermore, in the case of gas emerging from cylindrical burners, as established by our research, the Reynolds number is such a characteristic for a gas flowing out of cylindrical burners, and the fluctuating velocity is such a characteristic under conditions of isotropic turbulence.

Acknowledgment

The authors consider it their duty to express their gratitude to A. S. Predvoditelev and L. N. Khitrin for interest in the work.

References

1 Gol'denberg, S. A. and Pelevin, V. S., "Effect of Pressure on Normal Speed of Flame Propagation," *Izvestiia Akademii Nauk SSSR, Otd. Tekhn. Nauk* (*Bull. Acad. Sci. USSR, Tech. Sci. Div.*), no. 2, 1958.

2 Klaukens, H. and Wolfhard, H., "Measurements in the Reaction Zone," *Proc. Roy. Soc.*, vol. 193, no. 1035, 1948.

3 Cullen, R., *Trans. ASME*, vol. 75, no. 1, 1953.

4 Damköhler, G., "Der Einfluss der Turbulens auf die Flammengeschwindigkeit in Gasgemischen," *Zeitschrift fur Electrochemie*, vol. 46, no. 11, 1940.

5 Shchelkin, K. I., "On Combustion in Turbulent Flow," *J. Tech. Phys. (USSR)*, vol. 13, nos. 9–10, 1943.

6 Karlovitz, B., Denniston, D. and Wells, E., "Investigation of Turbulent Flames," *J. Chem. Phys.*, vol. 19, no. 5, 1951.

7 Leason, D., "Turbulence and Flame Propagation in Premixed Gases," *Fuel*, vol. 30, no. 10, 1951.

8 Wohl, K., Shore, L., Rosenberg and Weil, C., "The Burning Velocity of Turbulent Flames," Fourth Sym. on Combustion, 1953.

9 Scurlock, A. and Grover, J., "Propagation of Turbulent Flames," Fourth Sym. on Combustion, 1953.

10 Gol'denberg, S. A., "Certain Experimental Laws Holding in the Region of Turbulent Diffusion," *Izvestiia Akademii Nauk SSSR, Otd. Tekhn. Nauk* (*Bull. of the USSR Academy of Sciences, Technical Science Division*), no. 2, 1958.

11 Landau, L. D. and Lifshitz, E. M., "Mekhanika Sploshnykh Sred" ("Mechanics of Continuous Media"), Gostekhizdat, 1953.

12 Shchelkin, K. I., "Contribution to the Problem of Turbulent Combustion and Combustion Phases in Engines," *Izvestiia Akademii Nauk SSSR, Otd. Tekhn. Nauk* (*Bulletin of the USSR Academy of Sciences, Technical Science Division*), no. 3, 1953.

Estimate of Operation of Simplest Ramjet Combustion Chamber

A. V. TALANTOV

Continuing the investigations of Zel'dovich (1),[1] Tsien (2) and others, the author proposes an approximate method for designing a straight-through flow combustion chamber of constant cross section with a point (or linear) source of ignition. The method takes into account the conditions at the inlet of the combustion chamber and the finite duration of the combustion time. The following assumptions are made: Unidimensional flow at the inlet, flow velocity of combustion products and pressure both uniform over the transverse cross section during the combustion process. In addition, the position of the flame front is calculated in the present work under the condition that the combustion time in the zone is infinitesimally small, and the extent of the combustion zone is then found from the actual value of the combustion time. Additional assumptions are made to analyze the effect of the conditions at the combustion chamber inlet on the principal characteristics of the chamber. The error introduced thereby will be small, since the abscissa of the point of contact between the front of the flame and the wall changes very slightly, depending on whether it is assumed that combustion with a finite zone occurs or whether the front of the flame is assumed to be an infinitesimally thin surface. The point is that, according to the Michelson law, the magnitude of the surface needed for the combustion of the mixture entering the chamber is constant if the rate of flame propagation remains unchanged. The expansion of the combustion products and the rearrangement of the velocity profile over the transverse cross section during the combustion process, phenomena that behave differently under the two aforementioned assumptions, will affect the shape of the surface, and only through this factor will they affect the abscissa at which the flame will reach the wall. It was established by computation that even complete disregard of the effect of the expansion introduces an error on the order of several per cent.

IN THE case of a two-dimensional chamber in accordance with the customary assumptions, the dimensionless ordinate η of the flame front can be determined as a function of the fraction r of the liberated heat from the following equations.

1 The equation of conservation of energy and the adiabatic equation for the fresh mixture

$$\tau_m = 1 - \frac{k-1}{2} M_0^2(u_m^2 - 1) \qquad \tau_m = \pi^{\frac{k-1}{k}} \qquad [1]$$

where

τ_m, u_m = dimensionless temperature and velocity of the fresh mixture (referred to the corresponding parameters at the chamber inlet)
M_0 = Mach number at the chamber inlet
π = pressure at the section under consideration divided by the pressure at the inlet

2 The energy equation for the flow of combustion products

$$\tau_p = \lambda_p - \frac{k-1}{2} M_0^2(u_p^2 - 1) \qquad \lambda_p = 1 + \frac{q}{c_p T_0} \qquad [2]$$

where

τ_p, u_p = dimensionless temperature and velocity of combustion products
q = amount of heat delivered to 1 kg of gas

3 The equation of conservation of mass

$$\frac{\pi}{\tau_m} u_m(1 - \eta) + \frac{\pi}{\tau_p} u_p \eta = 1 \qquad [3]$$

4 The momentum equation

$$\frac{\pi}{\tau_m} u_m^2(1 - \eta) + \frac{\pi}{\tau_p} u_p^2 \eta = 1 + \frac{1}{kM_0^2}(1 - \pi) \qquad [4]$$

5 The equation for the fraction of liberated heat

$$r = (\pi/\tau_p) u_p \eta \qquad [5]$$

Under the assumptions made, r is also the fraction of combusted matter.

Six equations are sufficient to determine the unknown quantities π, u_m, u_p, τ_m, τ_p, η and r, one of which is the independent variable.

Instead of one of the foregoing equations, one can also use the simple approximate relation proposed by Tsien (2), between the dimensionless temperatures

$$\tau_p/\tau_m = \lambda_p \qquad [6]$$

We first determined the region of possible modes at the inlet of the combustion chamber, a region bounded by the conditions of occurrence of critical flow in the combustion products. The results of these calculations, made in accordance with the generally accepted gasdynamic relationships, are presented in the form of the dependence of the maximum permissible Mach number $M = M_{0\max}$ at the inlet to the combustion chamber, on the relative heating λ_p (Fig. 1). The same figure shows the corresponding limiting values of pres-

Translated from *Izvestiia Akademii Nauk SSSR, OTN, Energetika i Avtomatika* (*Bull. Acad. Sci. USSR, Div. Tech. Sci., Power and Automation*), no. 2, 1959, pp. 32–37.

[1] Numbers in parentheses indicate References at end of paper.

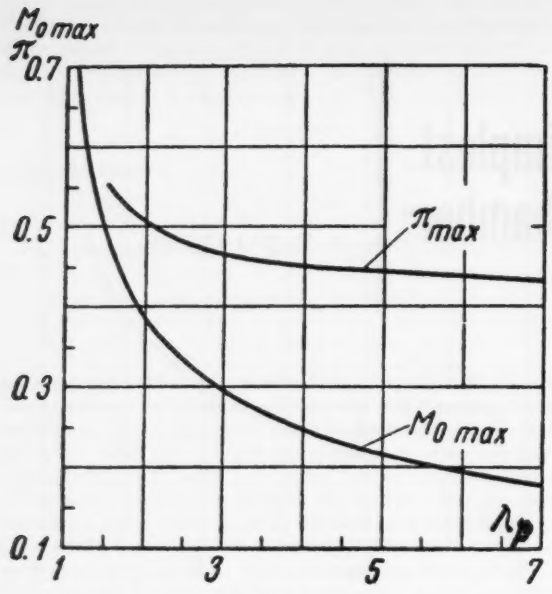

Fig. 1

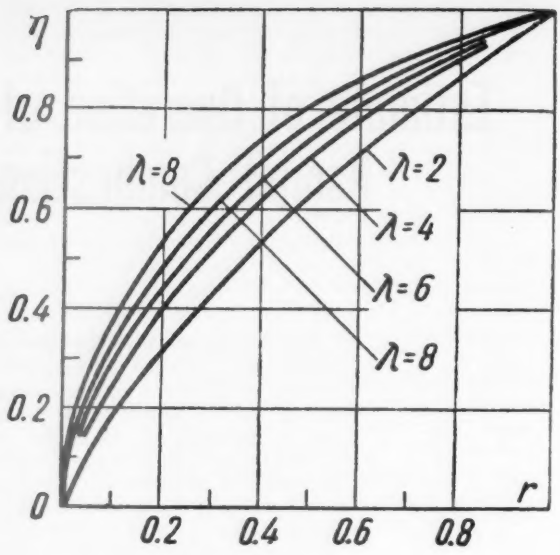

Fig. 2

sure drop π. It must be borne in mind that at infinitesimal combustion times critical phenomena occur somewhat earlier in fresh mixtures than indicated by Tsien (2), and that this effect may even not take place in the case of finite combustion time.

By solving the foregoing system of equations within the range bounded by critical flow and by $\lambda_p = 8$, we obtained the relations $\eta = f(r)$ (Fig. 2). It became evident that, the other parameters remaining constant, M_0 influences the value of η so little, that the curves $\eta = f(r)$ (Fig. 2) hold for all values of M_0 less than M_{0max}, accurate to within 1 per cent. For the sake of comparison, the same plot shows the analogous relation $\eta = f(r)$ obtained without equalization of the profile of flow velocity of the combustion products (extreme curve) (2). What is worthy of attention is that the compared curves differ little from one another and that, in plotting the geometry of the flame for combustion with a finite zone, the right-hand curves obviously yield results that are closer to the actual ones.

The next stage in the calculation is the plotting of the surface of the flame in the chamber. For this purpose it is convenient to use the equation for the conservation of mass of the fresh mixture, solved with respect to ΔX^0, the dimensionless distance between neighboring sections $i - 1$ and i, referred, as all other geometrical dimensions, to B_0, the half-width of the channel (from the axis to the wall)

$$\Delta X^0 = \sqrt{\left\{2\frac{(\pi/\tau_m)_{i-1}(1-\eta_{i-1})(u_m)_{i-1} - (\pi/\tau_m)_i(1-\eta_i)(u_m)_i}{[(\pi/\tau_m)_{i-1} + (\pi/\tau_m)_i]u_t^0}\right\}^2 - (\eta_i - \eta_{i-1})^2}$$

Here $u_t^0 = u_t/w_0$ is the dimensionless speed of flame propagation.

The calculation is carried out successively by sections; one takes two values of the dimensionless ordinates η with corresponding values of π, τ and u, and ΔX^0 is determined for these values.

It is possible then to determine the position of the flame front in the chamber

$$\eta = f(X^0)$$

where X^0 is the dimensionless abscissa, reckoned from the point of ignition.

The axial distance X_z^0 at the wall, needed to complete the combustion behind the initial flame front, is determined from

$$X_z^0 = w_c t/B_0$$

where

t = time of combustion of the mixture
w_c = flow velocity of the combustion product, which can be taken approximately as the mean between the flow velocity during the instant of crossing of the flame front and the flow velocity at the exit from the zone in the case of complete combustion of the mixture.

The length X_c^0 of the combustion chamber, which is the desired end result of the computation for a specified chamber cross section, is determined by adding the axial distances from the point of ignition to the point of contact between the flame and the wall to the axial length of the zone X_z^0.

The heat release rate q_t can be estimated from

$$q_t = Q/X_c^0 F B_0$$

where

Q = amount of heat liberated in the chamber
F = area of the chamber cross section

The results obtained with the foregoing approximate method permit us to conclude that the method can be used to evaluate the performance of the chamber operation.

To perform the calculations, one must know the dependence of u_t and t on the combustion conditions. This has been investigated most fully for a homogeneous mixture. The entire subsequent analysis of chamber operation is based on the assumption that the preparation of the mixture was completed before it entered the combustion chamber. This makes it possible to exhibit the dependence of chamber characteristics on the combustion processes in purest form.

An investigation of a combustion chamber operating with a homogeneous mixture yields certain ideas on operation with a heterogeneous mixture, since, to a certain extent, a similar dependence of the time of combustion and speed of flame propagation on the principal factors is observed in turbulent flow of both homogeneous and heterogeneous mixtures. Such an investigation is also of independent practical interest, for under certain ramjet operating conditions (high supersonic flight velocities) the main portion of the fed fuel has time to evaporate and to form a sufficiently homogeneous mixture, and more so in the case of combustion chambers in which the mixture is specially prepared.

The variation of u_t and t can be expressed as

$$u_t = Aw'^a u_n^b \qquad (w' = \epsilon w,\ a + b = 1)$$

where $A = 5.4$ is determined experimentally, and w' is the pulsational velocity. The pulsational velocity exponent a which ranges from 0.6 to 0.8, was assumed to equal 0.7.

The dependence of the time of combustion is

$$t = B\frac{l_0}{w'}\ln\left(1 + \frac{w'}{u_n}\right) \qquad (B = 1.16)$$

We disregarded in the computation the damping of the turbulence, which was partially offset by the increase in the flow velocity.

To estimate the influence of various factors on the required dimensions of the combustion chamber, operating with a homogeneous gasoline-air mixture, we performed the calculations for a two-dimensional chamber 200-mm wide with an inlet temperature 400 deg abs and atmospheric pressure, for three mixtures with $\alpha = 1.0$, 1.4 and 2.0, degree of turbulence $\epsilon = 0.05$, 0.1 and 0.2, and turbulence scales $l_0 = 0.5$, 1 and 2 cm, respectively. Experiments made with a Bunsen burner yield for the chosen mixtures, at this temperature, normal velocities u_n of 68, 48 and 12 cm per sec, respectively, and values of the parameter λ_p of 6, 5 and 4 at the given values of α.

Figs. 3 and 4 show plots of X^0 vs. w for various values of α, l_0 and ϵ.

It is seen that the combustion zone comprises the greater portion of the length of the flame proper (from 50 to 80 per cent). It is appropriate to note here that calculations which do not take the length of the combustion zone into account are unfounded.

The results obtained lead to the following conclusion: When striving to reduce the length of the chamber, one must first attack the combustion zone or the time of combustion. For a homogeneous mixture, the methods of attack are obvious—increase u_n and w', thereby increasing the speed of flame propagation and consequently also reducing the length X_f^0 of the inlet portion of the chamber. A third method, applicable to the zone only, is to reduce the scale of turbulence. Any action on the flow aimed at changing the extent of the zone should preferably be effected in the direct vicinity of the flame front (start of the zone), so as to reduce the undesirable attenuation effect, namely the drop in intensity and increase in the scale of turbulence.

The first component part of the chamber, up to X_f^0, can be reduced by changes in construction, say by installing a large number of stabilizers (within a practical limit).

When basing the length of the combustion chamber on the results of the calculations, it must be borne in mind that the heat liberated in the final portion is very small, and in practice one may sometimes forego several per cent of heat liberation for the sake of reducing the hydraulic losses and decreasing the size and weight of the chamber. This will increase the heat release rate in the chamber volume as a whole.

For the case of a combustion chamber of constant length, selected to yield the maximum heat release rate, a change in the foregoing parameters will lead to a drop in the combustion efficiency. Taking into account the variation of heat liberated along the length of the chamber, one can expect the variation in the combustion efficiency to be exponential.

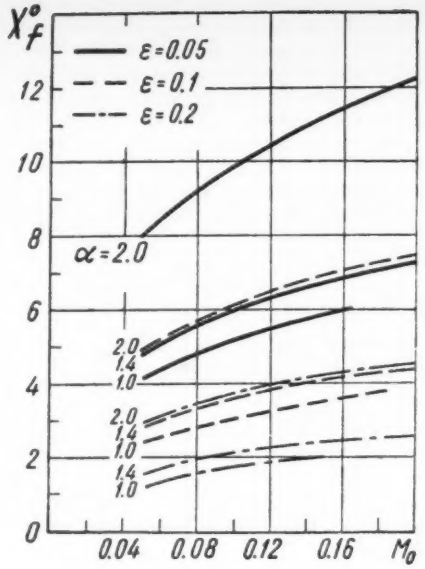

Fig. 3

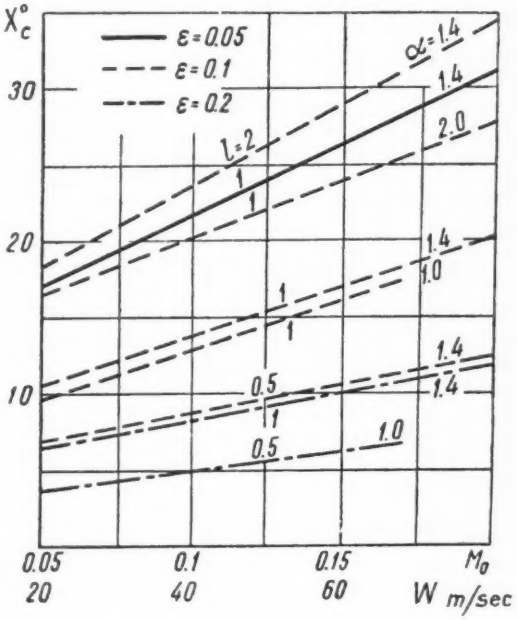

Fig. 4

The calculated values of the heat release rate q_t, shown in Figs. 5, 6 and 7, lead to certain conclusions concerning the influence of various factors on the heat release rate within the volume of the combustion chamber.

A striking fact is the exceedingly large range of variation in the heat release rate, from 5×10^6 to 220×10^6 kcal/m^3-hr, i.e., a change by a factor of several times 10. This range becomes even wider if the effect of temperature and pressure variation at the inlet are also taken into account.

The greatest influence on the heat release rate is exerted by variations in α; in the calculations performed, doubling α

(from 1.0 to 2.0) reduces the heat release rate by three or four times. This effect is observed also at large flow velocities.

In spite of the increase in the length of the flame with increasing flow velocity, the heat release rate increases. In the calculated range of w, from 20 to 80 m per sec, the value of q_t increases by approximately two or three times. This is due to an increase in the delivered heat, which is proportional to the flow velocity, i.e., it is more intense than the elongation of the zone. Consequently, in choosing a ratio of length to cross section of the combustion chamber so as to minimize its volume, the transverse cross section must be made narrower to the extent permitted by the increase in inlet velocity, limited by the criticality of the flow of combustion products or by the stability of chamber operation.

The heat release rate of the chamber increases approximately by two and a half times if the degree of turbulence increases by a factor of 4. The heat release rate depends on the scale of turbulence, and diminishes as the latter increases. In the range of l_0 under consideration, it changes by approximately three times. It is interesting to note that if the scale of turbulence is assumed proportional to the dimensions of the system, the heat release rate becomes inversely proportional to these dimensions. Thus, for example, the maximum heat release rate under our conditions can reach values of 400 $\times$ 10^6 kcal/m^3-hr atm abs if the transverse dimension of the chamber is reduced by one half (from 200 to 100 mm).

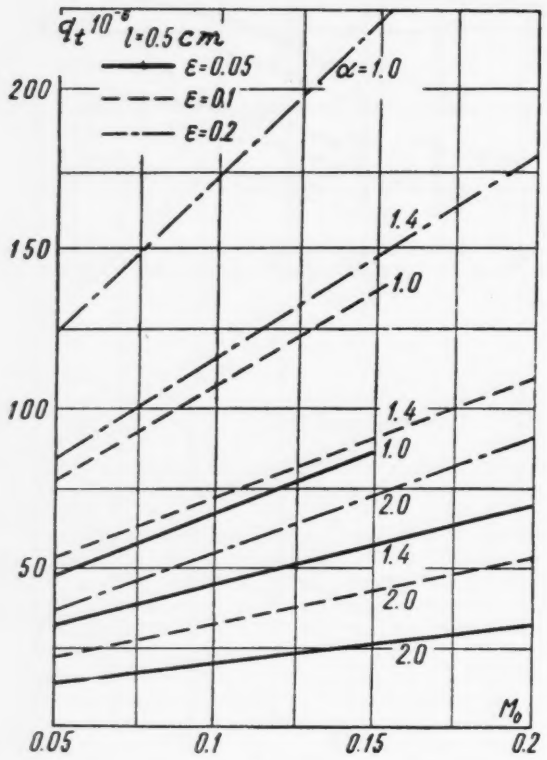

Fig. 5

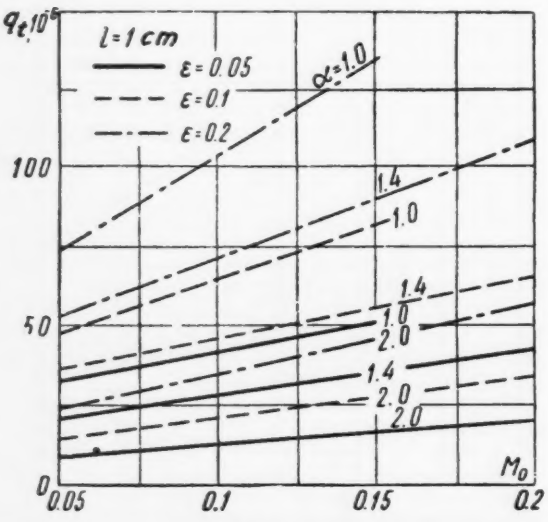

Fig. 6

Conclusions

The foregoing estimate of the operation of the simplest straight-through flow combustion chamber, using a homogeneous mixture, leads to the following conclusions:

1 The dimensions of the combustion chamber, calculated on the basis of a specified mean heat release rate, are exceedingly rough, for actually the heat release rate within its volume changes by a factor of several times 10 under differing inlet and outlet conditions.

2 The combustion chamber can be regulated only over a narrow range by varying α, if a sufficiently high efficiency in heat liberation is to be retained (we disregard here the problem of flame stabilization). It is possible to broaden the range of relation and still maintain satisfactory combustion chamber characteristics only if the combustion chamber has a substantial reserve volume at modes in which α is close to unity. The range of variation of α in the engine as a whole can be substantially broadened by using two- and multichannel combustion chambers with separate feed of fuel.

The principal premises that result from the calculations on

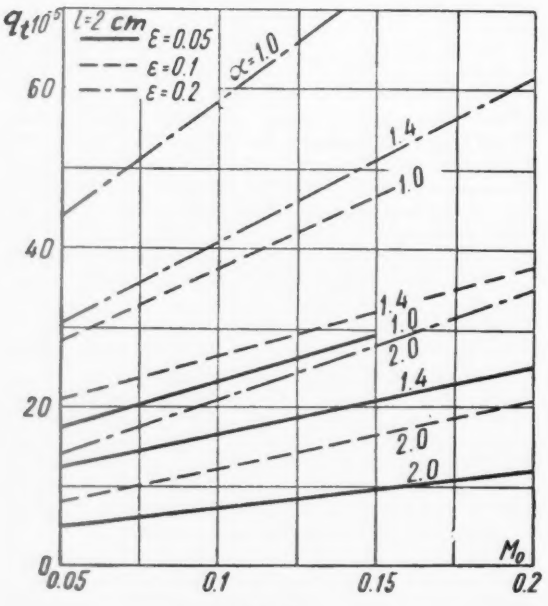

Fig. 7

the combustion of a homogeneous mixture in the simplest straight-through flow combustion chamber, can be extended, with some reservations, to include the process occurring in a ramjet combustion chamber. The presence of a set of stabilizers used in a real combustion chamber, stabilizers operating under identical conditions, does not prevent us from considering one of the elements, with a single stabilizer, as a simple straight-through combustion chamber. The most suitable scheme will indeed involve just such a flat element, for if the chamber has a row of concentric stabilizers, the ratio of the cross section of one chamber element to the length of the stabilizer periphery is quite small, and the curvature of the stabilizer can be neglected.

The conclusions remain valid also in the case of a combustion process distributed in depth, although the calculation becomes more complicated in this case.

References

1 Zel'dovich, Ya. B., "Remarks on the Combustion of a Fast Stream in a Tube," *J. Tech. Phys. (USSR)*, vol. XIV, no. 3, 1944.

2 Tsien, H., "Influence of Flame Front on the Flow Field, *J. Appl. Mech.*, vol. 18, no. 2, 1951.

One Problem in Nonstationary Heat Conduction

V. S. ZARUBIN

This paper is devoted to an analysis of the unsteady thermal process that occurs in the jacket of a cooled liquid fuel rocket engine.

BY UNSTEADY (nonstationary) heat exchange in a cooled liquid fuel rocket we mean the heat transfer during the launching, operation and stopping of the rocket engine, when the temperature of its jacket changes substantially with time. The temperature field of the jacket of an engine operating in the steady-state mode can be considered as the limiting field, which the temperature distribution in the jacket approaches in nonstationary heat transfer.

We examine the qualitative aspects of unsteady heat exchange by using as an example the launching of the rocket. We isolate a portion of the jacket and specify (arbitrarily) the initial temperature distribution (Fig. 1). The subscripts 1 and 2 identify the combustion products and the cooling liquids, respectively; the primes and double primes refer to the inner and outer walls of the rocket jacket; t is the temperature, and the subscripts $(_0)$ and $(_*)$ denote the initial and steady-state values of the parameters.

After the start of burning, combustion products with temperature t_1 begin to transfer their heat to the inner wall. Part of this heat goes to raise the temperature of the wall itself, and another part is transferred to the liquid and heats up the liquid itself, the spacers between the walls and the outer wall. The heat exchange between the outer wall and the surrounding medium can be neglected. The intermediate distribution is shown in Fig. 2.

In the course of time, the difference in temperature between the combustion products and the inner wall decreases, and equilibrium is established between the heat flow from the combustion products to the wall and from the wall to the cooling liquid. A constant temperature distribution is established in the inner wall. The cooling liquid also assumes a fixed temperature, defined for each section of the jacket. We assume that the outer wall and the ties between the wall have the same temperature as the liquid (Fig. 3).

Strictly speaking, the walls and liquid do not attain a constant temperature, and merely approach constancy as the duration of the process goes to infinity. However, one can assume the temperature distribution to be steady after a certain instant of time, at which the distribution differs from an ideally steady one by less than an arbitrarily selected definite small quantity.

If the thermal conductivity λ and the thermal diffusivity a of the wall material are assumed independent of the temperature and the jacket is assumed plane-parallel, the unsteady heat conduction is described by a differential equation with constant coefficients. Several problems formulated in this way, are contained, for example, in the book by A. V. Lykov.[1]

The problem considered here has the following distinguishing feature: The two walls (inner and outer) of the engine jacket are interconnected, with regard to heat flow, by the convective heat exchange through the cooling liquid, the temperature of which varies with the time. We next introduce the following assumption: At any instant of time, the heating dt_2 of the cooling liquid over the portion dF of the cooled surface is proportional to the temperature of the liquid over

[1] Lykov, A. V., "Teoriya Teploprovodnosti" (Theory of Heat Conduction), Gittl, 1952.

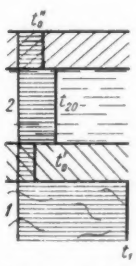

Fig. 1 Arbitrary initial distribution of the temperature in the jacket, during start of the engine. 1—combustion products, 2—cooling liquid

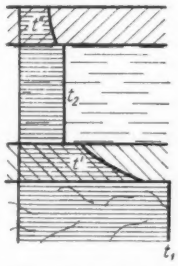

Fig. 2 Unsteady temperature field of the jacket during the starting time of the engine

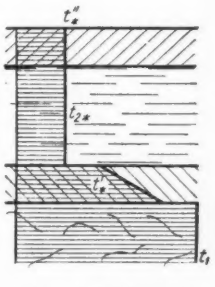

Fig. 3 Temperature field of the jacket during stationary engine operation

Translated from *Izvestiia Akademii Nauk SSSR, OTN, Energetika i Avtomatika* (*Bull. Acad. Sci. USSR, Div. Tech. Sci., Power and Automation*), no. 2, 1959, pp. 38–44.

the same area during the same instant of time.

In other words

$$q_3 = q_{2\max}(t_2 - t_{2\min})/(t_{2\max} - t_{2\min}) \quad [1]$$

where

q_3 = heat flux that goes into heating the cooling liquid during the given instant of time
$q_{2\max}$ = maximum heat flux over the given section
$t_{2\max}$ = maximum temperature of the cooling liquid over the given section
$t_{2\min}$ = temperature of the liquid at the inlet to the cooling system of the engine

In starting, $q_{2\max}$ and $t_{2\max}$ correspond to the steady-state values. The plot of Equation [1] is illustrated in Fig. 4, which shows the character of variation of t_2 in the cooling loop during starting.

We assume also that

$$t_2 = t_{2*} - (t_{2*} - t_{20})e^{-k\tau} \quad [2]$$

Here τ is the time, and the determination of the parameter k will be considered below. It is obvious that when starting the engine $t_{20} = t_{2\min}$, and $t_{2*} = t_{2\max}$; during stopping, we have $t_{20} = t_{2\max}$, and $t_{2*} = t_{2\min}$.

It should be noted that the problem can also be solved without introducing Equation [2], but the result is quite cumbersome. By representing t_2 in the form of Equation [2] we describe with sufficient accuracy the structure of this solution, and at the same time we are able to simplify it substantially. The coordinate system is illustrated in Fig. 5.

For the prime inner wall, the solution is defined by

$$\frac{\partial t'(x', \tau)}{\partial \tau} = a' \frac{\partial^2 t'(x', \tau)}{\partial x'^2} \quad [3]$$

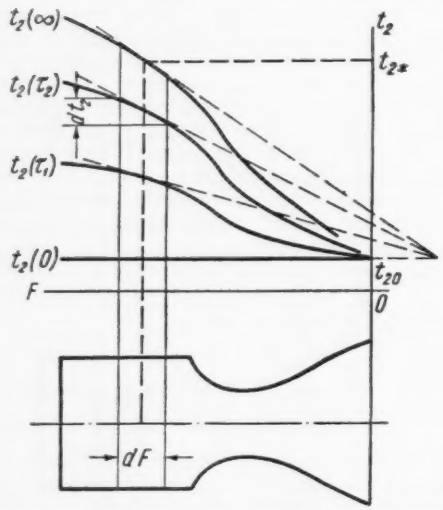

Fig. 4 Variation of the temperature of the liquid ir the cooling system during the start of the engine

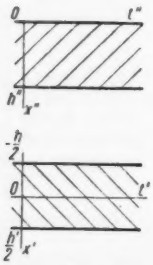

Fig. 5. Coordinate system used

with boundary conditions

$$-\lambda' \frac{\partial t'(\frac{1}{2}h', \tau)}{\partial x'} + \alpha_1[t_1^* - t'(\tfrac{1}{2}h', \tau)] = 0$$

$$\lambda' \frac{\partial t'(-\frac{1}{2}h', \tau)}{\partial x'} + \alpha_2'[t_2 - t'(-\tfrac{1}{2}h', \tau)] = 0 \quad [4]$$

and initial conditions (in the general case)

$$t'(x', 0) = t_0' + Dx' \quad [5]$$

For the outer wall the solution is defined by

$$\frac{\partial t''(x'', \tau)}{\partial \tau} = a'' \frac{\partial^2 t''(x'', \tau)}{\partial x''^2} \quad [6]$$

with boundary and initial conditions

$$\frac{\partial t''(0, \tau)}{\partial x''} = 0 \qquad -\lambda'' \frac{\partial t''(h'', \tau)}{\partial x''} + \alpha_2''[t_2 - t''(h'', \tau)] = 0 \quad [7]$$

$$t''(x'', 0) = t_0'' \quad [8]$$

The time τ is reckoned from the start of the nonstationary heat exchange. The symbols α_1, α_2', and α_2'' denote respectively the coefficients of heat transfer from the combustion products to the wall, from the inner wall to the liquid, and from the liquid to the outer wall, while t_1^* is the reduced temperature of the combustion products

$$t_1^* = t_1 + q_r/\alpha_1 \quad [9]$$

where

t_1 = actual temperature of the combustion products
q_r = the radiant heat flux assumed constant over the section under consideration

Let us apply to the variable τ the Laplace transformation

$$T(x, s) = \int_0^\infty t(x, \tau)e^{-s\tau}d\tau \quad [10]$$

The Laplace transformation is possible if the increase in the function $t(x, \tau)$ with increasing time is bounded. This condition is satisfied, since the temperature distribution in nonstationary heat transfer tends to a certain bounded steady state.

Taking Equations [2 and 5] into account, we apply the Laplace transformation to Equation [3] and to boundary conditions [4]. We obtain accordingly the equation

$$a'[d^2T'(x', s)/dx'^2] - sT'(x', s) + t_0' + Dx' = 0 \quad [11]$$

with boundary conditions

$$-\frac{dT'(\frac{1}{2}h', s)}{dx'} + \frac{N_1}{h'}\left[\frac{t_1^*}{s} - T'(\tfrac{1}{2}h', s)\right] = 0 \qquad \left(N_1 = \frac{\alpha_1 h'}{\lambda'}\right) \quad [12]$$

$$\frac{dT'(-\frac{1}{2}h', s)}{dx'} + \frac{N_2'}{h'}\left[\frac{t_{2*}}{s} - \frac{t_{2*} - t_{20}}{s + k} - T'(-\tfrac{1}{2}h', s)\right] = 0$$

$$\left(N_2' = \frac{\alpha_2' h'}{\lambda'}\right) \quad [13]$$

Here $T'(x', s)$ is the transform of the function $t'(x', \tau)$. Solution of Equation [11] in transform form is given by

$$T'(x', s) = \left(A - \frac{t_0'}{s}\right)\cosh \zeta \frac{x'}{h'} + \left(B - \frac{Dh'}{s\zeta}\right)\cosh \zeta \frac{x'}{h'} + \frac{t_0'}{s} + \frac{Dx'}{s} \qquad \left(\zeta = \sqrt{\frac{s}{a'}}h'\right) \quad [14]$$

We determine the constants A and B from the boundary conditions [12 and 13]; upon insertion in Equation [14] we obtain

$$T'(x', s) = \frac{N_1(t_1^* - t_0')(\cosh\varphi + N_2'\zeta^{-1}\sinh\varphi) + N_2'(t_{2*} - t_0')(\cosh\psi + N_1\zeta^{-1}\sinh\psi)}{sZ(s)} -$$

$$Dh'\frac{(2\zeta\sinh\tfrac{1}{2}\zeta + N_1N_2'\cosh\tfrac{1}{2}\zeta)\zeta^{-1}\sinh\zeta\,(x'/h') + N_2'(\zeta^{-1}\sinh\varphi - 2\cosh\psi) + N_1(\zeta^{-1}\sinh\psi - 2\cosh\varphi)}{sZ(s)} -$$

$$\frac{N_2'(t_{2*} - t_{20})(\cosh\psi + \zeta^{-1}N_1\sinh\psi)}{(s+k)Z(s)} + \frac{t_0'}{s} + \frac{Dx'}{s} \qquad [15]$$

The following symbols are used

$$Z(s) = \left(\zeta + \frac{N_1N_2'}{\zeta}\right)\sinh\zeta + (N_1 + N_2')\cosh\zeta$$

$$\varphi = \zeta\left(\frac{1}{2} + \frac{x'}{h'}\right) \qquad \psi = \zeta\left(\frac{1}{2} - \frac{x'}{h'}\right)$$

The solution in the original variables is determined in the following manner. We find the values of s for which the denominator of Equation [15] vanishes; i.e., we find the poles of the function $T'(x', s)$. These poles are

$$s' = 0 \qquad s'' = -k \qquad s_n = -\mu_n^2 a'/h'^2$$

where μ_n is the infinite set of roots of the transcendental equation

$$\cot\mu = (\mu^2 - N_1N_2')/\mu(N_1 + N_2') \qquad [16]$$

Subject to various mathematical limitations imposed on the transformed solution, limitations that are fulfilled in this particular case (the principal one is that $\lim T'(x', s) = 0$ when $s \to \infty$), the solution in the original variables is the sum of residues over the poles of $T'(x', s)$

$$t'(x', \tau) = \frac{\tfrac{1}{2}(t_1^* + t_{2*})N_1N_2' + N_1t_1^* + N_2't_{2*} + N_1N_2'(t_1^* - t_{2*})(x'/h')}{N_1N_2' + N_1 + N_2'} -$$

$$N_2'(t_{2*} - t_{20})e^{-N_\tau'N_k'} \times$$

$$\frac{\cos\sqrt{N_k'}\,(\tfrac{1}{2} - x'/h') + (N_1/\sqrt{N_k'})\sin\sqrt{N_k'}(\tfrac{1}{2} - x'/h')}{(N_1N_2'/\sqrt{N_k'} - \sqrt{N_k'})\sin\sqrt{N_k'} + (N_1 + N_2')\cos\sqrt{N_k'}} -$$

$$\sum_{n=1}^{\infty}\frac{2\cos\mu_n\exp(-\mu_n^2N_\tau')}{\mu_n^2 - N_1N_2' + (\mu_n^2 + N_1N_2')\mu_n^{-1}\sin\mu_n\cos\mu_n}$$

$$\left\{N_1(t_1^* - t_0')\left[\cos\mu_n\left(\frac{1}{2} + \frac{x'}{h'}\right) + \frac{N_2'}{\mu_n}\sin\mu_n\left(\frac{1}{2} + \frac{x'}{h'}\right)\right] + \right.$$

$$N_2'(t_{2*} - t_0')\left[\cos\mu_n\left(\frac{1}{2} - \frac{x'}{h'}\right) + \frac{N_1}{\mu_n}\sin\mu_n\left(\frac{1}{2} - \frac{x'}{h'}\right)\right] -$$

$$\frac{N_2'(t_{2*} - t_{20})}{1 - (N_k/\mu_n^2)}\left[\cos\mu_n\left(\frac{1}{2} - \frac{x'}{h'}\right) + \frac{N_1}{\mu_n}\sin\mu_n\left(\frac{1}{2} - \frac{x'}{h'}\right)\right] -$$

$$Dh'\left(\frac{N_1N_2'}{\mu_n}\cos\frac{\mu_n}{2} - 2\sin\frac{\mu_n}{2}\right)\sin\mu_n\frac{x'}{h'} -$$

$$D\frac{h'}{2}\left[N_1\cos\mu_n\left(\frac{1}{2} + \frac{x'}{h'}\right) - N_2'\cos\mu_n\left(\frac{1}{2} - \frac{x'}{h'}\right)\right] -$$

$$\left.D\frac{h'}{\mu_n}\left[N_2'\sin\mu_n\left(\frac{1}{2} + \frac{x'}{h'}\right) - N_1\sin\mu_n\left(\frac{1}{2} - \frac{x'}{h'}\right)\right]\right\} \qquad [17]$$

Here $N_\tau' = a'\tau/h'^2$ and $N_k = kh'^2/a'$.

Analogously, we obtain a solution for Equation [6] in the form

$$t''(x'', \tau) = t_{2*} - \frac{(t_{2*} - t_{20})\cos\sqrt{N_k''}(x''/h'')}{\cos\sqrt{N_k''} - (\sqrt{N_k''}/N_2'')\sin\sqrt{N_k''}} \times$$

$$\exp(-N_\tau''N_k'') - \sum_{n=1}^{\infty}\frac{2\nu_n^{-1}\sin\nu_n\cos\nu_n(x''/h'')}{1 + \nu_n^{-1}\sin\nu_n\cos\nu_n} \times$$

$$\left(t_{2*} - t_0'' + \frac{t_{2*} - t_{20}}{N_k''/\nu_n^2 - 1}\right)\exp(-\nu_n^2N_\tau'') \qquad [18]$$

where $N_\tau'' = \dfrac{a''\tau}{h''^2}$ $\quad N_k'' = \dfrac{kh''^2}{a''}$ $\quad N_2'' = \dfrac{a_2''h''}{\lambda''}$

and ν_n is the infinite set of roots of the equation

$$\cot\nu = \nu/N_2'' \qquad [19]$$

The characteristic Equation [19] (Fig. 6) is one of the principal equations in the theory of nonstationary heat conduction, and the values of its first few roots are tabulated as functions of N_2''.

Equation [16] can be rewritten as

$$\cot\mu = \frac{\mu}{N_1 + N_2'} - \frac{N_1N_2'}{\mu(N_1 + N_2')}$$

As μ increases, the second term in the right side can be neglected. The result is an equation similar to [19]. Starting with $n = 3$, the value of μ can be found with great degree of accuracy from the tables of roots of Equation [19].

Expanding into an infinite series within the interval $0 < \mu < \pi$ we get

$$\cot\mu = \frac{1}{\mu} - \frac{\mu}{3} - \frac{\mu^3}{3^2\cdot5} - \frac{2\mu^5}{3^3\cdot5\cdot7} - \ldots \qquad [20]$$

Inserting Equation [20] into Equation [16] and retaining the first three terms of the series, we obtain

$$\mu_1 \approx \left(1 + \frac{4}{5}\frac{(N_1 + N_2')(N_1 + N_2' + N_1N_2')}{N_1 + N_2' + 3} - 1\right)^{1/4} \times \left(\frac{2}{15}\frac{N_1 + N_2'}{N_1 + N_2' + N_1N_2'}\right)^{-1/2} \qquad [21]$$

The value of μ_1 obtained from Equation [21] can be improved by trial and error. The value of μ_2 is found by trial and error or graphically, as shown in Fig. 6, where

$$y_1 = \cot\mu \qquad y_2 = \frac{\mu}{N_1 + N_2'} \qquad y_3 = \frac{\mu^2 - N_2N_2'}{\mu(N_1 + N_2')}$$

The parameter k is found from the integral balance equation

$$\int_0^\infty \lambda'\frac{\partial t'(-\tfrac{1}{2}h', \tau)}{\partial x'}d\tau = \int_0^\infty \lambda''\frac{\partial t''(h'', \tau)}{\partial x''}d\tau + \int_0^\infty q_2d\tau + \int_0^\infty c_tm_t\frac{dt_t(\tau)}{d\tau}d\tau \qquad [22]$$

Here m_t is the weight of the ties between elements per unit of cooled surface, and c_t and $d_t(\tau)$ are, respectively, the bulk specific heat of the tie material and its temperature.

We assumed earlier that $t''(x'', \infty) = t_t(\infty) = t_{2*}$. Inserting Equations [1, 17 and 18] into Equation [22] and taking into

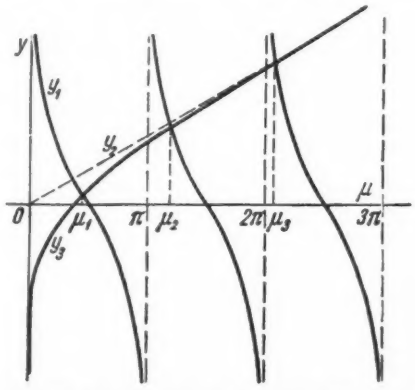

Fig. 6 Graphical determination of the roots of the characteristic equation

account that

$$\int_0^\infty q_{2\max}\frac{t_{2*}-t_{2\min}}{t_{2\max}-t_{2\min}}\,d\tau \equiv \int_0^\infty \alpha_2'\left[t'\left(-\frac{h'}{2},\tau\right)-t_{2*}\right]d\tau$$

we obtain

$$(c''h''\gamma''+c_1m_1)(t_{2*}-t_{20})=\frac{t_{2*}-t_{20}}{t_{2\max}-t_{2\min}}\frac{q_{2\max}}{k}-\frac{\alpha_2'}{k}\times$$

$$\frac{N_2'(t_{2*}-t_{20})(\cos\sqrt{N_k'}+(N_1/\sqrt{N_k'})\sin\sqrt{N_k'})}{(N_1N_2'/\sqrt{N_k'}-\sqrt{N_k'})\sin\sqrt{N_k'}+(N_1+N_2')\cos\sqrt{N_k'}}-$$

$$\frac{\alpha_2'h'^2}{a'}\sum_{n=1}^{\infty}\frac{2\mu_n^{-2}\cos\mu_n}{\mu_n^2-N_1N_2'+(\mu_n^2+N_1N_2')\mu_n^{-1}\sin\mu_n\cos\mu_n}\times$$

$$\left\{N_1\left(t_1^*-t_0'-D\frac{h'}{2}\right)-2Dh'\sin^2\frac{\mu_n}{2}+N_2'\left(t_{2*}-t_0'+\right.\right.$$

$$D\frac{h'}{2}-\frac{t_{2*}-t_{20}}{1-(N_k'/\mu_n^2)}\Big)\cos\mu_n+\frac{N_1N_2'}{\mu_n}\left[t_{2*}-t_0'+\right.$$

$$\left.\left.D\frac{h'}{2}\left(1+\frac{2}{N_2'}\right)-\frac{t_{2*}-t_{20}}{1-(N_k'/\mu_n^2)}\right]\sin\mu_n\right\} \quad [23]$$

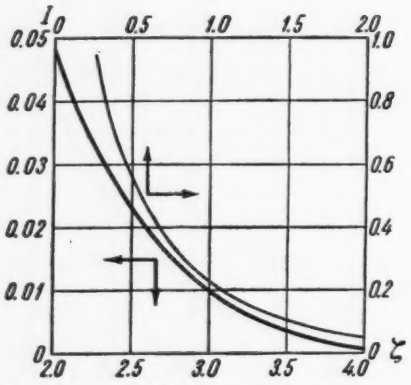

Fig. 7 Dependence of I on lower limit of integration

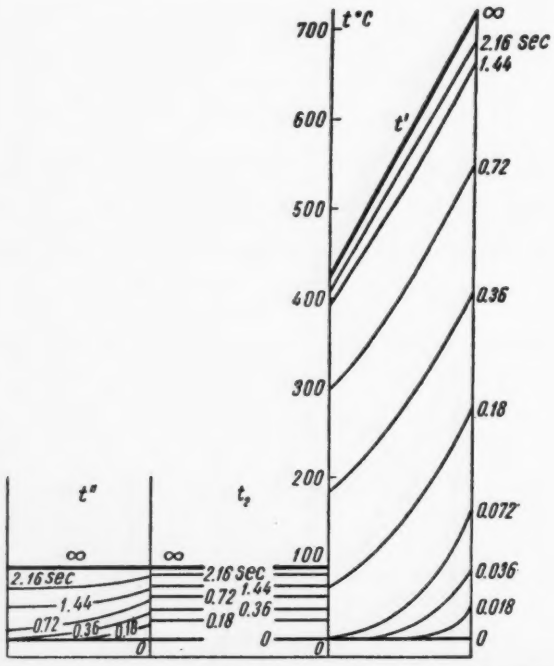

Fig. 8 Illustrative calculation of nonstationary heat transfer during the starting of an engine

Here c'' and γ'' are the specific heat and specific gravity of the material of the outer wall. The parameter k is determined from Equation [23] by trial and error.

The rapid convergence in time of the infinite sums in solutions [17 and 18] allows us to use a limited number of terms to determine the temperature distribution. Upper bounds for the residual terms of the series can be estimated in these solutions by means of the inequalities

$$\eta'<\frac{1}{\pi\mu_{m+1/2}}\left\{N_2'\left[t_{2*}-t_0'+D\frac{h'}{2}\left(\frac{2}{N_2'}+1\right)-\left|\frac{t_{2*}-t_{20}}{1-N_k'/\mu^2}\right|_{\min}\right]\sqrt{1+\frac{N_1^2+N_2'^2}{\mu_{m+1/2}^4}+\left(\frac{N_1N_2'}{\mu_{m+1/2}^2}\right)^2}+\right.$$

$$N_1\left[t_1^*-t_0'-D\frac{h'}{2}\left(\frac{2}{N_1}+1\right)\right]\times$$

$$\left.\left(1+\frac{N_2'^2}{\mu_{m+1/2}^4}\right)\right\}_{N\tau'_m}\int_{\mu^2_{m+1/2}}^{\infty}\frac{e^{-z}}{z}\,dz \quad [24]$$

$$\eta''<\frac{2N_2''|t_{2*}-t_{20}|}{\pi\nu_{m+1/2}[(\nu_{m+1/2}^2/N_k'')-1]}\int_{\nu^2_{m+1/2}}^{\infty}\frac{e^{-z}}{z}\,dz \quad [25]$$

Here m is the number of retained terms of the infinite sums, while η' and η'' are prescribed accuracy ranges, in degrees

$$\mu_{m+1/2}=\frac{1}{2}(\mu_m+\mu_{m+1}) \qquad \nu_{m+1/2}=\frac{1}{2}(\nu_m+\nu_{m+1})$$

In the expression

$$\left|\frac{t_{2*}-t_{20}}{1-(N_k'/\mu^2)}\right|_{\min}$$

contained in equality [24], it is necessary, to let $\mu\to\infty$ in the case of heating of the liquid, $t_{2*}>t_{20}$; in the case of cooling, $t_{2*}<t_{20}$, one must put $\mu=\mu_{m+1/2}$.

By specifying the required degree of accuracy η of the solution and by replacing the inequality sign of [24] by an equal sign, we evaluate the integral

$$I=\int_\zeta^\infty\frac{e^{-z}}{z}\,dz \qquad (\zeta=N\tau_m'\,\mu_{m+1/2}^2)$$

We find the value of ζ from Fig. 7 and compute the time τ_m beyond which the sum of the discarded terms lies within the interval of specified accuracy. One can proceed in a similar manner with Equation [25].

By way of an example, we show in Fig. 8 the results of computations for the nonstationary heat transfer in starting an engine, for the following data

$t_{20}=t_{2\min}=t_0'=t_0''=20$ C
$t_1=2720$ C
$t_{2\max}=t_{2*}=100$ C
$D=0$
$h'=1.5$ mm
$\lambda'=\lambda''=21.2$ kcal/m-hr-deg
$a'=a''=22.5\times10^{-3}$ m²/hr
$\alpha_1=1300$ kcal/m²-hr-deg
$q_r=1.5\times10^6$ kcal/m²-hr
$\alpha_2'=\alpha_2''=12{,}420$ kcal/m²-hr-deg

We assume $m_t=0$.

To take account of the pressure transients arising in the combustion chamber during starting, an additional relation was added to the right side of boundary condition [4], in the form

$$f=\alpha_1\left[t_1^*-t'\left(\frac{1}{2}h',\,0\right)\right]e^{-\beta\tau}$$

For the case under consideration, $t'(\frac{1}{2}h',\,0)=t_0'=20$ C, and $\beta=46$ sec^{-1}.

In each specific case, relations of this type can be introduced to account for the transients arising during stopping or changes in engine operating conditions.

Effect of the Rotation of a Planetary Atmosphere Upon the Orbit of a Close Satellite[1]

THEODORE E. STERNE[2]

Harvard University
Cambridge, Mass.

The rotation of a planetary atmosphere along with the planet changes all the orbital elements of a close satellite. Expressions are derived for such variations. The effects, although small, may be important to the precise interpretation of the motions of artificial Earth satellites. Rotation in the same sense as the satellite retards the rate of diminution of the orbital period, and unless allowed for, causes atmospheric densities inferred from satellite motions, to be as much as 10 per cent too low. The decrease of eccentricity is likewise retarded. The inclination i decreases secularly as found by Wildhack and Bosanquet, and a careful comparison by least squares of observation with theory shows good agreement for satellite 1957 Beta 1 and acceptable agreement for 1958 Beta 2. The node Ω regresses at a rate proportional to $\sin 2\omega$, and the argument ω of pericenter increases at a rate $\cos i$ times as great. Since the planet's rotational flattening changes ω secularly, atmospheric rotation does not change Ω and ω secularly. The mean anomaly at the epoch is not secularly changed. Equations are derived to permit the inference of atmospheric density from the mass and area of a satellite and from its observed orbital behavior, with due allowance for atmospheric rotation and for the dependence of density on distance from the flattened planet.

THE EFFECTS of the rotation of a planetary atmosphere upon the orbit of a close satellite do not appear to have been thoroughly and carefully considered anywhere. It is known (1)[3] that drag in the stationary atmosphere of a planet causes the mean distance a and eccentricity e of a satellite to decrease secularly, but causes no secular changes in the argument ω of pericenter, the inclination i, or the longitude Ω of the node. The decreasing period caused by the decreasing a has been used to infer (2,3) the density of the Earth's atmosphere at great altitudes from the decreasing periods of artificial Earth satellites. Rotational flattening (4,5) of the planet leaves a, e and i secularly unchanged but causes secular changes in ω and Ω, varying inversely as $a^{7/2}$. Drag and flattening thus combine to cause secular accelerations of the node and pericenter.

Wildhack (6) has considered semiquantitatively the effect of atmospheric rotation upon i. Bosanquet (7) has more recently considered this effect more accurately. We here consider still more accurately and generally the effect of atmospheric rotation upon all the orbital elements, and obtain their secular variations thus caused. The effects are small, but they may be of importance in the interpretation of observed features of the motion of artificial Earth satellites. In particular, it will be found that neglect of the effect of atmospheric rotation upon the rate of decrease of the period has led in practice to some underestimation of the atmospheric density, as inferred from the motion of artificial Earth satellites. A critical comparison will also be made of two observed rates of change of inclination of artificial Earth satellites with those predicted by the formulas to be derived in this paper.

Accurate equations will be derived to permit the inference of atmospheric density from the mass and area of a satellite and from its observed orbital behavior, with due allowance for atmospheric rotation and for the dependence of density on distance from the flattened planet.

Velocities and Forces

It is necessary to obtain expressions for the components S, T and W of drag force per unit mass, where S and T are in the plane of the orbit and along the radius vector r and perpendicular to it, respectively, in the sense of the orbital motion, and W is normal to the orbital plane in such a sense that the orbital motion appears clockwise when viewed along W. The effects sought are small. We take nonrotating right-handed rectangular axes $Oxyz$ with O at the planet's center, Oz being the planet's axis of rotation, and Ox and Oy being any two orthogonal axes in the plane of the planet's equator. The atmosphere is considered to rotate with the same angular velocity ω_s about Oz as the planet. The drag force per unit mass is $(\frac{1}{2})C_D A\ \rho\ v^2/m$; where C_D is the dimensionless aerodynamic drag coefficient, A is the cross-sectional area, ρ is the atmospheric density, m is the satellite's mass, and v is the velocity of the satellite relative to the atmosphere, which may be called the satellite's "airspeed." The drag force is in the direction opposite to the vector v.

The components of orbital velocity in the S, T and W directions are $\dot{r}$, $r\ \dot{w}$ and zero, respectively; where w is the true anomaly[4] (8). The angular velocity of rotation ω_s of the planet and its atmosphere has a component $\omega_s \cos i$ normal to the orbit, and a component $\omega_s \sin i$ about an axis, in the plane

Received Feb. 19, 1959.

[1] Presented in part at the Gainesville meeting of the American Astronomical Society, Dec. 27–30, 1958.

[2] Simon Newcomb Professor of Astrophysics; also Associate Director, Smithsonian Astrophysical Observatory.

[3] Number in parentheses indicate References at end of paper.

[4] Reference (8) is understood to be out of print, and as an introduction to the dynamical background and astronomical nomenclature here employed, (13) is alternatively cited.

of the orbit, perpendicular to the line of nodes. The former component of angular velocity gives rise to S, T and W components of atmospheric velocity $(0, \omega_s r \cos i, 0)$; the latter component of angular velocity gives rise to components of atmospheric velocity $(0, 0, -\omega_s r \sin i \cos u)$ in the same directions. Here u the argument of the latitude is the sum $(\omega + w)$. It follows that the airspeed v of the satellite has S, T and W components $(\dot{r}, r\dot{w} - \omega_s r \cos i, \omega_s r \sin i \cos u)$, and that v is given by

$$v^2 = \dot{r}^2 + r^2\dot{w}^2 - 2r^2\omega_s\dot{w}\cos i + \omega_s^2 r^2(\cos^2 i + \sin^2 i \cos^2 u)$$

exactly. The sum of the first two terms in the right-hand member is merely the square, given exactly (8) by

$$\frac{\mu}{a}\frac{1 + e\cos E}{1 - e\cos E}$$

of the ordinary orbital velocity, where

$\mu = MG$, the product of the planet's mass M and the constant G of gravitation
E = eccentric anomaly

Moreover, in the third term, $r^2\dot{w}$ is the areal constant, usually denoted by h, whose square is $\mu a(1 - e^2)$. Thus

$$v = \left(\frac{\mu}{a}\right)^{1/2}\left(\frac{1 + e\cos E}{1 - e\cos E}\right)^{1/2} \times$$

$$\left\{1 - \frac{\sqrt{1 - e^2}\,\omega_s \cos i}{n}\frac{1 - e\cos E}{1 + e\cos E} + \frac{1}{2}\frac{\omega_s^2}{n^2}\frac{(1 - e\cos E)^2}{(1 + e\cos E)^2}[\sin^2 i\cos^2 u(1 - e^2\cos^2 E) + e^2\cos^2 i \sin^2 E] + \text{still smaller terms}\right\}$$

where n is the mean orbital motion referred to the nonrotating axes, such that $n^2 a^3 = \mu$. For close Earth satellites the ratio ω_s/n is about $\frac{1}{15}$; the third term in the expansion is thus only about $\frac{1}{300}$ as large as the leading term, and will be ignored in this study. For satellites that are not close, the ratio will be larger, but the atmospheric density that will multiply this expression will then be so small that the product will still be unimportant. We thus take

$$v = \left(\frac{\mu}{a}\right)^{1/2}\left(\frac{1 + e\cos E}{1 - e\cos E}\right)^{1/2}\left(1 - d\frac{1 - e\cos E}{1 + e\cos E}\right) \quad [1]$$

where

$$d = (\omega_s/n)(1 - e^2)^{1/2}\cos i$$

Finally, therefore, the components of drag per unit mass are found to be

$$S = b\rho a e\, v \sin E \cdot \dot{E}$$

$$T = -b\rho a(1 - e^2)^{1/2} v\left(1 - d\frac{(1 - e\cos E)^2}{1 - e^2}\right)\dot{E}$$

$$W = -b\rho a\omega_s \frac{(1 - e\cos E)^2}{n}\sin i \cos u \cdot v \cdot \dot{E}$$

where b denotes the quantity $C_D A/2\ m$, and where use has been made of the relations

$$r = a(1 - e\cos E) \qquad nt = E - e\sin E$$

so that

$$\dot{r} = ae\sin E \cdot \dot{E} \qquad n = \dot{E}(1 - e\cos E)$$

Secular Variations of the Orbital Elements

The time-derivatives of the orbital elements are given (8) by

$$\frac{da}{dt} = 2\sqrt{\frac{a^3}{\mu}}[S\tan\varphi \sin w + T\sec\varphi(1 + e\cos w)]$$

$$\frac{de}{dt} = \sqrt{\frac{a}{\mu}}\cos\varphi[S\sin w + T(\cos w + \cos E)]$$

$$\frac{di}{dt} = \frac{rW\cos u}{\cos\varphi\sqrt{\mu a}}$$

$$\frac{d\Omega}{dt} = \frac{rW\sin u}{\cos\varphi \sin i\sqrt{\mu a}}$$

$$\frac{d\omega}{dt} = \frac{-aS\cos^2\varphi\cos w + rT\sin w(2 + e\cos w)}{\sin\varphi\cos\varphi\sqrt{\mu a}} - \frac{rw\sin u}{\cos\varphi\tan i\sqrt{\mu a}}$$

$$\frac{d\epsilon}{dt} = \frac{-2rS}{\sqrt{\mu a}} + 2\sin^2\left(\frac{\varphi}{2}\right)\frac{d(\omega + \Omega)}{dt} + 2\cos\varphi\sin^2\frac{i}{2}\frac{d\Omega}{dt}$$

where

$\sin\varphi = (1 - e^2)^{1/2}$
ϵ = mean longitude at the epoch, taken to be $t = 0$

From the expressions for S, T, da/dt and the relations (8)

$$\cos w = \frac{\cos E - e}{1 - e\cos E}$$

$$\sin w = (1 - e^2)^{1/2}\frac{\sin E}{1 - e\cos E}$$

it follows after some reduction that

$$\frac{da}{dt} = -2b\rho a^2\frac{(1 + e\cos E)^{3/2}}{(1 - e\cos E)^{1/2}}\left(1 - d\frac{1 - e\cos E}{1 + e\cos E}\right)^2\frac{dE}{dt}$$

If we integrate this with respect to t over one orbital period P and divide by the period we obtain the secular value of da/dt in the form

$$\dot{a}_{sec} = -\frac{2ba^2}{P}\int_0^{2\pi}\rho\frac{(1 + e\cos E)^{3/2}}{(1 - e\cos E)^{1/2}}\left(1 - d\frac{1 - e\cos E}{1 + e\cos E}\right)^2 dE \quad [2]$$

In the same way it is found from S, T and the expression for de/dt that

$$\dot{e}_{sec} = -(1 - e^2)\frac{abn}{\pi}\int_0^{2\pi}\rho\left(\frac{1 + e\cos E}{1 - e\cos E}\right)^{1/2}\left(1 - d\frac{1 - e\cos E}{1 + e\cos E}\right)\left\{\cos E - \frac{d}{2(1 - e^2)}(1 - e\cos E)(2\cos E - e - e\cos^2 E)\right\}dE \quad [3a]$$

Similarly, from W and the expression for di/dt

$$\left(\frac{di}{dt}\right)_{sec} = -\frac{ab\,\omega_s \sin i}{4\pi(1 - e^2)^{1/2}}\int_0^{2\pi}\rho(1 + \cos 2u)(1 - e\cos E)^{5/2}(1 + e\cos E)^{1/2}\left(1 - d\frac{1 - e\cos E}{1 + e\cos E}\right)dE \quad [3b]$$

which can be further reduced. One notices that ρ is a function of r, and therefore is an even function of E; except for

$1 + \cos 2u$, the integrand is an even function of E. However

$$\cos 2u = \cos 2\omega \cos 2w - \sin 2\omega \sin 2w$$

in which the term involving $\sin 2w$ is an odd function of E, contributing nothing to the integral. Dropping it, therefore, and expressing $\cos 2w$ in terms of $\cos E$, one finds

$$\left(\frac{di}{dt}\right)_{sec} = -\frac{1}{4\pi} ab\,\omega_s \sin i \frac{1}{\sqrt{1-e^2}} \int_0^{2\pi} \rho(1 - e\cos E)^{5/2}(1 + e\cos E)^{1/2}\left(1 - d\frac{1-e\cos E}{1+e\cos E}\right) \times \left[1 + \cos 2\omega \frac{(2-e^2)\cos^2 E - 1 + 2e^2 - 2e\cos E}{(1-e\cos E)^2}\right] dE \quad [4]$$

For $\dot{\Omega}$, one has

$$\dot{\Omega}_{sec} = -\frac{ab\,\omega_s \sin 2\omega}{4\pi\sqrt{1-e^2}} \int_0^{2\pi} \rho(1 - e^2\cos^2 E)^{1/2}\left(1 - d\frac{1-e\cos E}{1+e\cos E}\right)[2e^2 - 1 - 2e\cos E + (2-e^2)\cos^2 E]dE \quad [5]$$

For $\dot{\omega}$, one finds that

$$\dot{\omega}_{sec} = -\cos i \cdot \dot{\Omega}_{sec} \quad [6]$$

For $\dot{\epsilon}_{sec}$, one notices that the first term is an odd function of E and thus has zero for its secular value; the rest of the expression contains secular values of $d\omega/dt$ and $d\Omega/dt$ that have already been found, and is in fact

$$\dot{\epsilon}_{sec} = (1 - \cos i)\dot{\Omega}_{sec} \quad [7]$$

But the longitude of pericenter π is $\omega + \Omega$; hence

$$\dot{\pi}_{sec} = (1 - \cos i)\dot{\Omega}_{sec}$$

and since $\epsilon - \pi$ is the mean anomaly M_0 at the epoch t_0, it appears that M_0 has no secular variation

$$(\dot{M}_0)_{sec} = 0 \quad [8]$$

Hence the mean anomaly M at any time t is given by

$$M = M_0 + \int_{t_0}^{t} n\,dt$$

where

$n = \mu^{1/2}a^{-3/2}$

M_0 = constant

Period and Determination of Atmospheric Density

The secular variation of a is important because it provides a means of inferring the atmospheric density from the observed rate of change $\dot{P}$ of the period P. Since P varies as $a^{3/2}$ it follows from Equation [2] that

$$\dot{P} = -\frac{3}{2}(1-d)^2 C_D \frac{aA}{m} \int_0^{2\pi} \rho \times \frac{[1 + (1+d)/(1-d)^{-1}\,e\cos E]^2}{\sqrt{1 - e^2\cos^2 E}}\,dE \quad [9]$$

The integral can always be evaluated numerically for any assumed atmospheric model, and the resulting $\dot{P}$ compared with observation. However, very accurate analytical approximations can be obtained by approximating to ρ near $E = 0$ by the osculating exponential atmosphere

$$\rho = \rho_\pi e^{-Kz}$$

where

ρ_π = density at pericenter

z = height of the satellite above pericenter given by $z = a(1 - e\cos E) - a(1-e) = ae(1 - \cos E)$

$K = -(d/dz)\log_e \rho$

Here the density is assumed to depend only on the height above pericenter. In a later section the more accurate assumption will be made that the density depends on the height above the planet's spheroidal surface. If Kae is denoted by c, and if the variable of integration is changed to y defined by $\cos E = 1 - y^2/c$, Equation [9] becomes without further approximation

$$\dot{P} = -3C_D \frac{A}{m}\frac{(1+e)^{3/2}}{(1-e)^{1/2}}\left(1 - d\frac{1-e}{1+e}\right)^2 a\,\rho_\pi \sqrt{\frac{2}{c}} \int_0^{\sqrt{2c}} \frac{e^{-y^2}\left(1 - \frac{ey^2}{c}\frac{1+d}{1+e-d+ed}\right)^2 dy}{\left(1 + \frac{2e^2}{1-e^2}\frac{y^2}{c} - \frac{e^2}{1-e^2}\frac{y^4}{c^2}\right)^{1/2}\sqrt{1 - \frac{y^2}{2c}}}$$

The integrand can be expanded as $\exp(-y^2)$ times a power series in y^2 and can be integrated term by term to obtain the asymptotic expansion

$$\dot{P} \sim -3C_D \frac{A}{m}\frac{(1+e)^{3/2}}{(1-e)^{1/2}}\left(1 - d\frac{1-e}{1+e}\right)^2 \rho_\pi\, a\sqrt{\frac{\pi}{2c}}\left\{1 + \frac{f_1}{8c} + \frac{9}{128c^2}f_2 + \ldots\right\} \quad [10]$$

where

$$f_1(e,d) = 1 - 8ek - 4e^2/(1-e^2)$$

$$f_2(e,d) = 1 + \frac{8}{3}e^2\frac{1+5e^2}{(1-e^2)^2} + \frac{16ek}{3}\frac{(5e^2-1)}{1-e^2} + \frac{32}{3}e^2k^2$$

$$k = \frac{1+d}{1-d+e+ed}$$

Equation [10] provides accurate values of $\dot{P}$, unless c is smaller than about 2, because significant contributions to the integral in Equation [9] then come only from the neighborhood of $E = 0$. No assumption has been made about the smallness of e; the larger e is, the larger c is and more accurate is expression [10]. If the orbit is so nearly circular that $c < 2$, the asymptotic expansion in Equation [10] becomes useless; but then the osculating atmosphere remains a good approximation throughout the orbit, all parts of which then contribute significantly to the integral, which can be evaluated generally in terms of Bessel functions $I_0(c)$ and $I_1(c)$; thus, even when e is very small

$$\dot{P} = -3(1-d)^2 C_D \frac{A}{m} a\pi e^{-c}\rho_\pi \left\{\left[1 + e^2\left(j^2 + \frac{1}{2}\right) - \frac{e^3 j}{c} + \ldots\right]I_0(c) + e\left[2j - \frac{e}{c}\left(j^2 + \frac{1}{2}\right) + e^2 j\left(1 + \frac{2}{c^2}\right) + \ldots\right]I_1(c)\right\} \quad [11]$$

correctly through terms in e^3, where $j = (1 + d)/(1 - d)$.

It is clear that if one ignores the atmospheric rotation when inferring the atmospheric density ρ_π at perigee from the $\dot{P}$ of a satellite whose motion is direct, one will underestimate ρ_π. If the motion is retrograde, one will overestimate ρ_π. Equations [10 and 11] show that the relative error thus introduced is of the order of magnitude of d, which for a close Earth satellite of average inclination is a few per cent. For more distant satellites, the error could be as large as 10 per cent or more. Use of Equations [10 or 11] permits one to avoid this small error.

Allowance for the Planet's Flattening

In the preceding discussion, the effect of the planet's flattening has been ignored in deriving Equations [10 and 11] from Equation [9]. It can be included, and perhaps should be, because of the importance of density determinations, although at the expense of some complexity.

The radius of the spheroid, to the point under the satellite, is given by

$$a_0(1 - f \sin^2 i \sin^2 u)$$

where

f = flattening, $(a_0 - b_0)/a_0$, a_0 and b_0 being the planet's equatorial and polar radii

u = argument of the latitude, $\omega + w$

The height h above the spheroid is

$$h = a(1 - e \cos E) - a_0(1 - f \sin^2 i \sin^2 u)$$

which at pericenter has the value

$$h_\pi = a(1 - e) - a_0(1 - f \sin^2 i \sin^2 \omega)$$

so that

$$h - h_\pi = ae(1 - \cos E) + a_0 f \sin^2 i(\sin^2 u - \sin^2 \omega)$$

If the planet is spheroidal, and if the atmospheric density is a function of height above the spheroid, the osculating atmospheric approximation becomes

$$\rho = \rho_\pi e^{-K(h - h_\pi)}$$

$$= \rho_\pi \exp\,[-c(1 - \cos E) - q\,(\sin^2 u - \sin^2 \omega)]$$

where

$$q = Ka_0 f \sin^2 i \qquad [12a]$$

whose value for the Earth is of the order of 0.2. This value of ρ may be substituted into Equation [9], in the form

$$\rho = \rho_\pi e^{-c(1 - \cos E)} \sum_0^\infty (-)^s q^s (\sin^2 u - \sin^2 \omega)^s / s!$$

and in the series the terms that are odd functions of w, and thus of E, may be ignored because the rest of the integrand in [9] is an even function of E, and the odd terms cannot contribute to the complete integral. The even part of the series through terms in q^2, when expressed in terms of E is

$$1 + \frac{q_1 \sin^2 E}{(1 - e \cos E)^2} + \frac{q_2 \sin^4 E}{(1 - e \cos E)^4}$$

where

$$q_1 = (1 - e^2)[-q \cos 2\omega + (q^2/2) \sin^2 2\omega]$$

$$q_2 = (1 - e^2)^2 (q^2/2) \cos 4\omega \qquad [12b]$$

Substitution of the resulting ρ into Equation [9] leads to the same Equation [10] for $\dot{P}$ as before, but with

$$f_1 = 1 - 8ek - 4\frac{e^2}{1 - e^2} + 8q_1 \frac{1}{(1 - e)^2}$$

$$f_2 = 1 + \frac{8}{3} e^2 \frac{1 + 5e^2}{(1 - e^2)^2} + \frac{16}{3} ek \frac{5e^2 - 1}{1 - e^2} + \frac{32}{3} e^2 k^2 - \frac{16}{3} q_1 (1 + 10e + 8ek) + \frac{128}{3} q_2 (1 + 4e) \qquad [12c]$$

Terms in $q_1 e^3$ and $q_2 e^2$ have been ignored in f_1, and terms in $q_1 e^2$ and $q_2 e^2$ in f_2, since these terms can only be large if e is large, in which case c is large and the contributions of the neglected terms, multiplied by $1/8c$ and by $9/128c^2$, respectively, are very small.

The preceding result is valid when $c \geq 2$; a general result (Eq. [12d]) that allows for flattening even when $c < 2$ can be obtained in terms of Bessel functions, analogous to Equation [11]; it is

$$\dot{P} = -3C_D (A/m)(1 - d)^2 a \rho_\pi \pi\, e^{-c}[B_0 I_0(c) + B_1 I_1(c)] \qquad [12d]$$

where

$$B_0 = 1 + e^2\left(j^2 + \frac{1}{2}\right) - j\frac{e^3}{c} + q_1 \frac{e}{c}\left[2(j + 1) - \frac{3e}{c}\left(j^2 + 4j + \frac{7}{2}\right)\right] + q_2 \frac{3}{c^2}\left[1 - \frac{8e}{c}(j + 2)\right]$$

$$B_1 = 2ej - \frac{e^2}{c}\left(j^2 + \frac{1}{2}\right) + \left(1 + \frac{2}{c^2}\right) je^3 + q_1 \frac{1}{c}\left[1 - \frac{4e}{c}(j + 1) + e^2\left(1 + \frac{6}{c^2}\right)\left(j^2 + 4j + \frac{7}{2}\right)\right] - q_2 \frac{6}{c^2}\left[\frac{1}{c} - \left(1 + \frac{8}{c^2}\right) e(j + 2)\right]$$

correctly up to but not including terms in e^4, $q_1 e^3$ and $q_2 e^2$ which are very small.

The use of Equations [12c or d] should permit the inference of still more accurate atmospheric densities from physical and observational data relating to satellites and their orbits, than should the use of Equations [10 or 11].

Secular Decrease in the Inclination

Equation [3b] shows that the inclination decreases secularly, since the quantity d is small compared to unity and the integrand of the integral is never negative. The right-hand member of Equation [4] can be evaluated by the same substitutions as were employed to derive Equation [10]. The effect is small, and if the orbit is not so nearly circular as for c to be as small as 1 or 2, then Equation [13] should be sufficiently accurate

$$\left(\frac{di}{dt}\right)_{sec} \sim -\frac{C_D A}{4m} \omega_s \sin i\,(1 - e)^2 \left(1 - d\frac{1 - e}{1 + e}\right) a\rho_\pi \sqrt{\frac{1}{2\pi c}} \left\{1 + \frac{1}{8c}\left(1 - 4ek + 4e\frac{3 + 2e}{1 - e^2}\right) + \ldots \right.$$

$$\left. + \cos 2\omega \left[1 - \frac{1}{8c}\left(15 + 4ek + 4e\frac{5 + 6e}{1 - e^2}\right) + \ldots\right]\right\} \qquad [13]$$

One has

$$\sin^2 u - \sin^2 \omega = (1/2)[\cos 2\omega - \cos 2(\omega + w)]$$
$$= \cos 2\omega \sin^2 w + (1/2) \sin 2\omega \sin 2w$$

The planet's flattening in general causes ω to advance or regress, so that the term in $\cos 2\omega$ averages out over a long interval of time; the whole effect predicted by Equation [13] for a typical close Earth satellite (1957 Alpha 2) is of the order of a second of arc a day.

Formulas for Secular Changes in Eccentricity, Longitude of the Node, Argument of Pericenter and Mean Longitude at Epoch

From Equation [3a] by similar substitutions one finds the equation

$$\dot{\epsilon}_{sec} \sim -(1-e^2)\frac{C_D A}{m}\frac{(1+e)^{1/2}}{(1-e)^{1/2}}\left(1-d\frac{1-e}{1+e}\right)^2 \rho_\pi \frac{an}{\sqrt{2\pi c}}\left\{1-\frac{1}{8c}\left[3+4ek+\frac{4e^2}{1-e^2}+\frac{4ed}{1-d+e+ed}\right]+\ldots\right\} \quad [14]$$

that is accurate for c larger than 1 or 2, and which shows, as one would expect, that atmospheric rotation causes e to decrease less rapidly for a direct orbit in which d is positive, than it would if the atmosphere did not rotate.

From Equation [5], by the usual substitution, one finds that when c is larger than 1 or 2

$$\dot{\Omega}_{sec} \sim -(1-e^2)\frac{C_D A}{4m}\omega_s \sin 2\omega\left(1-d\frac{1-e}{1+e}\right)a\rho_\pi \frac{1}{\sqrt{2\pi c}}\left[1-\frac{1}{8c}\left(15-4e\frac{3-2e}{1-e^2}+4ek\right)+\ldots\right] \quad [15]$$

whose average value is zero over long intervals of time because of the advance or regression of ω caused by the planet's flattening.

By Equation [6], $\dot{\omega}_{sec}$ is merely $(-\cos i)$ times the value of $\dot{\Omega}_{sec}$ given by [15], whereas $\dot{\epsilon}_{sec}$ by [7] is $(1-\cos i)\dot{\Omega}_{sec}$.

Observational Comparisons: Decrease of Inclination

The artificial Earth satellites 1957 Beta 1 and 1958 Beta 2 permit comparison to be made of the secular decrease in declination predicted by Equation [13] with observation.

The satellite 1957 Beta 1 has been carefully observed by the Royal Aircraft Establishment, Farnborough, and reported upon by Cornford (9). Its inclination has been further discussed by Merson and King-Hele (10), while Bosanquet (7) has compared its observed decrease of inclination with that expected theoretically. We here repeat Bosanquet's comparison but with a more accurate theoretical decrease, and with more careful regard to the accuracy of the observed decrease so as to be able to apply a statistical test of significance to the difference, the observed decrease minus the expected decrease. If one divides Equation [13] by Equation [10] one obtains

$$\frac{di}{dP} = \frac{\omega_s}{12\pi}\sin i\,(1-e^2)\sqrt{\frac{1-e}{1+e}}\frac{k}{1+d}\,\frac{1+\frac{1}{8c}\left(1-4ek+4e\frac{3+2e}{1-e^2}\right)+\cos 2\omega\left[1-\frac{1}{8c}\left(15+4ek+4e\frac{5+6e}{1-e^2}\right)\right]}{1+\frac{1}{8c}\left(1-8ek-\frac{4e^2}{1-e^2}\right)} \quad [16]$$

from which the quantities A and m have disappeared. The right-hand member of Equation [16] has been evaluated by the use of the orbital data contained in (9) and integrated with respect to P over the 160 days between the limits of 1957 November $3^d.0$ and 1958 April $12^d.0$. The value of K needed to obtain c was obtained from the Smithsonian Interim Atmosphere, Model 2 (11); substantially the same results were obtained for di/dP when K was obtained from Rand's new model atmosphere (12). The integration was done by multiplying di/dP by dP/dt as listed by Cornford, and integrating with respect to t by Simpson's rule with intervals of 40 days for the first 120 days of the 150-day interval. For the last 40 days of the 160-day interval, the integration of di/dP was with respect to P, by Simpson's rule, at P-intervals of $1^d.665$. The theoretical change in i over the whole interval was thus determined to be $-0°.110$; or an average rate of $-2''.48$ per day. The observed change in i is stated by Merson and King-Hele (10) to be given by

$$i = 65°.331 - 0°.00018\,t - 0°.0000043\,t^2 \pm 0°.02 \quad [17]$$

the last number presumably being a standard deviation (s.d.) of the values given by the formula, and t being measured from U.T. (Universal Time, measured from Greenwich midnight) 1957 November $3^d.0$. The standard deviation must depend on t and cannot be right; but naive acceptance of the formula leads to an observed change over the 160^d of $-0°.139 \pm 0°.028$ (s.d.), so that the observed minus the expected change was $-0°.029 \pm 0°.028$, insignificantly different from zero—the agreement thus being satisfactory. Through distrust of the formula [17] the author was led to make his own least squares solution quadratic in the time, of the observed i given by Cornford (9), but rejected his first and fourth observed values (stated to be doubtful and apparently rejected also by Merson and King-Hele) and corrected his fifth tabulated value, 65°.35, to 65°.31 as shown in Cornford's own Figure 12 at $t = 59$ and plotted in the later and presumably critical publication (10). Cornford's values of 65°.22 on March 16, 65°.21 on March 20, and 65°.21 on March 21, all apparently excluded by Merson and King-Hele, have also been excluded here. With equal weights for the remaining 25 observations combined into 17 observational equations, the author has obtained the formula

$$i = 65°.326 - 0°.00006\,t - 0°.0000047\,t^2 \quad [18]$$

whose coefficients do not differ significantly from those in Equation [17] (the standard deviations being 0.019, 0.00039, 0.0000018) and obtained the weight, from the matrix of coefficients in the normal equations, of the value of i at $t = 160$ minus the value of i at $t = 0$ given by Equation [18] as 0.61. Such terminal values are of course not independent. In this way the observed change in i from $t = 0$ to $t = 160$ was found for satellite 1957 Beta 1 to be:

	Δi	Mean rate of change of inclination, per day
Observed	$-0°.130$ $\pm 0°.019$ (s.d.)	$-2''.93$ $\pm 0''.43$ (s.d.)
Expected	$-0°.110$	$-2''.48$
Difference	$-0°.020$ $\pm 0°.019$ (s.d.)	$-0''.45$ $\pm 0''.43$ (s.d.)

so that the difference between theory and observation is about 1.05 standard deviations, estimated from 14 degrees of freedom, of the observed quantity. The difference is statis-

tically insignificant, and the agreement must thus be considered good. If the insignificant difference were regarded as real, however, it could be explained completely by an average atmospheric wind, relative to the rotating Earth, blowing from west to east at about 130 mph at heights between 150 and 250 km.

Orbital data pertaining to satellite 1958 Beta 2 have been distributed by teletype from the Project Vanguard Computing Center; such data presumably have been obtained by "minitrack." Over the 196-day interval from July 3, 1958 to January 15, 1959 such data, in the right-hand member of Equation [16], have led to a predicted average rate of change of inclination of $-0''.0040$ per day. A least squares solution was carried out by the author with equal weights for the observations, in the form

$$i = A + B \sin \omega + C\,(t - t_0)/196$$

where A, B and C were the unknowns. The B term was included because it was expected theoretically to arise from the third spherical harmonic in the Earth's gravitational potential. A quadratic term, neither expected nor observed, was not included. The quantity C, the change in inclination from atmospheric rotation in 196 days, was found from 26 degrees of freedom to be $+0°.0065 \pm 0°.0053$ (s.d.). Thus the comparison of the observed and expected values for satellite 1958 Beta 2:

	Mean rate of change of inclination, per day
Observed	$+0''.119 \pm 0''.097$(s.d.)
Expected	$-0''.004$
Difference	$+0''.123 \pm 0''.097$(s.d.)

showed that they were in agreement, the difference being statistically insignificant. On the other hand, unlike the situation for 1957 Beta 1, the observational standard deviation was many times larger than the expected effect, which the observations are altogether too inaccurate to establish. The observations are consistent with there being no secular effect at all.

Concluding Remarks

The most important effects of the rotation of the atmosphere of a planet upon the direct orbit of a close satellite appear to consist of slight diminutions in the rates of decrease of period, mean distance and eccentricity, and of a gradually decreasing inclination. The first of these effects causes atmospheric densities, inferred from satellite motion, to be slightly underestimated unless such effects are allowed for by the use of equations like [10, 11, 12c or 12d]. In a retrograde orbit, the effects are reversed in sign. However, the astronomical convention of assigning to the inclination a value between 90 and 180 deg whenever the motion is retrograde, causes the inclination always to decrease.

Nomenclature

A = cross-sectional area, also a constant to be determined
a = orbital mean distance (semimajor axis)
a_0 = planet's equatorial radius
B = constant
B_0, B_1 = quantities defined after Equation [12d]
b = $C_D A/2m$
b_0 = planet's polar radius
C = constant
C_D = aerodynamic drag coefficient
c = Kae
d = $(\omega_s/n) \cos i\,(1 - e^2)^{1/2}$
e = orbital eccentricity
e = Napierian base
E = eccentric anomaly
f = planet's flattening, $(a_0 - b_0)/a_0$
f_1, f_2 = quantities defined after Equation [10] and in Equation [12c]
G = Newtonian constant of gravitation
h = areal constant, also height above spheroid
i = inclination, angle between orbit plane and planet's equator
I_0, I_1 = Bessel functions
j = $(1 + d)/(1 - d)$
K = $-(d/dz) \log_e \rho$
k = $(1 + d)/(1 - d + e + ed)$
M = mass of the planet, also mean anomaly
M_0 = mean anomaly at particular epoch
m = mass of the satellite
n = $2\pi/P$
P = satellite's period
q_1, q_2 = quantities defined by Equations [12b]
r = radius vector, mass center of planet to satellite
S = radial component of air resistance
T = component of resistance in orbit plane normal to radius vector
t = time
u = argument of latitude: Angle between radii to Ω and satellite
v = airspeed of satellite
W = component of resistance normal to orbit plane
w = true anomaly, angle between radii to pericenter and satellite
z = height above pericenter
ϵ = mean longitude at epoch, $\Omega + \omega + M_0$
π = longitude of pericenter, $\Omega + \omega$
μ = MG
ρ = atmospheric density
φ = $\sin^{-1} e$
ω = argument of pericenter: Angle between radii to Ω and to pericenter
ω_s = rate of absolute rotation of the atmosphere
Ω = ascending node, the point where the satellite positively traverses the planet's equator; also the longitude of the node, the angle between a standard equatorial direction and the radius to that point

Subscripts

π = values at pericenter
sec = secular or long term average values
dots over symbols denote time-derivatives

References

1 Sterne, T. E., "An Atmospheric Model and Some Remarks on the Inference of Density from the Orbit of a Close Earth Satellite," *Astronomical J.*, vol. 63, no. 3, March 1958, pp. 81–87.

2 Sterne, T. E., "Formula for Inferring Atmospheric Density from the Motion of Artificial Earth Satellites," *Science*, vol. 127, no. 3308, May 23, 1958, p. 1245.

3 Sterne, T. E., "High-Altitude Atmospheric Density," *Phys. Fluids*, vol. 1, no. 3, May-June 1958, pp. 165–170.

4 Sterne, T. E., "The Gravitational Orbit of a Satellite of an Oblate Planet," *Astronomical J.*, vol. 63, no. 1, Jan. 1958, pp. 28–40.

5 King-Hele, D. G., "The Effect of the Earth's Oblateness on the Orbit of a Near Satellite," Proc. Royal Society, Series A, vol. 247, 1958, pp. 49–72.

6 Wildhack, W. A., "Effect of Transverse Atmospheric Drag on Satellite Orbits," *Science*, vol. 128, no. 3319, Aug. 8, 1958, pp. 309–310.

7 Bosanquet, C. H., "Change of Inclination of a Satellite Orbit," *Nature*, vol. 182, Nov. 29, 1958, p. 1533.

8 Plummer, H. C., "Dynamical Astronomy," University Press, Cambridge, 1918, chap. III, VI and XIII.

9 Cornford, E. C., "A Comparison of Orbital Theory with Observations made in the United Kingdom on the Russian Satellites," Royal Aircraft Establishment, Farnborough, July 1958, reproduced by the National Academy of Sciences, National Research Council, Washington 25, D. C.

10 Merson, R. H. and King-Hele, D. G., "Use of Artificial Satellites to Explore the Earth's Gravitational Field: Results from Sputnik 2 (1957 β)," *Nature*, vol. 182, Sept. 6, 1958, pp. 640–641.

11 Sterne, T. E., Folkart, B. M. and Schilling, G. F., "An Interim Model Atmosphere Fitted to Preliminary Densities Inferred from USSR Satellites," *Smithsonian Contributions to Astrophysics*, vol. 2, no. 10, 1958, pp. 275–279.

12 Kallmann, H. K. and Juncosa, M. L., "A Preliminary Model Atmosphere Based on Rocket and Satellite Data," U.S. Air Force Project Rand Research Memo RM-2286, Oct. 30, 1958, ASTIA no. AD207752.

13 Smart, W. M., "Celestial Mechanics," Longmans, Green and Co., New York and London, 1953, chap. I through V.

Method for Determining Steering Programs for Low Thrust Interplanetary Vehicles

EDWARD RODRIGUEZ[1]

Autonetics Division
North American Aviation, Inc.
Downey, Calif.

A simple method is presented for determining possible thrust vector programs to transfer a low thrust space vehicle between coplanar circular orbits. A two-body physical model and constant vehicle thrust-to-mass ratio are assumed. Through relations between specific energy and specific angular momentum, this method determines possible steering programs and avoids the costly, difficult, time consuming trial and error processes of computing numerous trajectories to arrive at a possible steering program. Simple examples of steering programs with their machine computed trajectories illustrate the method.

THE PROBLEM of determining nominal steering programs for low thrust vehicles which travel from a satellite orbit about one planet to a satellite orbit about another is approached, in a preliminary analysis manner. A low thrust vehicle is considered to have a thrust acceleration of the order of $10^{-4} \times 32$ fps^2 (the thrust acceleration expected from ionic-type propulsion systems).

When such a vehicle approaches the region surrounding a destination planet within which the planet's gravitational field predominates, it is highly desirable that the vehicle's velocity relative to the planet be small. Excess velocity at this time means excess energy to be removed in the process of establishing the satellite orbit. Since the vehicle's thrust is very low, only a small relative velocity can be tolerated; otherwise the vehicle is unable to reduce the energy below escape level during the time it is within the planet's gravitational sphere, and is not captured. The vehicle may be designed to incorporate high thrust rockets which remove the excess velocity at the appropriate time, but this approach is probably too costly in payload. (The added weight consists not only of the weight of the rockets and fuel but also of the extra vehicle structure which must be designed to withstand the high thrust levels.)

The nominal steering program will therefore probably be designed not only to intercept the destination planet but also to match the planet's trajectory about the sun upon entering the planet's sphere of gravitational predominance. In this paper the problem of determining steering programs is examined only for the interplanetary phase of the transfer trajectory (during which the planetary gravitational fields can be neglected), and only a first approach toward solving this problem is presented. The approach is made by examining a similar but simplified problem with respect to a simplified physical model. The simplified physical model consists only of the sun and the vehicle.

The simplified problem considered is the determination of nominal steering programs which assure that the vehicle's trajectory tangentially intercepts any desired circular orbit about the sun which is coplanar with the vehicle's initial trajectory, and that the vehicle arrives there at the correct circular orbital speed. This is a great simplification over the real problem. The noncoplanarity and noncircularity of the planetary orbits introduce considerable difficulty. However, since the planetary orbits of most interest (those of Earth, Mars and Venus) are nearly coplanar and nearly circular, solutions obtained with respect to the simplified case should shed considerable light on the real problem and undoubtedly will form valuable data for preliminary design and feasibility considerations.

The most valuable papers in connection with this problem in the past are probably (1 and 2).[2] Standard works on celestial mechanics, such as (3) are, of course, basic to all space trajectory problems.

Basic Problem

In the assumed physical model, the sun's gravitational potential (U) is

$$U = -\mu/r \qquad [1]$$

and the vehicle's acceleration($d\vec{V}/dt$) is the sun's gravitational acceleration ($-\mu/r_2$) plus the sum of all other accelerations, herein designated as ($\vec{A}$). $\vec{A}$ is called the inertial acceleration. It is the acceleration directly sensed by inertial accelerometers. The equation of motion is

$$\frac{d\vec{V}}{dt} = -\frac{\mu}{r^2}\vec{l}_r + \vec{A} \qquad [2]$$

where

$\vec{V}$ = velocity vector
$\vec{A}$ = inertial acceleration vector
$\vec{l}_r$ = unit vector directed radially away from the sun

It is assumed that the vehicle is initially orbiting about the sun in an unpowered circular orbit, and that it is capable of applying and regulating its thrust magnitude so that its inertial acceleration magnitude is maintained constant and of the order of $10^{-4} \times 32$ fps^2. The initial condition is assumed because the trajectory of a low thrust vehicle upon escaping from the sphere of gravitational predominance of a planet differs little from the trajectory of the planet. It is not a necessary requirement in the method to be presented, however.

The analysis is limited to trajectories of possible interest in optimization studies. Fig. 1 shows the type of trajectory considered. The vehicle starts powered flight at point (1) at radius r_1, and ends powered flight at point (3) at radius r_3.

Presented at the ARS Semi-Annual Meeting, Los Angeles, Calif., June 9–12, 1958.

[1] Senior Engineer, Research, Advanced Engineering.

[2] Numbers in parentheses indicate References at end of paper.

At point (2) a discontinuity in steering direction may occur. The magnitude of the inertial acceleration vector is assumed to be constant during phase (1) to (2), and during phase (2) to (3), but not necessarily to be the same in both phases.

Possible steering programs may, of course, be found by trial and error: i.e., by proposing programs for $\vec{A}$ and solving the resulting differential equations (i.e., solving Eq. [2]) in turn by machine-computer methods until a program is found which results in a trajectory with the proper end conditions. This method is difficult, costly, time consuming and not generally useful to an understanding of the steering problems.

The new method presented attempts to circumvent these difficulties and provides greater insight into the nature of the problem. The principal ideas of the new method are simple. They involve the instantaneous specific energy (E), instantaneous specific angular momentum (h), and instantaneous orbit of the vehicle, which are defined as

$$E = \frac{V^2}{2} - \frac{\mu}{r} \qquad [3]$$

$$h = r^2\dot{\theta} \qquad [4]$$

(V, r and θ are defined in Fig. 1). The instantaneous orbit is the orbit the vehicle would follow if the inertial acceleration were instantaneously removed (i.e., it is the instantaneous "unpowered" orbit).

The instantaneous specific energy of the vehicle determines the size of the instantaneous orbit, since the semimajor axis (a) of any elliptical unpowered orbit is given exactly by

$$a = -\mu/2E \qquad [5]$$

The combination of instantaneous specific energy and specific angular momentum determines the eccentricity, or shape, of the instantaneous orbit, as the eccentricity (e) of any conical orbit is given exactly by

$$e = \sqrt{1 + (h/\mu)^2\,(2E)} \qquad [6]$$

For circular orbits $e = 0$

$$E = -\mu/2a \qquad [7]$$

and

$$h = \sqrt{\mu a} \qquad [8]$$

where a is the radius of the circular orbit.

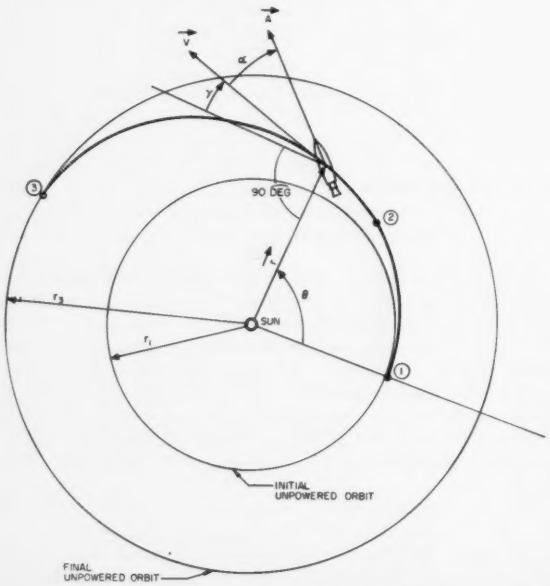

Fig. 1 Typical trajectory and definitions

The desired trajectory end conditions are achieved when the vehicle's instantaneous orbit becomes a circle of the desired radius. This condition is assured when E and h reach the values associated with the desired circular orbit radius. To accomplish the transfer it is thus only necessary (and sufficient) that the vehicle's specific energy and momentum be made to achieve the particular values associated with the desired orbit. Possible steering programs may therefore be studied by examining the effects of the magnitude and direction of the vehicle's inertial acceleration on the vehicle's specific energy and angular momentum. This approach is the essence of the method presented.

The time rates of change of specific energy and angular momentum are found to be given exactly by the following simple expressions (see Fig. 1 for meaning of α and γ)

$$\dot{E} = AV\cos\alpha \qquad [9]$$

$$\dot{h} = Ar\cos(\alpha + \gamma) \qquad [10]$$

Equation [10] is found in many texts. It expresses the familiar fact that the time rate of change of specific angular momentum is equal to the specific torque applied. Equation [9] is not commonly found in this form. It expresses the fact that the time rate of change of specific energy is equal to the product of the velocity and the component of inertial acceleration along the velocity vector. It may be derived by forming the dot product of each side of Equation [2] with the velocity vector $\vec{V}$ as follows

$$\frac{d\vec{V}}{dt}\cdot\vec{V} = \left(-\frac{\mu}{r^2}\vec{l}_r + \vec{A}\right)\cdot\vec{V}$$

or

$$V\dot{V} = -\frac{\mu}{r^2}\dot{r} + AV\cos\alpha$$

Now, since

$$E = \frac{V^2}{2} - \frac{\mu}{r}$$

we have

$$\dot{E} = V\dot{V} + \frac{\mu}{r^2}\dot{r}$$

thus

$$\dot{E} = AV\cos\alpha$$

Dividing Equation [9] by Equation [10] yields

$$\frac{dE}{dh} = \frac{V\cos\alpha}{r\cos(\alpha + \gamma)} \qquad [11]$$

Because Equations [9, 10 and 11] relate the direction and magnitude of the inertial acceleration vector to the changes of specific energy and specific angular momentum, they form the keys for determining steering programs. These equations are valid for any magnitude of inertial acceleration.

The E-h Diagram

Before developing possible steering programs, an energy-momentum (E-h) diagram is introduced. This diagram aids in obtaining understanding by providing a means for visualizing the effects of the key Equations [9, 10 and 11]. The E-h diagram is shown in Fig. 2. Each point in this diagram represents a particular size and shape instantaneous orbit. In fact, all possible instantaneous two-body orbits can be represented by the diagram. Note, however, that there is a region of the E-h diagram which is inaccessible (a region of imaginary eccentricities). The lines of constant eccentricity are determined from Equation [6].

As the vehicle is inertially accelerated, its E and h change in accordance with the key equations and describe a path in the

E-h diagram. To satisfy the transfer trajectory end conditions, this path need simply end at the particular E-h point associated with the destination circular orbit.

Thus all possible circular orbital transfers can be represented by all possible E-h diagram paths which go from the initial circular orbit's E-h point to the destination circular orbit's E-h point. (These paths may not enter the inaccessible region, however.) The vehicle's E-h path may not go from one circular orbit point to another by following the circular orbit line exactly, because whenever the vehicle's E and h are those of a circular orbit, the vehicle's velocity vector must be normal to the radius vector; hence, the vehicle cannot change orbital radius. Thus, to transfer from one circular orbit to another, the vehicle's E and h must enter the region of elliptical orbits (possibly also pass into the region of hyperbolic orbits) and then return to the line of circular orbits.

The slope of the motion of the E-h point in the diagram (as determined by Eq. [11]) has the following properties: Steering with $\vec{A} \perp$ to $\vec{V}$ ($\alpha = \pm 90$ deg), results in a constant energy motion in the diagram (horizontally). Steering with $\vec{A} \perp$ to $\vec{r}$ ($[\alpha + \gamma] = \pm 90$ deg), results in a constant angular momentum motion in the diagram (vertically). When the instantaneous orbit is circular (or nearly circular), steering with $\vec{A} \perp$ to $\vec{r}$ or $\vec{A} \parallel$ to $\vec{V}$ results in a motion tangent to the line of circular orbits.

The direction of the motion along the slope, however, is determined by Equations [9 and 10]. An important property of the direction of the motion of the E-h point along the slope is that it may reverse its direction while the steering direction is maintained constant relative to either $\vec{V}$ or $\vec{r}$, i.e., while either α or $(\alpha + \gamma)$ is kept constant. This can be seen by examining Equations [9 and 10] together. If α is kept constant, E will either increase or decrease but not reverse, as shown by Equation [9]; while h may reverse since $\cos(\alpha + \gamma)$ may change sign, as shown by Equation [10]. If on the other hand $(\alpha + \gamma)$ is kept constant, h will either increase or decrease but not reverse, as shown by Equation [10]; while E may reverse since $\cos \alpha$ may change sign, as shown by Equation [9]. The vehicle's E-h point must reverse its direction upon reaching the line of circular orbits (unless it is traveling on a slope tangent to the line of circular orbits), since it cannot enter the inaccessible region.

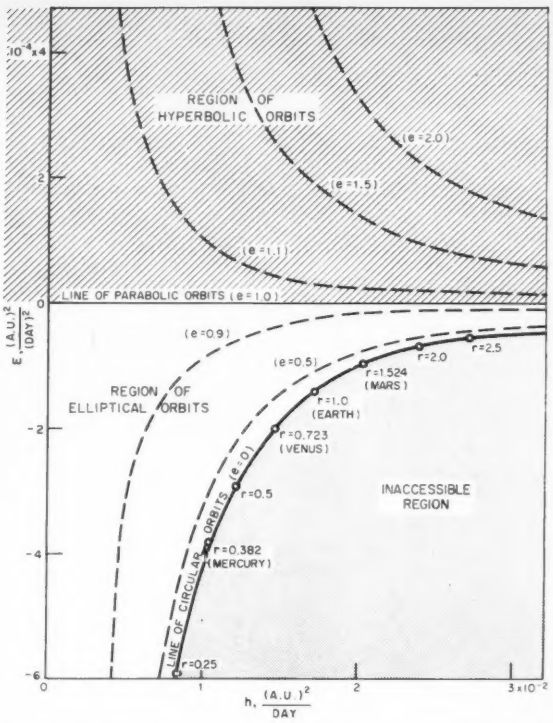

Fig. 2 Specific energy vs. specific angular momentum for two-body orbits

Steering Programs by Analytical Machine Techniques

Now we apply the key equations and the E-h diagram to develop steering programs which follow simple E-h diagram paths to the desired end points. First, these paths will be limited to combinations of steering with the inertial acceleration vector $\vec{A}$ parallel or normal to either the velocity vector $\vec{V}$ or to the radius vector $\vec{r}$. Second, more complicated paths will be developed.

Two simple steering programs are: Constant energy ($\vec{A} \perp \vec{V}$) and constant angular momentum ($\vec{A} \parallel \vec{r}$). If the vehicle has achieved either the specific energy or the specific angular momentum of the desired destination circular orbit, the required acceleration magnitude which assures that the vehicle's E-h point reaches the destination circular orbit point can be determined as will be shown.

For constant angular momentum ($\vec{A} \parallel \vec{r}$) transfers, let $(\alpha + \gamma) = +90$ deg, $\vec{A}$ positive when directed away from sun and r_3 the final circular orbit radius. Then $\dot{E} = AV \cos \alpha = AV(+\sin \gamma) = +A\dot{r}$, and

$$\int_{E_2}^{E_3} dE = A_{\substack{2,3 \\ h=\text{const}}} \int_{r_2}^{r_3} dr$$

thus

$$A_{\substack{2,3 \\ h=\text{const}}} = \frac{E_3 - E_2}{r_3 - r_2} = \frac{(-\mu/2r_3) - E_2}{r_3 - r_2} \qquad [12]$$

(Note that to use Eq. [12], the E_2 and r_2 of the initial orbit should be known.)

For constant energy ($\vec{A} \perp \vec{V}$) transfers, take $\alpha = +90$ deg and $\vec{A}$ positive when toward the right, looking along $\vec{V}$. Then $\dot{h} = Ar\cos(\alpha + \gamma) = -Ar\sin\gamma = -Ar\dot{r}/V$. Since $E_{2,3} = E_3 = -\mu/2r_3 = (V^2/2) - (\mu/r)$

$$V = \sqrt{2\mu\left(\frac{1 - (1/2r_3)r}{r}\right)}$$

thus

$$\int_{h_2}^{h_3} dh = \frac{A_{\substack{2,3 \\ E=\text{const}}}}{\sqrt{2\mu}} \int_{r_2}^{r_3} \frac{r^{3/2}}{\sqrt{1 - (1/2r_3)r}}\, dr$$

This integrates into (restricting $r_2 < 2r_3$)

$$A_{\substack{2,3 \\ E=\text{const}}} = \frac{\dfrac{\mu}{r_3^2}\left(1 - \dfrac{h_2}{\sqrt{\mu r_3}}\right)}{2 - \left(3 + \dfrac{r_2}{r_3}\right)\sqrt{\dfrac{r_2}{2r_3}\left(1 - \dfrac{r_2}{2r_3}\right)} + 3\left[\sin^{-1}\left(\dfrac{1}{\sqrt{2}}\right) - \sin^{-1}\sqrt{1 - \dfrac{r_2}{2r_3}}\right]} \qquad [13]$$

(Note that to use this equation the h_2 and r_2 of the initial orbit must be known.)

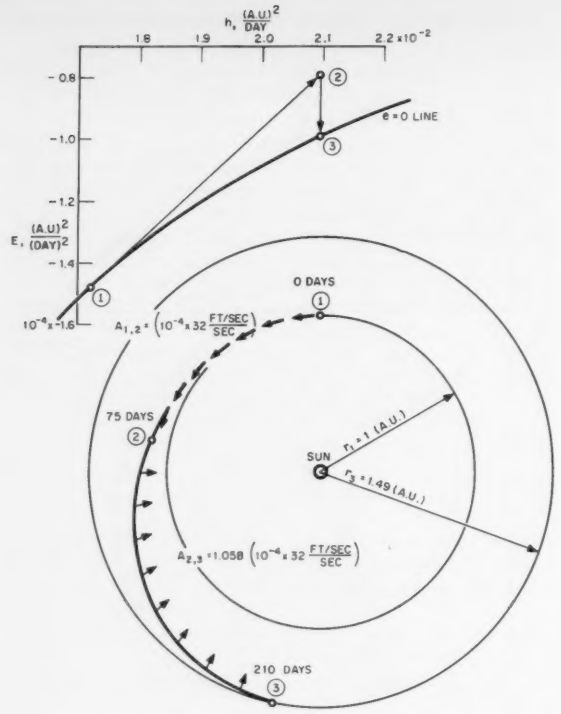

Fig. 3 Machine computed trajectory and corresponding *E-h* diagram path ($\vec{A}_{1,2} \perp \vec{r}$; $\vec{A}_{2,3} \| \vec{r}$)

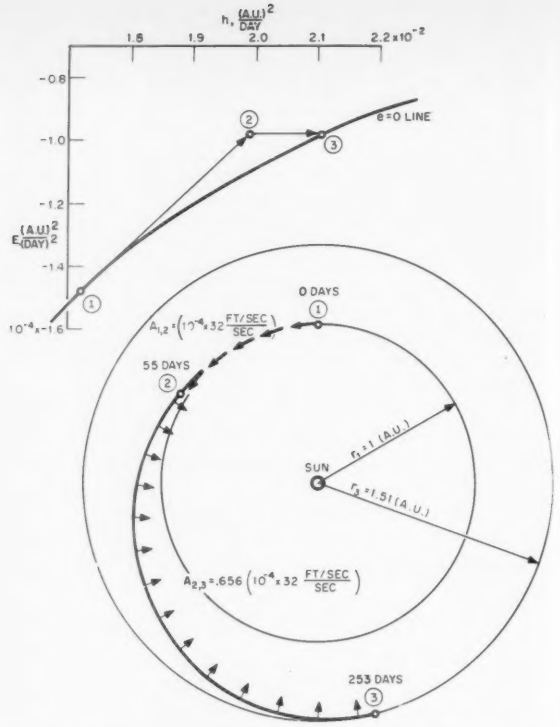

Fig. 4. Machine computed trajectory and corresponding *E-h* diagram path ($\vec{A}_{1,2} \perp \vec{r}$; $\vec{A}_{2,3} \perp \vec{V}$)

Now consider starting from the initial circular orbit and steering with $\vec{A}$ either parallel to $\vec{V}$ or perpendicular to $\vec{r}$ until the vehicle's *E-h* path intercepts either the E or the h line of the destination circular orbit. Because no trial and error is involved, these *E-h* paths can easily be determined by solving the differential equations of motion on a machine computer. When the machine computed trajectory indicates that the vehicle has reached the E or h or the destination orbit the conditions obtained are used as initial conditions for the second phase of the trajectory, and for determining the magnitude of $\vec{A}$ required for the second phase. $\vec{A}$ must satisfy either Equation [12] or Equation [13], whichever is appropriate. The second phase is thus also run off on the machine without trial and error, and a trajectory results which tangentially touches the destination circular orbit at the proper orbital speed.

To confirm the above analysis and to illustrate the technique, machine computed trajectories were run off on a digital computer. A simple computing program was used which generally gave accuracies slightly better than about 0.5 per cent. The initial circular orbit was taken as 1 astronomical unit (A.U.) from the sun, thus corresponding to the Earth's orbit. The destination circular orbits were taken close to 1.5 and 0.72 A.U. to correspond somewhat to martian and venusian orbits. No attempt was made to transfer to exactly 1.5 or exactly 0.72 each time, because the print-out interval from the computing machine did not make this convenient, and because the purpose of these trajectories was to illustrate and confirm this method rather than to determine an exact transfer trajectory. Figs. 3, 4, 5 and 6 show *E-h* diagram paths and corresponding machine computed trajectories for steering in phase (1) to (2) by keeping the inertial acceleration vector normal to the radius vector, and for steering in phase (2) to (3) by keeping $\vec{A}$ either normal to $\vec{V}$ (constant E) or parallel to $\vec{r}$ (constant h).

In each of these machine computed trajectories the destination orbit, which was determined prior to running the (2) to (3) phase, was within the machine accuracy of computation (0.5 per cent) of the orbital radius achieved when the velocity vector became locally horizontal, and vehicle speed at that time was also within computer accuracy of the correct orbital speed for the predicted destination orbit.

Now that some simple steering programs have been evaluated without trial and error, consider briefly more complicated programs (of possible interest in optimization studies). These may require some trial and error, but, as will be shown, the trial and error is a simple, rapidly converging process. First consider steering in the (1) to (2) phase as in the previous examples, that is, with $\vec{A}$ perpendicular to $\vec{r}$. This produces only a slightly curved *E-h* diagram path that starts out tangent to the line of circular orbits. Consider the program for the second phase to be any straight line connecting the initial phase *E-h* diagram path with the destination *E-h* point. That is, restrict dE/dh to be constant in the second phase, and consider solving the problem of finding the direction and magnitude program required of $\vec{A}_{2,3}$.

Equation [11] may be rewritten as

$$\tan(\alpha + \gamma) = \frac{r}{V \sin \gamma} \frac{dE}{dh} - \frac{1}{\tan \gamma} \qquad [14]$$

or

$$\tan \alpha = \frac{1}{\tan \gamma} - \frac{V}{r \sin \gamma \, (dE/dh)} \qquad [15]$$

The machine routine can be written so that at each interval of calculation either Equation [14] or [15] is satisfied (whichever is most convenient), thereby steering the vector $\vec{A}_{2,3}$ so that the vehicle's *E-h* diagram path follows the prescribed slope. The approximate magnitude of $\vec{A}_{2,3}$ required can be

estimated by extrapolating from the two simple programs which were solved previously without trial and error, or $|\vec{A}_{2,3}|$ may be found by extrapolating from approximate analytical solutions of the two simpler cases. (These analytical solutions are presented in the next section.) With the E-h diagram path following the prescribed slope, only the magnitude of $\vec{A}_{2,3}$ need be varied in the trial and error process. With approximations of the magnitude of $\vec{A}_{2,3}$ required available to start with, several trajectories should suffice to converge on the answer.

The technique described in this example is quite general. Any E-h path may be followed (from the initial to final circular orbit points), and the machine can be programmed to follow the specified path by applying the above equations. Then only one parameter—the inertial acceleration magnitude—need be varied in the trial and error process. Furthermore, this technique does not require that the inertial acceleration magnitude be constant; time variable programs, such as those associated with constant thrust propulsion systems may be employed. Of course, one may also specify that the inertial acceleration magnitude become zero at any point in the E-h diagram path (this corresponds to coasting) without introducing any particular difficulties, since exact solutions to the equations of motion in this case are well-known.

Steering Programs by Approximate Analytical Techniques

Useful approximate formulas may be developed for determining the entire (1) → (2) → (3) phases analytically for the simple programs $\vec{A}_{1,2} \perp \vec{r}$ and $\vec{A}_{2,3}$ either $\parallel$ to $\vec{r}$ or $\perp$ to $\vec{V}$. During phase (1) → (2) Equation [11] gives

$$\frac{dE}{dh} = \frac{V \cos \alpha}{r} = \frac{V \cos \gamma}{r} = \frac{h}{r^2}$$

or

$$\int_{E_1}^{E_2} dE = \int_{h_1}^{h_2} \frac{h}{r^2}\, dh$$

For magnitudes of $\vec{A}$ of the order of $10^{-4} \times 32$ fps^2 and for destination orbits not too far removed from the initial circular orbit, such as transfers between Earth, Mars and Venus, the radius r_2 does not differ much from that of the initial orbit. A fair approximation, taking r^2 in the above integral equal to r_1^2, is provided by

$$E_2 + \frac{\mu}{2r_1} \approx \frac{h_2^2 - \mu r_1}{2r_1^2} \qquad [16]$$

Also, if the (1) → (2) phase is carried out by keeping $\vec{A}$ along $\vec{V}$ and if $r^2 \cos^2 \gamma$ is taken equal to r_1^2 ($\cos^2 \gamma_1 = 1$) $= r_1^2$, which is also a fair approximation, there results the same approximate formula, Equation [16]. This means that during phase (1) to (2) it matters little whether one steers with $\vec{A}$ parallel to $\vec{V}$ or normal to $\vec{r}$. Note that the approximations assumed make the relationships between specific energy changes and specific angular momentum changes (as expressed by Eq. [16]) independent of the magnitude of $\vec{A}$ employed during the phase (1) to (2) trajectory.

Now if phase (2) to (3) is to be carried out by holding h constant, then $h_2^2 = \mu r_2$, yielding, from Equation [16]

$$E_2 \approx \frac{\mu r_2 - \mu r_1}{2r_1^2} - \frac{\mu}{2r_1}$$

Substituting this expression for E_2 and taking $r_2 = r_1$ reduces Equation [12] to the simple expression

$$\frac{A_{2,3}}{\substack{h=\text{const} \\ \mu/r_1^2}} \approx \frac{1}{2}\left(\frac{r_1}{r_2} - 1\right) \qquad [17]$$

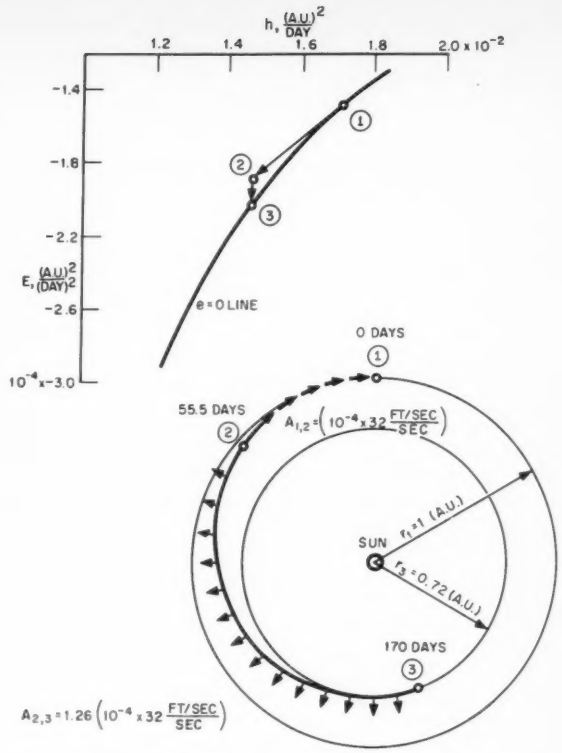

Fig. 5 Machine computed trajectory and corresponding E-h diagram path ($\vec{A}_{1,2} \perp \vec{r}$; $\vec{A}_{2,3} \parallel \vec{r}$)

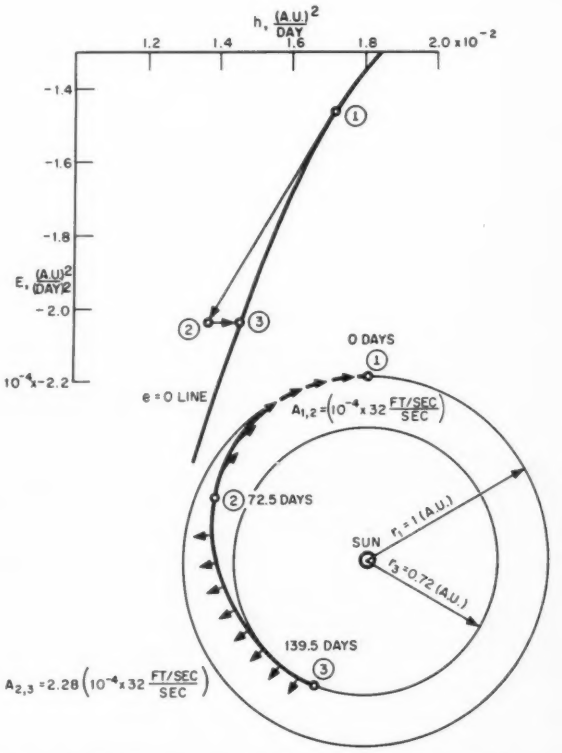

Fig. 6 Machine computed trajectory and corresponding E-h diagram path ($\vec{A}_{1,2} \perp \vec{r}$; $\vec{A}_{2,3} \perp \vec{V}$)

If phase (2) to (3) is to be carried out by holding E constant, then $E_2 = -\mu/2r_3$ and, from Equation [16]

$$h_2^2 = 2r_2^2\left(-\frac{\mu}{2r_3} + \frac{\mu}{2r_1}\right) + \mu r_1$$

Substituting this expression for h_2 and taking $r_2 = r_1$ in Equation [13] gives

$$\frac{A_{2,3}}{\frac{E=\text{const}}{\frac{\mu}{r_1^2}}} \approx \frac{\left(\frac{r_1}{r_3}\right)^2\left[1 - \sqrt{\frac{r_1}{r_3}\left(2 - \frac{r_1}{r_3}\right)}\right]}{2 - \left(3 + \frac{r_1}{r_3}\right)\sqrt{\frac{r_1}{2r_3}\left(1 - \frac{r_1}{2r_3}\right)} + 3\left[\sin^{-1}\left(\frac{1}{\sqrt{2}}\right) - \sin^{-1}\sqrt{1 - \frac{r_1}{2r_3}}\right]} \qquad [18]$$

Although the magnitude of $\vec{A}$ expressed in Equations [17 and 18] is the required magnitude for the (2) to (3) phase, it may also be the magnitude employed in the (1) to (2) phase, since the equations used for the (1) to (2) phase are approximately independent of the magnitude employed. Equations [17 and 18] are particularly interesting from the viewpoint of a preliminary system design engineer. They are applicable to transfers between any initial circular orbit r_1 and any destination circular orbit r_3. A surprising result is that, if one steers by the simple program $\vec{A}_{1,2} \perp \vec{r}$, then $\vec{A}_{2,3} \parallel \vec{r}$, approximately the same magnitude of $\vec{A}$ is required to transfer from "Earth" to "Mars" ($r_3/r_1 \approx 3/2$) as to transfer from "Earth" to "Venus" ($r_3/r_1 \approx 3/4$), and the required magnitude is approximately $10^{-4} \times 32$ fps^2—the acceleration level expected from ionic propulsion systems. A few values computed from Equations [12 and 13] using data obtained from the machine computed trajectories were compared with corresponding values obtained from Equations [17 and 18] to obtain an indication of accuracy. These comparisons indicated that for transfers from 1 A.U. to 1.5 or 0.72 A.U., Equations [17 and 18] give results which are within 6 per cent of the correct values.

Conclusion

A general method has been presented by which the determination of nominal steering programs for transferring a low thrust space vehicle from an initial orbit to a final coplanar circular orbit about the sun may be carried out with a minimum of trial and error machine computation. This method has been illustrated by considering some simple types of steering programs. The techniques presented, in particular the employment of the E-h diagram, permit investigations of and disclose in a simple manner all possible steering programs. The general method is not limited to interplanetary orbit transfers and to low thrust levels; it may also be applied to planetary or lunar orbit transfers and for any propulsion system.

It should be mentioned that the problem of determining how to rendezvous with a particular point (or small body) traveling in an "unpowered" orbit is relatively easy when the orbit is circular and coplanar with the vehicle's initial orbit. It is not easy when the orbit is noncircular or noncoplanar with the vehicle's initial orbit. In the former case, the time of transfer and the transfer angular distance (obtained by the method presented from a machine computed trajectory to the final circular orbit) fix the proper initial relative angular positions. In the latter case, the problem is much more complex and is a worthy subject for future study. Relations between specific energy and specific angular momentum, however, will be useful in determining steering programs in these cases, and an E-h diagram will be valuable in visualizing and understanding the connections between variations in the specific energy and the specific angular momentum of the vehicle and the corresponding steering direction and magnitude of the vehicle's inertial acceleration vector.

References

1. Stuhlinger, E., "The Flight Path of an Electrically Propelled Space Ship," JET PROPULSION, vol. 27, 1957.
2. Tsien, H. S., "Take-off from Satellite Orbit," JOURNAL OF THE AMERICAN ROCKET SOCIETY, vol. 23, 1953.
3. Moulton, F. R., "An Introduction to Celestial Mechanics," Macmillan Co., New York, 1914.

Technical Notes

Minor Circle Flight for Orbital Launched or Boost-Glide Vehicles

W. H. T. LOH[1]

Chance Vought Aircraft, Inc., Dallas, Texas

HYPERVELOCITY gliders may either take off from Earth by rocket boost or take off from satellite orbits by rocket control. These gliders designed to strike targets will, in general, fly great circle paths in reaching these targets. However, the possibility of reaching these targets by controllable flying paths other than great circles (minor circle paths) may be of interest. Although one recognizes that the great circle path is the shortest path between two given points, and that the great circle path is also the glider's natural automatic gliding path (in contrast to the minor circle path which needs a continuous accurate aerodynamic control to force the glider to fly along the desired path), nevertheless, one might use a minor circle path simply for strategic reasons. The approximate range equation of such a glider flying along a great circle path, derived recently by Allen and Eggers (1)[2] is

$$R = \left(\frac{R_0}{2}\right)\left(\frac{L}{D}\right)\ln\left[\frac{1 - (V_F^2/gR_0)}{1 - (V_i^2/gR_0)}\right]$$

or

$$R \cong \left(\frac{R_0}{2}\right)\left(\frac{L}{D}\right)\ln\left[\frac{1}{1 - (V_i^2/gR_0)}\right]$$

The approximate range equation of such a glider flying along a minor circle path was published (2) recently as

$$R = \left(\frac{R_0}{2}\right)\left(\frac{L}{D}\right)\sin\lambda_0 \ln\left\{\frac{[1 - (V_F^2/gR_0\sin^2\lambda_0)] - (1/\sin\lambda_0)\sqrt{(V_F^2/gR_0\sin\lambda_0)^2 - 2(V_F^2/gR_0) + 1}}{[1 - (V_i^2/gR_0\sin^2\lambda_0)] - (1/\sin\lambda_0)\sqrt{(V_i^2/gR_0\sin\lambda_0) - 2(V_i^2/gR_0) + 1}}\right\}$$

or approximately

$$R \cong \left(\frac{R_0}{2}\right)\left(\frac{L}{D}\right)\sin\lambda_0 \ln\left\{\frac{1}{[1 - (V_i^2/gR_0\sin^2\lambda_0)]} \times \frac{1 - (1/\sin\lambda_0)}{\left[1 - \frac{1}{\sin\lambda_0}\frac{\sqrt{1 - 2(V_i^2/gR_0) + (V_i^2/gR_0\sin\lambda_0)^2}}{(1 - V_i^2/gR_0\sin^2\lambda_0)}\right]}\right\}$$

The necessary aerodynamic control at any moment along the minor circle path was given (2) as a function of the instantaneous velocity V and minor circle angle λ_0

$$\sin\alpha \cong \sin\lambda_0 \frac{1 - (V^2/gR_0\sin^2\lambda_0)}{\sqrt{(1 - V^2/gR_0)^2 + (V^2/gR_0)^2\cot^2\lambda_0}}$$

In order to fly the vehicle along the desired minor circle path the automatic servo control must be designed in such a way that the aerodynamic forces produced by the control surfaces continuously satisfy this equation.

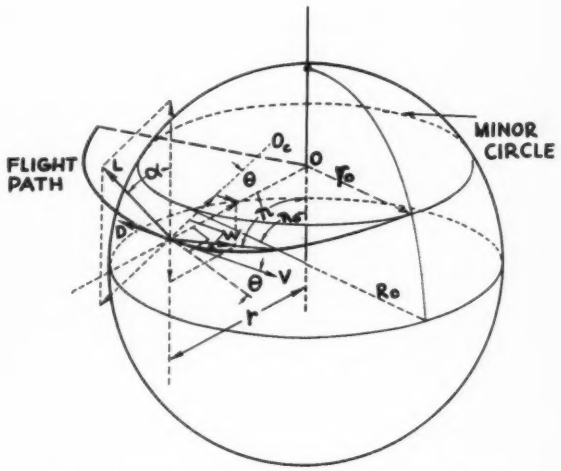

Fig. 1 Three-dimensional view on minor circle flight

Since, for the minor circle flight, the flight path angle, deceleration, altitude, distance from minor circle center, flight time, total aerodynamic heat input to the vehicle, time rate and maximum time rate of average and stagnation region heat input per unit area are just as important as the flight range itself, the present note is written to develop the relations for these additional parameters.

Using the same assumptions (1, 2) and the same equations (2), the following results are obtained:

1 Instantaneous range

$$R = \left(\frac{R_0}{2}\right)\left(\frac{L}{D}\right)\sin\lambda_0 \ln\left\{\frac{[1 - (V^2/gR_0\sin^2\lambda_0)] - (1/\sin\lambda_0)\sqrt{(V^2/gR_0\sin\lambda_0)^2 - 2(V^2/gR_0) + 1}}{[1 - (V_i^2/gR_0\sin^2\lambda_0)] - (1/\sin\lambda_0)\sqrt{(V_i^2/gR_0\sin\lambda_0)^2 - 2(V_i^2/gR_0) + 1}}\right\}$$

Received May 11, 1959.

[1] Staff Engineer to Assistant Chief Engineer, Technical.

[2] Numbers in parentheses indicate References at end of paper.

EDITOR'S NOTE: The Technical Notes and Technical Comments sections of ARS JOURNAL are open to short manuscripts describing new developments or offering comments on papers previously published. Such manuscripts are published without editorial review, usually within two months of the date of receipt. Requirements as to style are the same as for regular contributions (see masthead page).

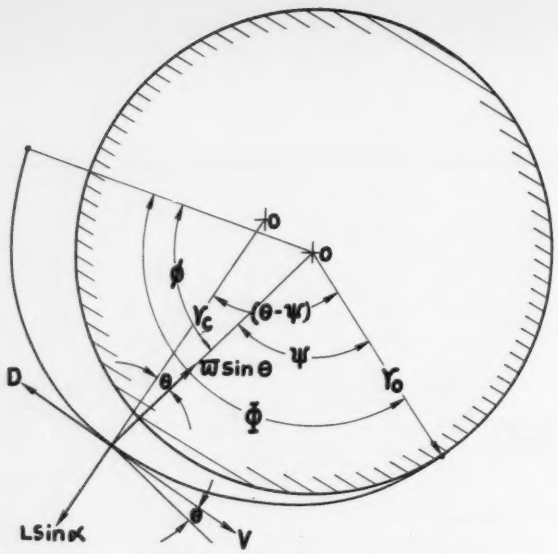

Fig. 2 Two-dimensional view on minor circle flight

2 Instantaneous flight path angle

$$\sin\theta = \frac{2\sin\lambda_0\,[(gR_0/V^2) - 1]}{R_0\,(L/D)\beta\sqrt{(1 - V^2/gR_0)^2 + (V^2/gR_0)^2\cot^2\lambda_0}}$$

3 Instantaneous deceleration and maximum deceleration

$$\frac{1}{g}\left(\frac{dV}{dt}\right) = -\left(\frac{D}{L}\right)\sqrt{\left(1 - \frac{V^2}{gR_0}\right)^2 + \left(\frac{V^2}{gR_0}\right)^2\cot^2\lambda_0}$$

$$\frac{1}{g}\left(\frac{dV}{dt}\right)_{\max} = -\left(\frac{D}{L}\right)\sqrt{\left(1 - \frac{1}{1+\cot^2\lambda_0}\right)^2 + \frac{\cot^2\lambda_0}{(1+\cot^2\lambda_0)^2}}$$

$$V^2\left(\frac{dV}{dt}\right)_{\max} = \frac{gR_0}{1+\cot^2\lambda_0}$$

4 Instantaneous altitude

$$y = \frac{1}{\beta}\left\{\ln\left[\frac{V^2/gR_0}{\sqrt{(1 - V^2/gR_0)^2 + (V^2/gR_0)^2\cot^2\lambda_0}}\right] + \ln\left[\frac{\sqrt{1 - (V_{R0}^2/gR_0)^2 + (V_{R0}^2/gR_0)^2\cot^2\lambda_0}}{(V_{R0}^2/gR_0)}\right]\right\}$$

5 Instantaneous distance from center of minor circle

$$r = r_0 + y\sin\lambda_0$$

6 Instantaneous time of flight

$$t = \sqrt{\frac{R_0}{4g}}\left(\frac{L}{D}\right)\int_V^{V_i} \times \frac{d(V^2/gR_0)}{\sqrt{(1/\sin^2\lambda_0)\,(V^2/gR_0)^3 - 2(V^2/gR_0)^2 + (V^2/gR_0)}}$$

7 Instantaneous total aerodynamic heat input to the vehicle from the very beginning

$$Q = \frac{m}{4}\left(\frac{C_F'S}{C_DA}\right)[V_i^2 - V^2]$$

8 Time rate and maximum time rate of average heat input per unit area

$$\left(\frac{dH_{av}}{dt}\right) = \frac{1}{2}\frac{C_F'}{C_DA}\frac{mg\sqrt{gR_0}}{(L/D)} \times \sqrt{\left(1 - \frac{V^2}{gR_0}\right)^2 + \left(\frac{V^2}{gR_0}\right)^2\cot^2\lambda_0}\left(\frac{V}{\sqrt{gR_0}}\right)$$

$$\left(\frac{dH_{av}}{dt}\right)_{\max} = \frac{1}{2}\frac{C_F'}{C_DA}\frac{mg\sqrt{gR_0}}{(L/D)} \times \sqrt{\left(1 - \frac{V_1^2}{gR_0}\right)^2 + \left(\frac{V_1^2}{gR_0}\right)^2\cot^2\lambda_0}\left(\frac{V_1}{\sqrt{gR_0}}\right)$$

$$V_1 = V_{\left(\frac{dH_{av}}{dt}\right)_{\max}} = \left\{\frac{2}{3}\left[\frac{1 - \sqrt{1 - (3/4)(1+\cot^2\lambda_0)}}{1+\cot^2\lambda_0}\right]\right\}^{1/2}\sqrt{gR_0}$$

9 Time rate and maximum time rate of stagnation region heat input per unit area

$$\left(\frac{dH_s}{dt}\right) = 6.8\times10^{-6}\sqrt{\frac{2mg}{C_LA\sigma}}\,(gR_0) \times \left\{\sqrt{\left(1 - \frac{V^2}{gR_0}\right)^2 + \left(\frac{V^2}{gR_0}\right)^2\cot^2\lambda_0}\right\}^{1/2}\left(\frac{V^2}{gR_0}\right)$$

$$\left(\frac{dH_s}{dt}\right)_{\max} = 6.8\times10^{-6}\sqrt{\frac{2mg}{C_LA\sigma}}\,(gR_0) \times \left\{\sqrt{\left(1 - \frac{V_2^2}{gR_0}\right)^2 + \left(\frac{V_2^2}{gR_0}\right)^2\cot^2\lambda_0}\right\}^{1/2}\left(\frac{V_2^2}{gR_0}\right)$$

$$V_2 = V_{\left(\frac{dH_s}{dt}\right)_{\max}} = \left\{\frac{5}{6}\left[\frac{1 - \sqrt{1 - (24/25)(1+\cot^2\lambda_0)}}{1+\cot^2\lambda_0}\right]\right\}^{1/2}\sqrt{gR_0}$$

The expression for time of flight may most easily be integrated by graphical means. When $\lambda_0 = \pi/2$, the minor circle becomes a great circle, and all the present results reduce respectively to the corresponding results already given (1) for great circle path.

Nomenclature

A = reference area for lift and drag expressions
C_D = drag coefficient
C_F' = equivalent skin friction coefficient

$$C_F' = \frac{1}{S}\int_S C_{Fl}\left(\frac{\rho_l}{\rho}\right)\left(\frac{V_l}{V}\right)dS$$

C_F = skin friction coefficient
D = drag, lb
g = acceleration due to force of gravity, fps²
H = convective heat transferred per unit area
L = lift, lb
m = mass of the vehicles
Q = convective heat transferred
r = distance shown in Figs. 1 and 2, ft
r_c = radius of curvature of flight path, shown in Fig. 2, ft
r_0 = distance shown in Figs. 1 and 2, ft
R_0 = radius of Earth, ft
R_g = glider distance from center of Earth, ft
R = flight range, measured along the surface of Earth, ft
s = distance along flight path, ft
S = surface area
t = time, sec
V = velocity, fps
W = weight
θ = angle of flight path to minor circle plane horizontal in radians, see Fig. 2

$\lambda_0, \lambda, \alpha$ = angles defined in Fig. 1
ρ = air density
σ = nose or leading edge radius of body or wing
β = constant in density-altitude relation: $\rho = \rho_0 e^{-\beta y}$. Here ρ_0 = reference density and y = altitude

Subscripts

i = initial condition or condition at the beginning of unpowered glide
F = final condition or condition at end of unpowered glide
l = local conditions
s = stagnation conditions
av = average values
max = maximum values

References

1 Eggers, A. J. and Allen, H. J., "A Comparative Analysis of the Performance of Long-Range Hypervelocity Vehicles," NACA TN 4046, Oct. 1957.

2 Loh, W. H. T., "Minor Circle Flight for Boost Glide Vehicles," ARS JOURNAL, vol. 29, no. 4, April, 1959, p. 300–301.

Control of Solid Propellant Burning Rates by Acoustic Energy[1]

MARTIN SUMMERFIELD[2]

Princeton University, Princeton, N. J.

This note presents the idea that acoustic energy beamed on the burning surface of a heterogenous solid propellant may enhance the normal burning rate by a significant factor, if the frequency and power level are sufficiently high. The theory is based on the concept of a steady-state combustion zone incorporating a granular diffusion flame, as described by the author in an earlier publication. It is speculated that acoustic stirring would hasten the gaseous reaction rate in the thin flame layer, raise the energy feedback to the surface, and so increase the burning rate. Since acoustic stirring would have its maximum effect on an unmixed diffusion flame, it is expected that heterogeneous propellants would respond more than homogeneous types. The author has no experimental verification of the idea as yet, but experiments are under way.

THIS presentation of the idea of controlling the burning rate of a solid propellant is probably premature, in the sense that direct experimental evidence is not yet available, but since considerable information has appeared in the public press on the subject in recent weeks, it appears worthwhile to present the idea in a technical paper for research engineers (1).[3]

The investigation of this idea on the part of the present author started on June 6, 1957, as a consequence of experimental findings concerning the structure of the flame zone of ammonium perchlorate-type propellants. This work was presented in part at the AMERICAN ROCKET SOCIETY annual meeting on Nov. 27, 1956 (ARS preprint 360–56), and later at the annual meeting on Nov. 17, 1958 (2). On June 6, 1957, H. J. Taback, a graduate student under the direction of the author, undertook to test the idea experimentally as part of his thesis. The big problem was to devise a means of generating the required high level of acoustic power in the combustion chamber. Acting on the advice of W. Welkowitz and M. Herold of Gulton Industries (October 1957), it was decided to try a high power whistle of the type developed by R. M. G. Boucher of France, which was an adaptation of the earlier Hartmann whistle. After various delays in the program, E. K. Bastress, presently a Ph.D. candidate at Princeton, picked up the project and is now engaged in systematic experimental tests. No definite results can be reported at this time.

Another program to test the feasibility of burning rate control has been started by Acoustica Associates, Inc., using different conditions and with a different kind of whistle named after its inventor, Levavasseur. The Acoustica project is based on the physical concepts outlined in this paper. This work is under the sponsorship of the National Aeronautics and Space Administration (1). It is reasonable to believe that, under this two-program attack, the feasibility of sonic burning rate control will receive a full test. The Acoustica-NASA project goes farther than the burning rate study: It includes the development of a thrust control system for solid rocket engines, which would use a sonic transducer to generate sound energy of the appropriate level to produce the thrust desired. The development of the system must, of course, await the burning rate studies.

Theoretical Foundations

As a result of a series of basic experimental researches on the combustion of simple ammonium perchlorate-polystyrene base solid propellants, carried out in the past three years at Princeton, the physical factors that determine the burning rates of such propellants appear to have been identified.

Briefly, these are: The linear rate at which a propellant burns is proportional to the rate of heat feedback from the hot gaseous combustion zone to the exposed solid surface. The rate of heat feedback is, in turn, proportional to the temperature gradient in this gaseous layer, thus, the thinner the combustion zone, the faster the rate.

The thickness of the combustion zone is inversely proportional to the rate of reaction in the gaseous layer, so that the faster the gaseous reaction, the faster the burning rate. In the case of a heterogeneous (composite) propellant, the speed of the gaseous reaction is controlled by two rate processes: The chemical kinetics of oxidation and the physical interdiffusion of the unmixed oxidizer and fuel gases. In the practical operating range of most composite propellants (above 500 psi), the slowest of these processes is the interdiffusional mixing. (At low pressures, less than 100 psi, the chemical kinetics is the rate-limiting process, a condition of great interest for fundamental combustion research, but of no practical interest here.)

Any physical factor that can speed up the interdiffusional mixing process in the gaseous combustion layer will speed up the burning rate. Thus, the finer the particle size of the ground perchlorate, the faster the burning rate is. Large amplitude gas oscillations, as in unstable combustion, probably interact with the burning process in this way.

One physical influence that immediately suggests itself is acoustic energy projected into the combustion layer by a separately energized whistle or other generator. Acoustic oscillation would produce a local stirring action in the combustion layer and, thus, a faster burning rate. This idea has occupied the attention of the Princeton group for some time, mainly as a means of verifying the burning rate theory developed (2) and incidentally as a practical means of controlling burning rates.

Received Aug. 18, 1959.

[1] This work was orginally started under the financial sponsorship of Princeton University in June 1957. It was continued later under the sponsorship of Project SQUID, a program of research supported by the Office of Naval Research, and is presently being continued under ONR sponsorship with research funds provided by the Advanced Research Projects Agency of the Department of Defense. The support provided by these sponsors is gratefully acknowledged.

[2] Professor of Jet Propulsion, Department of Aeronautical Engineering. Member ARS.

[3] Numbers in parentheses indicate References at end of paper.

Possible Magnitude of Burning Rate Increase

For simple propellants of the ammonium perchlorate plus polystyrene copolymer type, with no special additives, the burning theory leads to the following rate equation

$$\frac{1}{r} = \frac{a}{p} + \frac{b}{p^{1/3}}$$

where

r = linear burning rate
p = pressure
a = chemical kinetic reaction time parameter
b = diffusional mixing time parameter

In the extreme limit of instantaneous mixing by acoustic stirring, the parameter b can be made to vanish. For a typical propellant, as reported in (2), the resulting increase in r would be from 0.40 to 2.04 in./sec, measured at 500 psia. This is a fivefold increase. For other propellants, and at other pressures, the maximum possible increases would range from three- to tenfold.

The extent to which the mixing time parameter can be reduced by acoustic stirring is still a matter of speculation. No tests have yet been performed. A hopeful viewpoint is that a mere twofold variation would be adequate for practical purposes.

Estimate of Required Acoustic Power Level and Frequency

In order to estimate the necessary acoustic frequency, the microscopic details of the gas flow process in the thin combustion layer must be considered. The gases formed at the solid surface move outward at a certain velocity, spending a certain time, about 0.1 millisec at 500 psi in the flame layer, which is probably about 50-μ thick. For the acoustic stirring to be effective, it would be desirable to cause a full oscillation of the gas layer in this gas transit interval. A much longer oscillation period would hardly affect the mixing process. This consideration leads, therefore, to a minimum frequency of 10,000 cps.

The necessary amplitude can be estimated on the hypothesis that, to bring about a significant degree of mixing, the amplitude of lateral motion ought to be about equal to the flame layer thickness. Using the thickness of 50 μ and the frequency of 10,000 cps, the beam power comes to 5.4w/cm^2. In intensity units, this is 167 db.

A subsidiary consideration is the question of viscous damping adjacent to the solid surface (3). The "dead zone" thickness is a function of frequency; fortunately, at 10,000 cps it is only about 20 μ, so that the acoustic beam will be effective in most of the flame layer.

Proposed Experiments

Inasmuch as the above calculations of power level, frequency and burning rate increase are based on theoretical and somewhat idealized concepts of the flame structure of a composite propellant, direct experiments are needed to verify the predicted effect of acoustic stirring.

Experiments at Princeton will be carried out with small rocket motors of about 1000 lb-sec impulse fitted with acoustic generators fed by compressed air. Tests are planned on hollow tubular charges with an acoustic beam directed parallel to the port axis, and on end-burning charges with the acoustic beam perpendicular to the burning surface. Experiments will be made at various pressure levels, frequencies, power levels, and with various types of propellant, in an attempt to establish the magnitude of the acoustic effect and the optimum ranges of the parameters.

References

1 *Space Age News*, Los Angeles, Calif., Feb. 1, 1959; *Time Magazine*, March 16, 1959, p. 96; *Time Magazine*, July 27, 1959; *New York Times*, July 28, 1959. (Press releases by Acoustica Associates, Inc.)

2 Summerfield, M., Sutherland, G. S., Webb, M. J., Taback, H. J. and Hall, K. P., "Burning Mechanism of Ammonium Perchlorate Propellants," ARS preprint no. 737-58, Nov. 1958.

3 Rayleigh, J. W. S., "Theory of Sound," Dover Press, 1945.

Prediction of Inviscid Induced Pressures From Round Leading Edge Blunting at Hypersonic Speeds

E. S. LOVE[1]

Langley Research Center, NASA, Langley Field, Va.

A simple method is presented for predicting the inviscid induced pressures from round leading edge blunting at hypersonic speeds.

THE DEFICIENCIES of blast wave theory in the prediction of inviscid induced pressures from leading edge blunting are seen mainly in two regions: Near the leading edge and far downstream. These deficiencies have led to such modifications as shifting the point of origin of the blast in order to improve predictions near the leading edge (1, 2)[2] and taking the predicted surface pressure p to be the pressure increment $p - p_1$ in order to extend the usefulness of the predictions to the downstream region, as in (3). The former modification does not always give satisfactory results, and the amount of shift required cannot yet be predicted; the latter modification is in line with more exact predictions.

The present method might also be taken as a modification of blast wave theory, since it adopts the blast wave pressure decay laws (3). This method is intended primarily for application to rounded blunting, such as hemisphere cylinders and two-dimensional thick slabs with circular leading edges, but it may be suitable for other forms of bluntness, except in close proximity to the nose. For the rounded shapes the pressure at the tangency point of the nose and afterbody, referred to hereafter as shoulder pressure p_s (see sketch, Fig. 1) may be predicted as follows. For the hemisphere cylinder the modified-Newtonian plus Prandtl-Meyer theory (1) gives a good prediction, as shown in Fig. 1 in terms of both p_s/p_{max} and p_s/p_1. (The curves for axisymmetric shapes were obtained from calculations by R. D. Wagner Jr., of the Langley Research Center.) The shoulder pressure for the two-dimensional case was approximated by using a sonic leading edge approach; the utility of sonic leading edges in attacking blunt body problems has been demonstrated previously, as in (9). The present approach consists of:

1 Calculating from exact theory the ratio of the shoulder pressure to the stagnation pressure behind the shock p_s/H^* for a sonic cone cylinder and for a sonic wedge slab.

2 Using these ratios of p_s/H^* to determine the ratio of the shoulder pressure of the sonic wedge slab to that of the sonic cone cylinder by taking H^* to be approximately the same in both cases (a fair approximation for $M_1 \gg 1$).

3 Assuming that the ratio of shoulder pressures thus determined would be indicative of the ratio of shoulder pressures for round leading edge blunting. For $M_1 \gg 1$ this ratio is found to be essentially constant at a value of about 2.6. Application of this ratio to the curve for the axisymmetric case in Fig. 1 yields the curve for the two-dimensional case which also appears to be in reasonable agreement with experimental results at the higher Mach numbers. (The unpublished data at $M_1 \gg 9.6$ were obtained by Bertram, Feller and Blackstock of the Langley Research Center as part of an extensive study of induced pressures.)

The experimental data shown in Fig. 1 have been restricted to Reynolds numbers based on diameter (or thickness) of about 50,000 or greater in order to minimize boundary layer displacement effects. Note that the theoretical values of

Received June 4, 1959.

[1] Assistant Chief, Aero-Physics Division. Member ARS.

[2] Numbers in parentheses indicate References at end of paper.

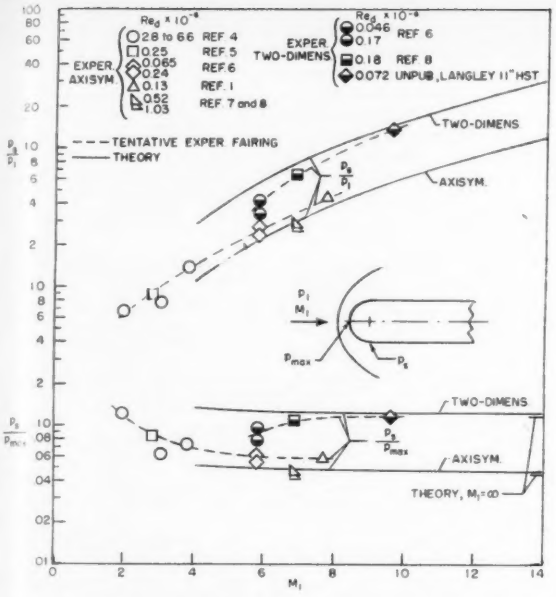

Fig. 1 **Effect of free stream Mach number on ratio of shoulder pressure to free stream static pressure and ratio of shoulder pressure to pressure at stagnation point, $\gamma = 7/5$**

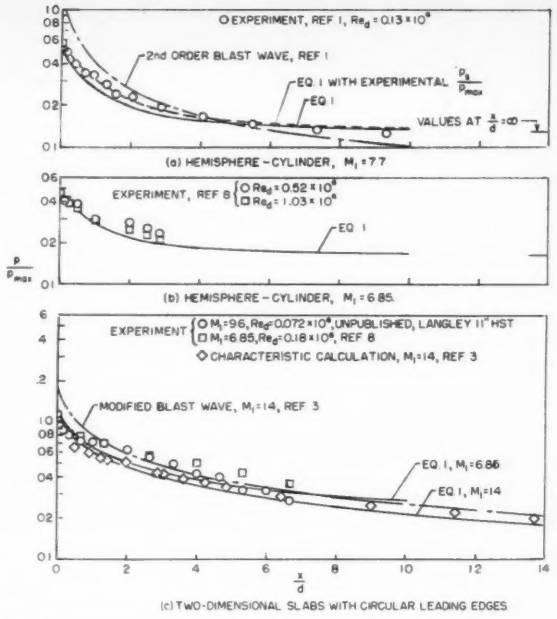

Fig. 2 Comparison of predictions and experimental results, $\gamma = 7/5$. (*a*) Hemisphere cylinder, $M_1 = 7.7$. (*b*) Hemisphere cylinder, $M_1 = 6.85$. (*c*) Two-dimensional slabs with circular leading edges

p_s/p_{max} are essentially invariant with Mach number; for $M_1 = \infty$, p_s/p_{max} is predicted to be 0.045 for the axisymmetric case and 0.117 for the two-dimensional case.

With these predictions of p_s/p_{max} and the adoption of the pressure decay laws of blast wave theory, the pressure distribution over the body downstream and within a few diameters (or thicknesses) of the shoulder is determined. To eliminate the deficiency of blast wave theory far downstream, the value of p/p_{max} at $x/d = \infty$ is taken to be p_1/p_{max}; this assumption can be supported by characteristics solutions and is the equivalent of the far downstream modification of blast wave theory (3) mentioned earlier, i.e., p taken to be $p - p_1$.

With the foregoing conditions and with x denoting distance downstream from the shoulder, the pressure distribution may be expressed as

$$\frac{p}{p_{max}} = \left[\frac{1}{1 + (x/d)^a}\right]\frac{p_s}{p_{max}} + \left[\frac{1}{1 + 1/(x/d)^a}\right]^b \frac{p_1}{p_{max}} \qquad [1]$$

which may be regarded as the second order form of the present method. In this expression the exponent a defines the pressure decay law of blast wave theory (3) and is $\frac{2}{3}$ for the planar blast wave (as for the two-dimensional slab) and 1 for the blast wave with cylindrical symmetry (as for the hemisphere cylinder). The value of the exponent b is determined by the requirement that the second term on the right in Equation [1] must, in addition to giving p/p_{max} its minimum value of p_1/p_{max} at $x/d = \infty$, maintain $p/p_{max} \geqq p_1/p_{max}$ for $0 \leqq x/d \leqq \infty$ with a minimum change in the pressure decay from that given by the first term only (the first order form of the present method). These conditions may be shown to give $b = p_s/p_1$. Thus all quantities in Equation [1] are known or may be readily calculated. The use of the shoulder as the origin for x is permissible in the adoption of the pressure decay law of blast wave theory because of the asymptotic form of this theory.

In Fig. 2, predictions by use of Equation [1] are compared with experimental results and blast wave theory. The prediction for the hemisphere cylinder at $M_1 = 7.7$, Fig. 2 (a), is in good agreement with the experimental results; the small differences shown may be due in part to boundary layer displacement effects. Note that the use of the experimental value of p_s/p_{max} would bring the predicted pressure distribution into excellent agreement with the experimental distribution. The curve given by second order unmodified blast wave theory is also shown; its deficiencies near the shoulder and far downstream are apparent.

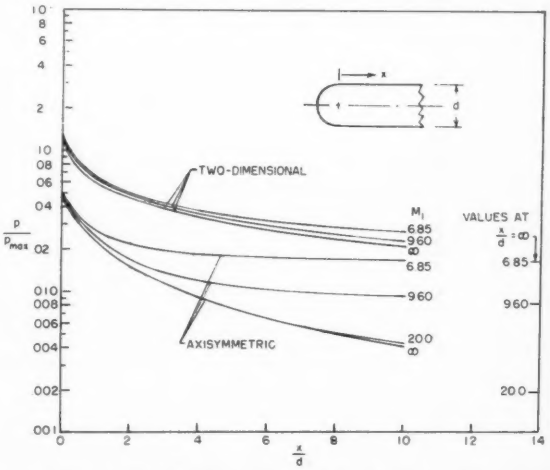

Fig. 3 Predicted pressure distributions, $\gamma = 7/5$

There appears to be slightly more scatter in the experimental data shown in Figs. 2 (b) and (c), but the predictions by Equation [1] appear to agree with the data within this scatter and the effects of Reynolds number. There is some indication in Fig. 2 (b) that as the boundary layer displacement effects are reduced, the experimental data come into closer agreement with the prediction. In Fig. 2 (c), the predicted curves for the two-dimensional case at $M_1 = 6.85$ and $M_1 = 14$ bracket the Mach range of the data shown; the characteristics solution (3) for $M_1 = 14$ and the present prediction for this Mach number agree closely. In this regard, the present method predicts a negligible effect of Mach number for the two-dimensional case over the range of x/d shown when M_1 is of the order of 14 or greater. Also shown is the blast wave theory for $M_1 = 14$, modified to satisfy the far downstream condition (3).

Fig. 3 presents several curves calculated by the present method to show more clearly the differences between the two-dimensional and axisymmetric predictions, as well as the effects of x/d and Mach number on the pressure distributions. Note that in Equation [1] the importance of the second term diminishes with increasing Mach number, particularly for the two-dimensional case for which the larger values of b make the second term insignificant except at large values of x/d.

Nomenclature

a = exponent, Equation [1], defining first order pressure decay
b = p_s/p_1
d = diameter or thickness
H^* = stagnation pressure behind shock for sonic cone (or sonic wedge)
M_1 = free stream Mach number
p = local pressure on body surface
p_1 = free stream static pressure
p_s = shoulder pressure, i.e., pressure at tangency point of nose and afterbody
p_{max} = pressure at stagnation point on body
x = axial distance from shoulder
γ = ratio of specific heats

References

1 Lees, L. and Kubota, T., "Inviscid Hypersonic Flow Over Blunt-Nosed Slender Bodies," *J. Aeron. Sci.*, vol. 24, no. 3, March 1957, pp. 195–202.

2 Casaccio, A., "Theoretical Pressure Distribution on a Hemisphere-Cylinder Combination," *J. Aeron. Sci.*, vol. 26, no. 1, Jan. 1959, pp. 63–64.

3 Cheng, H. K. and Pallone, A. J., "Inviscid Leading-Edge Effect in Hypersonic Flow," *J. Aeron. Sci.*, vol. 23, no. 7, July 1956, pp. 700–702.

4 Stine, H. A. and Wanlass, K., "Theoretical and Experimental Investigation of Aerodynamic Heating and Isothermal Heat-Transfer Parameters on a Hemispherical Nose with Laminar Boundary Layer at Supersonic Mach Numbers," NACA TN 3344, Dec. 1954.

5 Korobkin, I., "Local Flow Conditions, Recovery Factors,and Heat-Transfer Coefficients on the Nose of a Hemisphere-Cylinder at a Mach Number of 2.8," NAVORD Rep. 2865, May 1953.

6 Oliver, R. E., "An Experimental Investigation of Flow About Simple Blunt Bodies at a Nominal Mach Number of 5.8," *J. Aeron. Sci.*, vol. 23, no. 2, Feb. 1956, pp. 177–179.

7 Crawford, D. H. and McCauley, W. D., "Investigation of the Laminar Aerodynamic Heat-Transfer Characteristics of a Hemisphere-Cylinder in the Langley 11-Inch Hypersonic Tunnel at a Mach Number of 6.8," NACA Rep. 1323, 1957.

8 Bertram, M. H. and Feller, W. V., "A Simple Method for Determining Heat Transfer, Skin Friction, and Boundary-Layer Thickness for Hypersonic Laminar Boundary-Layer Flows in a Pressure Gradient," NASA Memo 5-24-59L.

9 Bertram, M. H. and Baradell, D. L., "A Note on the Sonic-Wedge Leading-Edge Approximation in Hypersonic Flow," *J. Aeron. Sci.*, vol. 24, no. 8, Aug. 1957, pp. 627–629.

Book Reviews

Ali Bulent Cambel, Northwestern University, *Associate Editor*

Air Intake Problems in Supersonic Propulsion, AGARDograph 27, edited by J. Fabri, Pergamon Press, New York, 1958, 82 + xx pp. $5.

Reviewed by Arthur A. Kovitz
Northwestern University

This book is a collection of four invited papers presented at the 11th AGARD Combustion and Propulsion Panel Meeting, Paris, December 1956. Preceding the papers is a useful introduction and summary by J. Fabri.

The turbojet or ramjet engine differs from the operation of a reciprocating engine primarily in the fact that thrust is obtained by internal acceleration of air. Both the air necessary for burning the fuel and the air necessary for thrust must be ingested through a frontal area usually smaller than that of the reciprocating engine. Supersonic flight speeds demand an air intake which must deliver a correct air flow rate at optimum pressure recovery.

For a given Mach number it is possible to design an optimum air intake. There is, of course, the need for an air intake which is efficient during off design operation as well as at the design point. Furthermore, the overall design of an air intake must also include its interaction with the powerplant itself.

The stated aim of this AGARD Combustion and Propulsion Panel was to emphasize this last aspect of the air intake problem. Four lectures were delivered to define the viewpoint of four scientists, engaged in air intake research, on the air intake-engine matching problem.

The first paper, in French, "The Role of the Air Intake in Estimating the Thrust of a Reaction Engine," by P. Carriére, undertakes to define some parameters in the supersonic operation of an air intake. *Flow coefficient, efficiency, external* and *internal drag* are defined and discussed. The effect of the air intake on the thrust of a supersonic ramjet is then computed. It is shown that in some cases the downstream portion of the ramjet configuration cannot take full advantage of the best performance of the air intake. However, off design operation (below design Mach number, in this case) usually demands corrective measures, such as variable area air intakes to avoid excessive off design losses.

The second paper by Marquis D. Wyatt is titled "Review of Supersonic Air Intake Problems." Among the specific problems discussed are:

(a) Pressure recovery. Normal shock intakes are to be avoided. *External compression* and *internal compression* intakes are described.

(b) Air intake location. The boundary layer developed on the approach surfaces must be removed ahead of the intake.

(c) Air intake drag. Friction drag is nearly independent of intake shape and is unavoidable. Cowl pressure drag depends upon shape. Additive drag, due to shock waves generated at the front of the air intake, can represent the largest contribution to total drag during off design operation.

(d) Stable internal flow. When the air intake system is choked certain low amplitude fluctuations sometimes occur. These are not important. However, during operation at Mach numbers below choking (subcritical), buzz-type instability occurs that is not well understood and is undesirable. Variable shape intakes are usually the answer to these instabilities. Finally, this flexibility in shape is also a help in the key problem of intake-to-engine matching.

The third paper by A. Ferri discusses "The Problems Related to Matching Turbo-Jet Engine Requirements to Inlet Performances as a Function of Flight Mach Number and Angle of Attack."

Pioneering Achievements in Missile Support Equipment at JPL

VEHICULAR EQUIPMENT . . . has been designed and developed having greater stamina and of much lighter weight. Specially designed prototype units were tested on rough terrain under the severest operating conditions. From these tests, significant design data resulted.

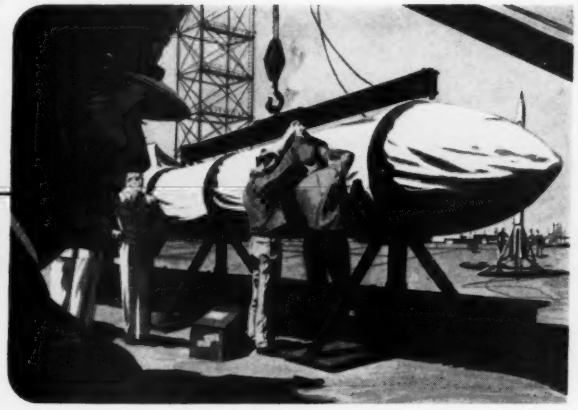

GROUND HANDLING EQUIPMENT . . . for servicing missiles and readying them for launching has been designed, developed and tested. However, a continuing program is in process at the Jet Propulsion Laboratory to further the state of the art in this important field.

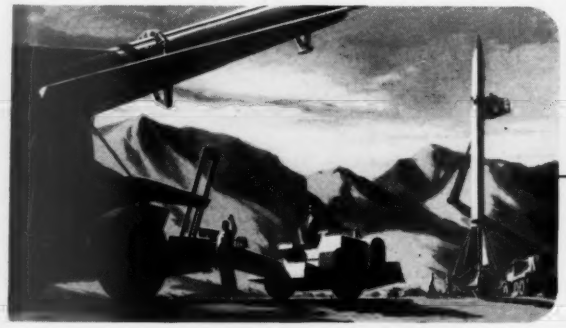

MOBILE MISSILE SYSTEMS . . . were designed, developed and tested for use in transporting and servicing missiles. A tractor-trailer with launching pad in one complete unit was developed. Other equipment for loading and transporting missiles via air, land or sea has been developed.

GROUND SUPPORT EQUIPMENT . . . is developed to operate under conditions of rain, snow, ice, and heat. Mud and desert sand also create difficult environmental problems. Objectives are ease of operation and handling permitting the missile to be readily unloaded from airplanes, or landing craft and quickly positioned for firing.

jpl

CALIFORNIA INSTITUTE OF TECHNOLOGY

JET PROPULSION LABORATORY

A Research Facility operated for the National Aeronautics and Space Administration

PASADENA, CALIFORNIA

Employment opportunities for Engineers and Scientists interested in basic and applied research in these fields

SERVOMECHANISMS • COMPUTERS • STRUCTURES • INSTRUMENTATION • MATHEMATICS
PACKAGING TECHNIQUES • MECHANICAL DESIGN AND DEVELOPMENT

Send professional resume, with full qualifications and experience, for our immediate consideration.

Solid Fuels are simple—

It is first pointed out that there are too many parameters to be controlled for exact matching of intake system to turbojet performance. A compromise is sought whereby only the most important are retained, depending upon the regime of operation.

Two primary parameters are invariably present. The first is Mach number ahead of the intake system. The second is air temperature.

The major difficulty in matching intake to engine requirements is unstable operation at Mach numbers greater than 1.6 when the flow is not choked. This is avoided by always designing for choked flow.

Variation of internal geometry is a recommended procedure. Placing the air intake behind a shock wave generated by a wing or fuselage can result in sufficiently low Mach number at intake entrance to allow much simplification in the design of the variable shape intake system.

Finally, it is pointed out that flow nonuniformities at intake entrance can have equal importance with variation in flight Mach number. Variable geometry air intakes are again recommended to reduce this effect and increase the range of safe operation with respect to angle of attack.

The fourth and last paper, in French, by L. Viaud, "Interpretation of Experiments on Supersonic Air Intakes," describes some of the experimental problems associated with meaningful wind tunnel testing of air intakes. A definition of a *standard air intake* is given, and certain experimental conditions are recommended. It is pointed out that it is difficult to compare results obtained in various wind tunnels. It is suggested that the standard air intake, as defined in the paper, could help in comparing experimental results from different wind tunnels.

This reviewer has never been engaged in supersonic air intake research. Nevertheless, he found this little volume extremely interesting and informative. In the course of discussing the intake-engine matching problem many operating features of the intake and engine itself were illuminated. However, there were not as many references as one might desire. This shortcoming is partially canceled by the possibility that many of the references would be dated at this time anyway.

It is the reviewer's impression that workers in the field will find this book to give a valuable overall picture of unclassified supersonic air intake research up to and including 1956.

Rocket Propellants, by Francis A Warren, Reinhold Publishing Corp., New York, 1958, ix + 218 pp. $6.50.

Reviewed by JOHN GUSTAVSON
Grand Central Rocket Co.

The title of this book is slightly misleading, since the treatment is strongly slanted toward solid propellants, a field with which the author is well-acquainted. The ratio of "solid-to-liquid" material is about four to one. Therefore, this is not the right book to choose for a reader seeking knowledge of liquid rocket propellants.

However, it presents a good semitechnical description of the fundamentals of solid propellant technology. The coverage includes manufacture and processing, ignition, burning, performance and industrial safety. The book is well-referenced, although numerous spelling errors of proper names tend to distract the reader.

The general treatment is more chemical than mechanical, undoubtedly due to the author's background. The book is illustrated with photos from ordnance plants and rocket companies as well as with sketches and a few graphs. In the chapter on liquids, the author overemphasizes the use of ozone. This highly unstable oxidizer has hardly left the research laboratory.

The book would have benefitted from a more extensive treatment of the safety problem, since the book probably will have its greatest circulation among high school students and laymen who want to become familiar with the propellants used in missiles and space vehicles. These readers may be prone to experiment, mixing their own propellants based on the tables in the book, and the results may be disastrous. This reviewer favors the inclusion of accurate data in a book, but when its market is mainly nontechnical, strong emphasis should be put on the necessary and often vital safety measures.

An Introduction to the Dynamics of Airplanes, by H. Norman Abramson, The Ronald Press Co., New York, 1958, 225 + viii pp. $5.50.

Reviewed by ROBERT H. SCANLAN
Schlumberger Well Surveying Corp.

The author presents standard material for an introductory senior or perhaps early graduate engineering course in aircraft dynamics. Within the range of the title are included airplane stability, dynamic load studies of various kinds, such as landing and gust loads, and the aeroelasticity topics of wing and panel flutter, lifting surface divergence and control effectiveness.

The book covers in an elementary way the various subject matters, grouped around the central theme of vibration theory, which comprise the domain of the modern aeroelastician, or still more broadly, the aircraft dynamicist. Thus we find an introduction to elementary vibration theory as well as a modicum of structural and unsteady aerodynamics facts, derivations of which are, for the most part, omitted.

The common, very useful mathematical and solution tools which are matrix theory, the Duhamel integral and the analog computer are introduced. Throughout, the presentation is simple and straightforward, with a good number of illustrative problems and references to the existing literature.

Chapter headings are: Vibrations of a Single-Degree-of-Freedom System, Vibrations of Multi-Degree-of-Freedom Systems, Elements of Matrix Algebra with Applications, Self-Excited Vibrations and Stability of Motion, Elementary Theory of Wing Flutter, Aeroelasticity, Problems

of Impulsive Loading—Landing Impact, Gust Response, and Buffeting, Introduction to Flight Stability, Miscellaneous Topics.

The chief *raison d'être* of this book would appear to be a rather pleasant, ordered assemblage of some of the basic material of the field. The author augments this material by qualitative discussions of the more advanced topics but thorough treatment is beyond the intended scope of his text.

The book should be useful in that it presents a correctly oriented introductory view of airplane dynamics to the newcomer.

Aircraft Hydraulics, edited by H. G. Conway, MacMillan Co., Inc., New York, 1957. Vol. I Hydraulic Systems, 146 pp, $7; Vol. II Component Design, 198 pp, $9.

Reviewed by ROBERT B. BANKS
Northwestern University

The very rapid pace at which advances are being made in the aircraft and missile industries has been paralleled by the very large number of books associated with the theoretical and practical aspects of high speed flight. During the past decade, books devoted to high speed aerodynamics, boundary layer theory, compressible fluid flow, aeroelasticity, missile trajectory and heat transfer have appeared in great number. However, one subject which has been neglected, as regards publication of reference books, is the subject of aircraft hydraulics and pneumatics. One does not need to point out the vital role which hydro-pneumatic equipment plays in present-day aircraft and missiles.

Such neglect of this subject extends beyond the aeronautical aspects of hydraulics and pneumatics; that is, even though hydraulic and pneumatic systems have been employed for many decades in countless numbers of industrial and commercial applications, the number of books on the subject has been exceedingly small. Furthermore, with a few exceptions, the texts which have appeared have been largely devoted to descriptions of the various components and qualitative discussions of their relationships in various types of circuits. The emphasis which most previous texts have put on the fundamentals of fluid motion has been very light. Previously, very little attention has been given to aspects of hydraulic circuit stability. As a consequence, almost no quantitative treatment has appeared in textbooks on hydraulics as regards control theory. This is in sharp contrast to the very great attention which has been devoted to the analogous problems of electrical circuits.

Therefore, the appearance of these two volumes on aircraft hydraulics is very timely. In a foreword by E. T. Jones, President of the Royal Aeronautical Society, it is announced that these two books are the first of a series "sponsored by the Society to meet the needs of students and engineers in the aeronautical field."

Volume I has the subtitle "Hydraulic Systems" and Volume II "Component Design." A third volume on the subject "Landing Gear Design" is to be published. The volumes are edited by H. G. Conway, Director and Chief Engineer, Short Brothers and Harland Ltd., Belfast. Nine other authors, all of whom have aircraft or other industrial affiliations, have contributed one or more chapters on various topics in these first two volumes.

Volume I The first chapter is entitled "Fluids for Hydraulic Systems." Properties of fluids are discussed, with particular emphasis on the effect of temperature and pressure on viscosity, compressibility and density. Aspects of gas absorption, foaming, miscibility, pour and boiling points, thermal and electrical properties and lubrication qualities are considered. Chapter II is devoted to the fundamentals of fluid flow as related to hydraulic systems. Equations for laminar flow in circular tubes and between parallel plates are derived. The Bernoulli and continuity equations are presented and employed in problems involving flow through orifices and sudden expansions and contractions. Chapter III continues the subject of fluid flow by presenting equations, nomograms and charts for laminar and turbulent flow in pipes. A portion of this chapter is devoted to pneumatics, primarily as related to the design and performance of accumulators.

The following two chapters are devoted to the subject of hydraulic systems and circuits. Criteria and considerations are presented for selection of the pumping unit, operating pressure and choice of fluid. A number of basic circuit diagrams are given. The remainder of the first volume is devoted to topics on installation, operation and testing of aircraft hydraulic systems.

Volume II The entire second volume is concerned with the design and performance of the components comprising the hydraulic system. Chapter I presents information on the subject of seals and packing. Various aspects of hydraulic pumps and motors are discussed in Chapter II, and, following this, a chapter is devoted to the subject of hydraulic jacks. Selectors, valves and miscellaneous hydraulic components are presented in subsequent chapters. The second volume concludes with a chapter on hydraulic servo controls and a chapter on the subject of pipe and tube selection.

There is no doubt that engineers engaged not only in aircraft hydraulic work but also those working in industrial hydraulics will find these volumes to be extremely useful. They will be of particular value to those involved with design and performance problems. No attempt has been made by the authors to incorporate any quantitative analysis of the servomechanism or other phases of control theory. This results in a very simple, nonmathematical presentation of the subject of aircraft hydraulics. It appears to be true, as E. T. Jones indicated, that the books in this new series, of which these two are the first, "will at least fill some of the gaps in current aeronautical literature."

New Patents

George F. McLaughlin, *Contributor*

Circular wing aircraft (2,876,964). H. F. Streib, Chula Vista, Calif.

Central opening in a circular wing with the airfoil section symmetrical about a vertical axis. An impeller in the opening draws air inward radially across the wing, and downward through the opening.

Method of bonding propellant grain to metal case (2,877,504). H M. Fox, Bartlesville, Okla., assignor to Phillips Petroleum Co.

Preparation of a rocket engine for firing by injecting a flowable material, capable of being cured to a firm set, into the space between a solid grain and the combustion chamber.

Quick release valve (2,877,780). E. M. Whitley and J. R. Greer, Mountain View, Calif., assignors to Beckman & Whitley, Inc.

An explosive cell opening into a cavity to create pressure when detonated, forcing a gate valve from closed to open position. A shoulder prevents the gate from closing after it has opened.

Jet inlet diffuser for supersonic flying wing (2,877,965). G. H. Wakefield, Takoma Park, Md.

Leading edge air inlet including an airfoil. Wedge-shaped upper and lower diffuser members, their edges pointed upstream, may have their angular positions adjusted according to the varying conditions encountered in supersonic flight.

Apparatus for measuring speed of moving objects (2,878,467). J. L. Barker and B. J. Midlock, Norwalk, Conn., assignors to Eastern Industries, Inc.

Unitary microwave transmitter and receiver system for directing a beam of microwaves along the path traveled by a body. System includes a single antenna for both transmitting and receiving microwaves.

Jet propelled airplane with jet diverter 2,879,014). S. W. Smith and C. M. Sperazz Sr., Williamsville, N. Y., assignors to Bell Aircraft Corp.

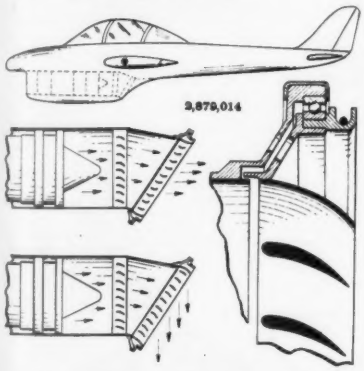

Pilot-controlled means for diverting the engine thrust forces between vertically downward directions and generally horizontal directions.

EDITOR'S NOTE: Patents listed above were selected from the Official Gazette of the U.S. Patent Office. Printed copies of patents may be obtained from the Commissioner of Patents, Washington 25, D. C., at a cost of 25 cents each; design patents, 10 cents.

Toy jet missile (2,879,624). R. A. Benson, Rockaway, N. J., assignor of one-half to R. J. Novotny.

Inflatable balloon with a discharge nozzle and guide fins. A sealing device secured to the neck of the balloon is manually detached to launch the missile.

Fluid sustained aircraft (2,879,957). A. M. Lippisch, Cedar Rapids, Iowa, assignor to Collins Radio Co.

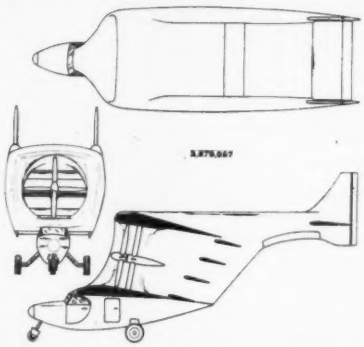

Wingless aircraft with a propeller within a central duct above the body. Vanes at the rear of the duct control the lift.

Variable area nozzle and aerodynamic brake (2,880,575). M. Scialla, Paterson, N. J., assignor to Curtiss-Wright Corp.

Inward and outward adjustment of the nozzle is accompanied by movement of a combined fairing and brake member to form a a smooth rearward continuation of the housing surface. The member is movable to a position for braking the propulsive thrust.

Supersonic variable throat nozzle (2880,-576). P. G. Kappus, Dayton, Ohio, assignor to the U. S. Air Force.

Means for disconnecting and jettisoning a separable convergent nozzle during flight from a tailpipe extension. Further means for disconnecting and jettisoning the extension, rendering the convergent-divergent nozzle solely effective to vary the tailpipe discharge area.

Automatic buzz control (2,880,579). D. L. Harshman, Lodi, N. J., assignor to Curtiss-Wright Corp.

Control for a jet engine having an air inlet arranged for supersonic entering air flow with the resulting shock wave marking the transition from supersonic to subsonic flow positioned within the inlet.

Convex panel wing construction (2,881,-994). H. E. Michael, Hawthorne, Calif., assignor to Northrop Aircraft, Inc.

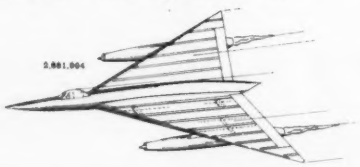

Method of securing a light gage metal skin to a delta wing frame to insure a minimum weight to lift ratio for the wing. Skin is secured along the chordwise ribs so that tension stresses on the panels will be perpendicular to the ribs.

Augmented-type afterburner (2,882,679). H. C. Karcher and O. T. Kreusser, Indianapolis, Ind., assignors to General Motors Corp.

Jet propelled aircraft with means for generating a high velocity gas stream containing a substantial portion of uncombined oxygen. Fuel is burned in an injector chamber. Entrance to a duct to the chamber receives boundary layer air adjacent the aircraft body.

Fuel supply system for ramjet engines (2,882,680). R. R. Jamison and F. D. Henderson, Bristol, England, assignors to Bristol Aero-Engines, Ltd.

Control of the supply of fuel during all phases of operation. Valve comprising two members, one held by a spring in one direction, and the other held in the opposite direction by fuel pressure. Fuel flows through an orifice between the members in proportion to the pressure arriving at the valve.

Air-jacketed combustion chambers for jet propulsion engines (2,882,681). F. J. Hudson and W. E. Gregory, Burnley, England, assignors to Joseph Lucas (Industries) Ltd.

An annular header for air under pressure at one end of the combustion chamber. Air is conveyed by passageways to inner and outer air jackets and the chamber in constant relative proportions, irrespective of nonuniformity between air flows in the header regions.

Tail cone release and ejection mechanism (2,882,862). C. A. Waldorff and R. E. Ainslie, Glenside, Pa., assignors to the U. S. Navy.

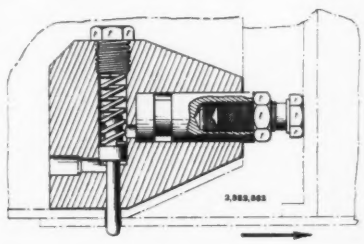

High pressure fluid directed into a port acts on the underside of a vertical piston, withdrawing a latch pin and releasing the tail cone. The fluid then passes to a horizontal piston which shoves the tail cone away from the supporting structure of the missile.

Breathing apparatus (2,882,896). H. W. Seeler, Dayton, Ohio, assignor to the U. S. Air Force.

Window portion of a breathing mask includes two spaced transparent members. The inner member has an opening to permit leakage of air preventing rupture in the space as altitude increases, but preventing flow of air into the space from the interior of the mask.

Breathing apparatus (2,882,897). W. B. McLean, China Lake, Calif., assignor to American Machine & Foundry Co.

A connection between a face mask and window permits the window to move slightly in and out. Movement of the window actuates a demand valve in the mask, shutting off air from the supply source.

Boosted into space by the 150,000-pound thrust of an Air Force Thor missile, the second-stage Agena satellite is powered into orbit by its own liquid-fuel rocket engine of 15,000 pounds thrust.

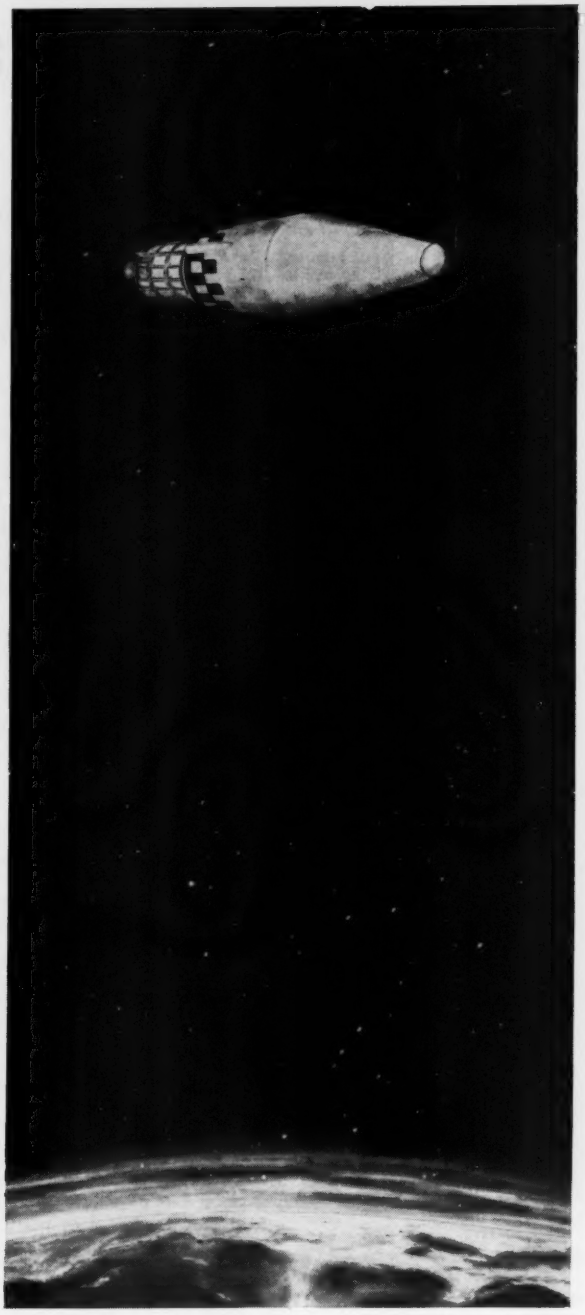

Once in orbit, the Agena satellite radios back to its tracking stations more than a hundred measurements of its performance and of the conditions it encounters as it circles the earth at 18,000 mph.

LOCKHEED

MISSILES AND SPACE DIVISION

MISSILE RESEARCH & DEVELOPMENT • BALLISTIC MISSILE SYSTEMS MANAGEMENT
ROCKETRY • ULTRASONIC AERODYNAMICS • SPACE INVESTIGATIONS • NUCLEAR PHYSICS
ADVANCED ELECTRONICS • HIGH-SPEED AUTOMATIC DATA REDUCTION
RAMJET PROPULSION TESTING

Technical Literature Digest

M. H. Smith, *Associate Editor*, and M. H. Fisher, *Contributor*
The James Forrestal Research Center, Princeton University

Jet Propulsion Engines

Residual Fuel Expulsion from a Simulated 50,000-pound-thrust Liquid-propellant Rocket Engine Having a Continuous Rocket-type Igniter, by Wesley E. Messing, *NASA Memo* 2-1-59H, Feb. 1959, 10 pp.

Analytical Investigation of the Significance of Turbine-inlet Temperature in High-energy Rocket Turbodrive Applications, by Harold E. Rohlik, *NASA Memo* 1-6-59E, Feb. 1959, 24 pp.

Materials Problems Encountered in Liquid Propellant Rocket Engines, by Donald E. Roda, *Soc. Automot. Engrs., Preprint* 4R, Jan., 1949, 6 pp.

Surveillance of Solid Propellant Rockets, by Carl Boyars, ARS JOURNAL, vol. 29, Feb. 1959, pp. 148–150.

State of the Art: Propulsion, *Space Aeron.*, vol. 31, March 1959, pp. 52–53.

General Equation for Rocket Velocity, by Sylvan Rubin, ARS JOURNAL, vol. 29, March 1959, pp. 219–220.

A Future for Hypersonic Ramjets, by Gordon L. Dugger, ASTRONAUTICS, vol. 4, April 1959, Part 1, pp. 38–39, 114–117.

Ramjet Trends, by Eugene Perchonok, ASTRONAUTICS, vol. 4, April 1959, Part 1, pp. 40–41, 100–102.

Ramjet Fuel-air Control, by Ludwig Muhlfelder, ASTRONAUTICS, vol. 4, April 1959, Part 1, pp. 42–43, 86.

Ramjet Combustion, by Roland Breitwieser, ASTRONAUTICS, vol. 4, April 1959, Part 1, pp. 44–45, 87–88, 90.

Supersonic Ramjet Diffuser Design, by R. B. Pearce Jr., ASTRONAUTICS, vol. 4, April 1959, Part 1, pp. 46–48, 68, 71.

Robert H. Goddard, an Autobiography, ASTRONAUTICS, vol. 4, April 1959, Part 1, pp. 24–27, 106, 108–109.

A Monopropellant Air-Turborocket, by James W. Mullen II, ASTRONAUTICS, vol. 4, April 1959, Part 1, pp. 36–37, 72.

Rocket Propulsion, by Charles J. Marsel, ASTRONAUTICS, vol. 4, April 1959, Part 2, pp. 7–11.

Rockets and Amateurs, by George P. Sutton, ASTRONAUTICS, vol. 4, April 1959, Part 2, pp. 12–14.

The Rocket: an Old Idea, an Old Challenge, by Saunders B. Kramer, Nancy Putnam and Alex Chwick, ASTRONAUTICS, vol. 4, April 1959, Part 2, pp. 15–17.

Propulsion Fundamentals, by B. Pinkel, *Rand Corp.*, P-1429, Feb. 1958, 28 pp.

Some Fundamental Considerations Relating to Advance Rocket Propulsion Systems, by J. H. Huth, B. W. Augenstein and R. D. Holbrook, *Rand Corp.*, RM-2194 (*ASTIA AD* 133047), March 1958, 35 pp.

Some Fundamental Considerations Relating to Advance Rocket Propulsion Systems, by John Huth, *Rand Corp.*, P-1479, Sept. 1958, 16 pp.

Direct Power Conversion: Part I—General Comments, by J. H. Huth, *Rand Corp.*, P-1524, Oct. 1958, 10 pp.

Suitability of Solid and Liquid Rocket Engines for Placing Manned Satellites on Orbit, by M. Goldsmith, *Rand Corp.*, P-1542, Nov. 1958, 12 pp.

Analysis of Flow-system Starting Dynamics of Turbo-pump-fed Liquid-propellant Rocket, by Richard P. Krebs and Clint E. Hart, *NASA Memo* 4-21-59E, April 1959, 45 pp.

Modeling Studies of Sub-atmospheric Combustors, by W. P. Jensen, P. M. Raymond and A. C. Tobey, *Wright Air Dev. Center, Tech. Rep.* 58-620, *ASTIA Document* 208857, Dec. 1958, 42 pp.

Experiments with Screens and Grids for Suppressing Jet Engine Noise, by H. U. Wisniowski, *Canada, Nat. Aeron. Estab. Lab., Rep.* LR-231, Oct. 1958, 9 pp.

Power for Satellites, by J. H. Huth, *Rand Corp.*, P-1511, Oct. 1958, 10 pp.

The Future for Solid Propellant Rockets, by K. W. Pearce, *J. Roy. Aeron. Soc.*, vol. 63, April 1959, pp. 221–226.

Turbo-ramjets—Best for Mach 2-3?, by Denis Desoutter, *Space Aeron.*, vol. 31, May 1959, pp. 61–62, 66.

Capabilities of Multistaged Chemical Rocket Systems, by J. E. Froehlich, *Inst. Aeron. Sci., Rep.* 59-82, Jan. 1959, 16 pp.

A Look at Rocket Propulsion for the Next 25 Years, by T. F. Dixon, *Inst. Aeron. Sci., Rep.* 59-54, Jan. 1959, 13 pp.

Thrust Control of Solid Propellant Rockets, by H. W. Ritchey, *Inst. Aeron. Sci., Rep.* 59-55, Jan. 1959, 7 pp.

Turbopumps for High Energy Propellants, by A. Ginsburg, W. L. Stewart and M. J. Hartmann, *Inst. Aeron. Sci., Rep.* 59-53, Jan. 1959, 18 pp.

Application of Oblique-shock Sensing System to Ram-jet-engine Flight Mach Number Control, by Fred A. Wilcox and Donald P. Hearth, *NACA RM* E54L22a, March 1955, 29 pp. (Declassified from Confidential by authority of *NASA Pub. Announcement* 4, p. 21, 3/16/59.)

Low-pressure Performance of Different Diameter Experimental Combustor Liners, by Ralph T. Dittrich, *NACA RM* E53L16a, Feb. 1954, 58 pp. (Declassified from Confidential by authority of *NASA Pub. Announcement* 4, p. 19, 3/16/59.)

Altitude Wind Tunnel Investigation of High-temperature Afterburners, by E. William Conrad and Carl E. Campbell, *NACA RM* E51L07, June 1952, 51 pp. (Declassified from Confidential by authority of *NASA Pub. Announcement* 4, p. 17, 3/16/59.)

Rocket Motors from the Core, by J. C. Chapman, *Thiokol Astronaut*, vol. 1, no. 1, 1959, pp. 3–7.

A Comparison of Two Approaches to an Electric Propulsion System, by Vernon H. Blackman, *Plasmadyne Corp.*, PLR-4, 30 pp.

A Five-stage Solid-fuel Sounding-rocket System, by Andrew G. Swanson, *NASA Memo* 3-6-59L, March 1959, 22 pp.

Optimum Exhaust Velocity Program-

EDITOR'S NOTE: Contributions from Professors E. R. G. Eckert, J. P. Hartnett, T. F. Irvine Jr. and P. J. Schneider of the Heat Transfer Laboratory, University of Minnesota, are gratefully acknowledged.

ming and Propulsion Efficiency, by Robert Fox, *AEC*, UCRL-5135, Feb. 1958, 11 pp.

Combustion Instability in Liquid Propellant Rocket Motors, Twenty-sixth Quarterly Progress Report for the Period 1 August 1958 to 31 October 1958, by D. T. Harrje, *Princeton University, Dept. Aeron. Engng., Aeron. Engng. Rep.* 216-z, 20 pp.

Ion Rocket Engine Systems—a Summary, by Robert H. Boden, *Aero/Space Engng.*, vol. 18, April 1959, pp. 60–66.

Performance Calculations for Hybrid Nuclear-Chemical Rocket Propulsion Systems, by Leon Green Jr. and James M. Carter, ARS JOURNAL, vol. 29, March 1959, pp. 180–186.

Liquid Injection for Solid Rocket Thrust Control, by Michael Grenus, *Space/Aeron.* vol. 31, April 1959, pp. 59–62.

Aerodynamics of Jet Propelled Missiles

Laminar Heat Transfer on Three-Dimensional Blunt Nosed Bodies in Hypersonic Flow, by Roberto Vaglio-Laurin, ARS JOURNAL, vol. 29, Feb. 1959, pp. 123–129.

An Experimental Investigation of Blunt Body Stagnation Point Velocity Gradient, by J. Christopher Boison and Howard A. Curtiss, ARS JOURNAL, vol. 29, Feb. 1959, pp. 130–135.

Dynamic Stability of Re-entry Vehicles, by Murray Tobak, ASTRONAUTICS, vol. 4, March 1959, pp. 32–33, 66.

Effect of Acceleration on the Longitudinal Dynamic Stability of a Missile, by E. V. Laitone, ARS JOURNAL, vol. 29, Feb. 1959, pp. 137–139.

Rapid Method for Computing High Altitude Gravity Turns, by Robert L. Sohn, ARS JOURNAL, vol. 29, Feb. 1959, pp. 139–141.

Calculation of Unsteady Supersonic Flow Past a Circular Cylinder, by Martha W. Evans and Francis H. Harlow, ARS JOURNAL, vol. 29, Jan. 1959, pp. 46–48.

Hypersonic Aerodynamics, Parts I and II, by Wallace D. Hayes, ASTRONAUTICS, vol. 4, March 1959, pp. 24–25, 72, 74; April 1959, Part II, pp. 34–35, 83–84, 86.

Low-speed Static Stability and Control Characteristics of a Model of a Right Triangular Pyramid Reentry Configuration, by John W. Paulson, *NASA Memo* 4-11-59L, April 1959, 15 pp.

On the Rotational Motion of a Body Re-entering the Atmosphere, by T. B. Garber, *Rand Corp.*, P-1407, June 1958, 32 pp.

Minor Circle Flight for Boost Glide Vehicles, by W. H. T. Loh, ARS JOURNAL, vol. 29, April 1959, pp. 300–301.

Aerodynamic Moment on Bodies Moving at High Speed in the Upper Atmosphere, by W. A. Gustafson, ARS JOURNAL, vol. 29, April 1959, pp. 301–303.

Thermal Analysis of Stagnation Regions with Emphasis on Heat-sustaining Nose Shapes at Hypersonic Speeds, by A. J. Hanawalt, A. H. Blessing and C. M. Schmidt, *J. Aero/Space Sci.*, vol. 26, May 1959, pp. 257–263.

Supersonic Flow Past a Family of Blunt Axisymmetric Bodies, by Milton Van Dyke and Helen D. Gordon, *NASA Rep.* 1, 1959, 48 pp.

The Effect of Sweep Back Angle on the Pressure Distribution of a Blunt Flat Plate at Hypersonic Speeds, Part 1: Studies of a Hemicylindrical Leading

Edge Flat Plate at Angles of Attack, $\Omega = 45°$ and $M_1 \sim 13.3$, by S. M. Bogdonoff and I. E. Vas, *Bell Aircr. Corp., Rep.* D 143-987-001, June 1957, 35 pp.

Preliminary Study of the Flow Over a Blunt Flat Plate at Various Angles of Attack at M = 13.3, Part 1: Studies of Flat and Hemicylindrical Leading Edges, by S. M. Bogdonoff and I. E. Vas, *Bell Aircr. Corp., Rep.* D 143-001, May 1956, 17 pp.

Longitudinal Stability Derivatives of Missile Shaped Bodies at Hypersonic Speeds, by Robert H. Tolson, IAS Student Branch Paper Competition, 1958; First Award Papers, by *Inst. Aeron. Sci.*, Minta Martin Aeron. Student Fund, 1958, 127 pp., pp. 92–111.

Investigation of Normal Force Distributions and Wake Vortex Characteristics of Bodies of Revolution at Supersonic Speeds, by J. F. Mello, *J. Aero/Space Sci.*, vol. 26, March 1959, pp. 155–168.

The Stagnation-point Boundary Layer on a Rotating Hypersonic Body, by Sinclaire M. Scala and Joseph B. Workman, *J. Aero/Space Sci.*, vol. 26, March 1959, p. 183.

Measurements of Local Heat Transfer and Pressure on Six 2-inch-diameter Blunt Bodies at a Mach Number of 4.95 at Reynolds Numbers Per Foot up to 81 $\times$ 10^6, by Morton Cooper and Edward E. Mayo, *NASA Memo*, March 1959, 39 pp.

Pressure Measurements on an Ogive-cylinder Body at Mach Number 4.04, by Douglas R. Lord and Edward R. Ulmann, *NACA RM* L51L20, Feb. 1952, 33 pp. (Declassified from Confidential by authority of *NASA Pub. Announcement* 4, p. 24, 3/16/59.)

Hypersonic Viscous Flow Past a Blunt Body with an Applied Magnetic Field, by Ching-Sheng Wu, *Princeton Univ., Dept. Aeron. Engng., Rep.* 443 (*AFOSR-TN*-58-1125; *ASTIA AD* 207 834), Nov. 1958, 26 pp.

An Exploratory Study at M-14 of the Flow about a Hemisphere Cylinder at Angle of Attack, by I. E. Vas and S. M. Bogdonoff, *Princeton Univ., Dept. Aeron. Engng., Rep.* 438 (Wright Air Dev. Center TN-58-331), Sept. 1958, 5 pp.

Motion of a Spinning Rocket Cluster, by O. H. VonRoos and Douglas B. Holdridge, *Calif. Inst. Tech., Jet Prop. Lab. Progr. Rep.* 20-376, Dec. 1958, 24 pp.

On the Flight Path of a Hypervelocity Glider, by Angelo Miele, *Purdue Univ., School of Aeron. Engng., Rep.* A-29-2, Jan. 1959, 31 pp.

Pressure Distributions on Flat Plates at Mach 4 and Low Density Flow, by Jerome Aeroesty, *Univ. Calif., Inst. Engng. Res., Tech. Rep.* HE-150-157, July 1958, 14 figs., 29 pp.

Study of the Oscillatory Motion of Manned Vehicles Entering the Earth's Atmosphere, by Simon C. Sommer and Murray Tobak, *NASA Memo* 3-2-59A, April 1959, 30 pp.

Heat Transfer and Fluid Flow

Heat Transfer in Separated Flows, by Howard K. Larson, *Inst. Aeron. Sci., Rep.* 59-39, Jan. 1959, 19 pp.

Experiments on Porous Wall Cooling and Flow Separation Control in Supersonic Nozzle, by Leon Green Jr. and Kenneth L. Nall, *Inst. Aeron. Sci., Rep.* 59-38, Jan. 1959, 21 pp.

A Shock Tube Investigation of Heat Transfer in the Wake of a Hemisphere Cylinder, With Application to Hypersonic Flight, by William E. Powers, Kenneth F. Stetson and Mac C. Adams, *Inst. Aeron. Sci., Rep.* 59-35, Jan. 1959, 24 pp.

Single Phase Transfer of Liquified Gases, by Robert B. Jacobs, *Nat. Bur. Standards, Circ.* 596, Dec. 1958, 42 pp.

A Direct Method to Measure the Thermal Diffusivity of Gases, by Herbert J. Bomelburg, *Aberdeen Proving Ground, Ballistic Res. Labs., Rep.* 1058, Nov. 1958, 23 pp.

Heat Transfer to RP-1 Flowing Turbulently at High Pressure in an Unsymmetrically Heated Rectangular Tube, *Rep.* R1156, by *North American Aviation, Inc., Rocketdyne Div.*, Jan. 1959, 37 pp.

Experimental Study of the Stability of Pipe Flow, I: Establishment of an Axially Symmetric Poiseuille Flow, by E. Reshotko, *Calif. Inst. Tech., Jet Prop. Lab., Progr. Rep.* 20-364, Oct. 1958, 11 pp.

Acoustic Propagation in a Diatomic Gas Subject to Thermal or Chemical Relaxation, by Walter E. Gibson and Franklin K. Moore, *Cornell Aeron. Lab., Inc., Rep.* HF-1056-A-2, (*AFOSR-TN*-58-1057; *ASTIA AD* 206988), Dec. 1958, 52 pp.

Transient and Steady State Heat Transfer Problems Associated with Rockets Utilizing Liquid Oygen, by Paul Lieberman, *Edwards Air Force Base, AF Flight Test Center, Rocket Engine Test Lab.*, Aug. 1956, 34 pp.

The High Temperature Heater and Evaporative Film Cooling of Nozzle Throat Sections of the Rosemont Aeronautical Laboratories Hypersonic Facility, by Rudolf Hermann, Hans Leitinger and Walter L. Melnik, *Wright Air Dev. Center, Tech. Rep.* 58-376 (*ASTIA AD* 204663), July 1958, 5 pp.

Exploratory Investigation of Transpiration Cooling to Alleviate Aerodynamic Heating on an 8° Cone in a Free Jet at a Mach Number of 2.05, by William J. O'Sullivan, Leo T. Chauvin and Charles B. Rumsey, *NACA Res. Mem.* L53HO6, Sept. 1953, 26 pp. (Declassified from Confidental by authority of *NASA PA* 1, p. 18, 11/14/58.)

Lag in Pressure Systems at Extremely Low Pressures, by William T. Davis, *NACA TN* 4334, Sept. 1958, 16 pp.

Experimental Investigation of Axial and Normal Force Characteristics of Skewed Nozzles, by David J. Carter Jr., and Allen R. Vick, *NACA TN* 4336, Sept. 1958, 40 pp.

Heat Transfer and Thermal Stresses in Sandwich Panels, by Robert T. Swann, *NACA TN* 4349, Sept. 1958, 34 pp.

Analysis of Turbulent Flow and Heat Transfer in Noncircular Passages, by Robert G. Deissler and Maynard F. Taylor, *NACA TN* 4384, Sept. 1958, 35 pp.

Application of the Method of Coordinate Perturbation to Unsteady Duct Flow, by Seymour C. Himmel, *NACA Tech. Mem.* 1439, Sept. 1958, 152 pp.

Shock Tubes, Part I: Theory and Performance of Simple Shock Tubes, by I. I. Glass, *Univ. of Toronto. Inst. Aerophys., Rev.* 12, Part I, May 1958, 141 pp., 19 tab., 1 plate, 179 figs.

Shock Tubes, Part II: Production of Strong Shock Waves; Shock Tube Applications, Design and Instrumentation, by J. Gordon Hall, *Univ. of Toronto, Inst. Aerophys. Rev.* 12, Part II, May 1958, 117 pp., 5 tab., 103 figs.

This is Martin-Activation

KEY TO MISSILE OPERATION

A New Division of The Martin Company

The Activation Division is organized to provide the facilities for the design, development, testing, and maintenance of check out and launch complexes for space vehicles and weapon systems bases throughout the world.

It offers to a select group of engineers an opportunity that is indeed unique in today's engineering specialities. It offers the challenge of not only devising a plan, but also of developing, testing, and seeing that plan put into operation.

Among the qualifications for t individuals we are seeking mu be included the willingness relocate, the desire to create a to participate in the develop end product operation. TO TH TYPE OF MAN, MARTIN-AC VATION offers the opportun for great personal advancem and recognition with a comp which has proven technolog ability.

MARTI
ACTIVATION

Extended Applications of Hot Wire Anemometry to High Speed Turbulent Boundary Layers, by Mark V. Morkovin and Ralph E. Phinney, *Johns Hopkins Univ., Dept. Aeron.*, (*AFOSR TN* 58-469; *ASTIA AD* 158279.), June 1958, 127 pp.

Solar Furnace; Support Studies, *Air Force Missile Dev. Center, Tech. Rep.* 58-7 (*ASTIA AD* 135014), 1958, 210 pp.

The Stability of Couette Flow in an Axial Magnetic ;Field, by E. R. Niblett, *Can. J. Phys.*, vol. 36, Nov. 1958, pp. 1509–1525.

Viscosity Equations for Gas Mixtures, by W. E. Francis, *Trans. Faraday Soc.*, vol. 54, Oct. 1958, pp. 1492–1497.

Calculation of Heat Transfer in the Turbulent Boundary Layer of Supersonic and Hypersonic Nozzles, by J. Persh, *Fusées et Récherche Aéron.*, vol. 3, no. 2, July 1958, pp. 86–96. (In French.)

A Method of Calculating the Pressure Distribution in Straight and Radial Cascades, by H. Krüger, *Ing.-Archiv.*, vol. 26, no. 4, 1958, pp. 242–267. (In German.)

Some Observations on the Effect of Radiation on the Refractive Indices of Certain Gases, by C. M. Crain, *J. Appl. Phys.*, vol. 29, Nov. 1958, p. 1605.

On the Behavior of Liquid Droplets after Impinging on Solid Surfaces, by Isaiah Gallily and Victor K. LaMer, *J. Phys. Chem.*, vol. 62, Oct. 1958, pp. 1295–1299.

A Theoretical Investigation of the Interaction between Shock Waves and Boundary Layers, by M. Honda, *J. Aero/Space Sci.*, vol. 25, Nov. 1958, pp. 667–678.

Magnetohydrodynamic-hypersonic Flow Past a Blunt Body, by William B. Bush, *J. Aero/Space Sci.*, vol. 25, Nov. 1958, pp. 685–690.

Flow Properties behind Strong Shock Waves in Nitrogen, by H. F. Waldron, *J. Aero/Space Sci.*, vol. 25, Nov. 1958, pp. 719–720.

A Note on the Interaction of Normal Shock Waves with a Thermal Boundary Layer, by John P. Appleton and Hubert J. Davies, *J. Aero/Space Sci.*, vol. 25, Nov. 1958, pp. 722–723.

Approximation of the Eigenvalues for Heat Transfer in Turbulent Flow, by Robert D. Cess, *J. Aero/Space Sci.*, vol. 25, Nov. 1958, pp. 723–724.

On the Length of Hypersonic Nozzles, by James T. Kenney and Ying-Nien Yu, *J. Aero/Space Sci.*, vol. 25, Nov. 1958, p. 724.

Hypersonic Flow Characteristics Including Real Gas Effects, by Kenneth L. Goldman, *J. Aero/Space Sci.*, vol. 25, Nov. 1958, p. 728.

Thermal Conductivity of an Electron Gas in a Gaseous Plasma, by T. Sekiguchi and R. C. Herndon, *Phys. Rev.*, vol. 112, no. 1, Oct. 1, 1958, pp. 1–10.

Relativistic Field Theory of Unstable Particles, by P. T. Matthews and Abdus Salam, *Phys. Rev.*, vol. 112, no. 1, Oct. 1, 1958, pp. 283–286.

Magneto-hydrodynamic Oscillations of a Perfectly Conducting Fluid Sphere Placed in a Uniform Magnetic Field, by Tsuneji Rikitake, *J. Phys. Soc. Japan*, vol. 13, Oct. 1958, pp. 1224–1230.

The Effects of Combined Electric and Magnetic Fields on Hypersonic Couette Flow, by Z. O. Bleviss, *Douglas Aircr. Co., Rep.* SM-23314, 47 pp.

A Series Solution to the Laminar Heat Transfer Problem at Hypersonic Speeds, by Hung-Ta Ho and Ronald F. Probstein, *Wright Air Dev. Center, TN* 58-263 (*ASTIA AD* 202333), Sept. 1958, 35 pp.

The Effect of a Nonisothermal Free Stream on Boundary Layer Heat Transfer, by E. M. Sparrow and J. L. Gregg *ASME Paper* 58-A-42, Nov. 1958, 5 pp.

Unsteady Laminar Boundary Layers over an Arbitrary Cylinder with Heat Transfer in an Incompressible Flow, by Kwang Tzu Yang, *ASME Paper* 58-A-49, Nov. 1958, 8 pp.

Laminar Heat Transfer in Rectangular Channels, by L. S. Han, *ASME, Paper* 58-A-124, Nov. 1958, 7 pp.

Prediction of Critical Pressures for the Two Phase Flow of Saturated Flow in Pipes, by D. O. Stuart and Glenn Murphy, *ASME, Paper* 58-A-112, Nov. 1958, 8 pp.

Growth of Bubbles in a Liquid of Initially Nonuniform Temperature, by S. G. Bankoff and R. D. Mikesell, *ASME, Paper* 58-A-105, Nov. 1958, 20 pp.

Flow Induced Noise in Heat Exchangers, by A. A. Putnam, *ASME, Paper* 58-A-103, Nov. 1958, 4 pp.

Heat-transfer and Friction Measurements with Variable Properties for Airflow Normal to Finned and Unfinned Tube Banks, by Robert G. Ragsdale, *NASA Mem.* 10-9-58E, Dec. 1958, 33 pp.

An Experimental and Analytical Study of Vortex Flow Temperature Separation by Superposition of Spiral and Axial Flow, by J. E. Lay, *ASME, Paper* 58-A-90, Nov. 1958, 9 pp.

A Survey and Correlation of Data on Heat Transfer by Forced Convection at Supersonic Speeds, by R. J. Monaghan, *Gt. Brit. Aeron. Res. Council, Rep. & Mem.* 3033 (formerly *ARC Tech. Rep.* 16528; *Roy. Aircr. Estab., TN Aero* 2259), 1958, 43 pp.

Contour Nozzles, by Ellis M. Landsbaum, *Calif. Inst. Tech., Jet Prop. Lab., Mem.* 20–169, Sept. 1958, 46 pp.

The Unsteady Wake Interaction in Turbomachinery and Its Effect on Cavitation, by Hsuan Yeh and J. J. Eisenhuth, *ASME, Preprint* 58-A-114, Nov. 1958, 8 pp.

Methods of Determining Surface Roughness, by M. K. Testerman, *Wright Air Dev. Center, Tech. Rep.* 58-230 (*ASTIA AD* 155828), June 1958, 42 pp.

The Radial Flow of Heat in an Infinite Cylinder, by T. P. Newcomb, *Brit. J. Appl. Phys.*, vol. 9, Nov. 1958, pp. 456–457.

Shock-tube Research in Hypersonic Aerodynamics, by P. H. Rose, *Instrum. Soc. Amer. J.*, vol. 5, Nov. 1958, pp. 72–80.

Molecular Diffusion Studies in Gases at High Temperature, I: The "Point Source" Technique, by R. E. Walker and A. A. Westenberg, *J. Chem. Phys.*, vol. 29, Nov. 1958, pp. 1139–1146.

Molecular Diffusion Studies in Gases at High Temperature, II: Interpretation of Results on the He–N_2 and CO_2–N_2 Systems, by R. E. Walker and A. A. Westenberg, *J. Chem. Phys.*, vol. 29, Nov. 1958, pp. 1147–1153.

Kinetic Studies of Hydroxyl Radicals in Shock Waves, II: Induction Times in the Hydrogen-oxygen Reaction, by G. B. Schott and J. L. Kinsey, *J. Chem. Phys.*, vol. 29, Nov. 1958, pp. 1177–1179.

Chemical Effects of Nuclear Transformations in the Gas Phase, by J. B. Evans, J. E. Quinlan, M. C. Sauer Jr. and J. E. Willard, *J. Phys. Chem.*, vol. 62, Nov. 1958, pp. 1351–1355.

Mechanism of Reaction of Recoil Hydrogen in the Gas Phase, by Mostafa Amr El-Sayed, Peder J. Estrup and Richard Wolfgang, *J. Phys. Chem.*, vol. 62, Nov. 1958, pp. 1356–1363.

Chemical Effects of the Nuclear Transformation, C^{12} (n, 2n) C^{11}, in Benzene: Influence of Phase, Temperature and Radical Scavengers, by B. Suryanarayana and Alfred P. Wolf, *J. Phys. Chem.*, vol. 62, Nov. 1958, pp. 1369–1372.

Similarity Flows behind Strong Shock Waves, by M. H. Rogers, *Quart. J. Mech. and Appl. Math.*, vol. 11, Nov. 1958, pp. 411–422.

Transverse Component of Velocity in a Plane Symmetrical Jet of a Compressible Fluid, by J. N. Kapur, *Quart. J. Mech. and Appl. Math.*, vol. 11, Nov. 1958, pp. 427–437.

A Lagrangian Formulation of the Boltzmann-Vlasov Equation for Plasmas, by F. E. Low, *Proc. Roy. Soc., London*, vol. A248, Nov. 11, 1958, pp. 282–289.

The Definitions of Terms Relating to Various Flow Regimes of a Gas—Some Proposals, by C. H. E. Warren and A. D. Young, *J. Roy. Aeron. Soc.*, vol. 62, Nov. 1958, pp. 801–804.

A Note on the Effect of Surface Finish on the Thrust of a Supersonic Conical Nozzle, by P. N. Rowe, *J. Roy. Aeron. Soc.*, vol. 62, Nov. 1958, p. 829.

Self-diffusion in Argon to 300 Atmospheres, by T. R. Mifflin and C. O. Bennett, *J. Chem. Phys.*, vol. 29, Nov. 1958, pp. 975–978.

Combustion, Fuels and Propellants

Investigation of a Resonance Burner Concept, Phase I, Summary Report Contract No. Nonr 2458(00), Rep. ARD 219, by *Hiller Helicopters, Advanced Res. Div.*, Dec. 1958, 21 pp.

Mechanism and Kinetics of the Reaction between Fuming Nitric Acid and/or Its Decomposition Products and Gaseous Hydrocarbons, by Francis R. Taylor, Rachel G. Franklin and Orenst N. Rudyj, *Wright Air Dev. Center, Tech. Rep.* 58-228 (*ASTIA AD* 155550), March 1958, 36 pp.

A Continuous Loss-in-weight Feeder for Nitrocellulose, by C. D. Cox, J. H. Pennington, P. H. Damon and A. H. Singleton, *Naval Prop. Plant, Mem. Rep.* 157, Dec. 1958, 30 pp.

Design and Operating Criteria for Fluorine Disposal by Reaction with Charcoal, by Harold W. Schmidt, *NASA Memo* 1-27-59E, Feb. 1959, 18 pp.

Recent Advances in Fluorine Chemistry and Technology, by John F. Gall, ARS Journal, vol. 29, Feb. 1959, pp. 95–103.

Multiple Flameholder Arrays: Flame Interactions, by F. H. Wright, ARS Journal, vol. 29, Feb. 1959, pp. 143–144.

Energy Release in Flames Stabilized by Cyclonic Flow, by William F. Kenney and Lyle F. Albright, *Ind. Engng. Chem.*, vol. 51, Feb. 1959, pp. 227–228.

Purification and Stabilization of Nitric Acid, by A. A. Krawetz and T. F. Young, *Ind. Engng. Chem.*, vol. 51, Feb. 1959, p. 229.

The Lithium Borohydride-Ammonia System: P-C-T Relationships and Densities, by Edward A. Sullivan and Sidney Johnson, *J. Phys. Chem.*, vol. 63, Feb. 1959, pp. 233–237.

Thermal Conductivity of Polycrystalline Boron, by Claude P. Talley, *J. Phys. Chem.*, vol. 63, Feb. 1959, p. 311.

Solid Propellant Aging; An Important Factor in the Relability of Rocket-

powered Missiles, by N. Fishman, *Ordnance*, vol. 43, Jan.-Feb. 1959, pp. 681–683.

Flow Field of a Flame in a Channel, by Mahinder S. Uberoi, *Phys. Fluids*, vol. 2, Jan.-Feb. 1959, pp. 72–78.

Recent Advances in Gaseous Detonation, by R. A. Gross and A. K. Oppenheim, ARS JOURNAL, vol. 29, March 1959, pp. 173–179.

Compression Sensitivity of Monopropellants, by G. A. Mead, ARS JOURNAL, vol. 29, March 1959, pp. 192–198.

Isothermal Compressibility of Liquid Oxygen and RP-1, by George T. Y. Chao, ARS JOURNAL, vol. 29, March 1959, pp. 199–203.

Recent Advances in Boron Technology, by Richard A. Carpenter, ARS JOURNAL, vol. 29, Jan. 1959, pp. 8–14.

A Ballistic Bomb Method for Determining the Experimental Performance of Rocket Propellants, by Donald N. Griffin, Charles F. Turner and George T. Angeloff, ARS JOURNAL, vol. 29, Jan. 1959, pp. 15–19.

Improvements in the Operating Characteristics of n-Propyl Nitrate, by R. W. Lawrence and W. P. Knight, ARS JOURNAL, vol. 29, Jan. 1959, pp. 29–32.

The Ignition Behavior of Various Amines with White Fuming Nitric Acid, by Rose L. Schalla and Edward A. Fletcher, ARS JOURNAL, vol. 29, Jan. 1959, pp. 33–39.

Application of Surface Decomposition Kinetics to Detonation of Ammonium Nitrate, by W. H. Andersen and R. F. Chaiken, ARS JOURNAL, vol. 29, Jan. 1959, pp. 49–51.

A Novel Combustion Measurement Based on the Extinguishment of Diffusion Flames, by A. E. Potter Jr. and James N. Butler, ARS JOURNAL, vol. 29, Jan. 1959, pp. 54–56.

Research on Supersonic Combustion, by Robert A. Gross, ARS JOURNAL, vol. 29, Jan. 1959, pp. 63–64.

A Rapid Method for Estimation of Specific Impulse, by B. A. Free and S. F. Sarner, ARS JOURNAL, vol. 29, Jan. 1959, pp. 64–67.

Rates of Selected Reactions Involving Nitrogen and Oxygen, by Norman Davidson, *AVCO Mfg. Corp., AVCO Res. Lab., Res. Rep.* 32, June 1958, 13 pp.

Round Robin 13C of the Joint Army-Navy-Air Force Panel on the Analytical Chemistry of Solid Propellants: Evaluation of the Karl Fischer Method for the Determination of Water in Ammonium Nitrate, by E. A. Burns and R. F. Muraca, *Calif. Inst. Tech., Jet Prop. Lab., Progr. Rep.* 20-354, April 1958, 31 pp.

The Equilibrium $Li_2CO_3(s) + CO_2 + H_2O \leftrightarrows 2Li^+ + 2HCO_3^-$, at High Temperature and Pressure, by William L. Marshall, Frank J. Loprest and C. H. Secoy, *J. Am. Chem. Soc.*, vol. 80, Nov. 5, 1958, pp. 5646–5647.

Competitive Oxidations, Part 1: Ethane + Propane Mixtures, by J. H. Knox, R. F. Smith and A. F. Trotman-Dickenson, *Trans. Faraday Soc.*, vol. 54, Oct. 1958, pp. 1509–1514.

Dissociation of the Hydrogen Molecule Ion by Electron Impact, by Eugene V. Ivash, *Phys. Rev.*, vol. 112, no. 1, Oct. 1, 1958, pp. 155–158.

Collision Cross Section and Energy Loss of Slow Electrons in Hydrogen, by G. Bekefi and Sanborn C. Brown, *Phys. Rev.*, vol. 112, no. 1, Oct. 1, 1958, pp. 159–164.

Photodetachment of O_{2-}, by D. S. Burch, S. J. Smith and L. M. Branscomb,

Phys. Rev., vol. 112, no. 1, Oct. 1, 1958, pp. 171–175.

Ignition Delay in the Burning of Perchloro-sulfo-nitrogen Associated with Various Combustibles, by H. Moutet, *La Récherche Aéron.*, no. 166, Sept.-Oct. 1958, pp. 23–34. (In French.)

Chemical Thermodynamics in Rocket Nozzles, by W. B. White, *Rand. Corp., Paper* P-1286, Feb. 1958, 12 pp.

The Equation of State of Hydrogen at High Pressures, by A. A. Abrikosov, *Rand Corp., Translation* T-61 (Translation of *USSR Acad. Sci., Astronomical J.*, vol. 31, 1954, p. 112) March 1958, 26 pp.

Efficiencies of Additives in the Transfer of Vibrational Energy in Ethylene and Nitrous Oxide, by J. W. Arnold, J. C. McCourbrey and A. R. Ubbelohde, F.R.S., *Proc., Roy. Soc., London*, vol. A248, Dec. 9, 1958, pp. 445–456.

Observations of Detonation in Solid Explosives by Microwave Interferometry, by G. F. Gawsey, J. L. Farrands and S. Thomas, *Proc. Roy. Soc., London*, vol. A248, Dec. 9, 1958, pp. 499–507.

Analytical Study of the Equilibrium Thickness of Boric Oxide Deposits on Jet-engine Surfaces, by Paul C. Setze, *NACA Res. Mem.* E57F13b, Oct. 1957, 20 pp. (Declassified from Confidential by Authority of *NASA PA* 2, p. 27, 12/10/58.)

Performance Comparisons of Navy Jet Mix and MIL-F-5624A(JP-3) Fuels in Tubular and Annular Combustors, by Richard J. McCafferty, *NACA Res. Mem.* E51J17, June 1954, 24 pp. (Declassified from Confidential by authority of *NASA PA* 2, p. 18, 12/10/58.)

Results of Turbojet Engine Operation Tests Using a 50-50- Mixture of JP-4 and Tributyl Borate as the Fuel, by Louis J. Schafer Jr. and Frances S. Stepka, *NACA Res. Mem.* E52L17a, Jan. 1957, 15 pp. (Declassified from Confidential by authority of *NASA PA* 2, p. 20, 12/10/58.)

The Thermal Stability of Unsymmetrical Dimethylhydrazine, by Adolph E. Spakowski, *NASA Mem* 12-13-58E, Dec. 1958, 12 pp.

Mechanisms of the Autodecomposition of Liquid Acetylenic Monopropellants, Experiment Inc., Progress report for January through June 1958, *TM*-1039, July 1958, 9 pp.

Evaluation of Liquefied Hydrocarbon Gases as Turbojet Fuels, by Robert R. Hibbard, *NACA Res. Mem.* E56I21, Dec. 1956, 44 pp. (Declassified from Confidential by authority of *NASA PA* 2, p. 26, 12/10/58.)

Development of an Indicator Test Paper to Detect Stability of Stored Propellants, by Phillip Rochlin, *Picatinny Arsenal, Feltman Res. and Engng. Labs., Tech. Rep.* 2567 (*ASTIA AD* 202006), Nov. 1958, 28 pp.

Sub Microsecond X-Ray Unit for Explosives Research, by S. W. Miller and C. J. Schoens, *Stanford Res. Inst., Poulter Labs., Tech. Rep.* 011-55, June 1955, 27 pp.

Use of Flash X-ray Techniques in Explosive Research, by Roy. McLeod, *Stanford Res. Inst., Poulter Labs., Tech. Rep.* 021-57, Sept. 1957, 55 pp.

Self-ignition Temperatures of Materials from Kinetic-reaction Data, by Daniel Gross and A. F. Robertson, *J. Res., Natl. Bur. Standards*, vol. 61, Nov. 1958, pp. 413–422.

Combustion—an Aeronautical Science, by Howard W. Emmons, *J. Aero/Space Sci.*, vol. 25, Dec. 1958, pp. 730–742.

Accelerated Flames and Detonation in Gases, by H. Jones, *Proc., Roy. Soc., London*, vol. A248, Nov. 25, 1958, pp. 333–345.

Instrumentation, Data Recording, Telemetering

Atlas Missile Instrumentation Checkout, by W. S. Hicks, *ARS Preprint* 761-59, March 1959, 10 pp.

Command Telemetry, by Leonard S. Taylor, *ARS Preprint* 752-59, March 1959, 6 pp.

On the Use of Ionization Gage Devices at Very High Altitude, by N. W. Spencer, R. L. Boggess, H. E. LaGow and P. Horowitz, ARS JOURNAL, vol. 29, April 1959, pp. 290–294.

A 960-mc Lunar Transmitter, by Leonard R. Malling, ASTRONAUTICS, vol. 4, May 1959, pp. 29–31, 104.

Miniaturized Digital Computing Systems, by Frederic A. Foss and Robert E. Lyons, ASTRONAUTICS, vol. 4, May 1959, pp. 42–43, 54.

Beyond Microminiaturization: Integrated Electronics, by Harry Kuhn, ASTRONAUTICS, vol. 4, May 1959, pp. 44–45, 126, 128, 130.

What Price Microminiaturization?, by David A. Young, ASTRONAUTICS, vol. 4, May 1959, pp. 46–47, 116.

Radar Contact with Venus, by John A. Newbauer, ASTRONAUTICS, vol. 4, May 1959, pp. 50, 124.

Accelerometers, Survey of the Ten Basic Types Available Commercially.

Instruments and Control Systems, vol. 32, April 1959, pp. 540–542.

Accelerometer Calibration, by Alvin B. Kaufman, *Instruments and Control Systems*, vol. 32, April 1959, pp. 544–547.

Bridge for Measuring the Impedance of Metal Microelectrodes, by R. C. Gesteland and Bradford Howland, *Rev. Sci. Instr.*, vol. 30, April 1959, pp. 262–264.

A Quantitative Rapid Response Atom Detector, by Kurt L. Wray, *Avco Mfg. Corp., Avco Res. Lab., Res. Rep.* 46, March 1959, 13 pp.

Preferred Precision Instrument Components, by *Bureau of Ordnance*, OP 1755 (first revision), April 1958.

Military Standard, Electronic Circuits. *Bureau of Aeronautics*, MIL-STD-439 (AER), May 1959, 157 pp.

Low Density Characteristics of an Aerobee-HI Pitot-static Probe, by J. A. Laurmann, *Univ. Calif., Inst. Engng. Res., Tech. Rep.* HE-150-156, May 1958, 10 pp,

The Calibration of Thermocouples by Freezing-point Baths and Empirical Equations, by R. P. Benedict, *J. Engng. for Power (ASME Trans.*, Series A), vol. 81, no. 2, April 1959, pp. 177–188.

The O.N.E.R.A. Telemeter, by H. LeBoiteux and G. Moussette, *Recherche Aéronautique*, no. 68, Jan.-Feb. 1959, pp. 3–8. (In French.)

Spaceflight

The Determination of Round Trip Planetary Reconnaissance Trajectories, by Richard H. Battin, *Inst. Aeron. Sci., Rep.* 59–31, Jan. 1959, 70 pp.

Minimum Time Interplanetary Orbits, by D. M. Cole, *J. Astron. Sci.*, vol. 5, Summer 1958, pp. 31–38.

Satellite Motions with Friction, by Leif N. Persen, *Zeitschrift für Angewandte Mathematik und Mechanik*, vol. 38, Nov.-Dec. 1958, pp. 437–442. (In German.)

Space Vehicles and Missiles, *Aviation Week*, vol. 69, Mid-December 1958, Section B, 46 pp.

Space Handbook: Astronautics and Its Applications, by *U. S. Congress, House, Select Committee on Astronautics and Space Exploration*, Washington, Govt. Print. Off., 1959, 252 pp.

Interplanetary Navigation by Optical Resection and Inertial Systems, by Joel Carroll, *Aero/Space Engng.*, vol. 18, March 1959, pp. 53–55, 75.

Relativity and Space Travel: A Reply to Professor Dingle, by R. Herman, *J. Brit. Interplan. Soc.*, vol. 16, Nov.-Dec. 1958, pp. 564–574.

What We Have Learned from Vanguard, by Milton Rosen, ASTRONAUTICS, vol. 4, April 1959, Part 1, pp. 28–29, 110–111.

Keeping Up to Date on Soviet Astronautics, by F. J. Krieger, ASTRONAUTICS, vol. 4, April 1959, Part 1, pp. 30–32, 76.

Biodynamics of Space Flight, by Edwin P. Hiatt, ASTRONAUTICS, vol. 4, Feb. 1959, pp. 24–25, 70, 72, 74, 77.

Weightlessness and Space Flight, by Harold J. von Beckh, ASTRONAUTICS, vol. 4, Feb. 1959, pp. 26–27, 84, 86.

Selecting a Space Cabin Atmosphere, by Karl E. Schaefer, ASTRONAUTICS, vol. 4, Feb. 1959, pp. 28–29, 104, 106.

Soviet Biological Experiments, by Irwin Hersey, ASTRONAUTICS, vol. 4, Feb. 1959, pp. 31, 80–81.

Psychophysiological Aspects of Manhigh, by David G. Simons, ASTRONAUTICS, vol. 4, Feb. 1959, pp. 32–33, 62–63.

Water Recovery in a Space Cabin, by R. A. Bambenek and J. D. Zeff, ASTRONAUTICS, vol. 4, Feb. 1959, pp. 36–37, 102.

Acceleration: How Great a Problem?, by John P. Stapp, ASTRONAUTICS, vol. 4, Feb. 1959, pp. 38–39, 98, 100.

Hazards of Sealed Cabins, by Eugene B. Konecci, ASTRONAUTICS, vol. 4, Feb. 1959, pp. 40–41, 48–51.

A Closed-cycle Breathing/Ventilation System, by Walter B. Moen and Paul Webb, ASTRONAUTICS, vol. 4, Feb. 1959, pp. 36–37, 102.

Aerophysics, Astrophysics

Some Consequences of a Theory of the Radiation Belt, by Professor S. F. Singer, *J. Brit. Interplanet. Soc.*, vol. 16, Nov.-Dec. 1958, pp. 558–563.

Missile Range Meteorology, by R. F. Durbin, *ARS Preprint* 757-59, March 1959, 10 pp.

Recent Results of High Altitude Research by Means of Rockets and Satellites, by H. K. Kallmann, *Rand Corp.*, RM-2275 (*ASTIA AD* 207200), Aug. 1958, 27 pp.

A Preliminary Model Atmosphere Based on Rocket and Satellite Data, by H. K. Kallmann and M. L. Juncosa, *Rand Corp.*, RM-2286 (*ASTIA AD* 207752), Oct. 1958, 39 pp.

Lines of Force of the Geomagnetic Field in Space, E. H. Vestine and W. L. Sibley, *Rand Corp.*, P-1541, Nov. 1958, 12 pp.

The Earth and Inertial Space, Part II: Shape of the Earth, by Richard H. Parvin, *Aero/Space Engng.*, vol. 18, May 1959, pp. 33–36.

Miniature Movies of the Planets, by Stuart C. Baker and John M. Kelso, ASTRONAUTICS, vol. 4, May 1959, p. 26–28, 104, 106.

Using TV Techniques in Astronomy, by J. Borgman, *Electronics*, vol. 32, May 8, 1959, p. 66.

Sputtering as It Is Related to Hyperbolic Meteorites, by Robert M. L. Baker Jr., *J. Appl. Phys.*, vol. 30, April 1959, pp. 550–555.

Collision Frequency of Electrons in the Terrestrial Atmosphere, by Marcel Nicolet, *Phys. of Fluids*, vol. 2, March-April 1959, pp. 95–99.

Cosmic-Ray Instrumentation in the First U. S. Satellite, by George H. Ludwin, *Rev. Sci. Instr.*, vol. 30, April 1959, pp. 223–229.

International Geophysical Year, Comité Special, Moscow, July 3–Aug. 9, 1958, Rocket and Satellite Symposium, Washington, National Acad. Sci., Feb 25, 1959. (Technical Papers.) Selected Papers:

1 **Cosmic Rays Observed by Satellite 1958 Alpha,** by Yuichiro Aono and Konnosuke Kawakami.

2 **On the Density of the Upper Atmosphere Derived from Observations of Satellites 1957 Alpha and Beta,** by S. Aoki, Paper A.3, 3 pp.

3 **An Interim Atmosphere Derived from Rocket and Satellite Data,** by I. Harris and R. Jastrow, Paper A.4.

4 **Decay of Spin in Sputnik I,** by J. W. Warwick, Paper A.5.

5 **A Short Program for the Determination of Satellite Orbits,** by I. Harris and R. Jastrow, Paper A.7.

6 **Progress of the British Upper Atmospheric Rocket Research Programme** by H. S. W. Massey, Paper B.1.

7 **Power Sources for Satellites and Space Vehicles,** by Harold A. Zahl and Hans K. Ziegler, Paper B.6.

8 **A Radioactive - ionization - gage Pressure-measurement System,** by N. W. Spencer and R. L. Boggess, Paper B.7.

9 **Preliminary Report on the Instrumentation and Operation of the Explorer Satellites,** by Henry L. Richter Jr., Paper B.8.

10 **Demise of Satellites of 1957 Alpha 1 and 1957 Beta,** by I. Harris and R. Jastrow, Paper B.9.

11 **General Aspects of Satellite Observation,** by M. Miyada, Paper C.3.

12 **Photographic Satellite Tracking with 35mm Cameras,** by M. J. Smyth, Paper C.4.

13 **A Comparison of Orbital Theory with Observations Made in the United Kingdom on the Russian Satellites,** by E. C. Cornford, Paper C.5.

14 **Australian Rocket-satellite Programme for the I.G.Y.,** by H. C. Webster, Paper C.6.

15 **Progress Report on the Japanese I.G.Y. Rocket Program,** by T. Hatanaka, Paper C.8.

16 **Surveying by Astrometry of Rocket-flashes,** by R. d'E. Atkinson, Paper C.9.

17 **Stellar Magnitude of Vanguard Satellites and of the Vanguard Third State Rocket Casing,** by R. Tousey, M. J. Koomen and I. S. Gullege, Paper C.10.

18 **The Analysis of Doppler Records from Earth Satellites,** by D. E. Hampton, Paper D.1.

19 **A Radio-interferometer Giving Continuous Information of Bearing,** by A. N. Beresford, Paper D.2.

20 **United Kingdom Tracking of Russian Satellites by Reception of Their 20 and 40 Mc/s Transmissions,** by W. T. Blackband, Paper D.3.

21 **Radar Observation of the Second Russian Earth Satellite,** by J. G. Davies, J. V. Evans, J. S. Greenhow, J. E. Hall, I. L. Neufeld and J. H. Thomson, Paper D.4.

22 **Some Simultaneous Radio Direction-finding and Doppler Frequency Shift Measurements on the Russian Artificial Earth Satellites,** by F. A. Kitchen, W. R. R. Joy and E. R. Billam, Paper D.5.

23 **Observation on the U.S.S.R. Earth Satellites and the Study of Radio Wave Propagation,** by W. C. Bain and D. R. Shearman, Paper D.6.

24 **Amateur Radio Measurements of Soviet Satellites I and II,** by J. Heywood, Paper D.7.

25 **The Use of Interferometer Observations of Satellites for Measurement of Irregular Ionospheric Refraction,** by Robert S. Lawrence and James W. Warwick, Paper D.8.

26 **Electron Densities in the Ionosphere from Radio Doppler Tracking of Artificial Earth Satellites,** by Warren W. Berning, Paper D.9.

27 **Micrometeorite Impact Measurements on a 20″ Diameter Sphere at 700 to 2500 Kilometers Altitude,** by H. E. LaGow, D. H. Schaefer and J. C. Schaffert, Paper F.13.

Prediction of Cratering Caused by Meteoroid Impacts, by M. Kornhauser, *J. Astron. Sci.*, vol. 5, Autumn-Winter, 1958, pp. 58–63.

Possible Explanation for the Radiation Observed by Van Allen at High Altitudes in Satellites, by P. J. Kellogg, *Nuovo Cimento*, vol. 11, no. 1, Jan. 1, 1959, pp. 48–66.

Russian Technical Articles*

Soviet Periodical Literature on Astronautics, by F. J. Krieger, *Rand Corp.*, P-1562, Dec. 1958, 12 pp.

Translations of Two Soviet Articles on Law Order in Outer Space, by F. J. Krieger and J. R. Thomas, *Rand Corp.*, T-98, Sept. 1958, 20 pp.: **For Equal Collaboration in the Peaceful Use of Cosmic Space,** by A. Galina, pp. 14–20 (translated from *Izvestiia*, Sept. 17, 1958, p. 5); and **On the Question of Interplanetary Law,** pp. 1–14 (translated from *Sovetskoe Gosudarstvo i Pravo*, no. 7, July 1958, pp. 52–58.)

Application of the Electric Analogy to the Solution of Radiant Heat Transfer Problems, by V. N. Adrianov, *Akad. Nauk SSSR, Izvestiia, Otdelenie Tekh. Nauk, Energetika i Avtomatika*, no. 1, 1959, pp. 20–25. (In Russian.)

Calculation of Heat Transfer and Friction on a Plane Plate in a Supersonic Flow in the Presence of Sweat Cooling, under the Condition of a Laminar Boundary Layer, by V. P. Motulevich, *Akad. Nauk SSSR, Izvestiia, Otdelenie Tekh. Nauk, Energetika i Avtomatika*, no. 1, 1959, pp. 33–38. (In Russian.)

Delineation of the Stability Areas of Nonlinear Automatic Control Systems Using Harmonic Linearization, by E. Popov, *Akad. Nauk SSSR, Izvestiia, Otdelenie Tekh. Nauk, Energetika i Avtomatika*, no. 1, 1959, pp. 53–64. (In Russian.)

Dynamics of Control Systems for the Study of Coulomb Friction in the Valve and in the Servomotor, with Consideration of the Nonlinear Characteristic of a Saturating Servomotor, by R. A. Nelepin, *Akad. Nauk SSSR, Izvestiia, Otdelenie Tekh. Nauk, Energetika i Avtomatika*, no. 1, 1959, pp. 65–73.

On the Transfer Function of a Relay Mechanism, by V. A. Besekerskii, *Akad. Nauk SSSR, Izvestiia, Otdelenie Tekh. Nauk, Energetika i Avtomatika*, no. 1, 1959, pp. 74–77. (In Russian.)

On the Carrying Capacity of a System of Parallel Information Channels, by I. A. Obseevich and M. S. Pinsker, *Akad. Nauk SSSR, Izvestiia, Otdelenie Tekh. Nauk, Energetika i Avtomatika*, no. 1, 1959, pp. 133–135. (In Russian.)

Electric Explosion of Spiral Wires in Vacuum, by I. F. Kvartskhava, V. V. Bondarenko, P. D. Meladze and K. V. Suladze, *Soviet Physics—JETP*, vol. 35(8), no. 4, April 1959, pp. 634–638.

Energy of the X-rays Emitted by Intense Pulsed Discharges in Hydrogen, by N. G. Koval'skii, I. M. Podgornyi and S. Khvashchevskii, *Soviet Physics—JETP*, vol. 35(8), no. 4, April 1959, pp. 656–660.

On the Motion of Bodies at High Velocities in a Weak Gravitational Field, by

---

* The Editors of Technical Literature Digest are making a systematic search for pertinent Russian articles, both in the original Russian and in translated form. For the balance of 1959, these will appear in a separate section with this heading, mainly to draw the readers' attention to the new listing. After that, they will appear item by item under the proper subject headings.

K. P. Staniukovich, *Soviet Physics—Doklady*, vol. 3, no. 3, May-June 1958, pp. 558–561.

On Motions with Homogenous Deformation in Magneto-hydrodynamics, by A. G. Kulikovskii, *Soviet Physics—Doklady*, vol. 3, no. 3, May-June 1958, pp. 507–509.

Some Remarks on the Structure of Shock Waves, by G. S. Golitsyn and K. P. Staniukovch, *Soviet Physics—JETP*, vol. 35(8), no. 3, March 1959, pp. 575–576.

The Stability of Shock Waves in Magnetohydrodynamics, by A. I. Akhiezer, G. Ia. Liubarskii and R. V. Polovin, *Soviet Physics—JETP*, vol. 35(8), no. 3, March 1959, pp. 507–511.

The deHaas-vanAlphen Effect in Pulsed Magnetic Fields, by A. M. Kosevich, *Soviet Physics—JETP*, vol. 35(8), no. 3, March 1959, pp. 512–514.

Stationary Relativistic Motions of a Gas in a Conducting Medium, by K. P. Staniukovich, *Soviet Physics—JETP*, vol. 35(8), no. 3, March 1959, pp. 529–531.

Unidimensional Motion in Magneto-hydrodynamics, by G. S. Golitsyn, *Soviet Physics—JETP*, vol. 35(8), no. 3, March 1959, pp. 538–541.

On the Theory of Gas Jets, by L. N. Sretenskii, *Soviet Physics—Doklady*, vol. 3, no. 2, March-April, 1958, pp. 252–254.

Synthesis of the Control Unit of an Optimum Servosystem from the Point of View of Its High Speed, by Sun Tsjan, *Avtomatika i Telemekhanika*, vol. 20, no. 3, 1959, pp. 273–288. (In Russian.)

Realization of Optimum Weight Function in Pulse Servosystems, by V. P. Perov, *Avtomatika i Telemekhanika*, vol. 20, no. 3, 1959, pp. 289–297. (In Russian.)

New Method of Constructing a Stability Plane within the Admissible Parameters of Control Systems, by V. I. Zubov, *Avtomatika i Telemekhanika*, vol. 20, no. 3, 1959, pp. 331–334. (In Russian.)

Choice of a Nonlinear Speed Feedback Characteristic for a Servosystem of Known Attitude, by B. N. Nanmov, *Avtomatika i Telemekhanika*, vol. 20, no. 3, 1959, pp. 335–345. (In Russian.)

Bibliography on Automatic Contrcl and Related Problems for 1956, *Avtomatika i Telemekhanika*, vol. 20, no. 3, 1959, pp. 381–399.

Electron Concentration in the Upper Ionosphere as Determined from Radio Signals of the First Earth Satellite, by Ia. L. Al'pert, F. F. Dobriakova, E. F. Chudesenko and B. S. Shapiro, *Soviet Physics—Doklady*, vol. 3, no. 3, May-June 1958, pp. 584–587.

Cosmic Radiation Measured on the Second Artificial Satellite, by S. N. Vernov, N. L. Grigorov, Iu. I. Logachev and A. E. Chudakov, *Soviet Physics—Doklady*, vol. 3, no. 3, May-June 1958, pp. 617–619.

Rocket Measurements of the Electron Concentration in the Ionosphere by Means of an Ultrashort-wave Dispersion Interferometer, by K. I. Gringauz, *Soviet Physics—Doklady*, vol. 3, no. 3, May-June 1958, pp. 620–623.

Investigation of Extensive Cosmic Ray Showers under Dense Substances, by S. I. Nikol'skii and A. A. Pomanskii, *Soviet Physics—JETP*, vol. 35(8), no. 3, March 1959, pp. 430–437.

Simulation of Nuclear Power Systems, by B. Ya Kogan, Yu. A. Nechaev and F. E. Tranin, *Avtomatika i Telemekhanika*, vol. 20, no. 3, 1959, pp. 349–354. (In Russian.)

Index to Advertisers